



University of
Nottingham

UK | CHINA | MALAYSIA

Histone modulation by nuclear localized meningococcal autotransporters

SHOMA DUTTA

B. Sc., M. Sc.

Thesis submitted to the University of Nottingham for the degree
of Doctor of Philosophy

December 2019

Molecular Bacteriology and Immunology Group

School of Life Sciences

Faculty of Medicine and Health Sciences

University of Nottingham

Declaration

I, do hereby declare that this thesis is my own work and this or any part of this has not been submitted elsewhere. Unless otherwise stated, all work contained here is my own.

Shoma Dutta

30th December 2019

Abstract

The meningococcal autotransporters Adhesion and penetration protein (App) and Meningococcal serine protease A (MspA) are secreted S6-peptidase family autotransporters which have previously been demonstrated to have various roles in meningococcal virulence including functioning as adhesins. One study from our group showed previously that FITC-labelled recombinant App or MspA passenger domain could be taken up by dendritic cells (DCs) and localised to the nucleus; App and MspA can also bind to, and cleave, recombinant histone H3. It was hypothesized the nuclear localisation of App and MspA occurred via nuclear-localisation sequences (NLS) present within them. This study aimed to shed more light on the nuclear localization of these autotransporters, and to identify the NLS of App and MspA.

In this study, nuclear localization was studied by expressing fluorescently labelled App and MspA fusion proteins using the expression plasmid pDsRed. Before identifying the NLS sequence of App and MspA, the nuclear localisation of DsRedApp and DsRedMspA were determined by confocal laser scanning microscopy. To achieve this, plasmids encoding DsRed-tagged proteins were transfected into Hep-2 cells (human epithelial carcinoma cell line) and HEK293T cells (human embryonic kidney cells with SV40 T-antigen) by transient transfection. The data confirmed that App and MspA were localized to the nucleus when expressed in either cell type. Proteolytic activity was not required for their nuclear localisation, as mutant proteins DsRedApp^{S267A} and DsRedMspA^{S241A} were also translocated.

In order to identify the motifs required to direct App and MspA to the nuclear compartment, various deletions were introduced into DsRedApp and

DsRedMspA, and the impact on nuclear localisation assessed. Three different mutants of App and two different mutants of MspA were expressed and their nuclear localisation properties assessed. Differences in the nuclear localisation patterns were observed between the wild-type and mutant App fusion proteins, with the mutant DsRedApp molecules lacking the putative NLS not showing nuclear localisation but remaining in the cytosol. Subsequent site-directed mutagenesis of serine residues within the deleted region also resulted in disruption of nuclear trafficking, confirming the localisation of a potential NLS within App between residues ⁹³³R and ⁹⁴⁰R.

In contrast, no classical NLS was predicted in MspA and a number of deletion mutants behaved like the wild type protein with respect to their nuclear localisation patterns. However, deletion of ⁹³³D to ¹⁰⁷³A of MspA resulted in a different pattern of localisation (punctuate cytoplasmic localisation) which was not observed with the other MspA mutants. The reason for this difference was unclear.

An additional aim of this study was to further characterise the proteolytic activity of App and MspA against histones, in terms of specificity and the requirement for histone post-translational modifications (PTMs), as it is known that histone clipping can influence chromatin structure and function. In histone clipping assays, a wide range of recombinant histones and epithelial cell-derived histones were used as cleavage substrates and the clipping products visualised by immunoblot analysis. Prior to these experiments, recombinant App and MspA were shown to have proteolytic activity against recombinant H1, H2B and H3 and against Hep-2 cell-derived H1, H2B and H3 (which possess post-translational modifications not found on the recombinant versions), demonstrating that histone PTMs do not effect App- and MspA-mediated

cleavage. Furthermore, by adding recombinant App or MspA to host cells *in vitro* and detecting histone cleavage products, we show that histone clipping occurs in intact cells following uptake and nuclear localization of the meningococcal autotransporters. Moreover, histone clipping was also observed in histones derived from sub-cellular chromatin preparations, indicating that the App and MspA-mediated proteolytic processing of histones occurs within intact chromatin.

List of Presentations

Poster/Oral presentations

Shoma Dutta, Dr. Neil Oldfield, Dr. Karl Wooldridge. Nuclear localisation and proteolytic activity of App and MspA meningococcal autotransporters. Presented at the Microbiology Society Annual Conference, 8 – 12th April 2019, Belfast, Northern Ireland, UK.

Shoma Dutta, Dr. Neil Oldfield, Dr. Karl Wooldridge. Nuclear localisation and proteolytic activity of App and MspA meningococcal autotransporters. Presented at the International Pathogenic *Neisseria* Conference (IPNC), 23-28th September 2018, Monterey, California, U.S.A.

Shoma Dutta, Dr. Neil Oldfield, Dr. Karl Wooldridge. Nuclear localisation and cellular response of meningococcal autotransporters. Presented at the School of Life Sciences Symposium, 11 - 12th July 2018, Nottingham, UK.

Shoma Dutta, Dr. Neil Oldfield, Dr. Karl Wooldridge. Nuclear localisation and cellular response of meningococcal autotransporters. Presented at the School of Life Sciences Symposium, 13 - 14th July 2017, Nottingham, UK.

Published (Abstract):

Dutta, Shoma, Oldfield, Neil and Wooldridge, Karl. Investigating the nuclear localisation and proteolytic activity of the meningococcal App and MspA autotransporters. Access Microbiology Volume 1, Issue 1A, 2019.

Acknowledgement

My sincere and deep appreciation to my supervisor's Dr. Karl Wooldridge and Dr. Neil Oldfield for providing me with the opportunity to complete this research work under their kind supervision and able guidance.

I would like to thank the Bangabandhu Fellowship trust, Ministry of Science and Technology, Bangladesh for funding my PhD at the University of Nottingham.

A special thanks goes to my assessor Dr. Kim Hardie for her valuable feedback and comments throughout the viva voice examination.

A very special thanks to my beloved husband for his support and understanding, and for listening my boring research stories. I am grateful to him for being with me as the best friend for the last two years sacrificing his own future.

I am most grateful to my son Shuvom, who is still a kid but tried every day to help me like a brave man during my whole PhD journey.

I am sincerely grateful to my amazing parents, my brother and my sister for all their love and supports throughout my life.

A special thanks to my friends Iyelola Turner, Rininta Firdaus, Banan Atwah and all other past and present members of MBIG for their companionship, encouragement, and much needed moral supports, as well as to Phil Bardelang, Jean Dubern for providing useful tips and suggestions and also to Ann Lowe.

Only words are not enough to describe how tough the journey was for us, especially for my son and for my husband. I am dedicating this thesis to them.

Shoma

Abbreviations

App	Adhesion and penetration protein
Ab	Antibiotic
AspA	Autotransporter serine protease A
ATCC	American Type Culture Collection
ATP	Adenosine triphosphate
ATs	Autotransporters
Amp	Amplification
AutA	Auto-transporter A
AutB	Auto-transporter B
Bam	β -barrel assembly machinery
BBB	Blood brain barrier
BCIP/NBT	5-bromo-4-chloro-3-indolyl phosphate/nitrobluetetrazolium
bp/kp	Base pairs/kilo base pairs
BSA	Bovine Serum Albumin
C3/C5	Complement 3/Complement 5 protein
CD	Cluster of differentiation
CEACAM	Carcinoembryonic antigen-related cell adhesion molecule
CFU	Colony-forming unit
CNS	Central nervous system
CO ₂	Carbon Dioxide
Cps	capsule synthesis operon
CR	Cysteine-rich domain

CSF	Cerebrospinal fluid
cspA	Cold shock protein A promoter
CTLD	C-type lectin-like domain
Cy5	Cyanine 5 fluorescent dye
Da/kDa	Dalton/kilodalton
DAPI	4', 6-diaminido-2-phenylindole
DCs	Dendritic cells
dH ₂ O	Distilled water
DMEM	Dulbecco's Modified Eagle's Medium
DNA	Deoxyribonucleic acid
dNTP	Deoxyribonucleoside triphosphate
<i>E. coli</i>	Escherichia coli
EDTA	Ethylenediaminetetraacetic acid
ELISA	Enzyme-linked immunosorbent assay
EpiCGS	Epithelial cell growth supplement
F	Forward
FBS	Fetal bovine serum
fHbp	Factor H-binding protein
g/mg/μg/ng	Gram/milligram/microgram/ nanogram
GAPDH-1	Glyceraldehyde 3-phosphate dehydrogenase
h/min/s	Hour/ minute/seconds
H1/H2A/ H2B	Histone 1/histone 2A/ histone 2B
H3.1/ H4	Histone 3. 1/histone 4
Hep-2	Human epithelial type II cells derived from human laryngeal carcinoma cells
HEK293T	Human embryonic kidney 293 cells, and contains the SV40

	T-antigen
His	Histidine
His6	Hexahistidine
HrpA	Haemagglutinin/haemolysin-related protein A
HrpB	Haemagglutinin/haemolysin-related protein B
Hsp	Heat shock protein
HSPGs	heparan sulfate proteoglycans
IgA1protease	Immunoglobulin A1 protease
IL	Interleukin
IMAC	Immobilized metal affinity chromatography
IMD	Invasive meningococcal disease
IPTG	Isopropyl β -D-1-thiogalactopyranoside
IU/ U/ mU	International units/ units/milli-units
Kb	Kilo base pair
kDa	Kilo Dalton
KpnI	restriction endonuclease enzyme isolated from <i>Klebsiella pneumoniae</i>
L/ml/ μ l	Litre/millilitre/microlitre
Lac	Lactose operator
LAMP	Lysosome-associated membrane proteins
LB	Lysogeny Broth
LbpB	Lactoferrin binding protein B
LBS	Lysine binding sites
LOS	Lipooligosaccharides
LPS	Lipopolysaccharides
LR	Laminin receptor

Lys	Lysine
M/mM	Molar/millimolar/
mAb	Monoclonal Antibody
MC58	A meningococcal serogroup B strain
MD	Meningococcal disease
methH	5-methyltetrahydropteroyl-triglutamate
MHC	Major Histocompatibility
MLEE	Multi-locus enzyme electrophoresis
MLST	Multi-locus sequence typing
MR	Mannose receptor
MS	Mass spectrometry
MspA	Meningococcal serine protease A
Mt	Mutant
MWCO	Molecular weight cut-off
Na ₂ PO ₄	Sodium phosphate
NaCl	Sodium chloride
NadA	Neisseria adhesion A
NalP	Neisserial autotransporter lipoprotein
NhbA	Neisseria heparin binding Antigen
NhhA	Neisseria hia homologue A
NLS	Nuclear localization signal
ODxxx	Optical density at xxx nM wavelength
OMP	Outer membrane protein
Opa	Opacity protein A
Opc	Opacity protein C
ORF	Open reading frame

OS	Oligosaccharide
P	Probability value
pAb	Polyclonal Antibody
PBMCs	Peripheral blood mononuclear cells
PBS	Phosphate buffer saline
PBST	PBS with 0.05%-0.1% Tween 20
pCold-TF	A fusion cold shock expression vector that expresses Trigger Factor (TF)
PCR	Polymerase chain reaction
pDsRed	A fusion expression vector that expresses Dsred
Pet	Plasmid-encoded toxin
pH	Unit of acidity/alkalinity
PMNs	Polymorphonuclear leukocytes
PorA	Porin A
PorB	Porin B
Prx	Peroxiredoxin
PTM	Posttranslational modifications
R	Reverse
RBCs	Red Blood Cells
rDnaK	Recombinant DnaK
Rpm	Revolution per minute
RT	Room temperature
rTF	Recombinant trigger factor
S/H/D/A/E	Serine/Histidine/Aspartate/Alanine/Glutamate
SDS-PAGE	Sodium dodecyl sulphate- polyacrylamide gel

	electrophoresis
SE	Standard error
Sec	The general secretion pathway (Sec pathway) of bacteria
SpeI	Restriction enzyme isolated from <i>Sphareotilus natans</i>
Sp	Species
SSM	Slipped strand mispairing
ST	Sequence type
TAE	Tris-Acetate-EDTA
Taq	<i>Thermus aquaticus</i> thermostable polymerase
Tat	Twin-arginine translocation
TF	Trigger factor
TLR	Toll-like receptor
TNF- α	Tumour necrosis factor- α
TxSS	TypeXsecretion system, where X represents number (1/2/3/4/5/6)
WT	Wild-type
μ M/nM	micromolar/nanomolar

Table of Contents

Declaration	i
Abstract	ii
List of Presentations	v
Acknowledgement	vi
Abbreviations	vii
Table of Contents	xiii
List of Figures	xvii
List of Tables	xxii
CHAPTER 1: Introduction	1
1.1. Meningococcal disease	2
1.2. History of meningococcal disease.....	3
1.3. Neisseria meningitidis	5
1.3.1. Classification.....	5
1.3.2. Epidemiology	6
1.4. Clinical Manifestations	8
1.5. Virulence factors.....	9
1.5.1. Capsule	10
1.5.2. Lipooligosaccharides	12
1.5.3. Adhesins	12
1.5.4. Iron-acquiring proteins.....	16
1.5.5. Factor H binding Protein	17
1.6. Meningococcal pathogenesis	17
1.7. Meningococcal vaccines	22
1.8. The autotransporter secretion pathway	25
1.9. Autotransporter proteins in <i>N. meningitidis</i>	29
1.9.1. IgA protease	30
1.9.2. NaIP	33
1.9.3. AutA and AutB	34
1.9.4. NadA and NhhA.....	35
1.9.5. App and MspA	36
1.10. Aim of the study.....	40

CHAPTER 2: Materials and Methods	41
2.1. Bacterial strains and growth conditions	42
2.2. List of the plasmids used in the study	42
2.3. Extraction, purification and quantification of DNA	44
2.4. Polymerase Chain Reaction (PCR)	44
2.5. Agarose gel electrophoresis	47
2.6. Restriction digestion	47
2.7. Ligation	47
2.8. Transformation of <i>E. coli</i>	48
2.9. Site directed mutagenesis.....	48
2.9.1. Lists of the Primers and Plasmids used in the mutagenesis	48
2.9.2. PCR mediated mutagenesis.....	49
2.9.3. Kinase-Ligase-DpnI (KLD) treatment	50
2.9.4. Transformation.....	50
2.10. DNA sequencing	50
2.11. Protein expression and purification	50
2.12. Desalting and concentration of proteins	51
2.13. SDS-PAGE analysis	52
2.14. Immunoblot analysis.....	52
2.15. Protein quantification	53
2.16. Cell culture	53
2.17. Cell viability assay	54
2.18. Transfection.....	55
2.19. Immunofluorescence staining and confocal microscopy	56
2.20. Histone purification from eukaryotic cells.....	56
2.21. Histone clipping assay	57
2.22. Cell lysis assay	58
2.23. Chromatin bound protein assay	59
CHAPTER 3: Nuclear localisation of meningococcal autotransporter App (Adhesion and Penetration Protein)	61
3.1. Introduction.....	62
3.2. Results.....	65
3.2.1. Nuclear localization of App into the host cell	65
3.2.2. Nuclear localization of App confirmed in HEK293T cells.....	70

3.2.3.	Quantification of nuclear localization	72
3.2.4.	Impact of catalytic serine residues on nuclear localisation of App proteins.....	73
3.2.5.	Identification of the App NLS sequence	78
3.2.6.	Mutation of serine residues in the putative NLS App sequence disrupts nuclear trafficking	87
3.2	Discussion	91
CHAPTER 4: Investigating nuclear localization signals in Meningococcal serine protease A (MspA).....		94
4.1.	Introduction.....	95
4.2.	Results.....	98
4.2.1.	Nuclear localization of MspA in host cells	98
4.2.2.	Role of MspA proteolytic activity in nuclear localization:	103
4.2.3.	Screening of regions of MspA which facilitate nuclear localization	106
4.3.	Discussion	116
CHAPTER 5: App and MspA mediated cleavage of host cell histones		120
5.1.	Introduction.....	121
5.2.	Results.....	125
5.2.1.	Purification of recombinant His-tagged App and MspA	125
5.2.2.	Purification of recombinant App and MspA proteins	127
5.2.3.	Purification of major histones from Hep-2 cells.....	134
5.2.4.	Identification of cell-derived histones	135
5.2.5.	Histone clipping assay by App and MspA.....	136
5.2.6.	Defining the reason behind the histone proteolytic processing of serine mutant of MspA	146
5.2.7.	Cellular histone clipping assay.....	169
5.2.8.	Cleaved histones H3 and H2B are associated with chromatin..	177
5.3.	Discussion	180
CHAPTER 6: General discussion		188
References	196
Appendix	230

List of Figures

Figure 1.1: Cross sectional view of the meningococcal cell membrane.....	10
Figure 1.2: Stages of the pathogenesis of <i>N. meningitidis</i>	18
Figure 1.3: A schematic overview of pathophysiology of meningitis.	22
Figure 1.4: Autotransporter secretion system.....	28
Figure 1.5: Schematic diagram showing the various domains of IgA1 protease with possible autocatalytic position sites and approximate NalP cleavage site.....	31
Figure 1.6: Models of autocatalytic processing and NalP-mediated proteolytic processing of App at the meningococcal surface.	39
Figure 2.1: Schematic overview of the subcellular fractionation procedure..	60
Figure 3.1: Schematic overview of the nuclear localization experiment	66
Figure 3.2: Confocal microscopic images showing co-localisation of App, VirD2 or IgA1 protease proteins tagged with DsRed with the nucleus in transfected Hep-2 cells.	69
Figure 3.3: Confocal microscopic images showing co-localisation of the DsRed-tagged recombinant proteins with the nucleus in transfected HEK293T cells.	71
Figure 3.4: Statistical analysis of co-localisation of fluorescent-labelled proteins and Hoechst-stained cell nuclei.	72
Figure 3.5: PCR-mediated generation of pDsRedApp ^{S267A}	74
Figure 3.6: DNA sequence chromatograms of pDsRedApp and pDsRedApp ^{S267A}	75
Figure 3.7: Nuclear localisation of DsRed-tagged App ^{S267A} and App proteins in transfected Hep-2 cells.	77

Figure 3.8: Predicted secondary Structure of App Protein	79
Figure 3.9: Inverse PCR- mediated generation of pDsRedApp ^{Δ901G-980Y}	80
Figure 3.10: Agarose gel analysis showing PCR confirmation of pDsRedApp ^{Δ901G-980Y}	81
Figure 3.11: Nuclear localisation of DsRedApp ^{ΔG901G-Y980}	83
Figure 3.12: Inverse PCR- mediated generation of pDsRedApp ^{ΔG901G-L965}	84
Figure 3.13: DNA sequence alignment of pDsRedApp and pDsRedApp ^{ΔG901 to L965} confirming the deletion.	85
Figure 3.14: Nuclear localization of DsRedApp ^{Δ901G-965L} in Hep-2 cells.	86
Figure 3.15: Generation of pDsRedAppNLS ^{S936AS939A}	88
Figure 3.16: Mutation of serine residues in the putative App NLS disrupt nuclear trafficking.....	89
Figure 4.1: Nuclear localization of DsRedMspA in Hep-2 cells.	100
Figure 4.2: Representative images showing the nuclear localization of DsRedMspA in transfected HEK293T cells.	101
Figure 4.3: Intensities of DsRed-labelled recombinant proteins in the nucleus was quantified.	102
Figure 4.4: DNA sequence of pDsRedMspA and pDsRedMspA ^{S241A}	104
Figure 4.5: Confocal microscopic images showing the colocalization of DsRed-tagged MspA ^{S241A} with the nucleus in transfected Hep-2 cells.	105
Figure 4.6: Predicted secondary structure of MspA WT and MspA ^{Δ1037A-1139I} showing how the 1037A to 1139I region deleted from MspA avoided helical regions of the protein.	107
Figure 4.7: Inverse PCR mediated generation of plasmid pDsRedMspA ^{Δ1037A-1139I}	108

Figure 4.8: Confocal images showing cellular localization of DsRedMspA ^{Δ1037A-1139I} in transfected Hep2 cells.	109
Figure 4.9: The 74 amino acids deleted from DsRedMspA to yield DsRedMspA ^{ΔD999-A1073}	110
Figure 4.10: Cellular localization of DsRedMspA ^{Δ999D-1073A}	112
Figure 4.11: DsRedMspA ^{Δ999D-1073A} shows various subcellular localization. .	114
Figure 4.12: Protein localization of DsRedMspA and DsRedMspA ^{Δ999D-1073A} . .	115
Figure 5.1: Nucleosome organization diagram.	121
Figure 5.2: PTMs of histone tails such as methylation, acetylation, phosphorylation, ubiquitinylation and ribosylation.	122
Figure 5.3: A schematic overview of the N-terminal tails of core histones. .	123
Figure 5.4: Representative images showing the induction of expression of recombinant autotransporter proteins in WCL.	126
Figure 5.5: Expression and purification of rpdApp protein.	128
Figure 5.6: Expression and purification of rpdMspA protein.	128
Figure 5.7: Purification of rpdApp ^{S267A} protein.	132
Figure 5.8: rpdMspA ^{S241A} expression and purification.	133
Figure 5.9: Successful histone purification from Hep-2 cells.	135
Figure 5.10: Representative immunoblotting images of purified histones..	136
Figure 5.11: Clipping assay utilizing recombinant or cell-derived native H1, and recombinant derivatives of App and MspA.	138
Figure 5.12: Clipping assay utilizing recombinant or cell-derived native H2A, and recombinant derivatives of App and MspA.	139
Figure 5.13: Clipping assay utilizing recombinant or cell-derived native H2B, and recombinant derivatives of App and MspA.	140

Figure 5.14: Clipping assay utilizing recombinant or cell-derived native H3, and recombinant derivatives of App and MspA. rpdApp^{S267A}. 142

Figure 5.15: Clipping assay utilizing recombinant or cell-derived native H4, and recombinant derivatives of App and MspA. 143

Figure 5.16: The serine protease inhibitor PMSF inhibits App and MspA mediated H3 clipping 145

Figure 5.17: PCR amplification of pColdTFMspA^{D135E} and pColdTFMspA^{D135ES241A}. 147

Figure 5.18: DNA sequence chromatograms confirming the desired mutations present in pColdTF-MspA^{D135E} and pColdTFMspA^{D135ES241A}. 148

Figure 5.19: SDS-PAGE and immunoblot analysis demonstrating purification of rpdMspA^{D135E} and rpdMspA^{D135ES241A}. 151

Figure 5.20: rH1 histone cleavage assay with different active and inactive recombinant MspA proteins. 152

Figure 5.21: Time course experiment for rH1 clipping assay. 154

Figure 5.22: Titration experiment to optimise rH1 cleavage assays using recombinant App and MspA proteins. 156

Figure 5.23: Final optimisation of the rH1 clipping assay. 157

Figure 5.24: Histone H2B clipping assay with recombinant App and MspA wild-type and mutant proteins. 158

Figure 5.25: Optimizing the incubation time for the rH2B clipping assay... 160

Figure 5.26: Titration experiment to optimise rH2B cleavage assays using recombinant App and MspA proteins.. 161

Figure 5.27: Optimized serine protease-mediated histone H2B clipping assay..... 163

Figure 5.28: rH3 Histone clipping assay with recombinant App and MspA wild types and mutant proteins. 164

Figure 5.29: Dose-time dependent histones rH3 clipping assays..... 166

Figure 5.30: Optimised serine protease mediated histone H3 clipping assay. 168

Figure 5.31: Toxicity of recombinant App autotransporter to Hep-2cells. ... 171

Figure 5.32: Toxicity of recombinant autotransporter MspA to Hep-2 cells. 173

Figure 5.33: Clipped Histones formed in Hep-2 cells by App and MspA. 176

Figure 5.34: Clipped histones accumulated within chromatin. 176

Figure 5.35: Schematic model presentation of the functional roles of histone cleavage in gene expression 186

List of Tables

Table 1.1: The main features of App and MspA proteins in <i>N. meningitidis</i> strain MC58.....	37
Table 2.1 Description of plasmids used in this study.....	42
Table 2.2 Primers for sequencing and PCR.....	46
Table 2.3 Following primers were used for site-directed mutagenesis	49

CHAPTER 1: Introduction

1.1. Meningococcal disease

Meningococcal disease refers to infection caused by *Neisseria meningitidis* (also known as the meningococcus). It has a high mortality rate if it is not immediately treated. The most notable clinical manifestations of meningococcal disease are meningitis and meningococcal sepsis. Meningitis is caused by the inflammation of the lining around the meninges, resulting from the penetration of organisms across the blood-brain barrier into the cerebral spinal fluid [1]. It is regarded as a medical crisis due to the rapid and severe neurological effects that are associated with the disease [2, 3]. Meningitis can be divided into two main types: bacterial and aseptic meningitis. Three principal organisms mainly cause bacterial meningitis: *Neisseria meningitidis*, *Haemophilus influenzae* and *Streptococcus pneumoniae*, whereas aseptic meningitis may be caused by non-bacterial organisms such as viruses, parasites or fungi, or by neoplasia and/or (less commonly), by certain drugs [1, 2]. Only *N. meningitidis* can cause both endemic and epidemic outbreaks.

N. meningitidis is a human nasopharyngeal commensal which persists in the upper respiratory tract, usually without causing disease symptoms [4], but occasionally, in susceptible hosts, it can cause invasive disease with high morbidity and mortality [5]. On average, the meningococcal carriage rate is approximately 10% of the population at any given time [6, 7]. Invasive meningococcal disease is the result of interplaying factors, including virulence factors of the organism, environmental conditions and host susceptibility [8]. In the case of hyper-virulent meningococci, the organism can invade the epithelial layers and can enter into the blood stream resulting in meningococcal sepsis, and can in some cases breach the blood-brain barrier (BBB) to cause meningitis

[9]. Meningococcal disease mainly affects infants, pre-school children, teenagers, and those older than 65 years. There is also an increased risk of meningococcal disease (due to increased transmission) where large groups of people get together, for example college students or military recruits [9].

Meningococcal disease has a prevalence rate which ranges from <1 to 1,000 cases/100,000 people per year which varies geographically and temporally [6, 10]. 10% of disease cases are lethal and around 30–50% of survivors of meningococcal disease develop permanent sequelae including neurologic disabilities, loss of hearing or visual loss, seizures, mental retardation or cognitive impairment, renal failure, hydrocephalus, and limb(s) amputation [11-13]. The incidence of the meningococcal disease has been reduced in the last few decades due to the development of vaccines [5].

1.2. History of meningococcal disease

Historically, meningitis has been described since the period of Hippocrates and possibly pre-renaissance physicians like Avicenna knew of meningitis. In 1768, Sir Robert Whyte was accredited with the first description of meningitis (in this case caused by *M. tuberculosis*). However, Gaspard Vieusseux was the first who gave a clinical description of meningococcal meningitis following the epidemics of meningococcal meningitis in Geneva in 1805 [14]. Another important milestone was in 1884, when the Italian pathologists Ettore Marchiafava and Angel Celli, first observed Gram-negative diplococci in the cerebrospinal fluid (CSF) from a meningitis patient's sample [14]. In 1887, the Austrian pathologist Anton Weichselbaum established the connection between the bacterium "*Diplococcus intracellularis meningitidis*", and the epidemic form of meningitis

[14]. Finally, the organism was renamed *Neisseria meningitidis*, after the German scientist and clinician Albert Neisser, who first described the closely related bacterium *Neisseria gonorrhoeae* [15].

Epidemics of meningococcal meningitis were also described in 1806 in New Bedford, Massachusetts and in the early 1900s in the African meningitis belt [16]. The disease patterns vary over time and with geographical areas, age group, and bacterial serogroups [10]. The late 19th century witnessed the identification of the causative agents of meningitis including *H. influenzae*, *S. pneumoniae*, and *N. meningitidis*.

The treatment of meningococcal disease by serum therapy was introduced in 1917 by Flexner [17] and sulfonamides were introduced in 1937 [18]. The first vaccine against meningococci was promoted in the 1960s [19]. During the pre-serum therapy and pre-antibiotic eras, 70–85% of disease cases were fatal. The development of new therapeutic methods including antisera, sulphonamides and penicillin resulted in a significant decline in mortality during the past century [8]. Currently, despite the availability of therapeutic and prophylactic antibiotics and immunizations against some serogroups, meningococcal meningitis is still reported in both developing and developed countries [10].

1.3. *Neisseria meningitidis*

The scientific classification of *N. meningitidis* is:

Phylum: Proteobacteria

Class: Betaproteobacteria

Order: Neisseriales

Family: Neisseriaceae

Genus: *Neisseria*

The genus *Neisseria* contains 25 species based on 16S rRNA gene sequence analysis, among them two well-characterized human pathogens *N. meningitidis* and *N. gonorrhoeae* that are the causative agents of meningitis/sepsis and gonorrhoea, respectively [20]. *N. meningitidis* is an obligate human commensal [21]. However, occasionally it causes nasopharyngitis, sepsis and meningitis. The organism is an encapsulated Gram-negative aerobic diplococcus; it is oxidase and catalase-positive, non-spore forming, aflagellated, and approximately 0.8 µm in diameter [22]. It's only known natural host is man. Other human commensal *Neisseria* species include *N. cinerea*, *N. elongata*, *N. flavescens*, *N. lactamica*, *N. mucosa*, *N. perflava*, *N. polysaccharea*, *N. sicca* and *N. subflava* [23].

1.3.1. Classification

Traditionally, meningococci have been classified serologically into serogroups, serotypes, serosubtypes and immunotypes, based on the surface structures polysaccharide capsule (serogroup), outer membrane proteins (OMPs; serotype and subtype) and lipooligosaccharide (LOS; immunotype). Based on the polysaccharide capsule structure or genetic differences in the capsule biosynthesis locus, meningococci are classified into 13 serogroups namely serogroups A, B, C, D, E, H, I, K, L, W, X, Y and Z [24-26]. Of the 13 serogroups,

six types, namely A, B, C, W, X, and Y, are responsible for the majority of invasive infections [27].

Based on differences in LOS structure, twelve immunotypes (L1 to L12) of meningococci can be distinguished [28] where L1 to L8 are common in serogroup B and C isolates and L9 to L12 more often associated with serogroup A.

Serotypes and serosubtypes are based on differences of the major outer membrane proteins PorB and PorA, respectively; *N. meningitidis* can be classified into 20 serotypes and 10 subserotypes [29, 30]. However, the phase and antigenic variation of surface antigens complicate the serological classification of meningococci.

N. meningitidis can also be classified by Multi Locus Sequence Typing (MLST), which is as a useful tool for epidemiological studies and population diversity studies. MLST is based on the DNA sequences of fragments of seven housekeeping genes (*abcZ*, *adk*, *aroE*, *fumC*, *gdh*, *pdhC*, *pgm*) allowing classification into sequence types (STs) [21, 31]. In this technique, small DNA fragments (433-501bp) from the seven housekeeping genes are amplified, sequenced and assigned with an allele number, the combination of the alleles defines an isolates sequence type (ST) [32]. Interestingly, this approach has demonstrated that most invasive meningococcal disease is caused by a limited number of genetically related strains, known as the "hyper-invasive lineages"[21, 33]. The MLST approach is increasingly being used using core genome sequences (cgMLST) to provide even greater resolution [34].

1.3.2. Epidemiology

Meningococcal meningitis remains a significant public health threat with 1.2 million cases and 170,000 deaths reported annually worldwide [35]. The

epidemiology of this organism is highly changeable through significant fluctuations in serogroup distribution and disease incidence. The reasons for the geographical serogroup variations are unknown but possible responsible factors are differences in environmental factors and the immunity of local populations. Meningococcal disease is mostly associated with six serogroups which are considerably diverse in their global distribution. In Europe and America, most cases of meningitis in modern times have been caused by serogroups B and C [36]. The main serogroup causing disease in the UK is serogroup B, and serogroup C was also common before the introducing of the MenC vaccine at the end of the last century. Nonetheless, cases of serogroup W disease in the UK have risen since 2009. Public Health England had shown that since 2008/9, when serogroup W accounted for only 1-2% of meningococcal cases, it has increased to cause 24% of cases in 2014/15 [37], However, MenW cases began to increase and exceeded 200 cases in 2015/16; the increase was due to a hypervirulent strain [38]. Despite 71% MenACWY vaccine coverage, the carriage of MenW increased substantially during 2015-2016 [39]. MenW disease has since slowed, however, and by August 2016, a 69% decrease was observed among English school leavers in 2015 (the first cohort to be immunised) compared to expected cases from pre- vaccination trends [40].

Serogroup A is the predominant serogroup responsible for meningococcal epidemics in the African meningitis belt [41]. It was also responsible for minor epidemics in China and Russia [22]. Serogroup W is not frequently encountered worldwide but was notable for a global epidemic following the 2000 Hajj pilgrimage [42]. Serogroups X and Y do not typically cause outbreaks, but

serogroup Y has emerged in the USA and Latin America, while serogroup X has been reported to cause small epidemics in parts of Africa [41, 43].

1.4. Clinical Manifestations

Meningococcal disease (MD) include bacteraemia with or without sepsis, sepsis with or without meningitis, meningococcal meningitis, meningococcal pneumonia, septic arthritis, pericarditis, myocarditis and endocarditis [44]. The most common clinical manifestations of MD are meningococcal meningitis and meningococcal sepsis that may co-exist. Initial symptoms of MD are usually non-specific and are very similar to self-limiting viral illnesses i.e. fever, nausea and loss of appetite, making recognizing the infection very challenging at the early stage [45]. Soon after, symptoms differ depending on whether the infection is in the bloodstream or the meninges; around 60% of patients develop meningococcal meningitis [22], and up to 20% progress to meningococcal sepsis, while others experience a combination of both clinical conditions [45].

The early symptoms of meningitis resemble upper respiratory infections. Headache, drowsiness, fever and neck stiffness are the usual presenting features. In severe bacterial meningitis, the patient may be exhausted and later there may be focal neurological signs. Meningococcal meningitis is associated with a purpuric rash in 70% of cases. Without septic shock, developing meningitis is the most typical clinical presentation of invasive meningococcal disease [22].

When meningitis is accompanied by sepsis it may present very rapidly with an abrupt onset of obtundation due to cerebral edema, probably as a result of endotoxin or cytokine release and it may also cause circulatory collapse

followed by septic shock. In meningococcal sepsis, non-blanching petechial hemorrhagic lesions are spread on the chest and extremities as a mirror image of the distributed intravascular coagulation [46, 47].

Chronic meningococemia is a rare condition in which patients can be unwell for weeks or even months with recurrent fever, sweating, joint pain and transient rash. Pivotal complications of meningococcal sepsis are shock, intravascular coagulation, renal failure, peripheral gangrene, arthritis and pericarditis [48] which can result in death or permanent disability [22, 49]. Other signs that a patient can experience include nausea, vomiting, photophobia and altered mental status. Additionally, inflammation and bleeding in small blood vessels, including those under the skin can result in a skin rash [50]. Non-specific symptoms including reduced feeding, irritability, a high-pitched cry and a bulging fontanelle are typical among infants and young children suffering from meningitis [46].

Early diagnosis and management, including rapid administration of antibiotics (such as ceftriaxone or penicillin), are essential for a full recovery. Otherwise, the mortality rate associated with meningococcal disease can be as high as 70–90%. Unfortunately, even with early management, around 25% of meningococcal disease survivors develop permanent sequelae [12].

1.5. Virulence factors

N. meningitidis develops several strategies to evade the human immune response and to survive inside the host. The major virulence factors are surface structures including capsule, lipooligosaccharide (LOS), pili, outer membrane protein (OMPs), adhesins, host-specific iron acquisition systems, surface-exposed and secreted virulence-associated proteins [36] (Figure 1.1). Many of

these virulence factors (such as capsule, pili, LOS, adhesins etc.) can undergo antigenic and phase variation whereby expression of the encoding genes is switched on or off enabling the bacterium to pre-adapt to its environment [51]. This can be accomplished by a variety of mechanisms including slipped strand mispairing [52] and insertion of mobile elements [51, 53].

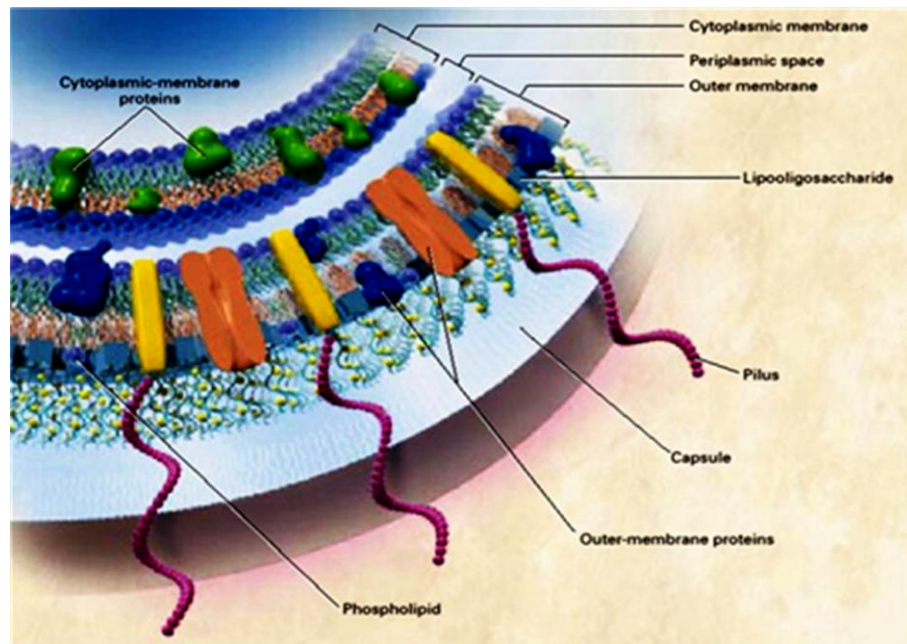


Figure 1.1: Cross sectional view of the meningococcal cell membrane.

The major virulence factors of *N. meningitidis* are depicted. Pili pass through the capsule and are the most protruding adhesins of encapsulated *N. meningitidis*. In addition, outer membrane (OM) adhesins are known to mediate interaction with specific host-cell receptors in appropriate phenotypes. Lipooligosaccharide (LOS) may interfere with the adhesion functions of OM proteins but can also contribute to cellular interactions by interacting with various cellular receptors. Adapted from: Rosenstein et al. [11].

1.5.1. Capsule

The capsule is one of the main virulence factors of *N. meningitidis*. This highly hydrated surface structure protects meningococci against environmental factors

as it extends meningococcal survival in aerosol droplets during transmission to a new host [54]. Once the bacteria are inside the host, the capsule provides defence against several host immune processes including phagocytosis, defensins, opsonisation and complement-mediated bacterial lysis [55, 56]. Encapsulation helps the bacteria to survive in the blood by its anti-phagocytic and anti-opsonic properties [57, 58]. High capsule expression can inhibit complement-mediated lysis by bactericidal antibodies [59]. However, capsule expression is also phase variable due to slipped-strand mispairing or through the reversible insertion of mobile elements [60]. In the carrier state, meningococci are often non-encapsulated, whereas the isolated invasive strains from patients are encapsulated [61].

The meningococcal capsule can hamper adhesion via some outer membrane adhesins; thus, the absence of capsule can promote meningococcal colonization of the nasopharynx [9, 62].

Molecular mechanisms involved in *N. meningitidis* capsule biosynthesis have also been identified, and genes involved in this process and in cell surface translocation are clustered at a single chromosomal locus termed *cps*. The biosynthesis and polymerization of capsular polysaccharide is mediated by genes clustered at the capsule biosynthesis locus [60]. The capsule biosynthesis genes termed as *css* followed by a letter representing the serogroup. Thus, sialic acid capsule biosynthesis genes are termed as *cssA-C* where *cs* refers to capsule synthesis and the final *s* indicates sialic acid [26].

Serogroups B, C, W and Y capsules are composed, wholly or partly, of sialic acid derivatives whereas serogroup A contains N-acetyl mannosamine residues [24, 25]. Sialic acid is a common component of human tissues. This molecular mimicry helps encapsulated bacteria to modulate the host immune

system [63] by bestowing the bacteria with anti-phagocytic properties which facilitate survival in the bloodstream or central nervous system [4].

1.5.2. Lipooligosaccharides

Meningococcal lipooligosaccharide (LOS) is similar to the LPS of some other Gram-negative bacteria, but lacks the repeating polysaccharide O-antigens [64]. Meningococcal LOS contains an oligosaccharide (OS) core which comprises with a distinct inner and outer core with a lipid A moiety. The inner core contains phosphorylated diheptose sugars (HepI and HepII) with a lipid that rooted in the outer membrane [4, 65]. The outer core is heterogeneous with the variable number of sugars [66]. This variation confers different antigenic features to the LOS, which used for meningococcal classification [67, 68]. In addition, meningococcal LOS is also prone to phase variation due to several mechanisms including Slipped -strand mispairing (SSM) of a poly-cytosine tract in the genes (e.g. *igtG*) involved in LOS biosynthesis [69]. This phase variation can allow for switching between immunotypes, which is proposed to play a significant role in meningococcal disease [70]. The biological activities and toxicity of meningococcal LOS are generally due to the lipid A portion [71]. During sepsis, the lipid A component of LOS has been shown to initiate the intense inflammatory response [72]. Meningococcal LOS also contains sialic acid, which makes the bacteria more resistant against antibody and complement systems and helps the bacteria to avoid phagocytosis [58]. The sialylated LOS mimics host-cell surface structures which can help the avoidance of the host antibody response [55, 73].

1.5.3. Adhesins

In the establishment of meningococcal infection, the first step is attachment of

N. meningitidis onto human upper respiratory mucosal surfaces where several structures, termed as major and minor adhesins, facilitate the meningococcal adherence.

1.5.3.1. Pili

Pili protrude from the bacterial surface beyond the capsule and have been recognized as major adhesins of meningococci [74]. The meningococcal pili belongs to the type IV pili (Tfp) family. Tfp consist of the major pilin PilE, and minor pilins (ComP, PilV, and PilX), which can be incorporated into the pilus and cause functional modulation [75]. Meningococcal pili are classified into two classes, designated class I and class II [6]. Several serological properties and structures are uniquely characterized in each class [76, 77]. Over 20 proteins are involved for a correctly assembled and functional Tfp [78]. Approximately 15 proteins (assigned PilC-X and ComP) are essential for the biosynthesis and various functional aspects of the meningococcal pili [79]. Pili are prone to phase and antigenic variation [80].

The type IV pili are involved in infection processes including adhesion to epithelial and endothelial cells, bacterial aggregation, twitching motility, inter bacterial interaction and transformation competence [79, 81]. The interactions between meningococcal adhesins and human nasopharyngeal cells, specifically non-ciliated columnar epithelial cells are mediated by the type IV Pili [82]. The role of pili as adhesins are well established where PilE and PilV are involved in adhesion to host cells. PilC1 also functions as an adhesin; however, the nature of the host cell receptor is still under investigation [20]. Johansson and colleagues proposed that CD46, a membrane-located human complement regulatory protein, is the receptor of meningococcal Tfp [83]. Although, another

study by Kirchner and colleagues showed that adherence of gonococci to urogenital mucosa could occur in a CD46-independent manner [84]. Recently, Bernard et al. have demonstrated that CD147, a member of an immunoglobulin (Ig) superfamily, can act as a receptor for PilE and PilV-mediated adhesion to brain and endothelial cells, and CD147 has also been implicated in meningococcal vascular colonization [85]. The function of PilX was also reported to be involved in bacterial aggregation and PilV for adhesion which can promote inter-bacterial interactions [86]. Imhaus et al. demonstrated that these two pilus components are localized in the periplasm, and play an indirect role by changing the number of Tfp per bacterium and in consequence regulating competence, aggregation and host-cell interaction [87]. Fussenegger reported that the type-4 pilus biogenesis process and transformation competence are functionally associated. PilE is involved in the uptake of DNA for transformation [88]. Merz et al. also demonstrated that Type IV pili (Tfp) are required for bacterial twitching motility where Tfp retract, produce substantial energy and facilitate cell movement [89]. Recently, it has been found that PilQ plays a role in adhesion to the host laminin receptor protein [90]. The host LAMR1, and galectin 3 binds the meningococcal PilQ, in addition to the major pilin PilE. LAMR1 and Gal-3 target common and specific meningococcal surface ligands and it has role during colonization by enhancing bacterial adhesion and cell invasion [91]. Recently it has been demonstrated that pili are involved in the activation of the β 2-adrenergic receptor (β 2-AR) which promotes endothelium signalling [92].

1.5.3.2. Opacity protein

Intimate adhesion is mediated by the opacity proteins, Opa and Opc, which share a similar molecular mass of ca. 30 kDa, and bind to carcinoembryonic

antigen cell adhesion molecule (CEACAM) receptors and extracellular matrix components, respectively [93]. CEACAMs may contain immunoreceptor tyrosine-based inhibitory motifs. Opa is expressed in *N. gonorrhoeae* and *N. meningitidis*; Opc is only expressed in *N. meningitidis* [94]. *N. meningitidis* produced opacity-associated (Opa) protein which can recognize multiple human cell receptors. Opa is an eight-stranded β -barrel structure with four surface-exposed loops. Structural variation occurs in three of these loops. Opc is produced by many, *N. meningitidis* strains but not all [95]. It has been shown to interact with fibronectin, vitronectin, and endothelial cell integrins [96-98]. The opaque appearance of meningococcal colonies is due to Opa protein expression, alongside type IV pili [20] which play an essential role mediating the adhesion and invasion of meningococci to the host epithelial, endothelial and phagocytic cells [99]. Similar to Opa, Opc has an β -barrel structure, but with five surface-exposed loops which mediate meningococcal-eukaryotic cell interactions and adherence, and is a target of bactericidal antibodies [77].

1.5.3.3. Porin A and Porin B:

The pore-forming proteins, PorA and PorB, play important roles in meningococcal pathogenesis and host interactions. In addition, porins act as adjuvants and stimulants of B-cells, which is mediated via TLR2 [100, 101]. Meningococcal PorA is an integral outer membrane porin that also plays fundamental roles in adhesion and invasion of host cells and complement binding [102]. It has also been shown to binding to the Laminin receptor (LR), a property that appears to play a role in the intimate contact with BBB cells [90]. PorA has a molecular mass of ca. 46kDa and is expressed in all meningococci strains [103, 104]. No homologue of PorA has not been found in *N. gonorrhoeae* [105]. PorB may target the mitochondrial outer membrane of

host epithelial cells, where it has been shown to exert anti-apoptotic activity on these cells [106] and also prompts the expression of the co-stimulatory molecule CD86 and of MHC class II, which are associated to the immune-potentialization of porin [106, 107]. However, Kozjak-Pavlovic et al. found that the integration of PorB into the mitochondrial membrane was associated with the sensitization of these cells to apoptosis [108].

1.5.3.4. HrpA-HrpB system

Haemagglutinin/hemolysin-related proteins are composed of the secreted effector protein HrpA and its cognate transporter HrpB [109]. It is the two-partner secretion system usually present in all *N. meningitidis* strains. They play a role in the adhesion of un-encapsulated bacteria to epithelial cell lines [109]. HrpA-HrpB have also been shown to be essential for the intracellular survival of *N. meningitidis* [109, 110].

1.5.3.5. Minor adhesins:

Several adhesins have been described as having essential roles in the pathogenesis of meningococcus and the process of adhesion. These proteins are surface-exposed on bacterial cells [111]. Some autotransporter proteins such as Neisseria hia homologue A (NhhA), Adhesion and penetration protein (App), Neisseria adhesion A (NadA), and Meningococcal serine protease A (MspA) may be retained on the bacterial cell surface and can act as minor adhesins [112]. These autotransporter proteins are described in more detail in section 1.9.

1.5.4. Iron-acquiring proteins

N. meningitidis possess host-specific iron acquisition mechanisms for survival and virulence [113]. In the meningococcus, iron acquisition is accomplished via expressing surface receptors that extract and import iron from different sources. Hemoglobin-binding outer membrane proteins (HmbR and HpuAB), transferrin-

binding proteins (TbpA and TbpB), together with lactoferrin-binding proteins (LbpA and LbpB), enable the meningococci to use hemoglobin, transferrin and lactoferrin, respectively, as sources of iron [114].

1.5.5. Factor H binding Protein

N. meningitidis expresses fHbp (factor H binding protein) which is a lipoprotein. It acts like the host factor H binding inhibitor proteins of the complement system by coating the bacterial surface with factor H protein. The protein is expressed on the surface of most strains [115]. FHbp is important for the survival of meningococci in the host. By producing fHbp (known as GNA 1870 [116] or LP2086 [115]), *N. meningitidis* can interact with human factor H (hfH) and can down regulate the host alternative complement systems, thus helping the bacteria to survive in the host bloodstream and tissues [117-119]. fHbp based vaccines can induce bactericidal antibodies capable of killing *N. meningitidis* [120]. fHbp is one of the antigenic components of the 4CMenB vaccine [121].

1.6. Meningococcal pathogenesis

In the establishment of the host carrier state, *N. meningitidis* adheres to the nasopharyngeal epithelial surface and eventually forms microcolonies that help the bacteria to exist as a commensal [122]. However, some strains of *N. meningitidis* are highly invasive and are habitually associated with disease [77]. Invasive infection usually takes place when the bacteria crosses the epithelial cells of nasopharynx and gain access to the blood-stream resulting in sepsis. When the bacterium crosses the blood-brain barrier (BBB), it leads to meningitis [123].

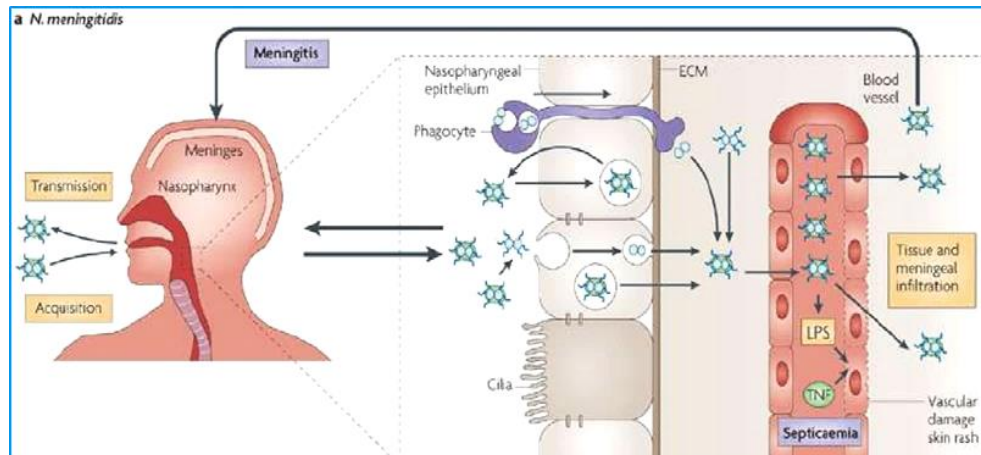


Figure 1.2: Stages of the pathogenesis of *N. meningitidis*. *Neisseria meningitidis* may be acquired via respiratory droplets. The organism establishes intimate contact with non-ciliated mucosal epithelial cells of the upper respiratory tract. Besides transcytosis, it can cross the epithelium either directly due to damage to the integrity of the monolayer or through phagocytes in a 'Trojan horse' manner. Once inside the bloodstream, *N. meningitidis* may proliferate throughout the body. Meningococci can pass across the blood brain barrier and enter the cerebrospinal fluid. Adapted from: Virji et al. [58].

Colonization of the human upper respiratory tract mucosa is the initial step for the establishment of a human carrier and invasive meningococcal illness [4]. About 1 to 10% of people carry *N. meningitidis* in their nose and throats without any clinical manifestation, even-though it can infect others by transmission. Meningococci can transmit from person-to-person via secretions and respiratory droplets which spread mostly as encapsulated bacteria, which are thought to be more resistant to desiccation [124]. The initial step of colonisation is adhesion to the epithelial cells of the nasopharynx, which is mediated by Type IV pili, that have also been implicated in different stages of the infective process [79].

Adhesion to the mucosal surface of the host is also essential for meningococcal survival. The presence of several adhesins in the meningococcus

and the specificity of binding to distinct receptors distributed over the surfaces of human cells demonstrates that the meningococcus can interact with different receptors or can mediate adhesion to different cell types at various sites [9]. The encapsulation of the bacteria can hamper adhesion, however, and phase variation of capsule expression may facilitate meningococcal transmissions from one site to another [125]. Meningococci can proliferate on non-ciliated epithelial cells, resulting in the formation of small microcolonies as well as cortical plaques on the apical surface. At this stage, an intimate association is established and it can trigger a series of specific signal events, which eventually result in the formation of pseudopodia that engulf the meningococcus [82]. After that, meningococci can pass through epithelium via phagocytic vacuoles as a result of endocytosis [126]. Binding of opacity proteins to the CEACAM protein and integrin receptor can stimulate endocytosis of *N. meningitidis* into the epithelial cells and facilitate the bacteria to cross the epithelium, from which it may gain access into the bloodstream [58]. In the bloodstream *N. meningitidis* can survive and proliferate with the help of virulence factors that the bacteria possess, some of which enable it to invade host defences [123]. The bacteria use different strategies to avoid the immune system such as complement system avoidance via fHbp expression. Survival in the bloodstream depends on encapsulation, which protects the bacteria from complement-mediated bacterial killing by hindering the insertion of the complement membrane attack complex; it also inhibits phagocytosis [127]. Likewise, shedding of outer membrane blebs which are rich in outer membrane proteins and bacterial endotoxin results in the diversion of antibodies and complement components away from the surfaces of intact bacteria [128]. Meningococcal intracellular survival is also influenced

by the expression of IgA1 protease that hampers phagosome maturation by degrading lysosome-associated membrane proteins (LAMP1) [129].

Only transient bacteraemia is expected when meningococci face an effective immune response. However, if the immune system is compromised, meningococcal sepsis can be established which is an acute meningococcal infection [20]. If *N. meningitidis* proliferates in the blood stream after evading defence mechanisms, it can cause sepsis, a deadly condition of the body. It happens when the LOS of *N. meningitidis* interacts with human cells resulting in the release of pro-inflammatory cytokines including interleukin 1 (IL-1), IL-6, and tumor necrosis factor (TNF) after its presence is detected via Toll-like receptors [130]. When the bacteria enter into the blood system, they can disseminate around the whole-body, including the brain. The brain is lined with endothelial cells that form a tight barrier between the blood and brain tissue. These cells are interconnected via tight junctions, and express a receptor called β -adrenergic receptor which promotes endothelial signalling, which leads to *N. meningitidis* translocation through the brain endothelium [92, 131]. Another host receptor, CD147, a member of the immunoglobulin superfamily (Ig), acts as a receptor for Tfp and facilitates adhesion of the bacteria to peripheral or human brain endothelial cells [85]. This leads to *N. meningitidis* accumulation on the endothelial surface. Protrusion of the apical side of the cell helps *N. meningitidis* to avoid being washed away by the bloodstream and can promote adhesion to and accumulation on the endothelial cells, create miscommunication in cell-to-cell contacts, and cause them to detach from each one-another. After passing the blood brain barrier, *N. meningitidis* first enters into the arachnoid space of the brain and starts uncontrolled multiplication. CSF is an ideal medium for bacterial uncontrolled growth because it provides nutrients, has few

phagocytic cells, and also has low levels of antibody and complement. Once the meningococci are in the CSF, bacterial components interact with host cells to initiate the production of cytokines including IL-6, IL-8, and TNF α , leading to a compartmentalized inflammatory response in the subarachnoid space [132]. The inflammatory response may be a precondition for bacterial invasion. Bacterial invasion and the inflammatory response progress in parallel and products of activated leukocytes can lead to permanent damage of the blood—brain and blood—CSF barrier [133]. LOS in particular, acting as an endotoxin causes blood clotting in the blood vessels of brain. In meningitis, neuronal damage is associated with a multi-factorial response including bacterial toxins, the cytotoxic products of immune competent cells and also secondary pathology to intracranial complications [133]. The most severe consequence is cerebral edema-increased intracranial pressure. It can cause decreased cerebral perfusion, hypoxia and neuronal necrosis [134].

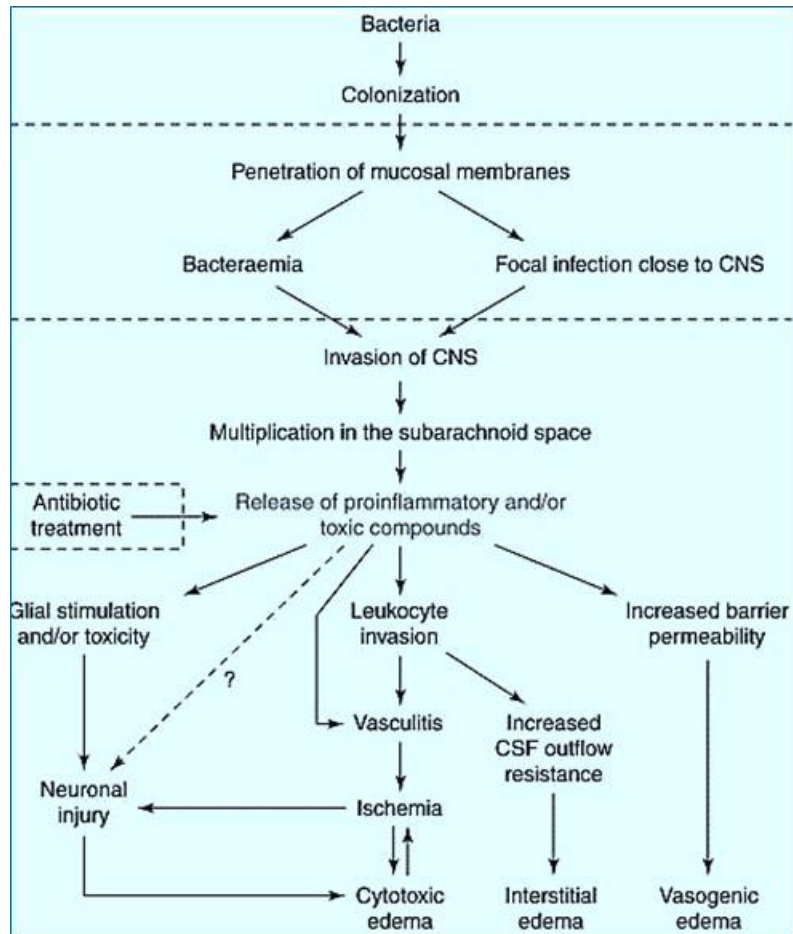


Figure 1.3: A schematic overview of the pathophysiology of meningitis. Following colonization of bacteria; under privileged condition the bacteria can enter into the blood and during bacteraemia it can invade into CNS. The bacteria multiply into the subarachnoid space and release proinflammatory response/toxic compounds. Then the bacteria stimulate macrophages, glial cells and cause leukocytes invasion which increased barrier permeability including blood-CSF and blood-brain barrier and also cause vasculitis. Adapted from: Nau et al. [135].

1.7. Meningococcal vaccines

Numerous attempts have been made to control meningococcal disease through the development and adoption of vaccines. Early meningococcal vaccines were

developed using capsular polysaccharides, which were first used about 40 years ago. Meningococcal purified plain polysaccharide vaccines have been used widely since the development of a highly immunogenic vaccine for serogroups A and C [136]. In the UK, MenC vaccine was included in the infant vaccination schedule from November 1990 and at the same time there was a catch-up campaign schedule targeting children up to 18 years of age. In Africa, the MenAfriVac campaign was used in an attempt to minimize the serogroup A epidemics in Africa. However, plain polysaccharide vaccines are poorly immunogenic in children below two years old [137] and also provide only short-term protection (3-5 years) [138]. Additionally, these vaccines cannot be boosted because repeated doses usually results in hyporesponsiveness [139]. To overcome the disadvantages of plain polysaccharide vaccines, conjugated vaccines were developed.

Conjugate vaccines contain the capsular polysaccharide of one or more serogroups conjugated to a carrier protein, which enhances the protective response for longer-lasting protection, and can be boosted without inducing hyporesponsiveness [140]. For serogroups A, C, W, and Y, conjugate vaccines have been shown to be very effective in preventing disease in all age groups. From August 2015, the Quadrivalent MenACWY vaccines replaced the MenC vaccine in the UK for 13-14 years-olds and new university entrants up to 25 years of age from August 2015. The catch-up vaccination programme has also been offered during 2015-17 to those who were aged 14-18 years in 2015 [37]. MenACWY vaccine has been given routinely to teenagers at around 14 to 18 years old in the UK.

Until recently, the development of a universal vaccine against serogroup B has been challenging. Serogroup B capsular polysaccharide is poorly

immunogenic and identical to the polysialic acid present in many human glycoproteins; additionally, antibodies generated against these targets may result in autoimmunity [141, 142] making serogroup B polysaccharide unsuitable to use as a vaccine antigen [143]. An approach to resolving this challenge was to focus on other surface-exposed virulence factors such as lipooligosaccharide or outer membrane proteins, either in purified or recombinant forms or in outer membrane vesicles. The first protein-based MenB vaccine contained outer membrane vesicles (OMVs) and showed discouraging results, particularly in children below four years [44, 144]. In particular, protection was only conferred against strains expressing homologous antigens due to the extensive antigenic diversity exhibited by meningococci and their major immunogenic antigens (such as PorA) [145].

Antigenic diversity of meningococcal surface proteins is the main problem when designing broadly protective meningococcal vaccines. Two different approaches have addressed the challenge of the antigen diversity: one based on multiple antigens identified by 'reverse vaccinology', which resulted in the development of the 4CMenB vaccine (Bexsero®) licensed so far in Europe, Australia, Canada and Chile [9, 121, 146] the other based on the combination of two variants of the surface antigen factor H-binding protein (fHbp), which has recently been licenced in the United States (Trumenba®) [147]. Since September 2015, the 4CMenB vaccine has been introduced into the childhood immunization schedule in the UK. This NHS immunisation scheme covers babies only; other risk groups, including toddlers and teenagers, are not currently entitled to the vaccine on the NHS. The multivalent vaccine contains recombinant group B Neisserial adhesion protein (NadA), fHbp, Neisseria heparin-binding antigen (Nhba), and outer membrane vesicles (OMV) from *N.*

meningitidis group B strain NZ98/254. Using different strategies, Pfizer have developed and licensed the vaccine (Trumenba) based on two variants of factor H-binding protein [148]. Successful implementation of an anti-serogroup B vaccine will help change the epidemiology and disease burden in countries where serogroup B disease remains a significant problem.

1.8. The autotransporter secretion pathway

Gram-negative bacteria possess at least six well-defined secretion systems for transporting secreted proteins across the cell envelope to the extracellular milieu [149]. These are designated type I to type VI [150]. These types of pathways are grouped into the Sec-dependent and Sec independent pathways [151].

In the Sec dependent systems, the Sec machinery is involved in the secretion of the proteins across the inner membrane [151]. Sec-independent systems are one-step systems where no periplasmic intermediate is involved. The twin arginine (Tat) pathway is an alternative pathway to the Sec pathway across the inner membrane [152]. In *N. meningitidis* four secretory pathways are active namely the autotransporter pathway (T5aSS), the two-partner secretion pathway (T5bSS), the trimeric pathway T5cSS (collectively known as T5SS) and the type one secretion pathway (T1SS) [153, 154]. Recently, another mechanism has been discovered which is the Slam-dependent pathway for cell-surface exposure of lipoproteins [155].

Autotransporter proteins are secreted via the Type V secretory system [156]. It is a transport system where a single polypeptide was originally thought to facilitate its own translocation across the outer membrane [112] and is

arguably the most widely used transportation system in Gram-negative bacteria [156, 157]. The classic autotransporter proteins have three distinct domains: an N-terminally located signal peptide (leader) sequence which mediates inner membrane translocation via the Sec (general secretion system) system, a C-terminal β -domain that is required to translocate the central passenger domain across the outer membrane, and the central function-determining passenger domain which is translocated to the extracellular environment [158-160].

The word autotransporter was coined because previously it was assumed that all the classical monomeric autotransporters contained all information for the translocation process without requiring any accessory factors or energy [161]; the C-terminal domain was thought to form a transmembrane pore through which the passenger domain could translocate to the bacterial cell surface [162, 163]. However, the β -barrel pore is too narrow to allow transport of the corresponding passenger domain in the partially folded state and several studies have shown that expression of the outer membrane protein assembly factor is a prerequisite for passenger domain secretion [5]. Initially, the signal sequence of autotransporters directs the protein transportation across the inner membrane via the Sec machinery, which is followed by cleavage of the peptide by a signal peptidase [162]. Then, certain accessory factors including periplasmic chaperones such as Skp, SurA, DegP are used to escort the secreted protein across the outer membrane [164-166]. Although *N. meningitidis* lacks DegP, the bacterium encodes the closely related homologue DegQ, which can functionally replace the former [167]. In the translocation process of the secreted protein from the inner membrane to OM, the β barrel assembly machinery (Bam) complex is required for folding and insertion of the β -barrel domain into the outer membrane, and to allow the passenger domain to be

translocated to the cell surface (Figure 1.4) [168, 169]. The Bam complex in *E. coli* is composed of the outer membrane β -barrel protein BamA (formerly known as YaeT in *E. coli* or Omp85 in *N. meningitidis*) and four associated lipoproteins that are exposed to the periplasm (BamB, BamC, BamD, and BamE) [170]. It was hypothesized that the β -domain of autotransporter and the β -barrel domain of BAM complex make a hybrid form which is wide enough to allow passenger domain translocation [171]. The study of Dorbnak et al. demonstrated that protein folding at the cell surface likely provides the energy to drive translocation [172]. After OM translocation, the passenger domain may remain associated with the β -domain or alternatively it may be cleaved but remain loosely attached to the bacterial cell surface, or it may be completely detached from the bacterial cell surface and released into the extracellular milieu. Depending on the individual autotransporter the cleavage may be due to autoproteolytic activity or due to the action of other proteases bound to the bacterial outer membrane. This latter scenario is encountered with IgA1 protease and other secreted serine proteases [112, 157, 173, 174].

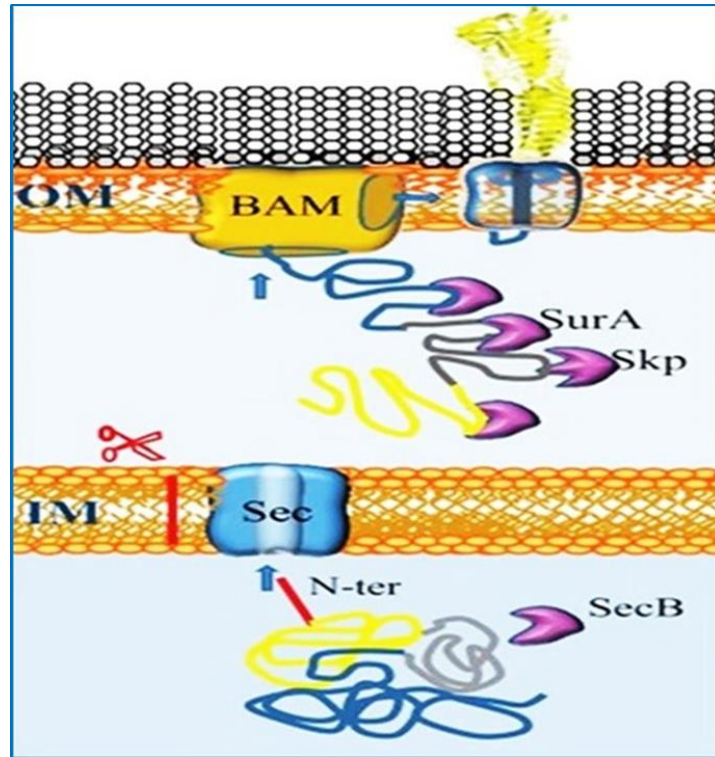


Figure 1.4: Autotransporter secretion system. They are synthesized with a cleavable N-terminal signal sequence (red) for translocation across the inner membrane (IM) via the Sec apparatus. After periplasmic transit, escorted by chaperones like Skp and SurA, the C-terminal β -domain (blue) is integrated as a β -barrel into the OM by the BAM complex. Presumably, during this integration, the passenger domain is transported to the cell surface [175]. A segment that connects the passenger with the β -domain (grey) forms an α -helix that plugs the channel within the barrel. Adopted from: Tommassen et al. [5].

Autotransporters can be categorised into four categories based on the size of translocator domain and its position relative to the passenger domain: classical autotransporters (T5aSS); two-partner autotransporters (T5bSS); trimeric autotransporters (T5cSS); fused two-partner autotransporters (T5dSS) and inverted autotransporters (T5eSS) [157].

T5cSS is the trimeric autotransporter secretion system. Like the classical ATs, trimeric ATs consist of a passenger domain and a C-terminal translocator

domain. However, the translocator domain is much shorter. The proteins assemble into the outer membrane as trimers, where each protomer contributes four β -strands to form a single 12-stranded β -barrel [149]. In contrast to many classical ATs, none of the trimeric ATs that have been studied so far are cleaved from the cell surface and released into the extracellular milieu. The trimeric autotransporters typically act as adhesins where they can mediate bacterial adherence to eukaryotic cells or extracellular matrix proteins or can promote bacterial biofilm formation [157]. In some cases, they can also bind circulating host factors, such as immunoglobulins or complement components [176, 177]. So, this secretion pathway may have evolved to enable high-affinity multivalent interaction with host molecules [178]. It is exemplified by members of the Oligomeric Coiled-coil Adhesins (Oca) family [179].

1.9. Autotransporter proteins in *N. meningitidis*

Eight autotransporter proteins have been identified in meningococci, namely IgA1 protease, NhhA, NadA, adhesion and penetration protein (App), meningococcal serine protease A (MspA); AutA, AutB, and NalP (AspA). The majority of these proteins have been studied in depth by our research group [178, 180-184]. Two have close homologues in *N. gonorrhoeae*, namely App and IgA protease [58]. NhhA and NadA belong to the Oca family [154].

In *N. meningitidis*, the classical autotransporters (type Va) is one of the important class and it is the largest subgroup of autotransporters. Many classical ATs contain a serine protease domain. Many of them have been shown to play roles as virulence factors. Among of them, IgA1 protease is perhaps the best-characterised virulence factor involved in meningococcal pathogenesis. Several additional autotransporter proteins including Neisseria hia homolog A (NhhA),

Adhesion and penetration protein (App), Neisseria adhesion A (NadA) and Meningococcal serine protease A (MspA), are also associated with host-pathogen interactions. Some act as adhesins, but may also have additional virulence-associated activities [185]. In general, autotransporter proteins contribute to virulence and play important roles including adhesion to cell surfaces, proteolytic degradation of host molecules, iron acquisition, cytotoxicity, immune evasion and serum resistance [162]

Three of the meningococcal autotransporters: IgA1protease; App and MspA, harbor S6-peptidase domains within their respective passenger domains. Such autotransporter peptidases are associated with adherence or cleavage of extracellular or intracellular host proteins resulting in toxicity and modulation of host response [159, 186]. NalP is a lipoprotein which harbors a S8-peptidase domain, AutA and AutB are surface exposed, and NhhA & NadA are two trimeric autotransporter proteins.

1.9.1. IgA protease

IgA1 protease is a serine protease which has a chemotrypsin-like fold. The passenger domain of IgA1-protease contains two subdomains: a protease domain and a peptide domain both of which are connected by a γ -peptide [187]. The passenger domain is connected with the β -domain via a linker peptide. The protease domain is released into the milieu via autoproteolytic cleavage at sites located between the protease domain and γ -peptide/ between γ -peptide and α -peptide/ between the α -peptide and the linker peptide but the processing sites depend on the strains (Figure 1.5) [188]. Alternatively, the whole passenger domain with linker peptide can be released by NalP-mediated cleavage, expression of which is prone to phase variation due to single strand mispairing

[183, 188, 189]. van Ulsen and his colleagues reported that in *N. meningitidis*, two different variants of IgA protease were involved in two different and mutually competing proteolytic events mediating the release of passenger domain [183].

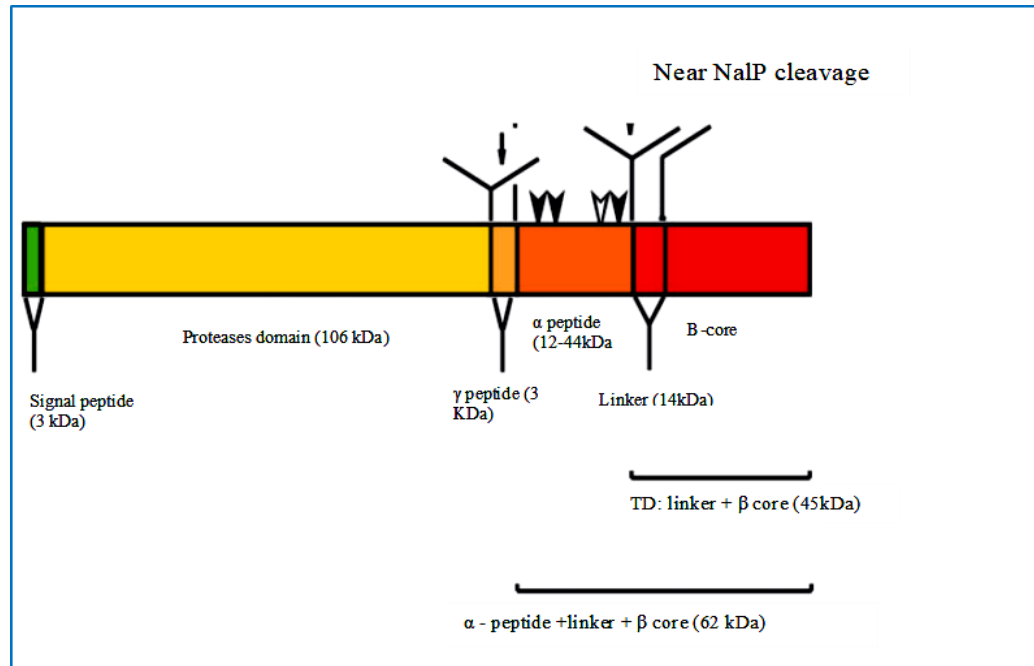


Figure 1.5: Schematic diagram showing the various domains of IgA1 protease with possible autocatalytic position sites and approximate NaIP cleavage site. NaIP-mediated IgA protease fragment contains the protease domain and α-peptide domain. Arrowheads indicate Nuclear localization signals (NLS) position and the open arrow heads show NLS position in α-peptide. Adapted from: Roussel et al. [188].

Furthermore, IgA1 protease appears to degrade IgA1 by cleavage at a site located in the region between Fab and Fac domains [190], releasing inactive monomeric Fab fragments [191], that can block the interaction of IgG and IgM [192]. Cleavage of IgA1 may also inhibit IgA-mediated agglutination and consequent clearance of the bacteria in the nasopharynx [5]. IgA1 protease has

no activity against IgA2. IgA1 protease can also cleave lysosome-associated membrane protein LAMP. LAMP1 contains an IgA1-like hinge region with potential cleavage sites for the neisserial type 1 and type 2 IgA1 proteases. LAMP1 degradation prevents acidification of the bacterium-containing endosome and thus promotes bacterial intracellular survival in the epithelial cells *in vitro* [193] and transcytosis across the polarized epithelial monolayers [129].

The α -peptide of IgA1 contains nuclear-targeting signals (NLS) that are rich in arginine residues, and which facilitate trafficking of IgA1 protease to the nucleus of eukaryotic cells [183, 187]. When IgA1 protease is released from the bacterial cell surface via NalP-mediated cleavage the released passenger domain contains an α -peptide, which targets the nucleus following uptake by eukaryotic cells. Besbes and colleagues showed that meningococcal IgA1 protease carrying an α -peptide moiety and harboring a nuclear localisation signal (NLS), allowed efficient intra-nuclear transport and when the NLS was absent in the α -peptide there was no nuclear transportation [194]. Jose et al. and colleagues also described different variants of IgA1 protease regarding the number of NLSs and sequence variability [195]. In absence of NalP, IgA protease-containing α -peptide remains covalently attached to the translocator domain at the cell surface and the protease domain without the α -peptide can be released by the autocatalytic processing [183]. Due to the absence of NalP expression, the α -peptide that is attached at the bacterial surface can stimulate biofilm formation by binding polyanions like environmental DNA(e-DNA) [196]. The α -peptide also binds heparin and may mediate serum resistance and adhesion [188]. Nuclear-localized IgA1 protease can cleave the transcription activator NF- κ B, and thus prevent immune activation [188, 194]. It is predicted that α -peptide associated IgA1 proteases may bind with DNA dependent NF- κ B

responsive promoters [194]. The NF- κ B protein family of closely related transcription factors play important roles in gene expression of proteins with roles in the immune response. It was reported that α -peptide containing IgA1 protease is transported to the nucleus of infected cells where it cleaves the p65/RelA component of NF- κ B complex and the expression of NF- κ B regulated genes was altered [194].

1.9.2. NaIP

NaIP (Neisseria autotransporter lipoprotein) has a S8 family (subtilisin-like) protease domain [183]. The gene is common to most, but not all, meningococcal strains [197]. The expression of NaIP is phase-variable due to slipped strand mispairing which determines the length of a poly-cytosine tract in the coding region [183, 197]. A study by our group demonstrated that *nalP* was phase ON in approximately half of serogroup B strains tested and no significant differences were noticed between carriage and invasive strains [197]. The passenger domain of NaIP is released from the bacterial surface by autoproteolytic processing. However, after cleavage between the passenger domain and the β -domain, the passenger domain remains temporarily attached at the outer membrane of cell surface by an N-terminal lipid moiety anchor [189]. In this location, it can cleave other surface-exposed proteins including several autotransporters (IgA1, MspA, App, and NHBA) and lipoproteins (LbpB) [181, 183]. The release of these proteins has significant consequences on meningococcal pathogenesis. NaIP-mediated IgA protease and App can both stimulate apoptosis [153]. Another important target is NHBA, which is responsible for heparin binding [198]. NaIP-mediated cleavage can release the C-terminal part of NHBA that can in turn bind environmental DNA (e-DNA),

which is nuclear or mitochondrial DNA, and result in inefficient biofilm formation [196]. Conversely, in the absence of NalP expression, the α -peptide of IgA protease and NHBA are retained on the cell surface, which facilitates colonization and biofilm formation. NalP expression may abrogate dispersal of biofilms and invasion or spreading to a new host [5].

Once released, NalP can be internalized by host cells and its proteolytic activity can increase host cell metabolic activity [184]. NalP can also cleave the complement factor C3, thus contributing to the ability of meningococci to survive in host serum by avoiding complement activation [198, 199].

1.9.3. AutA and AutB

AutA and AutB are surface-exposed classical small autotransporters. The *autA* gene is distributed among all the *Neisseria* sps. whereas *autB* is restricted to the two pathogenic *Neisseria* sp.: *N. meningitidis* and *N. gonorrhoea*. The expression of *autA* and *autB* is prone to phase variation due to slipped strand mispairing of AAGC nucleotides repeated downstream of the start codon [200]. The *autB* gene is phase off in the majority of meningococcal genomes containing an intact *autA* gene [201]. The two proteins, AutA and AutB, do not release their passenger domains into the milieu. Instead there are exposed at the bacterial cell surface covalently attached to the β -domain [200, 201]. AutA expression can induce bacterial autoaggregation and biofilm formation [200]. Autoaggregation is mediated by the interaction of AutA proteins on neighbouring cells. AutA can also bind DNA, which acts as an adhesin between cells [5]. In addition, it is associated with resistance to host immune defences such as phagocytosis [202]. AutA was also reported to be a potent CD4⁺T-cell and B-

cell stimulating antigen [178]. AutB expression can also enhance biofilm formation indicating that AutB also has a role in colonization [201].

1.9.4. NadA and NhhA

NadA and NhhA are trimeric autotransporters which function as virulence factors. NhhA has homology to the Hia and Haf adhesin of non-typeable *H. influenza* [203]. The *nhhA* gene is ubiquitously present in meningococci [204]. NhhA protein expression is required for efficient colonization since it binds to extracellular matrix proteins, heparin sulfate and laminin. NhhA protects against complement activation by binding with activated complement regulatory protein vitronectin and thus conveys serum resistance by inhibiting membrane attack complex formation [205]. It was reported that NhhA can also induce apoptosis of macrophages [206]. This research study also reported that an *nhhA* mutant was less virulent after intraperitoneal injection of mice [206]. In addition, it was also reported that NhhA functions as an immune modulatory agent [100]. It was found that NhhA induced the differentiation of monocytes into macrophages whereas the differentiation of monocytes into dendritic cells that produce an anti-inflammatory response was blocked. This response prevents dissemination and help to sustain asymptomatic colonization by *N. meningitidis* [100].

Neisserial adhesion A (NadA) is also a surface-exposed trimeric autotransporter protein, and a component of the 4CMenB vaccine. The protein has similarity with the virulence factor YadA of *Yersinia enterocolitica* [153]. *Neisseria* NadA has been implicated in host adhesion and invasion. The *nadA* gene is present in 30% of *N. meningitidis* with a lower prevalence carrier state [207, 208]. In saliva, secreted 4-hydroxyphenylacetic acid acts as an inducer of NadA expression suggesting an important role for NadA in mucosal colonization

[209]. NadA has also been shown to promote the bacterial invasion of the host cells [210]. By producing of NadA in *E. coli* it has been shown to increase adherence to activated human monocytes and macrophages and purified NadA induced TNF- α and IL-8 production by these cells [211]. NadA is considered to be a good vaccine candidate because it is a surface exposed molecule which plays a role in adhesion, and can induce high level of bactericidal antibodies [212].

1.9.5.App and MspA

App and MspA are chemotrypsin-like serine proteases which have homology with IgA protease [182, 213]. Both proteins belong to the S6-peptidase family based upon common ancestry and shared features including the nature, order and relative positions of catalytic residues. The following table summarizes the main structural aspects of App and MspA (Table 1.1).

Table 1.1: The main features of App and MspA proteins in *N. meningitidis* strain MC58.

Features	App	MspA
Accession number	NP_274977.1	NP_274990.1
Sequence identity	Hap (56%) IgA1 protease (39%)	IgA1 protease (36%) App (33%)
Molecular Weight (kDa)	159.966 (full-length protein) 124.633 (passenger domain)	157.645 (full-length protein) 123.996 (passenger domain)
Full-length autotransporter	1457a.a	1431a.a
Signal peptide	42 (M ¹ -A ⁴²)	26 (M ¹ -S ²⁶)
Passenger domain	1137 (G ⁴³ -N ¹¹⁷⁹)	1126 (S ²⁷ -A ¹¹⁵²)
β-domain	262 (Q ¹¹⁹⁶ -W ¹⁴⁵⁷)	248 (D ¹¹⁷⁹ -K ¹⁴²⁶)
Catalytic triad	H ¹¹⁵ , D ¹⁵⁸ , S ²⁶⁷	H ¹⁰⁰ , D ¹³⁵ , S ²⁴¹
Proteolytic processing	autocleavage/NaIP mediated	autocleavage/NaIP mediated
Putative autocleavage site(s)	956F↓NTL ⁹⁵⁹ 1178A↓NSG ¹¹⁸¹	870F↓NTL ⁸⁷³
Predicted NLS	(⁹³³ RRRSRRSR ⁹⁴⁰)	Not Identified

The table summarises and compares the main structural features of App and MspA proteins of *N. meningitidis* serogroup B strain MC58. The number above the amino acids sequence refer to amino acid position in the full-length proteins

prior to signal peptide cleavage. The table is adapted from the thesis of Dr. Kharilla.

App expression is common for all meningococcal strains [180] whereas the *mspA* gene is absent or disrupted in some strains, and its expression is prone to phase variation [197].

App and MspA are both immunogens. App can be expressed during meningococcal infection and carriage, and can induce antibody responses [180]. Similarly, expression of MspA in the host has been shown to induce bactericidal antibody responses [182].

App and MspA may remain anchored to the cell surface, where they mediate adhesion to human epithelial and endothelial cells. Both proteins were shown to facilitate adhesion to human brain microvascular endothelial cells (HBMEC), dendritic cells (DCs) and red blood cells [182, 214, 215]. App is required as an adhesin for optimal meningococcal adhesion to host epithelial cells [214].

App and MspA can be released from the bacterial cell surface by autoproteolytic cleavage. However, as with IgA protease, two different secretion forms due to the different proteolytic cleavage events are also common for App and MspA [183]. In the case of NaIP-mediated cleavage, both proteins are released from the cell surface in a larger form with a C-terminal extension named the α -peptide (Figure 1.6). The α -peptide of App is proposed to contain a putative nuclear localization signal (which is two arginine rich segments similar to the NLS of the α -peptide of IgA protease). This type of NLS is not found within the α -peptide of MspA and MspA has not been shown to play any role in biofilm formation [196].

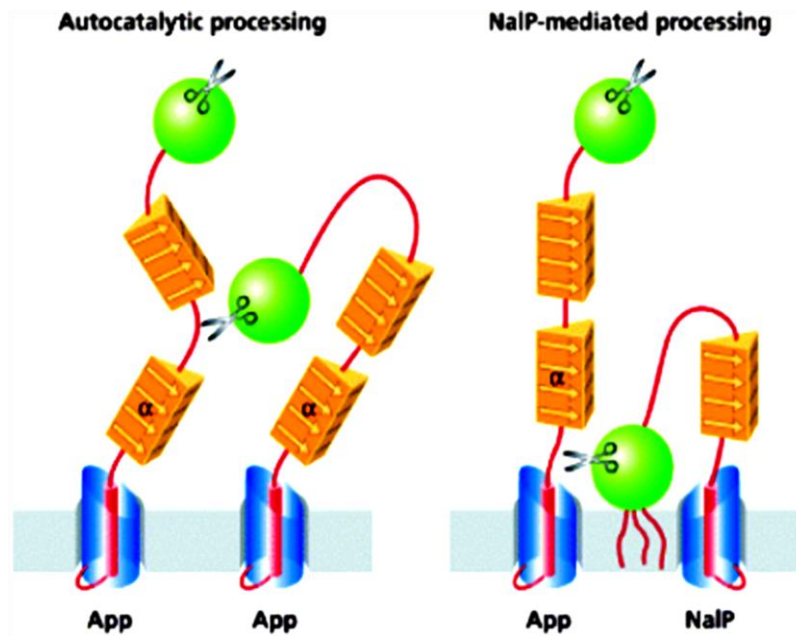


Figure 1.6: Models of autocatalytic processing and NalP-mediated proteolytic processing of App at the meningococcal surface. Here, 'α' indicates the α-peptide of App and the protease domain is shown in green. The passenger domain without α peptide is autocatalytically released at the bacterial cell surface, but NalP-mediated proteolytic processing releases the passenger domain of App containing the α-peptide. The figure shows a model in which one App molecule acts on another molecule and it is also possible that an intra-molecular cleavage event is responsible for the observed processing [153].

In the absence of NalP expression, the α peptide of passenger domain of App remains associated with cell surface and it could contribute to biofilm formation [216]. In *E. coli* App and MspA expression mediated adhesion to Chang epithelial cells and App also mediated adhesion of meningococci to the same epithelial cells [214]. It is interesting that encapsulation did not interfere in the adhesion function indicating that these large proteins can extend beyond the capsule.

App can also mediate inter-bacterial interaction by bacterial aggregation on cell layers by binding the NLS to e-DNA [214].

A recent study by our research group demonstrated that recombinant

App and MspA passenger domains (akin to the NalP-released fragments) could be taken up by dendritic cells. Cross-linking experiments identified the mannose receptor (MR) and transferrin receptor as App- and MspA-ligands which were involved in the uptake process [215]. Mannose receptor is a member of the calcium dependent lectin receptor superfamily that plays a role in innate immune response and mediates endocytosis [175, 217]. The transferrin receptor is a transmembrane homo-dimeric glycoprotein and is required for internalization of iron-loaded transferrin through endosome [218]. Following uptake, the internalised App and MspA trafficked to the cell nucleus, and exposure to App and MspA triggered apoptosis. Cross-linking also indicated that App and MspA bound to histone proteins, and cleavage of recombinant histone H3 by App and MspA was demonstrated, a potential mechanism by which apoptosis is induced in these cells [215]. Significantly, a transgenic mouse model of meningococcal infection was used to demonstrate the involvement of App and MspA in meningococcal pathogenesis [215].

1.10. Aim of the study

App and MspA are secreted virulence proteins with structural similarities to IgA1 protease. However, further knowledge of their respective roles in pathogenesis is required. We hypothesized that, due to the large size of the internalized App and MspA fragments, nuclear localization of App and MspA was NLS-dependent. This study also aims to more fully assess the interactions of App and MspA with human core histone proteins in terms of specificity and the role of PTMs in modulating activity.

CHAPTER 2: Materials and Methods

2.1. Bacterial strains and growth conditions

In this study, *Escherichia coli* strain JM109 (Promega) was used for the routine propagation of plasmids. For protein expression, *E. coli* BL21-Gold (DE3) was used. Bacteria harbouring plasmids were cultured on LB agar plates containing the appropriate antibiotics: 100 µg ml⁻¹ Ampicillin or 50 µg ml⁻¹ Kanamycin. The plates were incubated at 37°C; broth cultures were incubated at the same temperature in a shaking incubator while being aerated by shaking at 200rpm.

2.2. List of the plasmids used in the study

Table 2.1 Description of plasmids used in this study.

Plasmid	Description	Source or Reference
pColdTF-App	Expression vector encoding 6 × histidine-tagged ⁴³ G - ¹¹⁷⁹ N of MC58 App fused to trigger factor	Dr. Ahmed Khairalla
pColdTF-App ^{S267A}	Catalytic serine (²⁶⁷ S) residue of App substituted with an alanine residue	Dr. Hibah Albasri
pColdTF-MspA	Expression vector encoding 6 × histidine-tagged ²⁷ S - ¹¹⁵² A of MC58 MspA fused to trigger factor	Dr. Ahmed Khairalla
pColdTF-MspA ^{S241A}	Catalytic serine (²⁴¹ S) residue of MspA substituted with an alanine residue	Dr. Hibah Albasri
pColdTF-MspA ^{D135E}	Catalytic aspartic acid (¹³⁵ D) residue of MspA substituted with glutamate.	This study
pColdTF-MspA ^{D135ES241A}	Catalytic aspartic acid (¹³⁵ D) and serine (²⁴¹ S) residues of MspA	This study

	substituted with glutamate and alanine residues, respectively	
pDsRed monmer-C1	DsRed expression vector	Clontech
pDsRedApp	MC58 App passenger domain (⁴³ G - ¹¹⁷⁸ N) in pDsRed monomer-C1	Dr. Osman A. Dufailu
pDsRedMspA	MC58 MspA passenger domain (²⁷ S - ¹¹⁵² A) in pDsRed monomer-C1	Dr. Osman A. Dufailu
pDsRedVirD2	<i>virD2</i> of <i>Agrobacterium tumifaciens</i> in pDsRed monomer-C1	Dr. Rob Delahay
pDsRedIga1Protease	MC58 <i>igaA1</i> in pDsRed monomer-C1	Dr. Osman A. Dufailu
pDsRedApp ^{S267A}	Catalytic serine residue (²⁶⁷ S) of App substituted with an alanine residue	This study
pDsRedMspA ^{S241A}	Catalytic serine residue (²⁴¹ S) of MspA substituted with an alanine residue	This study
pDsRedApp ^{Δ901G-980Y}	Residues ⁹⁰¹ G to ⁹⁸⁰ Y deleted from App	This study
pDsRedAppDel ^{Δ901G-965L}	Residues ⁹⁰¹ G to ⁹⁶⁵ L deleted from App	This study
pDsRedAppNLS ^{S936AS939A}	Serine residues at amino acid sites 936 and 939 of App NLS substituted with alanine residues	This study
pDsRedMspADel ^{Δ1037Q-1136I}	Residues ¹⁰³⁷ Q to ¹¹³⁷ I deleted from MspA	This study
pDsRedMspADel ^{Δ999D-1073A}	Residues ⁹⁹⁹ D to ¹⁰⁷³ A deleted from MspA	This study

2.3. Extraction, purification and quantification of DNA

Plasmid DNA was extracted from bacterial cells using the GenElute plasmid miniprep kit (Sigma Aldrich-UK) by following the manufacturer's instructions.

The GenElute PCR clean up kit (Sigma Aldrich-UK) was used to clean up both PCR products and products of restriction digestion.

The Gel Extraction kit (Sigma Aldrich-UK) was used for the purification of DNA fragments from agarose gels. Bands of interest were first confirmed with minimal UV exposure.

The manufacturer's instructions were followed in each case.

The concentration and the purity of DNA were confirmed using a NanoDrop ND-1000 Spectrophotometer (Thermo Scientific) at 260/280nm wavelength. DNA preparations were generally accepted as pure when the 260/280 absorbance ratios were in the range of 1.8-2.0.

2.4. Polymerase Chain Reaction (PCR)

PCR was performed using Q5 High Fidelity DNA polymerase and/or Phusion High Fidelity DNA polymerase with selected primer pairs. All primers were purchased from Sigma and are listed in Table 2.2. PCR reactions were undertaken according to the manufacturer's recommendation. Briefly, a master mix was used, containing 1µl DNA template, each of the respective primers (Table 2.2) to a final concentration of 0.5 µM, 60 µl 5 × Q5 reaction buffer, final concentration of dNTPs 0.2 mM, 3 µl High Fidelity DNA polymerase and added water to make final volume 300 µl. 50 µl aliquots of the master mix were dispensed into six reaction in PCR tubes.

Inverse PCR was performed using Phusion High Fidelity DNA polymerase with respective primers (Table 2.2) which incorporated with SpeI restriction enzyme to delete the targeting region and the reaction was done with following the manufacturer's instructions. The final concentrations of the constituents of the reaction mixture were as followed : 0.5 μ M primer, 1 \times Q5 reaction buffer, final concentration of dNTPs 0.2 mM and DNA concentration <250ng. The PCR was performed under the different thermo-cycling conditions as follows.

For Q5 High Fidelity DNA polymerase, the PCR conditions were initial template denaturation step at 98°C for 30 s, denaturation at 98°C for 10 s, annealing for 30 s, and extension at 72°C and time used based on the amplicon size, usually 30 s/kb and followed by 30 cycles of incubation. The annealing temperature were differed depending on the primer pair (Appendix). The final extension was done at 72°C for 5 min.

For Phusion High Fidelity DNA polymerase, the PCR conditions were as follows: initial template denaturation step at 98°C for 5 min; denaturation at 98°C for 30 s; annealing at indicated temperature based on the primer pair (Appendix) for 30 s then extension at 72°C for 30s/kb repeated for 30 cycles and followed by a final extension at 72°C for 10 min.

Then the PCR product was cleaned up with Gene elute-PCR clean up kit (Sigma-Aldrich) and then quantified with NanoDrop ND-1000 Spectrophotometer (Thermo Scientific).

Table 2.2 Primers for sequencing and PCR

Primer	Primer sequence(5' to 3')	Purpose
AppDsRedF1	GGCT GGTACC GGACACACTTATTTCCGGCATC	DNA sequencing
AppDsRedR1	GCGT GGATCC GGCATAACGGCTGATCAGGTC G	
MspADsRedF1	GGCT GGTACC TCCATTGTCCGCAACGATGTCTG	DNA sequencing
MspADsRedR1	GCGT GGATCC CCGACCGGCTGATCAGTTCTG	
DsredMono C	AGCTGGACATCACCAACCACAGCCG	DNA sequencing
AppdelRed-AmpF1	CCCAAACGGCAACCTTAGCCTCGTGGGCAAT GC	Confirming Amplicon expected size
AppdelRed-AmpR1	GCAATCAGCGCGTCAAGGCTTTGC	
AppReddel ^{901 to 980} mt1-F5	GG ACTAGT CGCAGCGACAAATTGAAGCTGGC G	Deletion of G901 to Y980 fragments of Passenger domain of App
AppReddel ^{901 to 980} mt1-R5	GG ACTAGT GCCTAATCCGTGCCTGACGGCAG CG	
AppReddel ^{908 to 965} mt2-F2	GG ACTAGT AACGGTCAGGGAACATTCCGC	Deletion of G901 to L965 fragments of Passenger domain of App
AppReddel ^{908 to 965} mt2-R2	GG ACTAGT GTTGTCAAGGTTTAAATTGCC	
MspAReddel ^{1037 to 1139} mt1-F4	GG ACTAGT CGTATGCCGAACCTGGCC	Deletion of A1037 to I1139 fragments of Passenger domain of MspA
MspAReddel ^{1037 to 1139} mt1-R4	GG ACTAGT CGGACAGATATTGGACTTGGC	
MspAReddel ^{999 to 1073} mt2-F3	5'GG ACTAGT GACACGAACGACCTGACA	Deletion of D999 to

MspAReddel ⁹⁹⁹ to 1073mt2-R3	5'GG ACTAGT TCGGTTCCTGTAATTGG	A1073 fragments of Passenger domain of MspA
MspAdelRed- AmpF1	CTGGGCAAAGCACACCTGTACG	Confirming Amplicon expected size

Sequences in bold indicate restriction enzyme recognition sequences *BamHI*, *KpnI* and *SpeI*.

2.5. Agarose gel electrophoresis

DNA was separated using 0.7%(w/v) agarose gels, pre-stained with 10 µg ml⁻¹ Syber safe stain (Invitrogen) and run in 1 × Tris-Acetate-EDTA buffer (TAE buffer) (Appendix). DNA in 1 × DNA loading dye were loaded on the gel, separated, and their sizes estimated by comparison to 1 kb DNA Ladder (N3232S; New England Biolabs). Gels were run at 100 V for 60 min. Finally, DNA fragments were visualized using UVitec scanner (Bio-Rad).

2.6. Restriction digestion

Restriction enzymes were purchased from New England Biolabs-UK. Reaction mixtures were incubated in a water bath at 37°C for ≥3 h.

2.7. Ligation

DNA fragments were ligated using T4 DNA ligase (New England BioLabs). Reactions were performed by mixing 100 ng of DNA, 1 µl 10 × ligation buffer,

1 µl T4 DNA ligase and nuclease-free water to a final volume of 10 µl. The mixture was incubated at 16°C for overnight.

2.8. Transformation of *E. coli*

DNA was transformed into *E. coli* strain JM109 competent cells by heat shock transformation. 50 µl of *E. coli* JM109 were thawed on ice for 5 min. 50 ng of DNA was added to the cells and then the cells were incubated on ice for 5 min. For heat shock transformation, the cells were incubated in a water bath at 42°C for 30 s and immediately transferred to ice for 5 min. After that, 950 µl of SOC medium (New England BioLabs) was added and the cells was incubated at 37°C for 1.5 h with shaking before being plated onto LB agar plates containing appropriate antibiotic(s). The resulting colonies were screened by overnight culturing in LB broth containing the same antibiotics followed by plasmid extraction, restriction digestion and DNA sequencing.

2.9. Site directed mutagenesis

2.9.1. Lists of the Primers and Plasmids used in the mutagenesis

Site directed mutagenic primers were designed using the NEBaseChanger online tool (<http://nebasechanger.neb.com/>). Each primer was designated based on the amino acid targeted for mutation. Each case the encoding nucleotide triplet was altered to encode a non-polar amino acid.

Table 2.3 Following primers were used for site-directed mutagenesis

Primer	Template	Primer sequence (5' -3')
AppRed ^{S267A} -F	pDsRedApp	ATTTGGCGAC GCC GCCTCACCAATG
AppRed ^{S267A} -R		GAGCCTCCTGTTGGTAAA
MspA ^{S241A} -F	pDsRedMspA	CGCCGGAGAC GCT GGTTCCCCC
MspA ^{S241A} -R		ATTGCGTAGGTGTTAAGG
MspA ^{D135E} -F	pColdTF-MspA or pcoldTF-MspA ^{S241A}	CCCGGACTAC GA A ^T ACCACCTTC
MspA ^{D135E} -R		TGCGGGTTGCGTGATACG
AppRedNLS ^{SS936&939AA} -F	pDsRedApp	CGCCGCCGT GCG CGCCGT GCG CGC CGTTCC
AppRedNLS ^{SS936&939AA} -R		GGCGCATCTGTCGCACTGCCGGTTT GCG

The sequence in bold represents the target residues of amino acid substitution.

2.9.2. PCR mediated mutagenesis

Site-directed mutagenesis was carried out using the Q5 Site-Directed Mutagenesis kit. Each reaction mixture containing 15-20 ng plasmid DNA, 2 × Q5-Hot Start High-Fidelity master mix to a final 1 × concentration; each of the respective primers (Table 2.3) to a final concentration of 0.5 μM and total volume of final reaction mixture was 25 μl with dH₂O. The PCR conditions used were as following: initial denaturation step at 98°C for 30 s, denaturation at 98°C for 10 s, followed by 30 cycles, recommended annealing for 30 s, and extension at 72°C for 5 min. The temperature for annealing were used varied depending on the respective primer pair used (Appendix); the extension time

used based on the expected size of the amplicon, generally 30 s/1kb and final extension step was 72°C for 5 min.

2.9.3. Kinase-Ligase-DpnI (KLD) treatment

1µl of PCR-product was mixed with 1µl 10 × KLD enzyme mix (from the Q5 Site-Directed Mutagenesis Kit) in the presence of 2µl from 5 × KLD reaction buffer. The reaction mixture was made up to 10µl with dH₂O and incubated at 37°C for 5 min.

2.9.4. Transformation

5µl from the reaction mixture was transformed into *E. coli* JM109 competent cells as per section 2.8.

2.10. DNA sequencing

DNA sequencing was provided by Source Bioscience UK, and the data analysed using DNAMAN software.

2.11. Protein expression and purification

E. coli BL21-Gold (DE3) cells harbouring pColdTF-based plasmids were cultured on LB agar containing ampicillin (100 µg ml⁻¹) and subsequently overnight fresh cultures were 1:50 diluted and as grown as 500ml LB broth cultures to a mid-phase optical density (OD₆₀₀ of 0.5). The culture was then cooled down at 15°C for 30 min without shaking. Recombinant protein expression was induced with 1mM IPTG for 24 h at 15°C. Cells were harvested by centrifugation at 4200 × *g* at 4°C for 10 min in an Allegra X-22R centrifuge (Beckman Coulter). Cell pellets were frozen at -80°C until use or re-suspended in lysis buffer (50mM sodium

phosphate, 300mM NaCl, 10mM imidazole, pH 7.4). Sonication was performed for 8 min on ice in short bursts (15s on and 15s off) using a model 705 Sonic Dismembrator (Fisher Scientific) at amplitude 15 microns. The cell lysate was centrifuged at $8500 \times g$ at 4°C for 15 min and the his-tagged recombinant protein present in the soluble lysate purified by immobilized metal ion chromatography (IMAC) using an AKTA Prime Plus (GE-Healthcare) and 5ml HisTrap-HRP Ni-column (Fisher Scientific). The column was washed with buffer containing 50mM NaH_2PO_4 , 300mM NaCl, 50mM (or 30mM) imidazole, pH 7.4 before the soluble lysate was loaded through the column. The flow through was then reloaded and unbound protein collected as FT, and loosely bound protein removed by washing using the same wash buffer as used previously. Finally, the bound protein was eluted from the column with elution buffer (50mM NaH_2PO_4 , 300mM NaCl, 500mM imidazole, pH 7.4). 1 ml elutes were collected based on the corresponding peak area ratios from the purification chromatogram and proteins resolved by SDS-PAGE.

2.12. Desalting and concentration of proteins

The fractions containing the desired protein were combined and desalted using dialysis tubing-Spectra/Por dialysis membrane (Spectrum labs) by incubated at 4°C overnight with shaking into 20% (v/v) glycerol in Phosphate Buffer Saline (PBS).

Purified, desalted protein samples were then concentrated by using 30MWCO membrane cut-off Vivaspin centrifugal concentrators (Sartorius).

2.13. SDS-PAGE analysis

For SDS-PAGE analysis, mini-protein III apparatus (Bio-Rad) was used. Prior to loading, samples were mixed with 6 × SDS sample buffer (Alfa-Ashar) and heat denatured at 100°C for 5 min. Proteins were electrophoretically separated using different percentage of mini-gel based on the molecular weight of the proteins. Colour Plus protein marker (P7712S; New England BioLabs) was used to estimate the molecular weights of the proteins. 1 × Tris Glycine SDS running buffer (Alfa-Ashar) was used for electrophoresis which was run at 130 V until the marker reached to the baseline of the gel. After electrophoresis, the proteins were detected by staining the gel with Coomassie blue stain for 1 h. Gels were scanned using the Uvitec scanner (Bio-Rad).

2.14. Immunoblot analysis

Protein mixtures were separated by SDS-PAGE and were electro-transferred onto nitrocellulose membranes (0.2µm; GE-Healthcare Life Science) in semi-dry blotting buffer (5.8g Tris base, 2.9g Glycine, 3.7ml 10% (w/v) SDS and 200ml methanol/L) using a Trans-Blot SD semi-dry transfer cell (Bio-Rad) at 10 V for approximately 30 min. After transfer, the membrane was blocked with blocking buffer (5% [w/v] skimmed milk [Millipore] in PBS-Tween (PBS containing 0.1% (v/v) Tween-20) or Bovine Serum Albumin (BSA, Sigma-Life Science) in PBST for 1 h at room temperature or overnight at 4°C. Then the membrane was treated with appropriate polyclonal or monoclonal primary antibody diluted appropriately in blocking buffer and incubated for 1.5 h at RT or overnight at 4°C with gentle agitation. The membrane was washed three times with 0.1% (v/v) PBST, for 5 min each. Then the membrane was incubated with secondary

antibody (anti-mouse/rabbit/goat IgG antibody conjugated to alkaline-phosphatase [Sigma], (1:30000 diluted in blocking solution) for 1.5 h with shaking at RT. After incubation the same washing steps were followed. For the detection of the protein, then the membrane was incubated with substrate 5-Bromo-4-chloro-3-indolyl phosphate / nitro blue tetrazolium liquid substrate system (NBT /BCIP Tablets, Sigma-Aldrich or Roche) and finally washed briefly with dH₂O and visualized with Uvitec scanner (Bio-Rad).

2.15. Protein quantification

Protein concentration was determined using the Pierce BCA protein assay kit (Thermo Scientific), used according to the manufacturer's instructions.

2.16. Cell culture

In this study, Hep-2 (Human epithelial cell-2) and HEK293T (human embryonic kidney 293 cells, and contains the SV40 T-antigen) cells were used. The Hep-2 and HEK293T cells was generously provided by Dr. Osman Dufailu and Dr. Luisa Martinez, University of Nottingham respectively. The cells were cultured in complete growth media consisting of Dulbecco's Modified Eagle's Medium (DMEM media Low glucose, Sigma-Aldrich; appendix for the detail composition of the medium), supplemented with 10% Fetal bovine serum (FBS), 1% (v/v) Penicillin/Streptomycin (10,000 U Penicillin with 10 mg ml⁻¹ Streptomycin in 0.9% (w/v) NaCl, Sigma-UK) and Epithelial growth supplement/Endothelial growth supplement (ECGS, 100×; ScienceCell). Cultures were incubated at 37°C, in a humidified atmosphere of 5% CO₂ (Sanyo CO₂ incubator) in T75cm² flasks (Corning T75 cell culture flask, Corning, NY). When the cells were 85-90% confluent, then the cells were passaged by washed with PBS and then

incubating with pre-warmed dissociation reagent (trypsin-EDTA solution; Sigma-LifeScience). After detachment of the cells, pre-warmed complete fresh medium was added and centrifuged at $300 \times g$ for 5 min. Then the supernatant was aspirated off and the cell pellet suspended with 1 ml of fresh culture medium and the cell suspensions used for cell counting, sub-culturing and experiments.

2.17. Cell viability assay

5×10^5 Hep-2 cells were seeded into 6-well plates and incubated at 37°C in a humidified atmosphere of 5% CO_2 until 80% confluent. Then the old medium was replaced with fresh culture medium containing purified recombinant autotransporter proteins (ranging from 40nM to 400nM final concentration) and the cells were incubated for 20 h. Cell viability was assessed by microscopic evidence and cellular metabolic activities of the cells. Images of the viable cells were captured using an Invitrogen EVOS XL Core Cell Imaging System at $10\times$ objective. Three separate images from three different batches of the cell viability assay were considered. Cell viability of autotransporter treated cells were compared with Staurosporine (2 μM) as positive control and untreated cells as negative control.

The viable cells were counted with 0.4% (w/v) trypan blue solution with haematocytometer.

Alternatively, the XTT cell viability kit (Cell Signalling Technologies) was also used to determine the cell viability. Here, Hep-2 cells were seeded in 96-well plates (1×10^4 cells well⁻¹) and incubated overnight.

The medium was replaced with serum free medium containing 40nM final concentration of autotransporters and 50 μl XTT detection solution [XTT reagent: electron coupling solution PMS (50:1)] was added into each well and incubated

for 24 h. Then the absorbance of formazan formed was measured at 450 nm using a Spark microplate plate reader at different time points. Each sample were tested with triplicate replicates and in three independent experiments. In parallel, negative control cells (untreated) and positive control cells (Staurosporine; 40nM final concentration) were also analysed. Data analyse with GraphPad Prism 7.

2.18. Transfection

Hep- 2 cells and HEK293T cells were seeded onto 12mm glass coverslips in 24-well plates at a cell density of 100,000 cells well⁻¹. Once the cells had reached 80-90% confluency, the medium was removed and 500µl pre-warmed antibiotic free medium added into each wells. Adherent cells were transiently transfected with 1µg of the desired DsRed-based fusion construct. pDsRedIgA1protease and pDsRedVirD2 were used as positive controls for nuclear localisation, pDsRed was used as a positive control for transfection, and untreated cells were used as a negative transfection control.

All transfection experiments were carried out with antibiotic-free Opti-MEM (1 × Reduced Serum Free Medium) using Lipofectamine3000p DNA Transfection reagent (Invitrogen) following the manufacturer's instructions. After 48 h of post transfection, the cells were washed with PBS and used for immunofluorescence staining and microscopic analysis.

2.19. Immunofluorescence staining and confocal microscopy

Transfected cells were grown for 48 h following transfection and fixed with 4% (w/v) paraformaldehyde in PBS at room temperature for 15 min. After permeabilisation with 0.1% (v/v) Triton X-100 in PBS for 20 min, cell nuclei were stained with 0.1% (v/v) Hoechst 33342 (200ug/ml-Immunochemistry) in PBS and incubated for 20 min. Cells were washed with ice-cold PBS for three times after each step. Then coverslips were sealed with antifade Prolong gold mounting reagent (Invitrogen). Nuclear localisation of fluorescently-labelled proteins was determined by confocal laser scanning microscopy and quantified using Velocity 6.3.1 software (Perkin Elmer). Confocal images were obtained using a Zeiss LSM 710 confocal microscope with lasers at 405 nm and 560 nm for excitation of DAPI/Hoechst and DsRed respectively. Images were analysed by Zen 2.3 Lite software. The intensity of the proteins was analysed using Velocity 6.3.1 software (PerkinElmer-UK).

2.20. Histone purification from eukaryotic cells

Cell-derived histones were purified from Hep-2 cells grown in 175cm² flasks in DMEM (Dulbecco's Modified Eagle's Medium) complete growth medium (described in the section 2.16). When the cells were 90-95% confluent, cells were harvested and the histones were extracted and purified using the Active Motif Histone Purification kit.

Harvested cells were suspended in 500µl extraction buffer and incubated overnight on a rotating platform at 4°C. The supernatant containing crude histone was obtained by centrifugation at 13,000 × *g* in a micro-centrifuge at

4°C (Thermo Scientific-UK). The supernatant was neutralised with 5 × Neutralisation buffer until the pH was adjusted to 8.0. The neutralized crude histone sample was then loaded onto a pre-equilibrated column with equilibration buffer and the flow through was collected by centrifuged at 50 × *g* for 3 min. The column was then washed thrice with 3 ml wash buffer by centrifugation for 3 min at 50 × *g*. For H2A/H2B purification, the column was eluted with 3ml H2A/H2B elution buffer by gravity flow. Four 1 ml eluted fractions were collected into sterile 1.5 ml Eppendorf tubes. Subsequently, H3/H4 histones was eluted by applying four 1 ml aliquots of H3/H4 elution buffer. Purified histones were precipitated for buffer exchange according to the manufacturer's instructions (Active Motif-UK). Aliquots were taken during different stages of the purification process and proteins resolved on SDS-PAGE and immunoblot analysis was performed with specific rabbit polyclonal antibodies: anti-Histone H3 (N-terminal, ab18521; 1:5000 dilution), anti-Histone H3 (C-terminal, ab1791; 1:5000 dilution), anti-Histone H2B (N-terminal, ab18977; 1:5000 dilution), anti-Histone H2B (C-terminal, ab1790; 1:5000 dilution), anti-Histone H4 (C-terminal, ab10158; 1:4000 dilution) or anti-Histone H2A (C-terminal, ab18255, 1:2000 dilution). Alternatively, a mouse mAb was used: anti-Histone H3 (C-terminal, ab24834; 1:5000 dilution).

2.21. Histone clipping assay

Initially, 3µg of cell-derived histones (H1, H2B/H2A or H3/H4) or 1.5 µg human recombinant histones - H3.1 (M2503S), H1 (M2501S), H2B (M2505S) or H4 (M2504S; New England Biolabs) were incubated with 40nM purified recombinant autotransporter protein in a total reaction volume of 40µl of PBS for each sample and incubated at 37°C for 16 h with shaking (60rpm).

The histone clipping assay was subsequently optimised for different parameters such as incubation period, histone quantity and autotransporter protein concentration. The reaction was stopped with the addition of 6 × SDS-PAGE sample buffer and heat denaturation for 5min at 95°C. Cleavage products were separated on 16% (w/v) SDS-PAGE gels and detected by immunoblot analysis using the specific antibodies detailed in section 2.20. For inhibition experiments, the protease inhibitor, Phenylmetanesulfonyl fluoride (PMSF 1mM; Sigma) was used.

2.22. Cell lysis assay

Hep-2 cells (5×10^5) were seeded into 6-well plates and incubated for 24 h at 37°C in a humidified atmosphere of 5% CO₂. Then the cells were washed with PBS and used fresh culture medium containing purified recombinant autotransporter proteins were treated with various range (40nM, 100nM, 150nM, 250nM and 500nM) and the cells were incubated for 12 h/16 h/20 h. After incubation the culture medium was discarded. Then the whole cell lysates obtained by using ice-cold RIPA buffer (Sigma-Life Science) supplemented with PhosSTOP phosphatase inhibitors (Roche) and Complete mini EDTA-free protease inhibitor cocktail (Roche) and placed on ice for 30 min. Scraped cells were homogenized using a 21-gauge needle and incubated on ice for 10 min. The cell debris were removed by centrifugation at $13,000 \times g$ for 15 min at 4°C. Proteins in the supernatant were heat denatured at 95°C for 5 min and stored at -20°C until use. Each sample was subsequently subjected to immunoblotting analysis using the antibodies listed in section 2.20.

2.23. Chromatin bound protein assay

Chromatin extraction were performed using a commercial subcellular protein fractionation kit (Thermo-scientific) from cultured Hep-2 cells. Cells (2×10^5 /well) were seeded into 12 well plates and growth overnight and followed as the outline of ATs treatment (in the section of 2.22). The cells were treated with various concentration of recombinant ATs (150nM, 200nM and 250nM). A schematic of the method (Figure 2.1) is shown which shows the stepwise separation and extraction of chromatin-bound proteins from the cells.

After sequential extraction of cytoplasmic and membrane proteins, the soluble nuclear extract was isolated with ice-cold NEB (Nuclear extraction buffer) containing protease inhibitors. Chromatin-bound proteins were extracted by adding 5 μ L of 100mM CaCl₂ and 3 μ L of Micrococcal Nuclease in NEB extraction buffer. Chromatin-bound nuclear extract in the supernatant were transferred to a clean pre-chilled tube on ice. Then the supernatant was denatured by heat and analysed by western blot using specific anti-histone antibodies (describe in the section 2.20 Immunoblotting analysis).

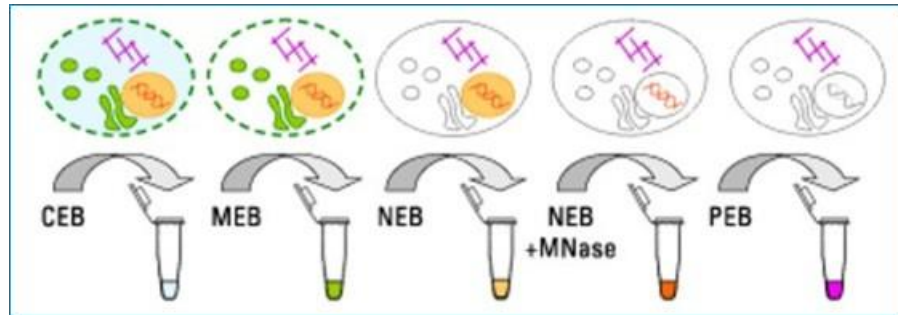


Figure 2.1: Schematic overview of the subcellular fractionation procedure (Thermoscientific). Cellular compartments were sequentially extracted by incubating cells with cytoplasmic extraction buffer (CEB) followed by membrane extraction buffer (MEB) and nuclear extraction buffer (NEB). Adding micrococcal nuclease (MNase) to NEB extracts chromatin-bound proteins from the cell pellet.

**CHAPTER 3: Nuclear
localisation of meningococcal
autotransporter App (Adhesion
and Penetration Protein)**

3.1. Introduction

There is a growing recognition that some secreted proteins target the host cell nucleus, where they may modify gene expression and thus host cell biology, with implications for the pathogenesis of Gram-negative bacteria [219]. Host nuclear targeting of pathogenic bacterial proteins is an emerging pathogenic mechanism whereby bacterial proteins can be translocated into the nucleus of the host cell and can interact with the nuclear machinery including the chromosome and their associated chromatin (histones) resulting in an alteration of cell physiology and even cytotoxicity [220]. It is evident that invasive meningococcal infections cause cytopathic effects associated with the tissue damage and extensive cell injury [127, 221-223] and also apoptosis of infected epithelial cells [224, 225].

In Gram negative bacteria, autotransporter proteins are secreted virulence factors. Several meningococcal autotransporter proteins have been characterized to date and they are all known or putative virulence factors. Among the meningococcal autotransporters, App (Adhesion and penetration protein) is a secreted protein required for optimal meningococcal adhesion to epithelial cells [214] and shows homology with the Haemophilus Adhesion and penetration (Hap) protein of *Haemophilus influenzae* [226, 227] which belongs to the SPATE (Serine protease of autotransporters of Enterobacteriaceae) family [180, 186]. This family is associated with toxicity and/or host immune system modulation via adherence and/or cleavage of intra and extracellular host proteins [179]. Several studies on App revealed that App gene expression is common to all serogroups and occurs during meningococcal infection. App has been shown to stimulate T and B cells, and to induce a bactericidal antibody

response [180, 213]. In addition, a significant contribution of App to pathogenesis was demonstrated using a transgenic mouse model where CD46-expressing transgenic mice were infected with either wild-type or a meningococcal mutant lacking both App. A statistically significant difference in survival between the groups of mice infected with wild-type and App mutant bacteria was demonstrated at 72 h post infection [215].

App comprises all the structural components of an autotransporter protein: an N-terminal signal peptide, a central passenger domain and a translocator β -domain. The functions of passenger domains of autotransporters are various and are usually related to virulence [228]. The passenger domain of App may be released via auto cleavage, or by the action of the autotransporter NaIP [183]. App auto cleavage (at least partially) releases a secreted protein fragment harboring a peptidase domain which is *ca.* 100kDa and, alternatively in the presence of the proteolytic autotransporter NaIP, a larger *ca.* 140kDa secreted App fragment is released which contains the peptidase domain and α -peptide domain [183]. This α -peptide is a unique feature of some of the autotransporters of pathogenic *Neisseria* which may contain nuclear localization signals (NLSs) [187, 194] and has been implicated in biofilm formation via binding of the NLS to eDNA. It is also hypothesized that the presence of an NLS-containing α -peptide may mediate the ability of autotransporters to enter into the host cell nucleus resulting in differential cellular responses.

It is known that in eukaryotic cells, molecules smaller than 40kDa can be transported between the cytoplasm and nucleus by diffusion through the nuclear pore complex, but larger macromolecules (such as App passenger domain) require an active transport mechanism. Active transport is mediated by peptide motifs - nuclear localization signals (NLSs) [229] which bind to NLS

receptors and mediate the nuclear translocation of the large proteins [230]. Several bacterial and viral proteins have been reported with functional NLSs in species as varied as *E. coli*, *Helicobacter pylori*, Influenza A, SV40 virus, *Shigella Spp.*, *Salmonella Spp.*, *Klebsiella pneumoniae* and *Yersinia Spp.*[231-237]. Jose et al. defined four different variants of meningococcal α -peptide based on the number of NLSs and sequence variability [195]. Interestingly, predicted NLSs are present in both meningococcal IgA1 protease and App in their respective α -peptide regions. Pohner et al. and Bebes et al. demonstrated IgA1 protease nuclear accumulation in the host cell nucleus [187, 194]. A recent study in our research group demonstrated the uptake and nuclear targeting of App autotransporter proteins into dendritic cells (DCs) [215].

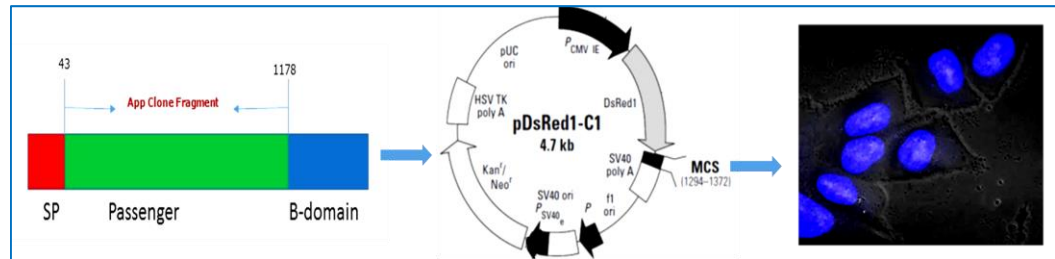
As a consequence of the previous findings we aimed to further investigate App nuclear trafficking in human epithelial cells and to define the functional NLS sequence present in App. To achieve this, the passenger domain of App (or mutated derivatives) was expressed as a fusion with the fluorescent DsRed protein in the mammalian expression vector pDsRed and the sub-cellular localization of these tagged-App proteins determined using confocal microscopy.

3.2. Results

3.2.1. Nuclear localization of App into the host cell

Hep-2 epithelial cells were initially used as a human cell model to characterise the sub-cellular localisation of recombinant App and its derivatives. As the starting point, optimisation experiments were performed to achieve efficient transfection and also to confirm expression of DsRed-tagged proteins (data not shown). Different parameters were optimised including incubation period of transfected cells, the concentration of DNA used and the fluorescent staining protocol. The best results were obtained using one μg DNA per transfection with Lipofectamine reagent and 48 h post-transfection incubation (data not shown). After 48 h, the cells were washed, fixed, permeabilised and subjected to fluorescent staining using Hoechst stain and the DsRed tagged proteins visualised with the confocal microscope (described in the section 2.19). Nuclear localization of the DsRed-fused proteins was confirmed by co-localisation of the red emission protein with the blue Hoechst nuclear marker. A schematic showing an overview of the experiments is shown in (Figure 3.1).

[A]



[B]

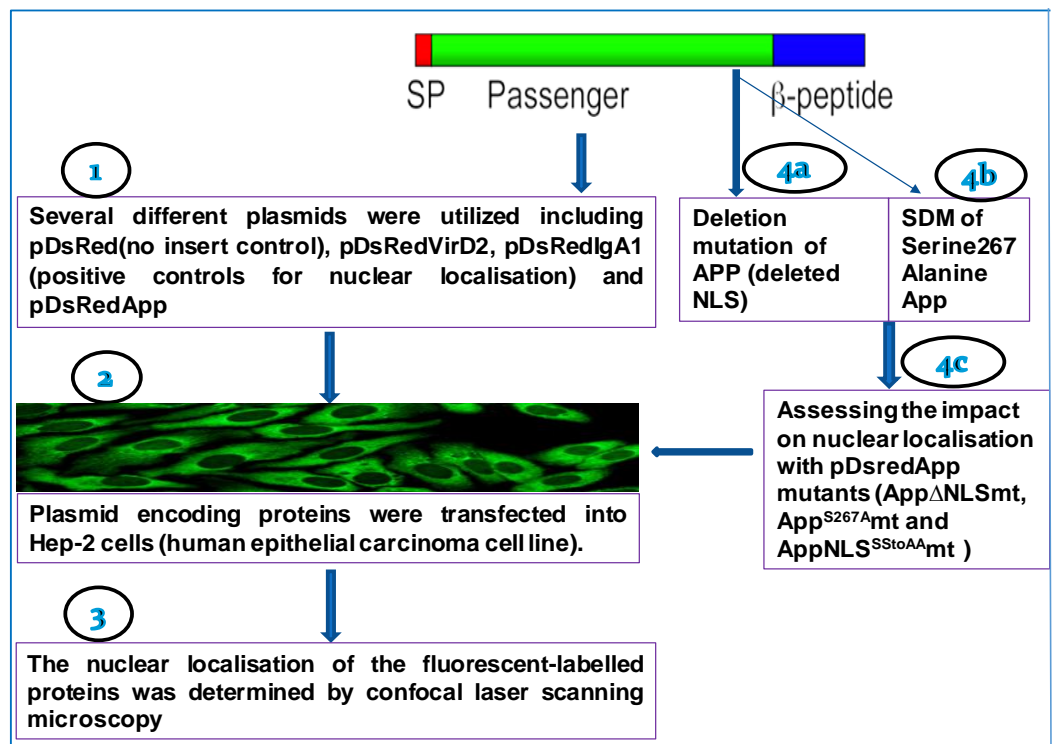


Figure 3.1: Schematic overview of the nuclear localization experiments. [A] DNA encoding the App passenger domain was cloned into pDsRed (pDsRedApp plasmid generously provided by Dr.Osman Difailu, University of Nottingham) and transfected into tagged Hep-2 cells to facilitate expression of DsRed-tagged App passenger domain. [B] Overview of the sequential experimental flow to investigate the nuclear localization of App.

In these experiments, untreated Hep-2 cells were used as negative control and pDsRed-transfected cells were used as transfection control and non-nuclear localising fluorescent protein control. pDsRedVirD2 and pDsRedIgA1 α -protease were used as positive controls for nuclear localisation as they both encode proteins harbouring known NLS sequences [194, 238]. In non-transfected Hep-2 cells, only blue-staining nuclei were evident and DsRed expression was fully absent in the red channel (Figure 3.2). In the case of cells transfected with pDsRed, cells were stained red throughout the cells indicating that the DsRed protein was uniformly distributed across cells when expressed in Hep-2 cells (Figure 3.2). It has been reported that the two NLSs of VirD2, a protein of the plant pathogen *Agrobacterium tumefaciens*, is capable of directing proteins into the eukaryotic cell nucleus [238]. As expected, the expressed DsRed-tagged VirD2 protein localised to the cell nucleus. In the merged panel, DsRed was observed to co-localise with the nuclear stain (Figure 3.2), demonstrating nuclear localisation of the VirD2 protein.

As the NLS-harboured α -peptide of IgA protease can act as a carrier for nuclear transport [194], the pIgA1 α -red construct was used as another positive control for nuclear localisation. Consistent with this study, our data also provided evidence of DsRed-tagged IgA1 protease localization into the nucleus of the transfected cells (Figure 3.2). In the case of pDsRedApp, the DsRed-tagged App passenger domain was also translocated into the nucleus of the transfected cells similar to the positive controls (Figure 3.2). Interestingly, in many cases, the DsRedApp-expressing cells appeared to be undergoing apoptosis based on their visual appearance which supported the finding by our group that App induces apoptosis [215]. It was also noted that the transfection efficiency was low for

App compared with VirD2 and DsRed, presumably as a consequence of the apoptotic effect. Overall, the data is consistent with the previous work by our group where App which had been added to dendritic cells was taken up and trafficked to the nucleus [215].

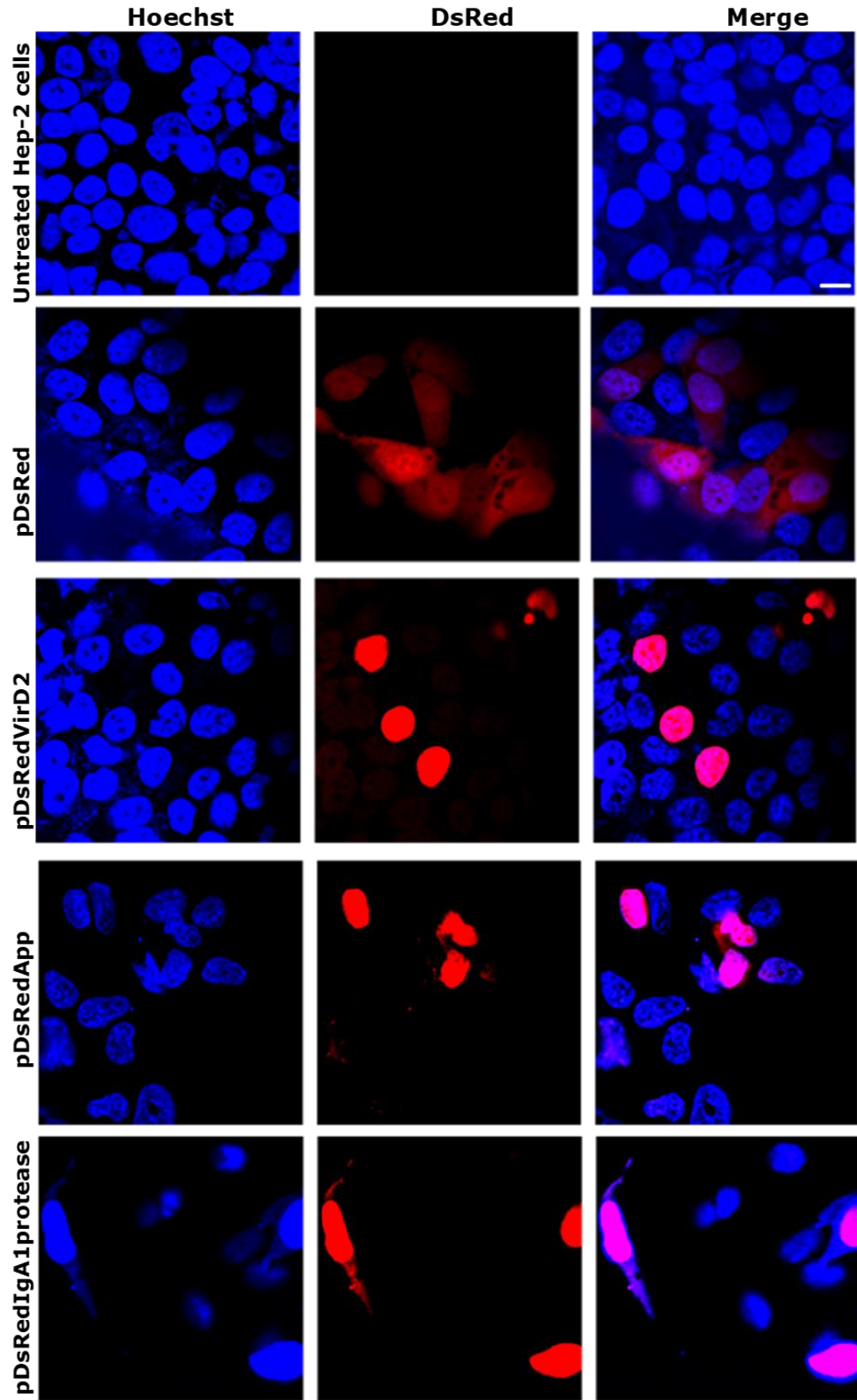


Figure 3.2: Confocal microscopic images showing co-localisation of App, VirD2 or IgA1 protease proteins tagged with DsRed with the nucleus in transfected Hep-2 cells. Untreated Hep-2 cells served as negative control, pDsRed-transfected cells served as transfection control and showed the uniform distribution of red (DsRed) colour throughout the cell. Plasmids encoding DsRed-tagged VirD2 and IgA1 protease served as controls for nuclear localisation. Similarly, DsRed-tagged App localised to the nucleus of transfected (red) cells. All scale bars, 10µm. Representative images are from one of three independent experiments.

The result confirmed that the passenger domain of App was trafficked to the nucleus of Hep-2 cells.

3.2.2. Nuclear localization of App confirmed in HEK293T cells

The nuclear localization experiments were carried out primarily with human epithelial laryngeal cells (Hep-2 cells). For comparison, the nuclear localization was also observed in another cell line - HEK293T cells (Human embryonic kidney cells).

To investigate any cell specificity of the observed nuclear localisation of the recombinant App passenger domain in epithelial cells, the DsRed tagged recombinant proteins were expressed in a second cell line: HEK293T using the same protocols as were used previously for Hep-2 cells. Similar nuclear localization of DsRedVirD2 and DsRedApp was observed in Hep-2 cells and HEK293T cells (Figure 3.3).

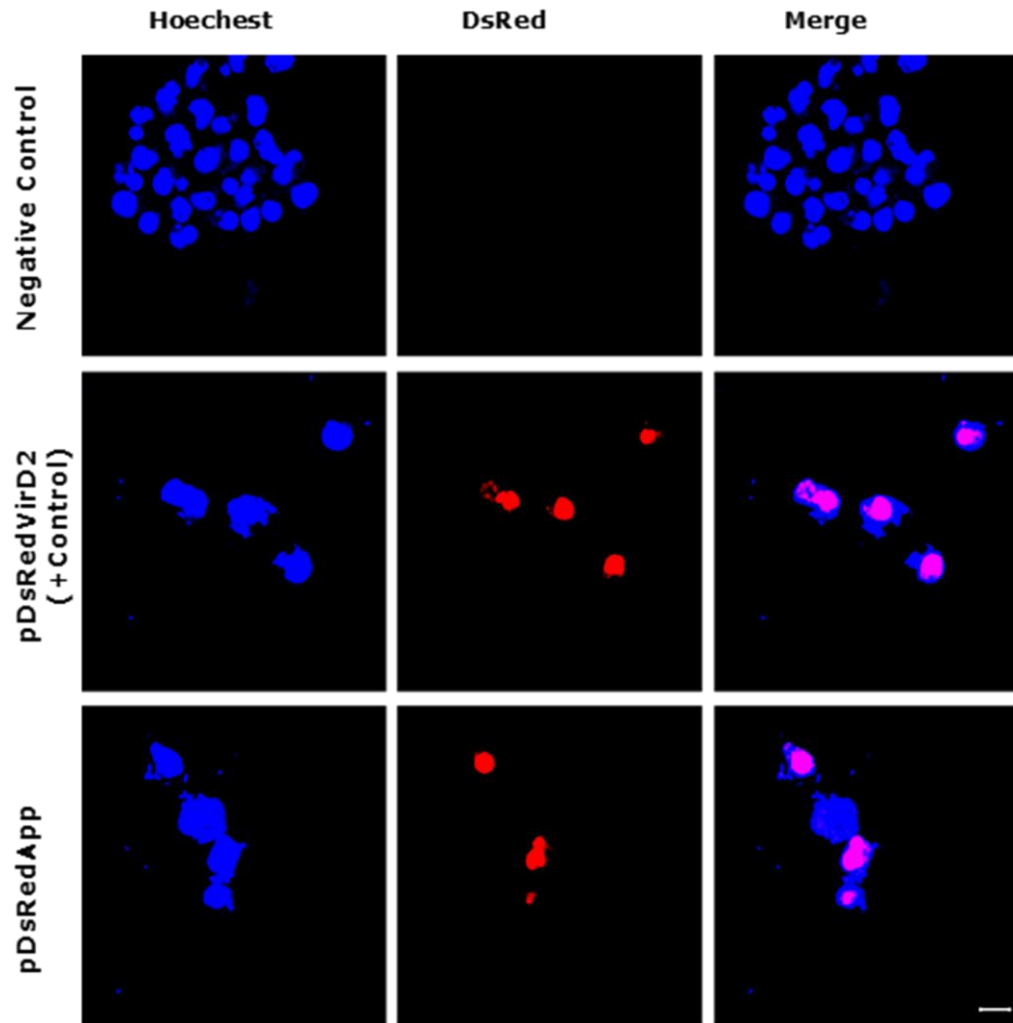


Figure 3.3: Confocal microscopic images showing co-localisation of the DsRed-tagged recombinant proteins with the nucleus in transfected HEK293T cells. In this experiment, untreated cells were included as a negative control. In parallel pDsRed used as transfection control and pDsredVirD2 used as positive control for NLS.

Transfection experiments were carried out with HEK293T cells and the nuclear localisation of DsRed-tagged App visualised in comparison to VirD2-expressing and untreated cells. Recombinant App- and VirD2-DsRed tagged proteins were localized into the nucleus of the cells, and a similar level of DsRed emission was

observed. No red signal was detected into the untreated HEK293T cells. All scale bars, 10µm.

3.2.3. Quantification of nuclear localization

The fluorescence intensity of DsRed-labelled protein in the nucleus (as defined by Hoechst stain) of transfected cells was measured using velocity software. This was evaluated from an equal number of cells (fifteen) for each sample, and quantification of the expression of the proteins were calculated in three different experiments. There was a statistically significant difference in the fluorescence intensity of VirD2, App, and IgA1 protease compared to DsRed ($p < 0.0001$).

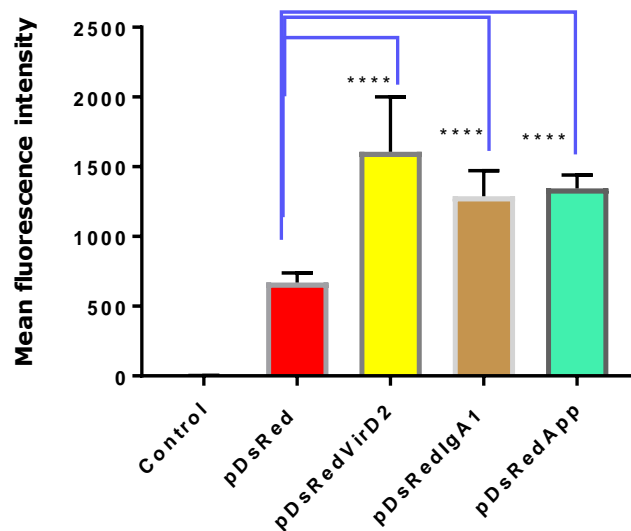


Figure 3.4: Statistical analysis of co-localisation of fluorescent-labelled proteins and Hoechst-stained cell nuclei. Hep-2 cells were transfected with plasmids encoding DsRed-labelled proteins and Hoechst was used to detect the DNA within cell nuclei. Mean fluorescence intensities of the nuclear regions were derived from cells in four different fields. Error bars: mean of values + SD. The data was analysed by one-way Anova multiple comparison test and Tukey's test. Here, **** means highly significant nuclear localisation, $p < 0.0001$.

This data provides evidence that the passenger domain of App can translocate to the nucleus of human epithelial cells.

3.2.4. Impact of catalytic serine residues on nuclear localisation of App proteins

We next aimed to determine the possible contribution of the catalytic serine residue of the passenger domain of App in nuclear trafficking.

3.2.4.1. Mutation of pDsRedApp:

To understand the possible role of catalytic serine mutant of App in nuclear trafficking, plasmid pDsRedApp^{S267A} was generated by site-directed mutagenesis using the Q5 site-directed mutagenesis kit (described in the section 2.9). Here, pDsRedApp was used as DNA template, and primers AppRed^{S267A}-F and AppRed^{S267A}-R used to substitute the serine-encoding codon with nucleotides (GCC) encoding an alanine residue at position 267 of App.

The PCR product was confirmed by agarose gel electrophoresis and a DNA fragment of the expected size of *ca.* 8.1 kb was observed (Figure 3.5).

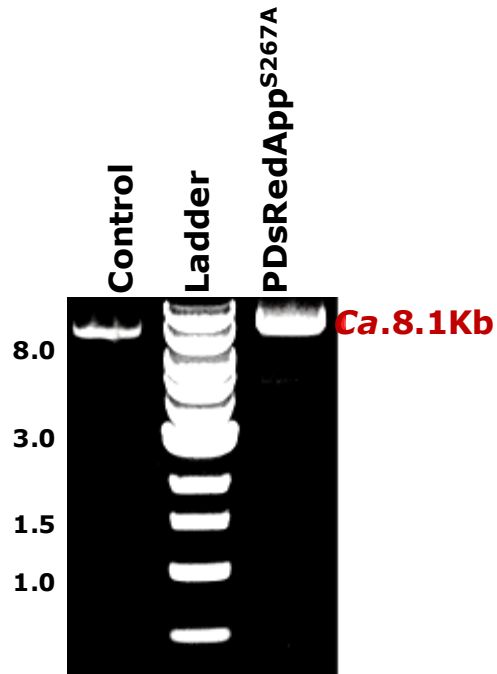
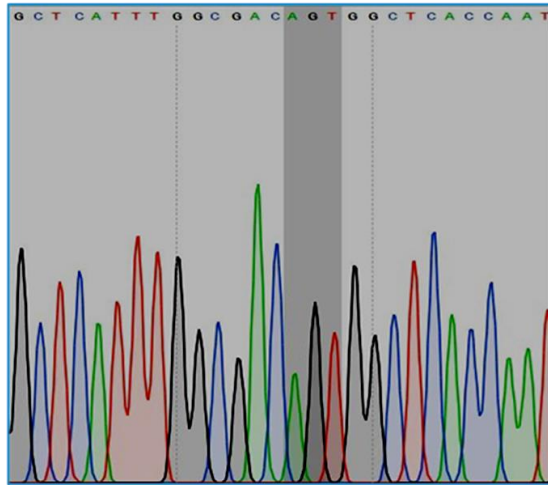


Figure 3.5: PCR-mediated generation of pDsRedApp^{S267A}. Agarose gel analysis showing the PCR amplification of pDsRedApp^{S267A}. pDsRedApp plasmid DNA was used as a template with mutagenic primer pairs AppRed^{S267A}-F and AppRed^{S267A}-R (Table: 2.3) to amplify the whole plasmid while generating a single serine to alanine substitution at position 267 of App protein by PCR. Lane 1: Control, Lane 2: 1kb DNA ladder, Lane 3: PCR product corresponding to pDsRedApp^{S267A}.

The PCR product was then treated with enzyme mixture KLD (containing kinase, ligase and DpnI) according to the manufacturer's instructions (described in the section 2.9.3). Then the KLD-treated DNA was used to transform into *E. coli* JM109 cells. Several colonies were screened for by DNA sequence analysis for the presence of the desired mutation.

pDsRedApp



pDsRedApp^{S267A}

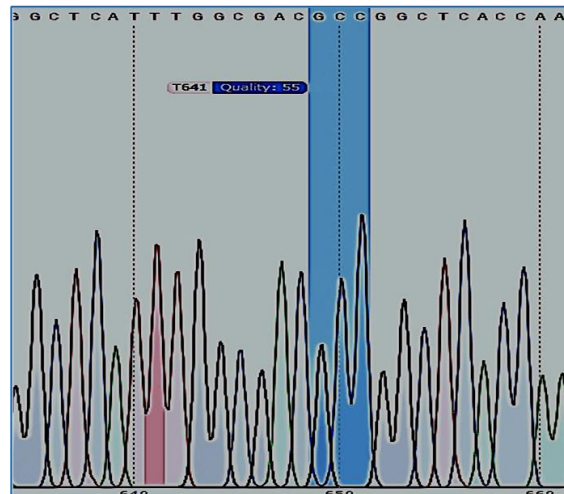


Figure 3.6: DNA sequence chromatograms of pDsRedApp and pDsRedApp^{S267A} showing the substitution of the triplet AGT encoding ²⁶⁷S of meningococcal App to a GCC codon encoding an alanine, to generate pDsRedApp^{S267A}.

3.2.4.2. Nuclear localisation of DsRedApp^{S267A}

DsRed-tagged App and App^{S267A} plasmids were expressed in transfected Hep-2 cells with VirD2 pDsRed-expressing cells as a positive control. No apparent

difference in the nuclear localization of wild type App and App^{S267A} was observed in transfected Hep-2 cells. The nuclear localization ability of DsRedApp^{S267A} was indistinguishable from DsRedApp or the positive control VirD2 protein. We found that pDsRedApp^{S267A} indeed localized to the nucleus in the Hep-2 cells and the expression of the levels of pDsRedApp^{S267A} mutant into the cells are similar to those of pDsRedApp wild-type (Figure 3.7). This finding indicates that App proteolytic activity was not required for the nuclear localization of this protein.

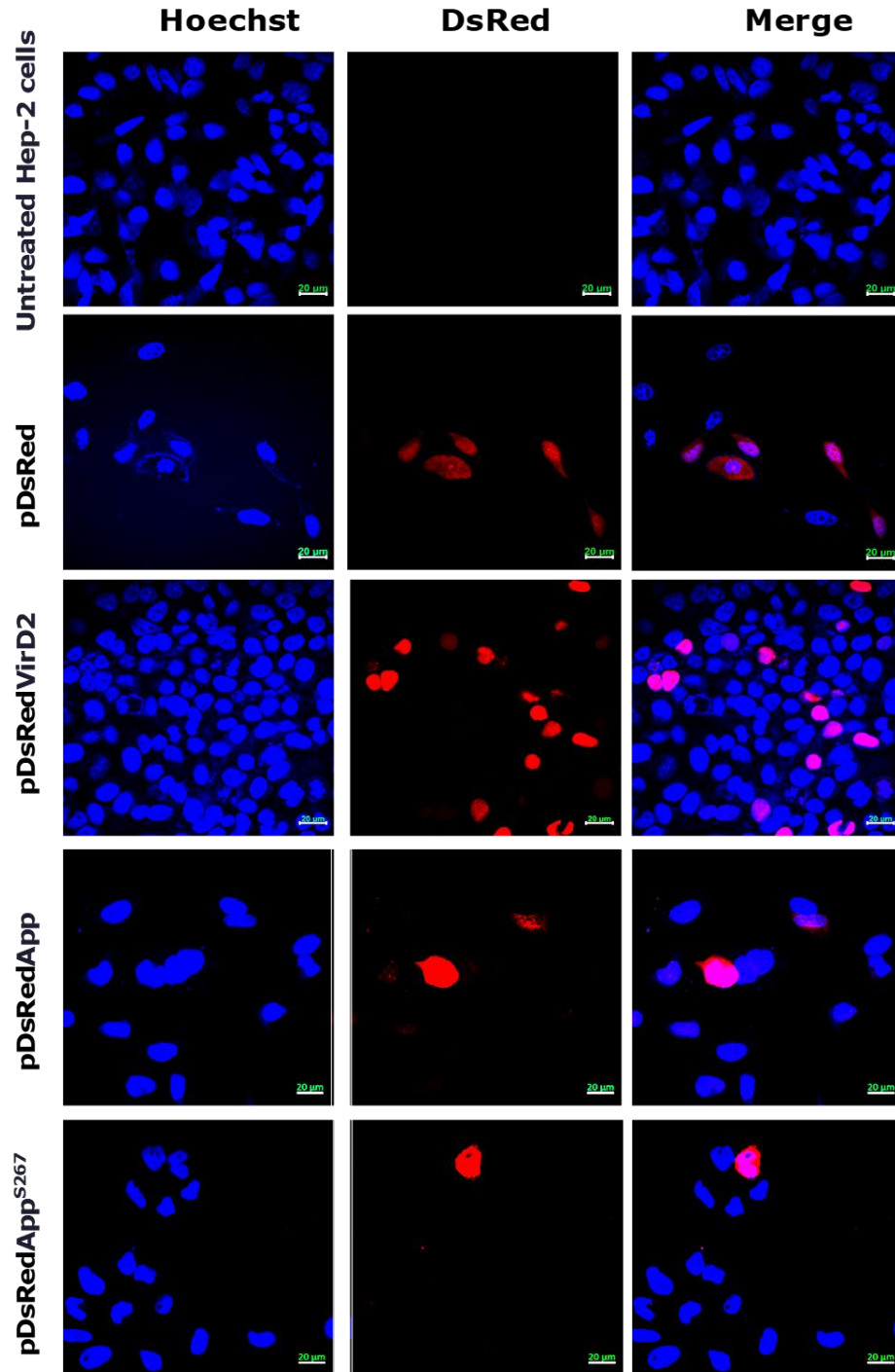


Figure 3.7: Nuclear localisation of DsRed-tagged App^{S267A} and App proteins in transfected Hep-2 cells. Hep-2 cells were transfected with the appropriate plasmids and were analysed by confocal microscopy 48 h post-transfection. The nuclear accumulation of the expressed proteins from pDsRedApp and pDsRedApp^{S267}, respectively, showed similar results as DsRedVirD2.

All scale bars, 20µm. Images from one of three independent experiments are shown here.

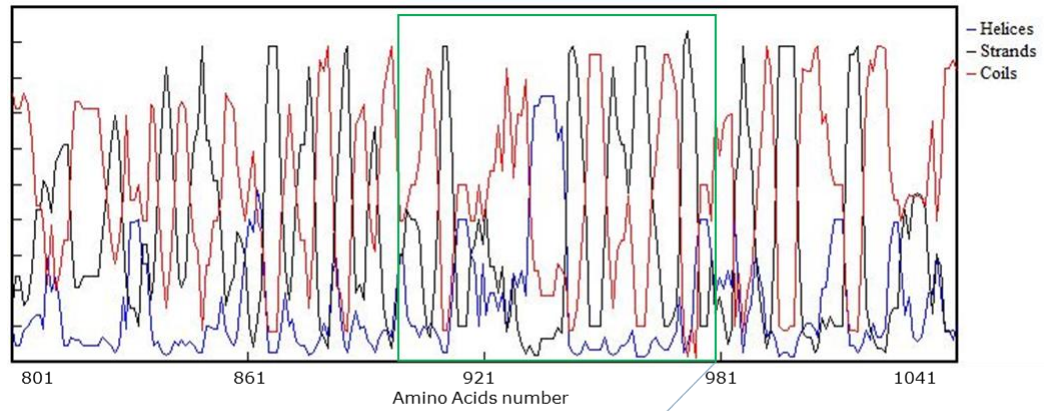
3.2.5. Identification of the App NLS sequence

The ability of DsRedApp to translocate to the nucleus suggested that the App passenger domain contains at least one NLS which is able to mediate active transport, or there are other alternative ways by which the App protein could get into the nucleus. Earlier studies suggested the presence of a putative NLS sequence in MC58 App (⁹³³RRRSRRSR⁹⁴⁰ in MC58 App) [180]. To investigate the role of this putative NLS sequence and surrounding regions in nuclear localisation, a derivative of pDsRedApp was generated (pDsRedAppΔ^{G901 to Y980}) and nuclear localization experiments were performed using Hep-2 cells with the same approach described above for pDsRedApp.

3.2.5.1. Deletion of App residues 901-980

Before designing the inverse PCR primers, the secondary structure of the protein was predicted using DNAMAN software in order to avoid regions of secondary structure such as longer alpha-helices (Figure 3.8), where mutagenesis might cause gross structural changes. In this mutation, the putative NLS-encoding sequence of pDsRedApp was deleted by inverse PCR using primers AppReddel⁹⁰¹⁻⁹⁸⁰mt1-F5 and AppReddel⁹⁰¹⁻⁹⁸⁰mt1-R5 to delete residues G⁹⁰¹ to Y⁹⁸⁰ of the App passenger domain. The PCR amplicon was resolved by agarose gel electrophoresis as shown in Figure 3.9.

AppwT



Deleted fragment G901 to Y980

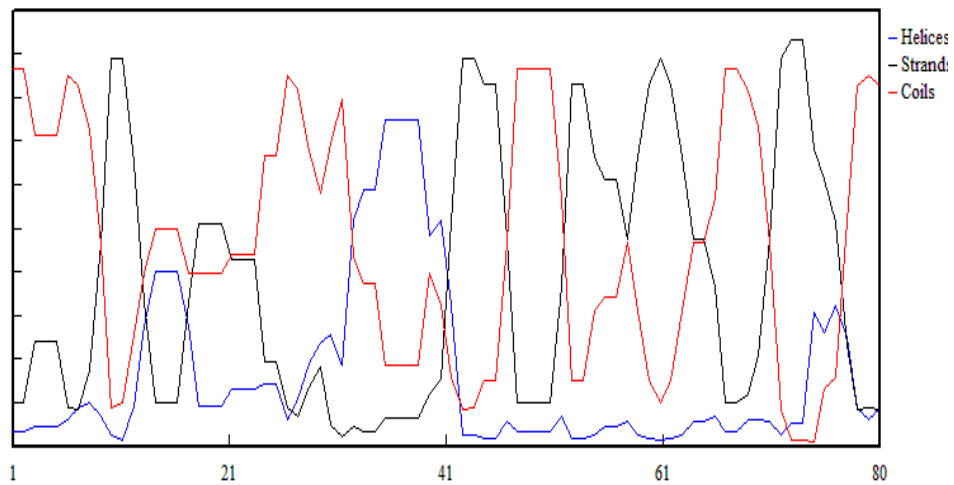


Figure 3.8: Predicted secondary structure of App Protein. Here, the secondary structure of AppwT shown from S⁸⁰¹ to W¹⁰⁴¹. The fragment G⁹⁰¹ to Y⁹⁸⁰ was deleted from App protein. The secondary structure of the protein and the structure probability were done with DNAMAN software.

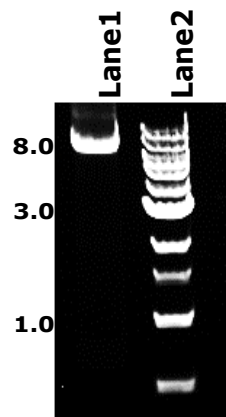


Figure 3.9: Inverse PCR- mediated generation of pDsRedApp^{Δ901G-980Y}. Inverse PCR was performed to the region encoding 80 amino acids from ⁹⁰¹G to ⁹⁸⁰Y of App from pDsRedApp using primers AppReddel⁹⁰¹⁻⁹⁸⁰mt1-F5 and AppReddel⁹⁰¹⁻⁹⁸⁰mt1-R5 (Table-2.2). Lane 1: PCR product of pDsRedApp^{Δ901G-980Y}, Lane 2: 1 kb DNA Ladder.

3.2.5.2. Confirming the deletion in pDsRedApp^{Δ901G-980Y}

pDsRedApp^{Δ901G-980Y} was confirmed by PCR using primers of AppdelAmpF-1 and AppdelAmpR-1. Amplification generated a 930 bp product from pDsRedApp, whilst the corresponding amplicons from mutant plasmids C1, C2 and C4 were lower, reflecting the loss of 240 nucleotides from the region (Figure 3.10).

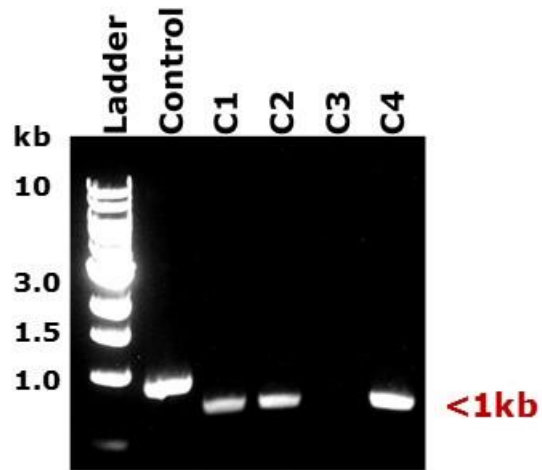


Figure 3.10: Agarose gel analysis showing PCR confirmation of pDsRedApp^{Δ901G-980Y}. pDsRedApp was used as a control DNA template to amplify a 930 bp fragment spanning the region deleted in pDsRedApp^{Δ901G-980Y} using primer pair AppdelAmpF-1 and AppdelAmpR-1 (Table-2.2). The corresponding amplicon from C1, C2 and C4 was 240 bp smaller confirming truncation in these clones. Lane 1: 1 kb DNA ladder, Lane 2: Control (pDsRed), Lane 3 to 6: amplicons from four different putative positive mutants (C1-C4).

DNA sequence analysis of pDsRedApp^{Δ901G-980Y} confirmed that the target region (encoding G⁹⁰¹ to Y⁹⁸⁰) was deleted in pDsRedApp^{Δ901G-980Y} and that the sequence was otherwise unaltered. The region encoding Glycine at position 901 to Tyrosine at 980 position was deleted from the template plasmid pDsRedApp. The deletion was confirmed by sequence alignment using DNAMAN.

3.2.5.3. Nuclear localization of pDsRedApp^{Δ901G-980Y}

To determine the role of App residues ⁹⁰¹G to ⁹⁸⁰Y in nuclear trafficking, the localisation properties of this protein were determined. Hep-2 cells were transfected transiently with DsRed-fused constructs either encoding the full

passenger domain of App (pDsRedApp) or its mutant derivative (pDsRedApp^{ΔG901-Y980}) and the localisation of the encoded recombinant proteins determined by confocal microscopy. pDsRedVirD2 and pDsRedApp used as positive controls, pDsRed used as transfection control and untreated cells used as negative control. As before, we observed that DsRed was distributed throughout the cytosol of transfected cells, no red signal was observed in untreated cells whereas a significant amount of red signal was detected in cells expressing the NLS-containing VirD2 (pDsRedVirD2), which was completely located into the nucleus of transfected cells and the full passenger domain of App containing pDsRedApp was strongly accumulated into the nucleus (Figure 3.11). Interestingly, we found that the mutant protein expressed from pDsRedApp^{ΔG901-Y980} had a different distribution compared with wild-type (Figure 3.11); the mutant protein did not accumulate in the cell nucleus, but displayed a punctate distribution within the cytosol. This finding indicated that the sequence required for nuclear localisation was localised to the region deleted in this mutant.

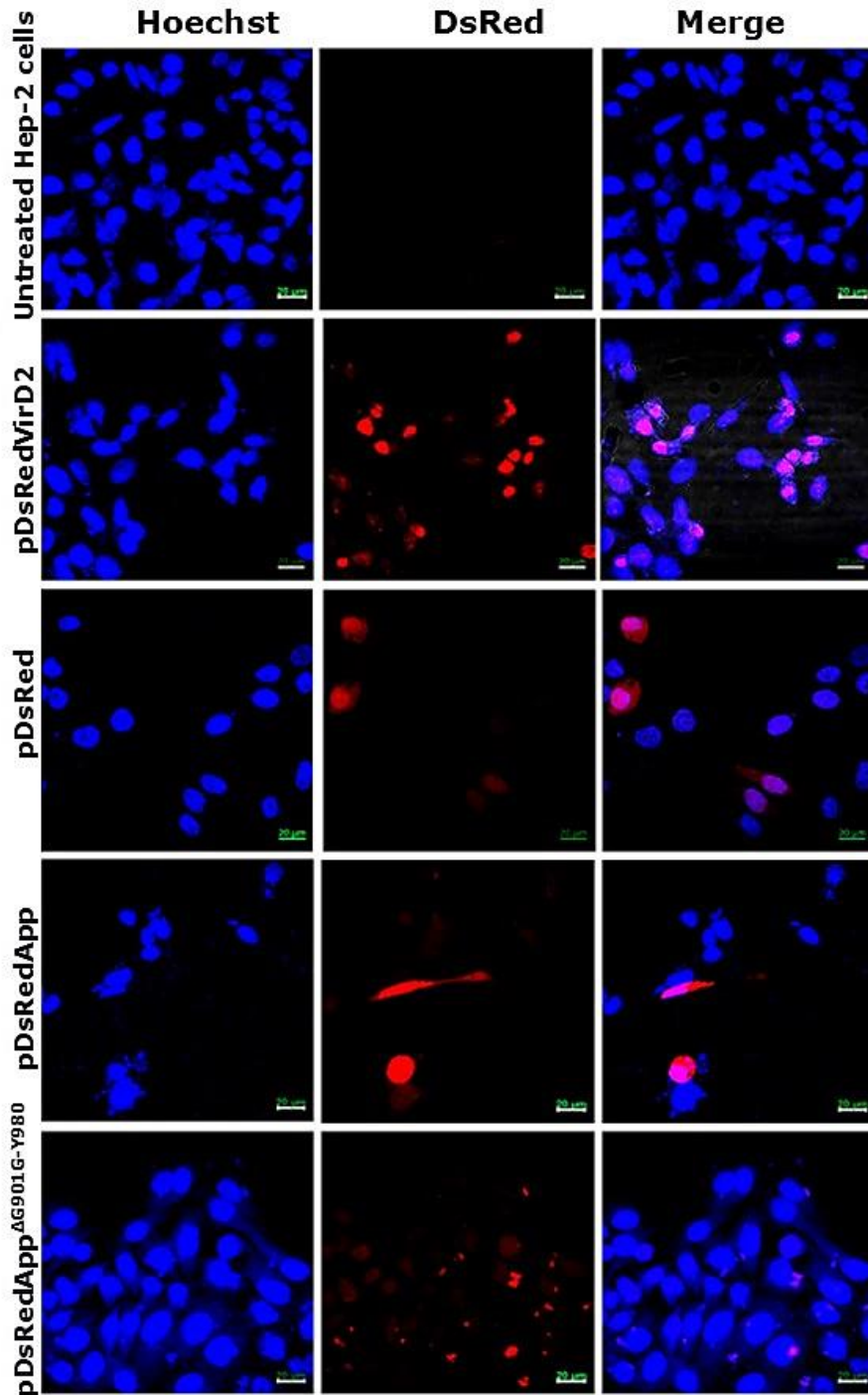


Figure 3.11: Nuclear localisation of DsRedApp^{ΔG901-Y980}. Hep-2 cells were transfected with each of the plasmids pDsRedApp, pDsRedApp^{ΔG901-Y980}, pDsRed, pDsRedVirD2 or were left untransfected. Cells were fixed 48 h after transfection and analysed by confocal microscopy. All scale bars 20 μm. Representative images from three experiments.

3.2.5.4. Refining the region required for the nuclear localization of App

To define further the crucial region of App required for nuclear trafficking, another truncated mutant was constructed lacking amino acids G⁹⁰¹ to L⁹⁶⁵ from App. The construct was confirmed by amplification across the deleted region and DNA sequencing.

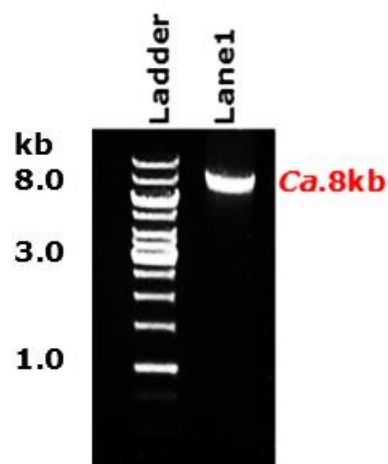


Figure 3.12: Inverse PCR- mediated generation of pDsRedApp^{ΔG901G-L965}. Inverse PCR was performed to remove the region encoding 65 amino acids (Glycine at position 901 to Leucine 965) from pDsRedApp with forward AppReddel^{901 to 965}mt2-F2 and reverse primer pair AppReddel^{901 to 965}mt2-R2 (Table-2.2). Lane 1: 1 kb DNA Ladder, Lane 2: PCR product of pDsRedApp^{ΔG901 to L965}.

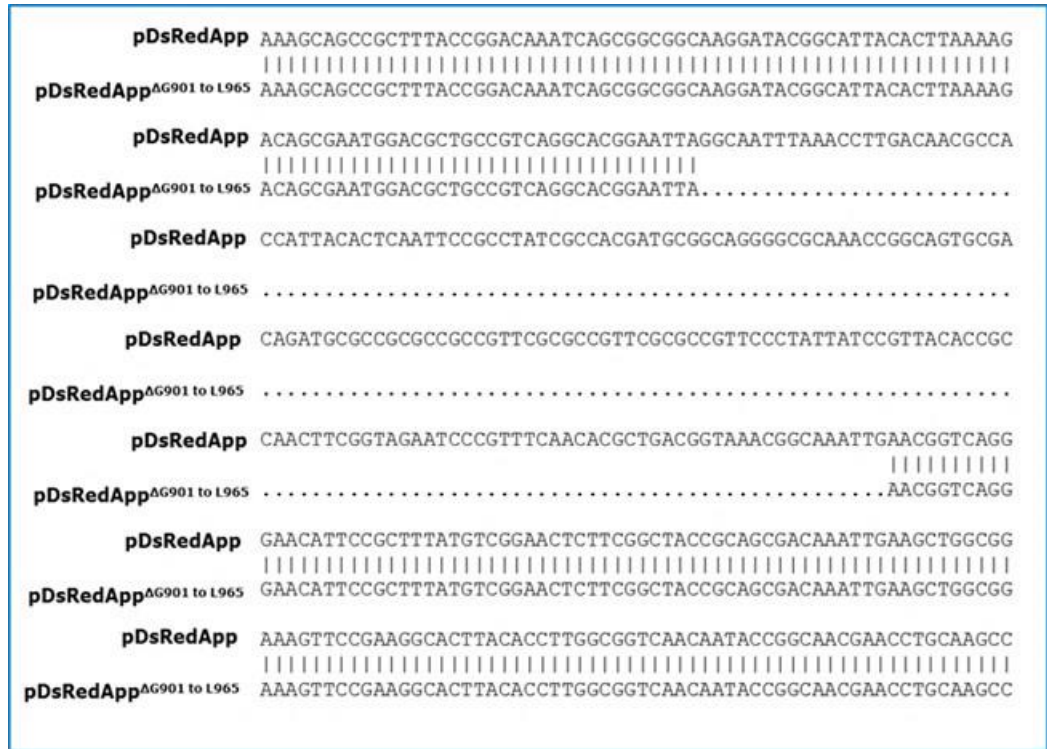


Figure 3.13: DNA sequence alignment of pDsRedApp and pDsRedApp^{ΔG901 to L965} confirming the deletion. The DNA sequence encoding amino acids G⁹⁰¹ to L⁹⁶⁵ was deleted from the template plasmid pDsRedApp and the sequence of the mutant aligned with the *app* gene of MC58. Here, the upper line sequence represents pDsRedApp and lower line is for pDsRedApp^{ΔG901 to L965}.

3.2.5.5. Nuclear localization of pDsRedApp^{Δ901G-965L}

pDsRedApp^{ΔG901-L965} transfected cells showed similar distribution of tagged protein to pDsRedApp^{ΔG901-Y980} transfected cells, whereas the pDsRedApp positive control showed co-localization of the expressed protein with the nucleus (Figure 3.14). The experimental evidence showed that both mutant App proteins (App^{ΔG901-Y980} and App^{ΔG901-L965}) lost their ability to access the cell nucleus indicating the App NLS is localized to between G⁹⁰¹ and L⁹⁶⁵.

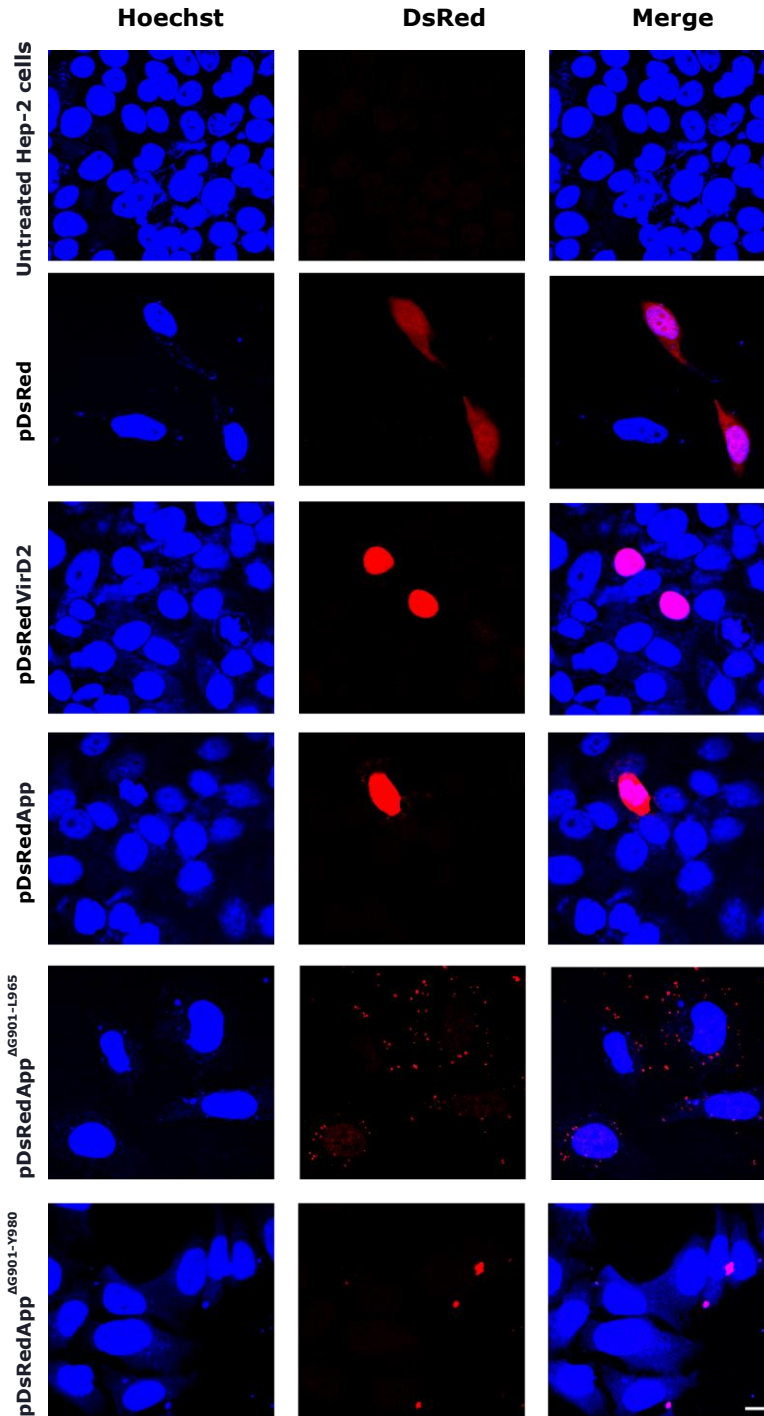


Figure 3.14: Nuclear localization of DsRedApp^{ΔG901G-965L} in Hep-2 cells. Cells were transfected using pDsRed, pDsRedVirD2, pDsRedApp, pDsRedApp^{ΔG901-L965} and pDsRedApp^{ΔG901-Y980}. Representative images indicate that App is localized to the

nucleus, but the mutated App derivatives are not. All the scale bars 5µm. One of three independent experiments is shown here.

3.2.6. Mutation of serine residues in the putative NLS App sequence disrupts nuclear trafficking

The data shown so far in this chapter shows that deletion of residues 901-965 of MC58 App disrupts nuclear localisation. Furthermore, we previously proposed a putative NLS sequence in MC58 App (⁹³³RRRSRRSR⁹⁴⁰) [180]. Several studies have reported that the subcellular localization of the nuclear-localising protein is influenced by the serine residues in the NLS [235, 239, 240] as they are involved in the interaction between the NLS and importin which acts to transport the protein through the nuclear pores [241]. In order to define whether or not the serine residues of putative NLS sequence have a significant role in the nuclear trafficking of App; the replacement of two serine residues (at positions 936 and 939) was undertaken.

3.2.6.1. Mutation of App serine residues in the putative App NLS

We generated the mutant plasmid pDsRedAppNLS^{S936AS939A} via site-directed mutagenesis where serine residues at 936 and 939 were substituted with alanine. Then the PCR product was confirmed based on molecular size and by DNA sequencing (Figure 3.15).

pDsRedApp

```
ACGGAATTAGGCAATTTAAACCTTGACAACGCCACCATTACACTCAATTCGCCTATCGC
T E L G N L N L D N A T I T L N S A Y R
CACGATGCGGCAGGGGCGCAAACCGGCAGTGCACAGATGCGCCGCGCCGCCGTTCGCGC
H D A A G A Q T G S A T D A P R R R S R
CGTTCGCGCCGTTCCCTATTATCCGTTACACGCCAACTTCGGTAGAATCCCGTTTCAAC
R S R R S L L S V T P P T S V E S R F N
```

pDsRedAppNLS^{S936AS939A}

```
ACGGAATTAGGCAATTTAAACCTTGACAACGCCACCATTACACTCAATTCGCCTATCGC
T E L G N L N L D N A T I T L N S A Y R
CACGATGCGGCAGGGGCGCAAACCGGCAGTGCACAGATGCGCCGCGCCGCCGTTCGCGC
H D A A G A Q T G S A T D A P R R R A R
CGTTCGCGCCGTTCCCTATTATCCGTTACACGCCAACTTCGGTAGAATCCCGTTTCAAC
R A R R S L L S V T P P T S V E S R F N
```

Figure 3.15: Generation of pDsRedAppNLS^{S936AS939A}. pDsRedApp was used as a template with AppRedNLS^{S936AS939A}-F and AppRedNLS^{S936AS939A}-R mutagenic primers (Table-2.3) to amplify the whole plasmid while generating serine to alanine substitution at positions 936 and 939 of App by PCR and confirmed by DNA sequencing.

3.2.6.2. Effects of NLS serine substitutions on App nuclear localisation

To determine whether the serine residues in the putative NLS were required for optimal nuclear trafficking of App; the nuclear localization of protein encoded by pDsRedAppNLS^{S936AS939A} was investigated in transfected Hep-2 cells. As before, DsRedApp and DsRedVirD2 were predominantly localised to the nucleus. In contrast to the wild type (DsRedApp), DsRedAppNLS^{S936AS939A} did not localise to the nucleus but was scattered as red punctate dots in the cytosol of the Hep-2 cells (Figure 3.16). The serine substitutions therefore altered the nuclear trafficking ability of App and demonstrated the requirement for the two serine

residues in the functional NLS sequence. This finding supports the hypothesis that residues ⁹³³RRRSRRSR⁹⁴⁰ constitute a functional NLS in App.

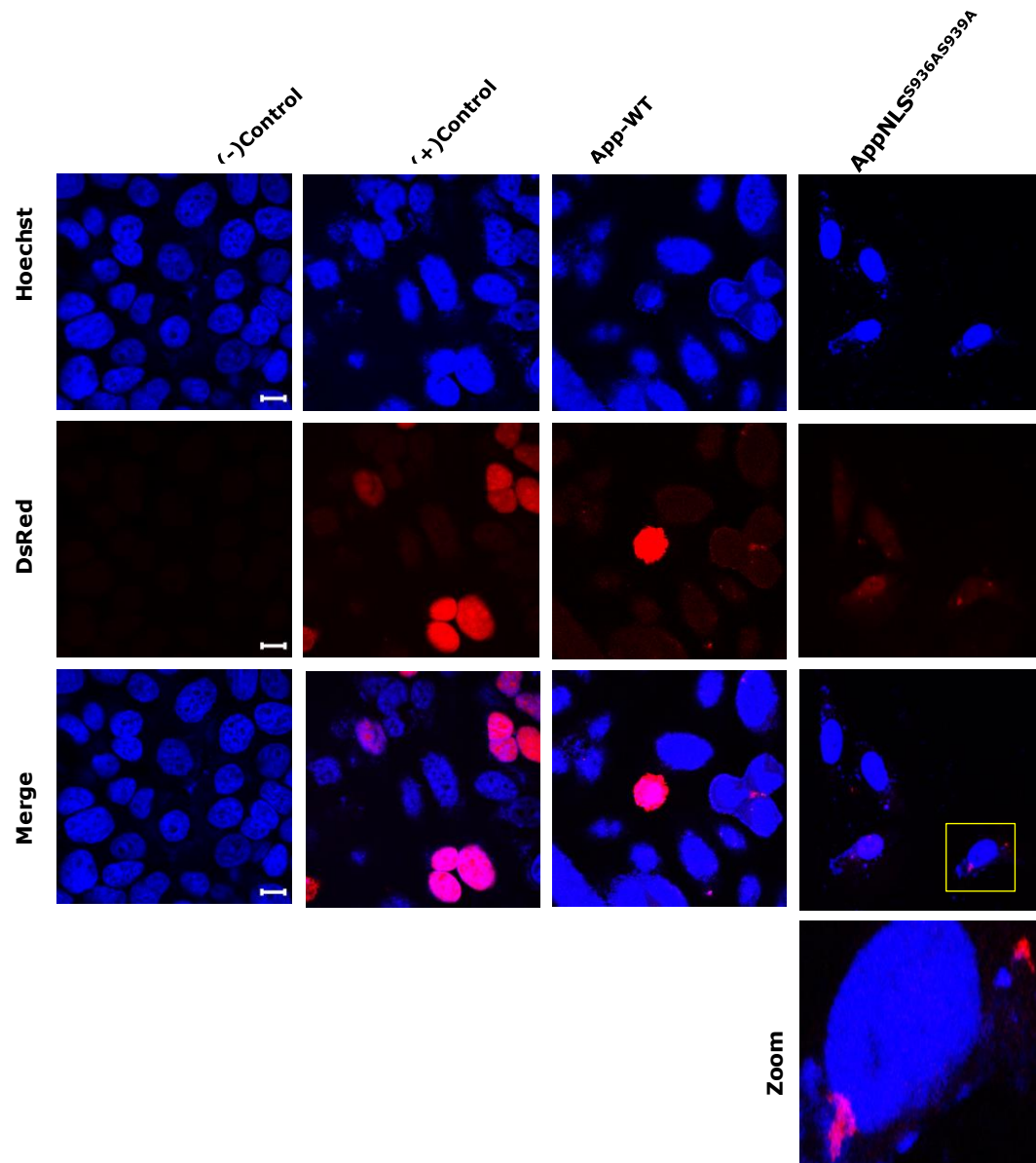


Figure 3.16: Mutation of serine residues in the putative App NLS disrupt nuclear trafficking. Untreated Hep-2 cells were used as negative control, VirD2-expressing cells were used as positive control. DsRed-tagged App as well as VirD2 co-localised with the blue nuclear stain in transfected cells, but AppNLS^{S936AS939A} was not localised to the nucleus although showed perinuclear

localization which might be associated with nuclear membrane or nuclear pore.
All the scale bars 20 μ m (except zoom).

Based on the experimental evidence we concluded that App nuclear localization is NLS dependent and the functional NLS is in the region 901-965, and likely between 933R to 940R in MC58.

3.2 Discussion

Secreted proteins play essential roles in the pathogenesis of Gram-negative bacteria. In some cases such proteins have been shown to interact with nuclear molecules of the host cell after uptake and nuclear targeting, resulting in alteration of the host cell physiology [220]. Secreted proteins include cytolethal distending toxins from Gram-negative bacteria [242], *Salmonella enterica* SspH1 [243] *Yersinia* YopM [232], OspcF of *Shigella* species [233] have been reported to target to the host cell nucleus. It was previously shown by our group that meningococcal App and MspA are members of this group of secreted proteins which are taken into the nucleus of human DC cells [215].

Work described in this chapter provides experimental evidence for nuclear targeting of App via NLS-based import. App is a large protein with a molecular weight of 190kDa including a secreted passenger domain of 125kDa. This is larger than the diffusion limit for transport into the nucleus. Macromolecule transport between nucleus and cytoplasm is an active process involving a peptide motif which is rich in arginine and lysine referred to as a nuclear localization signal or sequence (NLS) which 'tags' proteins for nuclear transport and binds to a nuclear receptor leading to their import into the cell nucleus through the nuclear pore complex [236].

Importantly, it was reported that NLS motifs of meningococcal IgA1 α -protease served to promote the accumulation of this protein in the eukaryotic cell nucleus [187]. Nuclear translocation of this IgA1 α -protease autotransporter in Hec-1-B was observed by Besbes et al, who reported that an NLS harboring- α -peptide acts to promote nuclear transport of IgA protease and that fragments having or lacking the α -peptide differ in their access to the cell nucleus [194].

The App passenger domain used in this study corresponds to the larger, α -peptide-containing, meningococcal protein of IgA1 protease. Preliminary studies suggested that App contains one putative NLS (⁹³³RRRSRRSR⁹⁴⁰ in MC58 App) which is arginine-rich, but the experimental confirmation of this remained to be established [180].

The nuclear targeting of App was analysed by expressing the full-length passenger domain of App as a DsRed-fusion protein and visualising the distribution of the protein across the host cell by confocal microscopy. Hep-2 cells were used as a human epithelial cell model that is relatively easy to culture, transfect and has been used for cell biology studies using meningococcal bacteria or proteins previously [184]

The finding that the passenger domain of App was translocated into the host cell nucleus was consistent with previous observations by our group [215]. In addition, App-transfected cells showed evidence of apoptosis, which was previously reported by our group [215]. Mutations abolishing the proteolytic activity of App resulted in a protein which was still translocated to the nucleus indicating that the proteolytic activity of App is not required for nuclear localization.

In contrast, two different truncated mutant DsRedApp proteins showed a clear disruption in nuclear trafficking and showed a punctate distribution within the cytosol. This difference in the distribution indicated that the truncations had removed NLS sequence(s), thus effecting the nuclear targeting of App.

App nuclear localization may have role in cell death because we observed an apoptotic appearance in cells expressing wild-type App, but this was not evident in cells expressing App derivatives which were unable to access the

nucleus. So, a possible explanation is that the presence or absence of App nuclear trafficking ability may provoke different cellular responses.

Several studies have reported that serine residues within the NLS can influence nuclear transport by their phosphorylation [244, 245]. Therefore, we expressed DsRedAppNLS^{S936AS939A} which confirmed the importance of these residues for nuclear trafficking. The mutant protein lost the ability to access the nucleus indicating that the residues function within a NLS. Several studies have reported similar evidence, for instance, Lee and colleagues who reported nuclear targeting by the HsdM protein of *Klebsiella pneumoniae*, but HsdMpΔNLS and two substituted derivatives (lysine residues with alanine in the NLS) were localized to the cytoplasm, not to the nucleus [237].

To extend our understanding of the role of App in pathogenesis, and in particular to determine whether it can induce cellular or molecular changes after host cell nuclear targeting, the molecular interactions of the nuclear-targeted proteins need to be investigated; the interaction of both App and MspA with histones are described in chapter-five.

**CHAPTER 4: Investigating
nuclear localization signals in
Meningococcal serine protease
A (MspA)**

4.1. Introduction

Meningococci interact with various cells of the host and their secreted virulence factors have been attributed various roles in colonization, persistence and damage to the host [58]. Meningococcal serine protease A (MspA) is an outer membrane and secreted protein with significant roles in meningococcal virulence [182, 215].

MspA is chymotrypsin-like serine protease; it is an adhesin which also shares homology with IgA protease and App [180, 182]. MspA is 157-kDa protein which has *ca.* 33% and *ca.* 36% overall amino acids identity with App and IgA protease, respectively [182].

In *N. meningitidis*, an intact *mspA* gene is not present in all strains; in some strains (ST-11) the gene contains a premature stop codon resulting in the gene not being expressed. MspA expression is phase variable due to a polycytosine tract in the coding region [153, 181, 182]. The reversible ON /OFF switching of *mspA* expression may allow bacteria to adapt to different microenvironments and aid escape from the adaptive immune system [69]. Interestingly, the phase-variable expression of *mspA* is serogroup-specific. A study reported that approximately 90% of *mspA* genes were phase ON in both invasive and carriage strains of serogroup B, demonstrating the importance of MspA expression in that serogroup. By contrast significantly less phase ON *mspA* genes were found amongst invasive and carriage serotype Y isolates [197].

MspA exhibits autoproteolytic cleavage resulting in release of the functional passenger domain from the cell surface into the external milieu. The secreted MspA fragments vary between strains and are also influenced by the activity of another autotransporter, NaIP [183]. NaIP-mediated cleavage results in the release of a large form of the passenger domain protein, with a C-terminal

extension called the α -peptide. The α -peptide of IgA protease and App contain the nuclear localisation signal (NLS), but such sequences have not been recognised in the MspA protein [182]. The α -peptide of MspA does not contain positively charged amino acids residues such as those found in NLS sequences of other proteins including App. Nonetheless, it was reported by our group that MspA targeted the host cell nucleus after being taken up into dendritic cells: a process mediated by the mannose and transferrin receptors [215]. Heterologous expression of MspA in *E. coli* mediated adhesion to epithelial and endothelial cells were reported [182].

As mentioned in the previous chapter, research into the nuclear targeting of bacterial secreted proteins is an emerging field in cellular microbiology. The subcellular targeting of the bacterial protein may induce host cell pathology, but the exact effects of this remains unclear. However, a few bacterial proteins have been found to be targeting the nucleus and induce host pathology. For example, CDT (cytolethal distending toxin) can induce S/G2 cell cycle arrest and cell death after nuclear translocation [220, 246, 247]. Previously, we mentioned in Chapter three a few bacterial proteins with ability in nuclear localization into the host cell, in particular outer membrane protein A of *Chlamydia trachomatis* [248], a transposase of *Acinetobacter baumannii* Ac [249], the SspH1 secreted protein of *Salmonella enterica* [231], YopM of *Yersinia spp* [232], and IpaH9.8 and OspcF of *Shigella* species [233] were all found to induce host cell pathology after nuclear targeting. The secreted MspA protein is a large protein, which exceeds the active diffusion limit for transport across the nuclear membrane. In eukaryotic cells, many cytoplasmic proteins with molecular weights greater than 40kDa are transported into the nucleus via specific NLSs [250, 251] but such a signal has not been identified in MspA.

This study was designed to characterise the mechanism by which MspA is targeted to the nucleus of mammalian cells, and to identify the motif responsible for nuclear trafficking of this molecule.

4.2. Results

A significant amount of work-related to identification of a functional NLS in the App autotransporter was discussed in chapter three. Here we followed a similar sequential flow of experiments as presented in Figure 3.1B.

4.2.1. Nuclear localization of MspA in host cells

To investigate whether MspA could target the nucleus of the host cells, like App protein, we first examined this using the DsRed-tagged fusion proteins encoded by plasmids (pDsRedMspA plasmid generously provided by Dr. Osman Dufailu, University of Nottingham). Hep-2 cells or HEK293T cells were transfected transiently using pDsRedMspA (encoding the whole passenger domain of MspA fused to DsRed), pDsRedVirD2 and pDsRedApp respectively (following the same procedure described in the section 2.18). Cells were fixed 48 h post-transfection, permeabilised and were subjected to fluorescent staining with Hoechst before imaging with confocal microscopy. The subcellular distribution of DsRed-tagged expressed proteins were analysed using confocal laser scanning microscopy. The nuclear localization of the DsRed tagged proteins were evaluated by co-localization with the blue nucleus of the transfected cells.

In this experiment, untreated cells were included as a negative control. In parallel DsRed tagged, NLS-containing VirD2 and App, showed co-localisation with the nucleus whereas pDsRed showed the red protein distributed throughout the cell.

Both experiments showed the nuclear targeting ability of MspA in Hep-2 cells (Figure 4.1) and HEK293T (Figure 4.2). pDsRedMspA transfected cells

showed the red fluorescence emission on top of the blue marker for the nucleus indicating DsRed-tagged MspA protein was localized into the nuclei of the cells.

It is worth mentioning that the DsRed-MspA fusion protein has a molecular mass greater than 40kDa, yet showed precise nuclear localization in Hep-2 cells and HEK293T cells. This finding is consistent with the previous finding that MspA is taken up and targeted to the nucleus by dendritic cells [215].

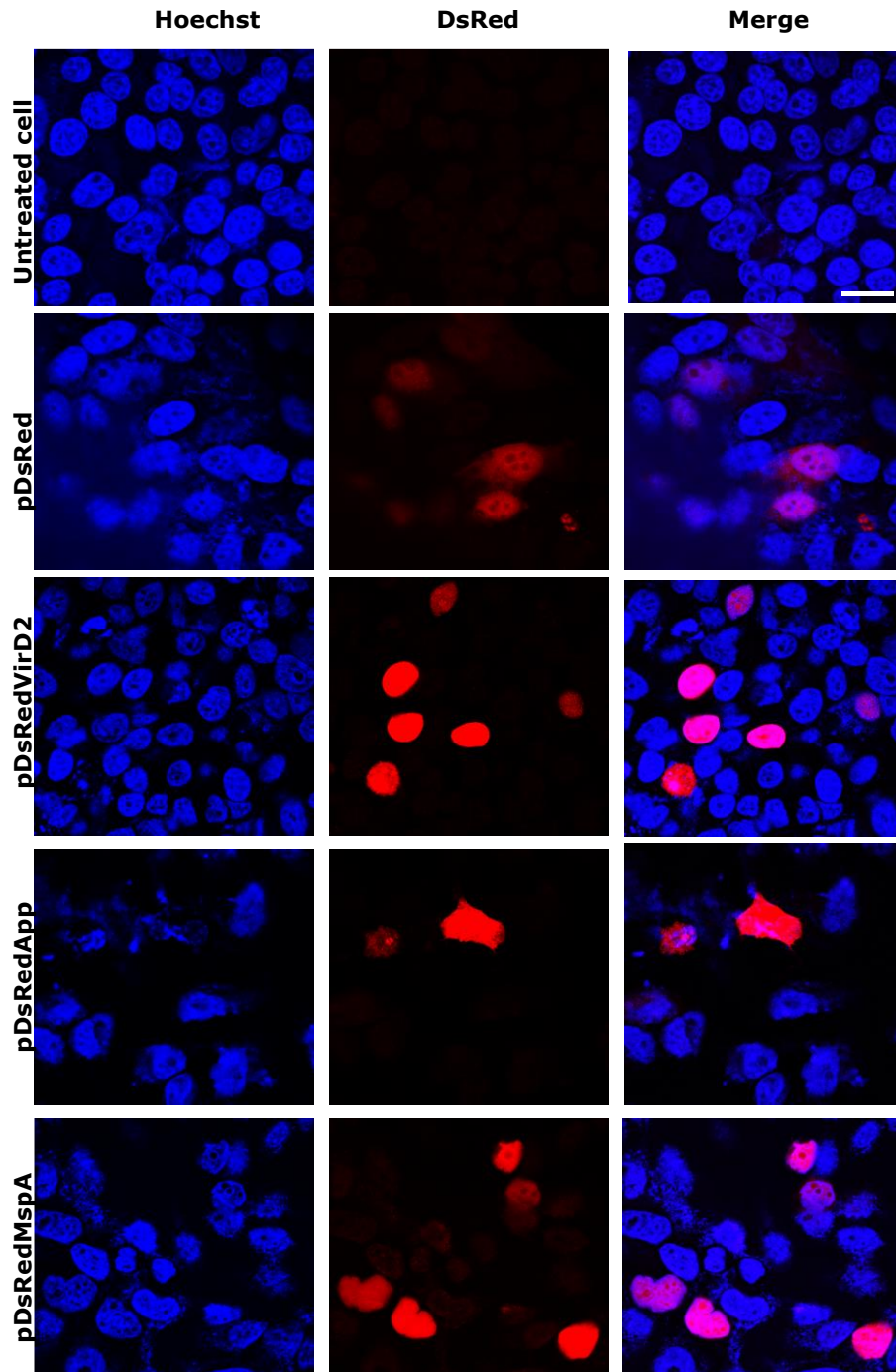


Figure 4.1: Nuclear localization of DsRedMspA in Hep-2 cells. Hep-2 cells were transfected with pDsRedMspA. In parallel pDsRedApp and pDsRedVirD2 were used as positive controls. Co-localization of DsRed-tagged recombinant proteins with Hoechst (stain for cell nuclei) in transfected cells was observed with

confocal microscopic images. All scale bars, 10 μ m and one of three independent experiment images is represented here.

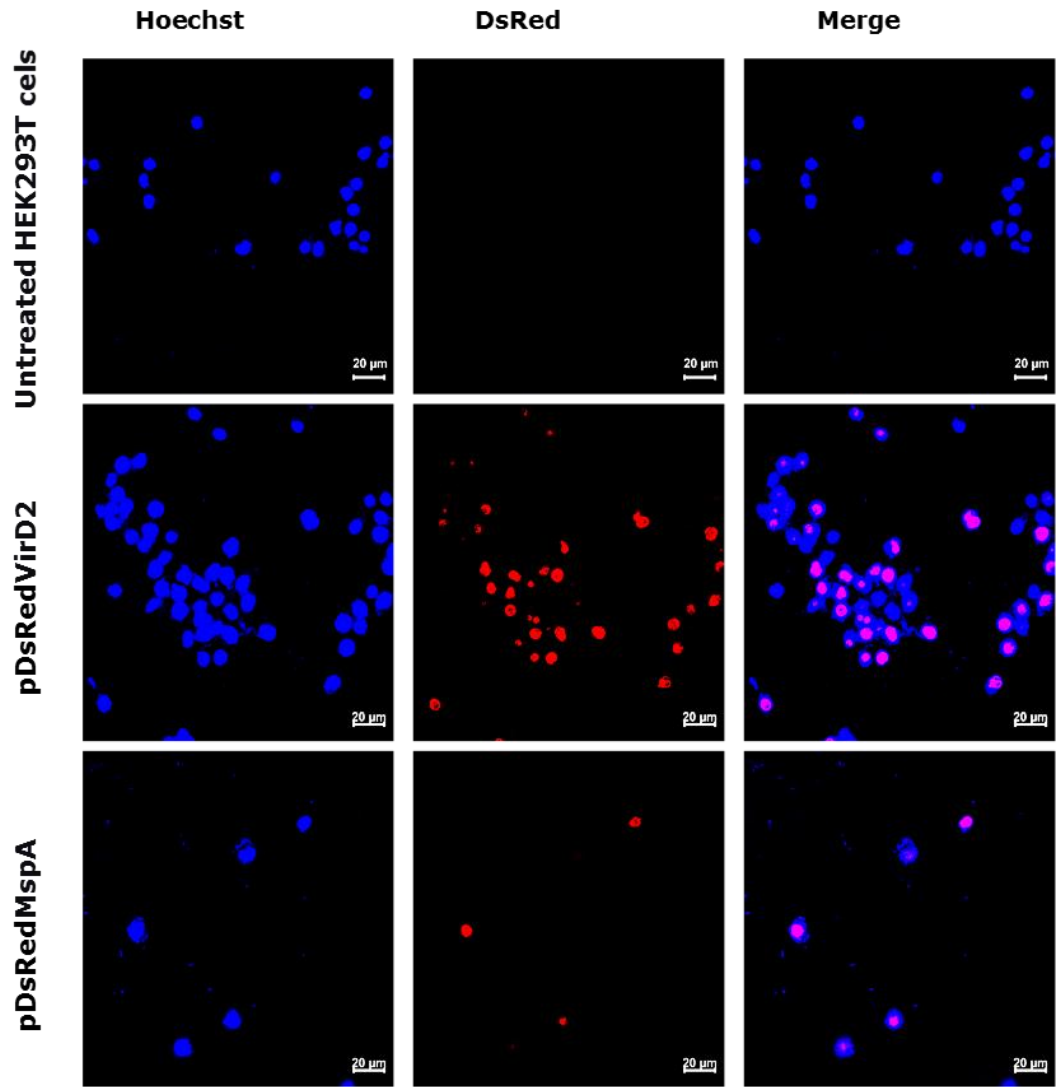


Figure 4.2: Representative images showing the nuclear localization of DsRedMspA in transfected HEK293T cells. HEK293T cells were transfected with pDsRedVirD2 and pDsRedMspA and after post-transfection the fixed cells were subjected to fluorescence staining as following the same protocol for Hep-2 cells. One of the two independent experiments shown here. All scale bars 20 μ m. Recombinant VirD2 and MspA showing similar level of co-localization with the blue nucleus of transfected cells. It is mentionable that the transfection

experiment for HEK293T cells was not optimised. For the consistency of the experiment, the same conditions were used for Hep-2 cells and HEK293T cells.

Having shown the nuclear localization of DsRedMspA, we quantified the co-localisation of DsRed labelled recombinant proteins (including DsRed, VirD2, App and MspA proteins) with the respective nuclei of transfected Hep-2 cells. Mean fluorescent intensities were derived from twenty different cells from three independent experiments. Figure 4.3 shows the descriptive statistics of the nuclear localisation of the fluorescent-tagged proteins. The red fluorescence intensities were measured coming from the region bounded by the nucleus (*i.e.* stained with Hoechst). From this, it can be concluded that there is significant co-localization of the VirD2, App and MspA proteins with the nucleus.

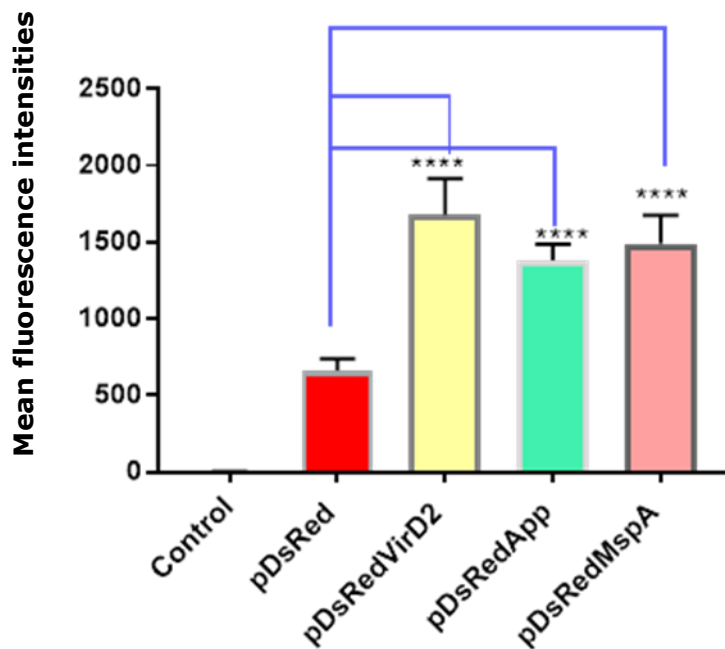


Figure 4.3: Intensities of DsRed-labelled recombinant proteins in the nucleus was quantified. Mean intensities were derived from the three independent experiments. Error bar means the value of SD. The experiment then analysed

with one-way ordinary Anova test and Tukey's test showed significant P value denotes **** $p < 0.0001$.

4.2.2. Role of MspA proteolytic activity in nuclear localization:

Several studies have shown that the catalytic serine residue of a protease plays a significant role in the proteolysis of host proteins, for instance, nuclear cleavage of histone H3 by MspA which may alter cell biology [215]. However, the role in the nuclear localization process has not been tested. Based on this, we attempted to investigate whether the proteolytic activity of MspA has any direct contribution to nuclear trafficking of this protein.

4.2.2.1. Construction of pDsRedMspA^{S241A}

Site directed mutagenesis was used to replace the active site serine to alanine. The 'AGC' codon encoding the relevant serine residue (position 241) in pDsRedMspA was substituted with 'GCT' encoding alanine using primer pair MspA^{S241A}Red-F and MspA^{S241A}Red-R (followed procedure describe in the Section 2.9.2). The PCR amplicon was confirmed based on the expected band size of the plasmid pDsRedMspA^{S241A} (not shown). The PCR product was then used in the KLD reaction (described in the section 2.9.3) and transformed into *E. coli* JM109 (described in the section 2.9.4). Thirteen kanamycin-resistant colonies were screened by plasmid extraction and DNA sequencing, but only one of them showed the presence of the desired substitution, and no PCR generated errors (Figure 4.4).

pDsRedMspA

```
GGCTTACTCGTCGGCGGCAGCCTGACCGACCAACCCCTTAACACCTACGCAATCGCCGGA
G L L V G G S L T D Q P L N T Y A I A G
GACAGCGGTTCCCCCCTGTTTGCCTTCGAC
D S G S P L F A F D
```

pDsRedMspA^{S241A}

```
GGCTTACTCGTCGGCGGCAGCCTGACCGACCAACCCCTTAACACCTACGCAATCGCCGGA
G L L V G G S L T D Q P L N T Y A I A G
GACGCTGGTTCCCCCCTGTTTGCCTTCGACAAG
D A G S P L F A F D K
```

Figure 4.4: DNA sequence of pDsRedMspA and pDsRedMspA^{S241A}. The AGC encoding serine was substituted to GCT encoding alanine in pDsRedMspA^{S241A} using site-directed mutagenesis using primer pairs MspARed^{S241A}-F and MspARed^{S241A}-R (Table-2.3).

4.2.2.2. Nuclear targeting by DsRedMspA^{S241A}

The nuclear localization of the inactive serine mutant protein encoded by pDsRedMspA^{S241A} was investigated in Hep-2 cells. As before, pDsRed, pDsRedMspA and pDsRedVirD2 were used as controls. No substantial reduction in nuclear localization of DsRedMspA^{S241A} was observed compared to DsRedMspA; with DsRedMspA and DsRedMspA^{S241A} both showing a similar pattern of nuclear targeting to DsRedVirD2 (Figure 4.5).

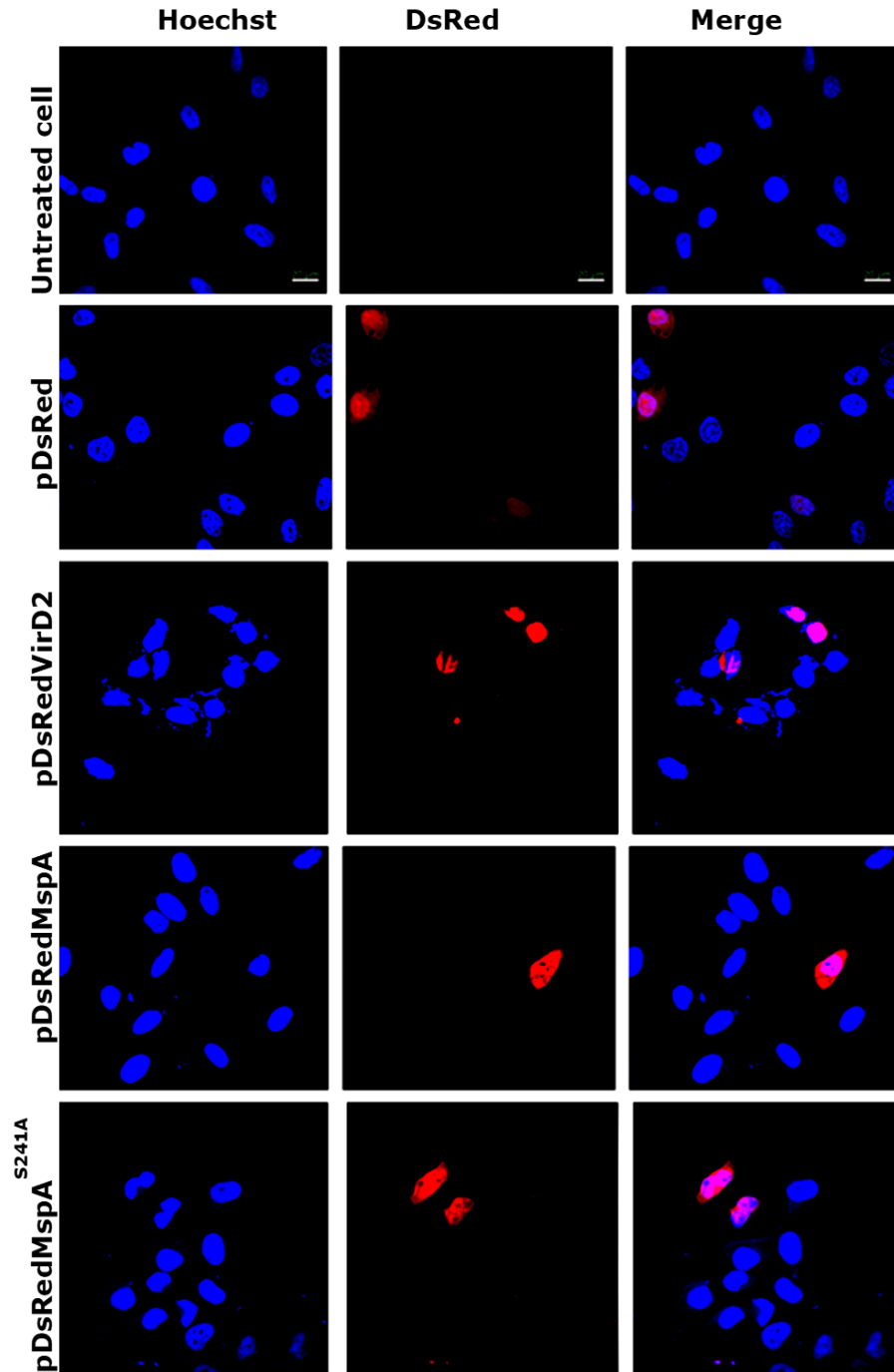


Figure 4.5: Confocal microscopic images showing the colocalization of DsRed-tagged MspA^{S241A} with the nucleus in transfected Hep-2 cells. Here, Hep-2 cells were transfected with pDsRed, pDsRedMspA, pDsRedMspA^{S241A} and pDsRedVirD2, respectively. The images do not show any noticeable difference

in nuclear localization between DsRedMspA and DsRedMspA^{S241A}. All scale bars 20µm. One of three experiments presented here.

This finding suggested that proteolytic activity does not influence nuclear targeting of MspA protein. Work described in chapter three, a similar result was found for App.

4.2.3. Screening of regions of MspA which facilitate nuclear localization

In this study the nuclear targeting of MspA in host cells has been confirmed, but how does a large molecule the size of MspA access the cell nucleus? Based on the theory of signal-mediated transportation of a large protein from the cytoplasm to the nucleus, it is likely that MspA contains an undefined NLS. To help localize this, we deleted two different, but overlapping regions from DsRedMspA.

4.2.3.1. Construction of pDsRedMspA^{Δ1037A to 1139I}

In work described in chapter three, we localized a functional NLS sequence in the α-peptide of App. In line with this, we created a mutant of DsRedMspA bearing a deletion between A¹⁰³⁷ to I¹¹³⁹ corresponding to the C-terminal region of MspA (akin to the α-peptide of App). This fragment contains some basic amino acids including arginine, lysine and serine residues. Before mutation, the secondary structure of MspA was analyzed with DNAMAN software to avoid the long helix portion (Figure 4.6). In this mutation, pDsRedMspA was used as DNA template and primer pair MspAReddel^{1037 to 1139}mt1-F4 and

MspA^{Reddel}^{1037 to 1139}mt1-R4 used for inverse PCR. The resulting PCR product had a deletion of approximately 300bp in *m*spA (expected size <8kb) and was designated as pDsRedMspA^{Δ1037A to 1139I} (Figure 4.7) after re-ligation using the unique *SpeI* site introduced at the site of deletion by the primers used. The deletion within pDsRedMspA^{Δ1037A-1139I} was confirmed by DNA sequencing.

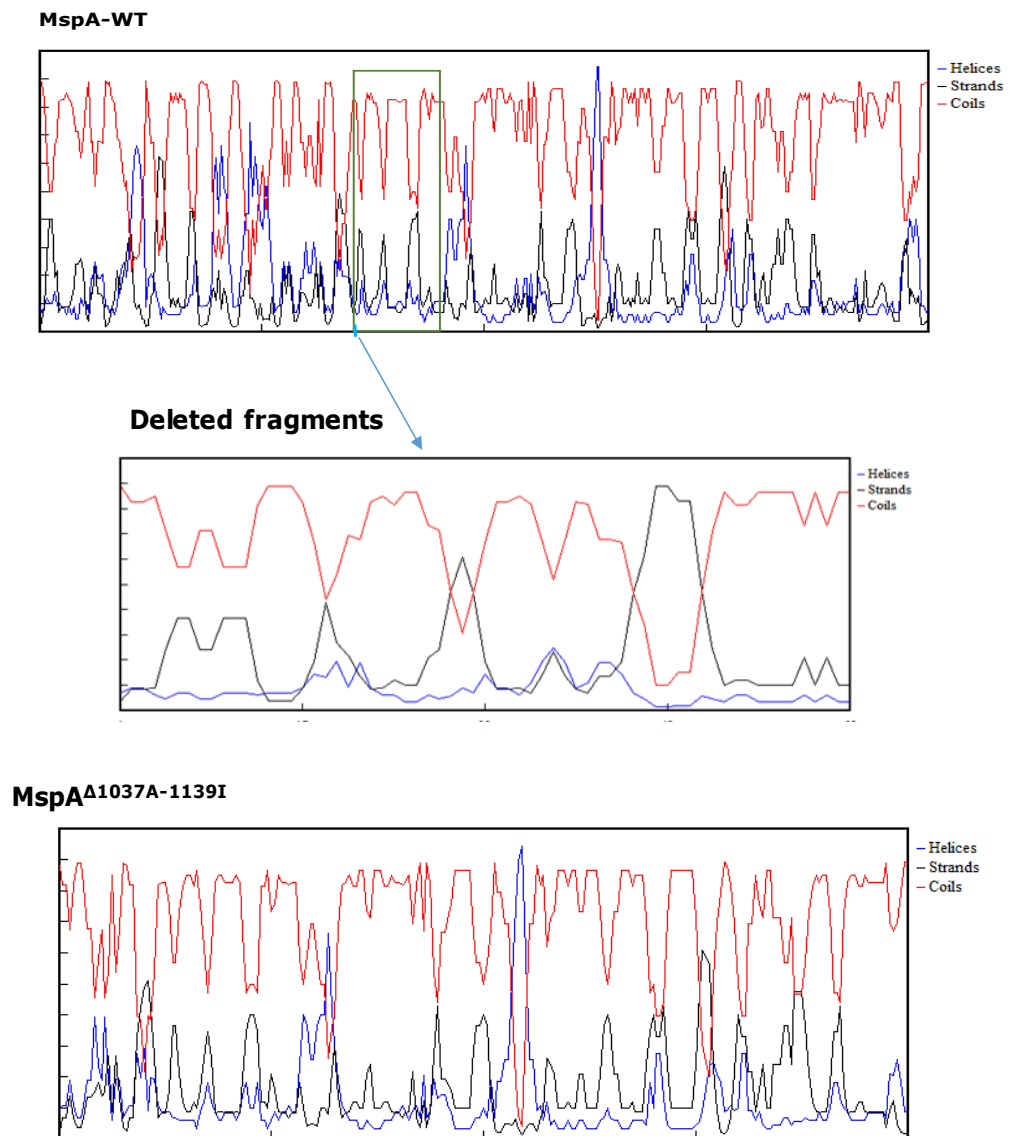


Figure 4.6: Predicted secondary structure of MspA WT and MspA^{Δ1037A-1139I} showing how the 1037A to 1139I region deleted from MspA avoided helical regions of the protein.

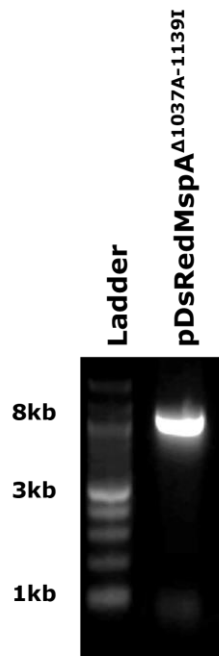


Figure 4.7: Inverse PCR mediated generation of plasmid pDsRedMspA^{Δ1037A-1139I}. 102 amino acids (A¹⁰³⁷ to I¹¹³⁹) were removed from DsRedApp via inverse PCR mediated deletion of the relevant region of *mspA* contained in pDsRedMspA and primer pair MspAReddel^{1037 to 1139}mt1-F4 and MspAReddel^{1037 to 1139}mt1-R4 used (Table-2.2). Lane1: DNA Ladder, lane2: I-PCR product representing pDsRedMspA^{Δ1037A-1139I}.

4.2.3.2. Subcellular localization assay of DsRedMspA^{Δ1037A-1139I} using Hep2-cells

DsRedMspA^{Δ1037A-1139I} was expressed in Hep-2 cells and its subcellular location observed in the transfected cells based on the red emission patterns of DsRed (Figure 4.8). Interestingly, no significant difference was appeared between the DsRedMspA and DsRedMspA^{Δ1037A-1139I}. This result indicated that the deletion of 102 amino acids had no direct effect on nuclear localization suggesting that this motif has no direct effect on MspA nuclear localization.

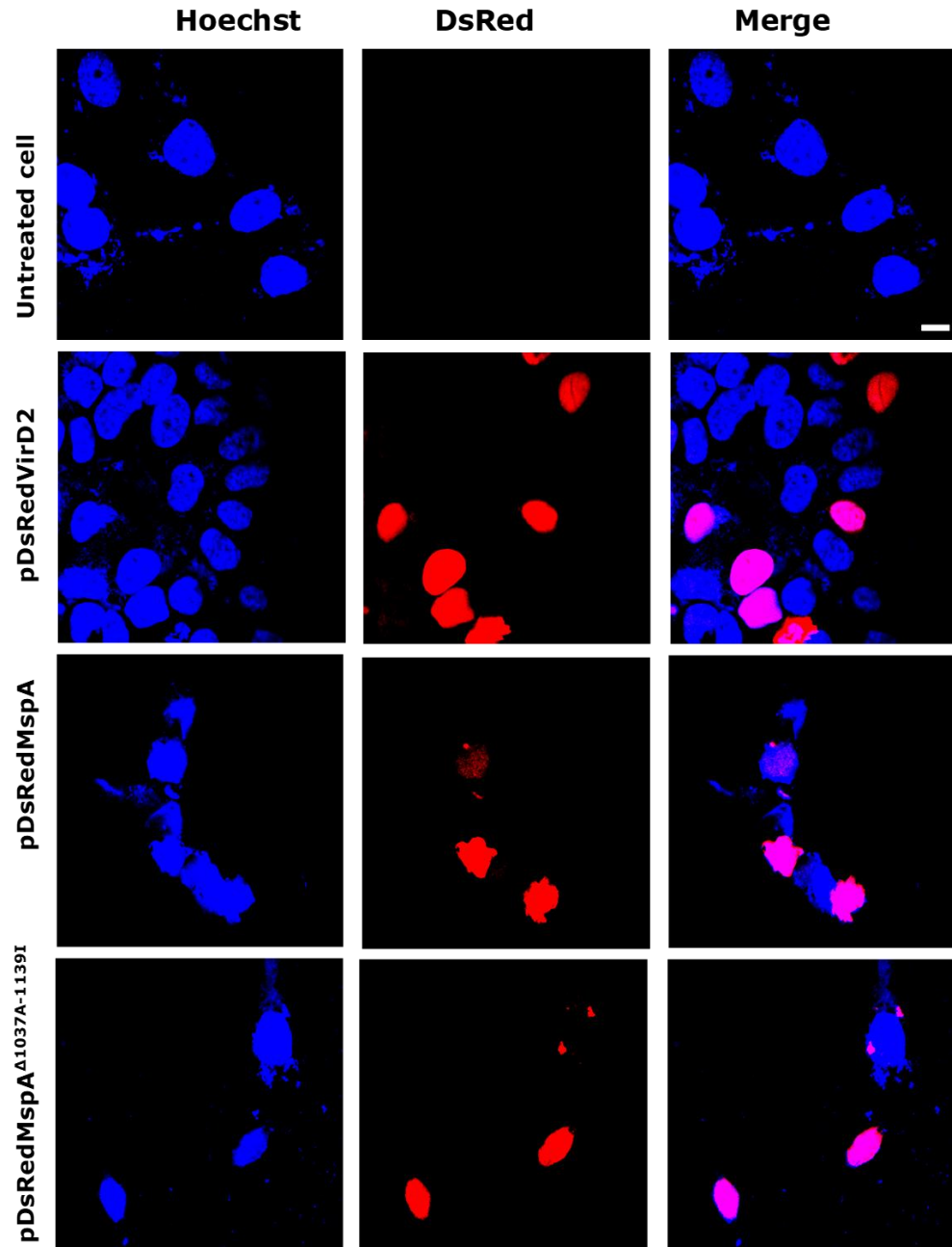


Figure 4.8: Confocal images showing cellular localization of DsRedMspA^{Δ1037A-1139I} in transfected Hep2 cells. Here Hep-2 cells were transfected with pDsRedVirD2, pDsRedMspA or pDsRedMspA^{Δ1037A-1139I} and the cell nuclei were stained with Hoechst before being viewed under confocal scanning microscope. The respected images illustrating the nuclear localization for DsRedVirD2, cytoplasmic and nuclear localization for pDsRedMspA and DsRedMspA^{Δ1037A-1139I}.

All the scale bars 10µm. Representative images from one of three experiments are shown here.

4.2.3.3. Characterising the specific motif that is required to direct MspA to the nuclear compartment

In the previous section 4.2.3.2, the truncated mutant DsRedMspA^{Δ1037A-1139I} exhibited clear localization into the nucleus suggesting the deleted region did not contain any NLS. Therefore, in order to identify the MspA motif required for nuclear trafficking, another truncated version of DsRedMspA was constructed. Mutagenesis of pDsRedMspA was carried out by inverse PCR in order to delete the amino acids D⁹⁹⁹ to A¹⁰⁷³ to generate pDsRedMspA^{ΔD999-A1073}. Kanamycin-resistant colonies were screened by DNA sequencing to confirm the mutation.

74 amino acids deleted from DsRedMspA
DISRQVQHSDATRQALQAWQNSQTELARIDSQVQYLSA
QLKQTDPLTGILTRAQNLCAAQGYSADIRQVAKAA

Figure 4.9: The 74 amino acids deleted from DsRedMspA to yield DsRedMspA^{ΔD999-A1073}. R indicates an arginine residue and K indicates a lysine residue.

4.2.3.4. Nuclear trafficking of DsRedMspA^{ΔD999-A1073}

To determine the ability of DsRedMspA^{ΔD999-A1073} to localize to the nucleus, pDsRedMspA^{ΔD999-A1073} was used for Hep-2 transfections and DsRed expression analyzed using the same approach as before. The cellular distribution of DsRedMspA^{ΔD999-A1073} showed different results compared to DsRedMspA. The wild type MspA was predominately accumulated in the nucleus and cytoplasm whereas the mutant MspA protein was located in the cytoplasm of most of the transfected cells, although some transfected cells showed evidence of red

protein accumulation in the nucleus at a substantial level (Figure 4.10). This difference in cellular localization suggested that the removal of these 74 amino acids containing some basic amino acids reduced the nuclear access of MspA. Alternatively, this deletion may have affecting MspA protein nuclear trafficking.

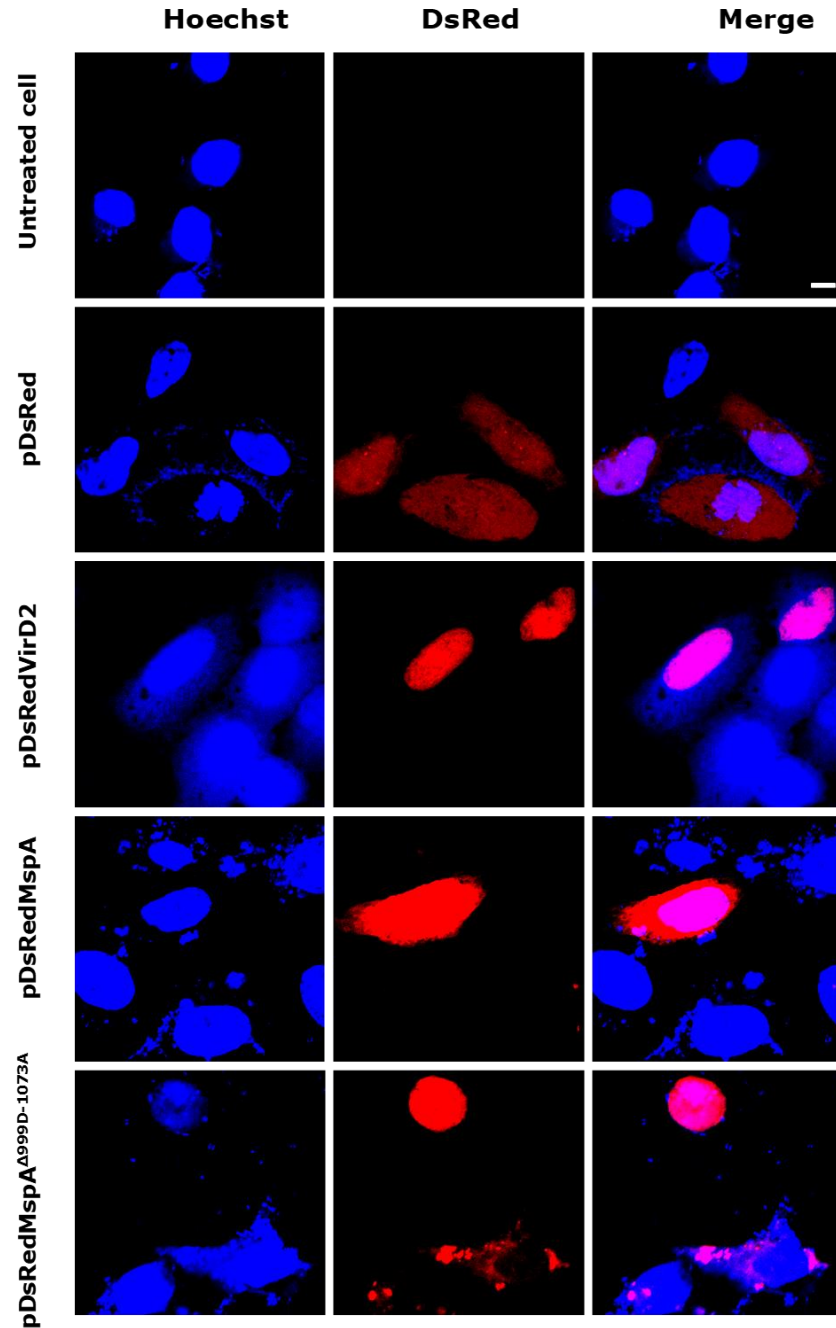


Figure 4.10: Cellular localization of DsRedMspA^{Δ999D-1073A}. Hep-2 cells were transfected with appropriate pDsRed plasmids encoding proteins of interest. The cells were fixed, stained with Hoescht and the distribution of DsRed-tagged proteins observed using confocal microscopy. All scale bars 5um. Representative images from one of three experiments are shown here. The DsRed tagged

MspA^{Δ999D-1073A} mutant showing localization into cytoplasm and for another cell showed accumulation into the nucleus of Hep-2 cells.

The MspA construction MspA^{Δ999D-1073A} mutant showed a different pattern of localization which was not observed with the other constructs of MspA (Figure 4.11). The pDsRedMspA^{Δ999D-1073A} mutant is located in the cytoplasm with some transfected cells and some are located into the nucleus. 21% cells showed nuclear localization and most of other cells showed punctate distribution into the cytoplasm (Figure 4.12).

This result demonstrated this mutant protein may not be as potent as the wild type of MspA for the nuclear trafficking.

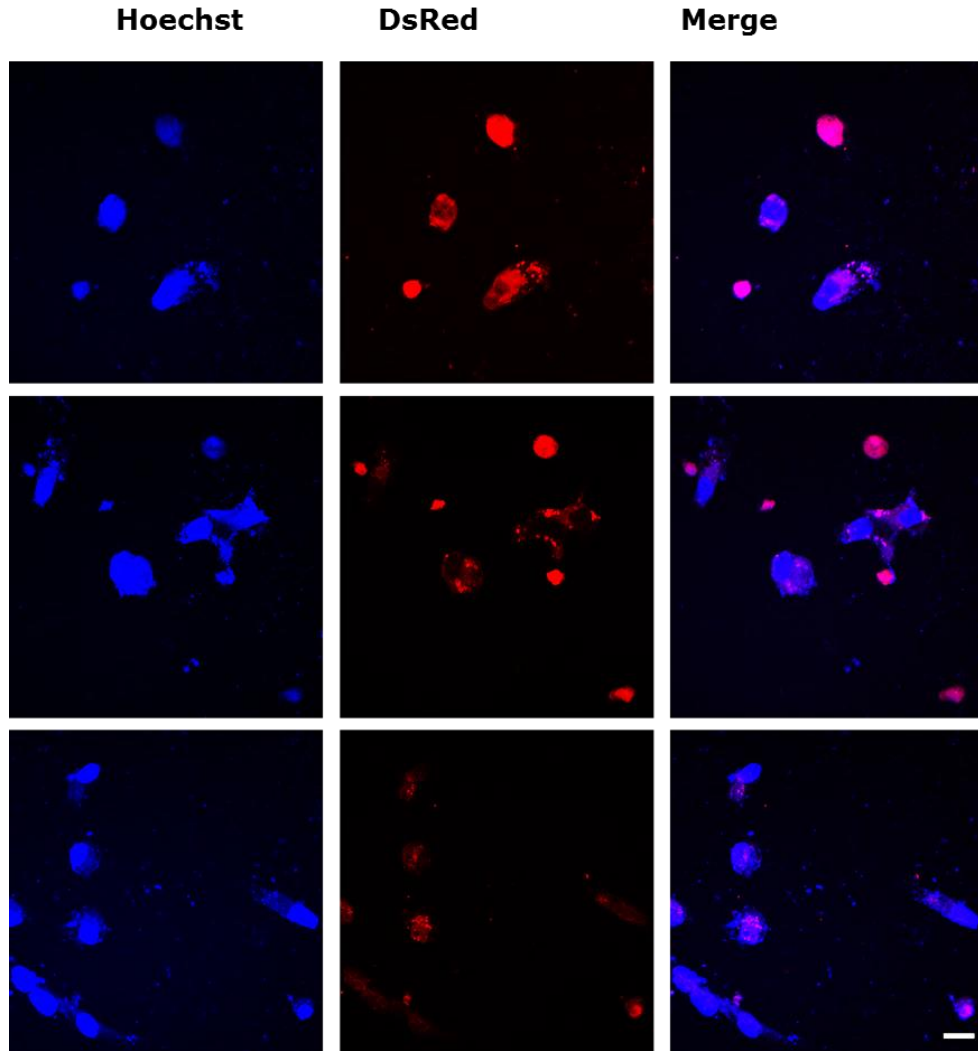


Figure 4.11: DsRedMspA^{Δ999D-1073A} shows various subcellular localization. Here, representative images showing the red (DsRed) and merge (DsRed + Hoechst) channels of different fields of MspA^{Δ999D-1073A} transfected cells. All the scale bars denoted 20μm.

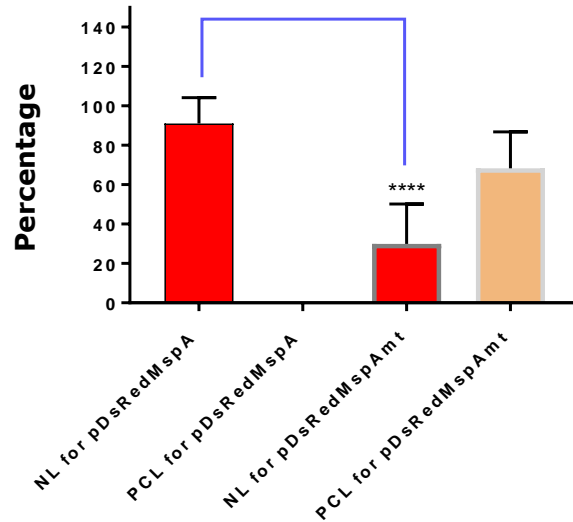


Figure 4.12: Protein localization of DsRedMspA and DsRedMspA^{Δ999D-1073A}. Here the data represents the percentage of transfected cells with nuclear localized (NL) or punctate cytoplasmic localised (PCL) DsRedMspA and DsRedMspA^{Δ999D-1073A}. The data was analysed by one-way Anova test and Dunnett's multiple comparisons test. Error bars: mean of values + SD. Here, **** means highly significant difference in nuclear localisation, the nuclear localization of the DsRedMspA vs DsRedMspA^{Δ999D-1073A} showed p-value is 0.0001. The results were calculated here from ten different fields from three independent experiments.

This result demonstrated that the region (D⁹⁹⁹ to A¹⁰⁷³) does not necessarily function as NLS but has an indirect impact on nuclear trafficking of MspA.

4.3. Discussion

This chapter describes the investigation of MspA nuclear targeting in host cells with the aim of identifying a functional NLS region. *N. meningitidis* is an extracellular pathogen which can interact with eukaryotic cells using several distinct cellular receptors [252]. The microorganism has a range of surface structures to communicate with host cells including Type IV pili, LOS and a number of outer membrane proteins, such as Opc and Opa opacity proteins, App [180], NadA [210] NhhA [204], and MspA [182] mediating the interaction of the meningococcus to host cells.

Previous studies have identified and characterized, MspA as an immunogenic meningococcal autotransporter protease with importance in meningococcal virulence [182]; however, the precise pathogenic mechanism remains unclear, although cleavage of histones is one possibility. Investigating the nuclear localization of MspA may lead to a better understanding of the role of the autotransporter protein in meningococcal pathogenesis. Moreover, it is becoming increasingly apparent that nuclear targeting by secreted proteins is a potential pathogenic mechanism in bacteria, although the nuclear targeting of the bacterial protein in question must be verified with experimental evidence first. Understanding the nuclear localisation of MspA may lead to a clearer explanation of the role of this autotransporter in meningococcal pathogenesis.

It was previously suggested that MspA protein targeted the nucleus after uptake by dendritic cells, although with the caveat that additional experiments were required to verify this [215]. To continue this research, the nuclear translocation of MspA was first confirmed in this study with the same approach used to demonstrate App nuclear localization and App was used as a positive control for a protein containing an NLS, with an additional positive control:

VirD2. The confocal microscopic images confirmed that MspA protein was clearly localized into the nucleus and also in the cytoplasm. The transfection efficiency of MspA was better than App, and no apoptosis was visually observed with MspA transfection. This result indicates the protein has a role of the nuclear localisation into the host cell and also showed consistency with the previous finding of our group [215].

The nuclear localization quantification of the co-localization of DsRed and Hoechst stain of the nuclei of the transfected cell provided evidence of that MspA localization is significant compared with DsRed.

To further support of the nuclear targeting potential of MspA, the nuclear localization experiments were carried out with different cell lines, including HEK293T cells. No apparent difference in nuclear targeting by DsRedMspA was observed, however, due to time restraints, experiments with HEK293T cells were only carried out two times. Ideally, they should be repeated at least three times to confirm this finding.

To exclude a requirement for MspA proteolytic activity during nuclear localisation, the active site serine residue in MspA was substituted with alanine. The serine mutant version of DsRedMspA was expressed and localized to the nucleus just like the wild type DsRedMspA. This would suggest that the serine residue (and the proteolytic activity it confers) are not required for nuclear localization, or that the alanine replacement can overcome any detrimental effect of the loss of the serine on nuclear localization.

In the context of the MspA passenger domain, it is not clear if any specific region is required to facilitate nuclear localization. The protein does not appear to possess any functional NLS sequence that can direct the protein into the nucleus. The molecular mass of the MspA passenger domain is greater than

40kDa, which suggests the presence of an active NLS sequence. So, we aimed to define which motif or region of MspA was required for nuclear trafficking. It was reported by Besbes et al. that nuclear trafficking by meningococcal autotransporter proteins differs depending on the presence or absence of the α -peptide region [194]. In the previous chapter, we also found that App nuclear trafficking was NLS dependent. To define the functional motifs required for MspA nuclear trafficking, truncated mutants were made where different regions of MspA were deleted, and then their nuclear targeting capacity was investigated.

Firstly, amino acids between A¹⁰³⁷ to I¹¹³⁹ were removed as this region contains several basic residues at positions from 1122 to 1133, but the nuclear localisation of this deletion mutant did not show any distinguishable difference from DsRedMspA. This result indicated that the mutation did not have any effect on nuclear targeting either because it is not required for nuclear targeting or, alternatively, another region of the protein can compensate for the loss of this fragment; however, this prediction requires additional experimental confirmation. Our finding suggests that the α -peptide region of MspA does not contain any NLS signal.

In subsequent analysis, an overlapping fragment was removed to create another truncated mutant (MspA ^{Δ 999D-1073A}). The subcellular localization of this protein showed a difference to DsRedMspA; the protein was able to localize to the nucleus in a few transfected cells whereas most of the transfected cells showed the punctate localization in the cytoplasm only. This deletion of the fragment reduced the nuclear localization but did not abolish it. The sequence analysis and secondary structure prediction of this stretch of amino acids suggest it is mostly structured into helices. It is possible that the lack of this region affected the structure (and or stability) of the expressed MspA.

Overall, in this study, we did not find any specific region of MspA which controls nuclear trafficking. It might be possible that MspA translocation into the nucleus occurs via an NLS-independent pathway, but further studies are required to determine the mechanism by which MspA accesses the nucleus in host cells.

CHAPTER 5: App and MspA mediated cleavage of host cell histones

5.1. Introduction

Having suggested the nuclear localization of the App and MspA proteins, the question of the mechanism of interaction of these proteins with the chromatin of the nucleus has also been asked. In all eukaryotic cells, DNA is wrapped with histone proteins and packed into the nucleus of the cell via its compaction into chromatin. Chromatin is subjected to biological processes including gene regulation and transcription, replication, mitosis and apoptosis. Chromatin is made of repeating units of nucleosomes, which consist of approximately 147 base pairs of DNAs wrapped around a histone octamer consisting of two copies of each of the core histones (H2A, H2B, H3, and H4) form the centre of the nucleosomes. Core Histones contain H2A-H2B dimer and H3-H4 tetramer [253]. Linker histone H1 is positioned on top of the nucleosome core particles stabilizing higher-order chromatin structure [254].

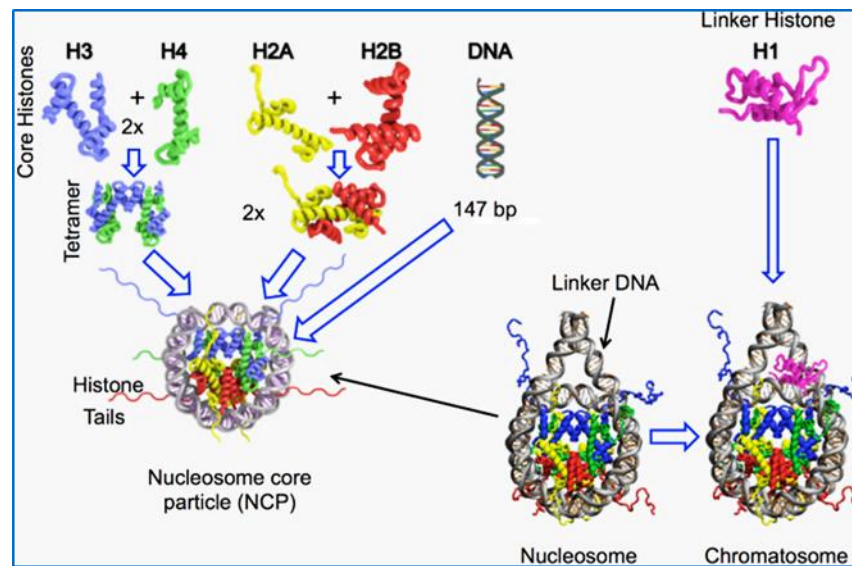


Figure 5.1: Nucleosome organization diagram. Adapted from: Draizen, Shaytan et al. [254]. A nucleosome contains an octamer of histone molecules. An octamer contains an H3-H4 tetramer and two H2A-H2B dimers.

The core histones contain two common domains: histone folding and histone tail domains. The N-terminal tail of four core histones and the C-terminal tail of H2A and H2B protrude outside the nucleosome, which undergo a variety of post-translational modifications (PTMs) including methylation, acetylation, propionylation, butylation. Most of the modifications happen in the N-terminal extensions of the histones and are reversible in nature.

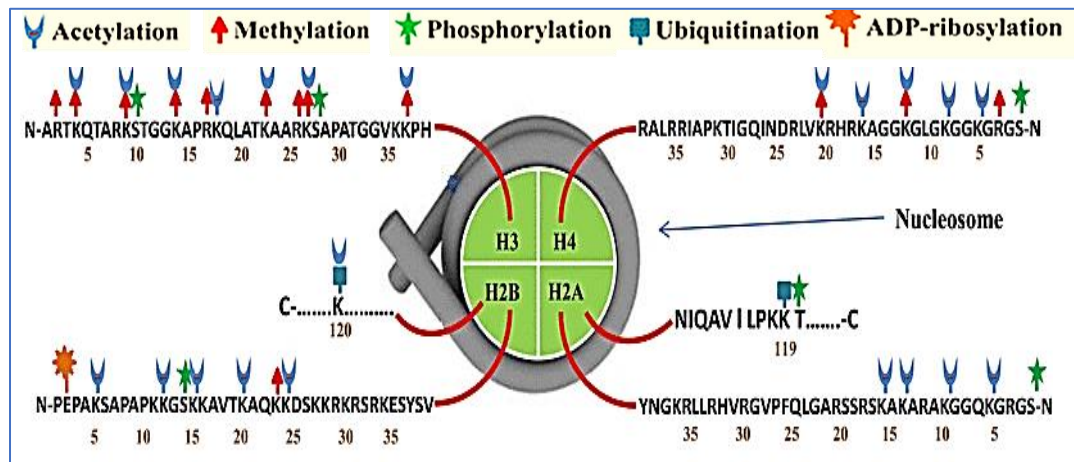


Figure 5.2: Histones undergoes various reversible PTMs during different biological processes. PTMs of histone tails such as methylation, acetylation, phosphorylation, ubiquitinylation and ribosylation. Here showed- Adapted from: Azad and Tomar et al. [255].

In eukaryotic cell nuclei, all the DNA-template processes are imprinted in the chromatin structures. Histone proteins make a significant contribution to the regulation and maintenance of chromatin structure. Post-translational modifications (PTMs) of histone help to modulate chromatin functions. Emerging evidence suggests that it is not only PTMs like methylation, acetylation and phosphorylation of amino acids, but also histone clipping (*i.e.* proteolysis of the N-terminal tails of histones), which play a fundamental role in the epigenetic regulation of cellular processes [255, 256].

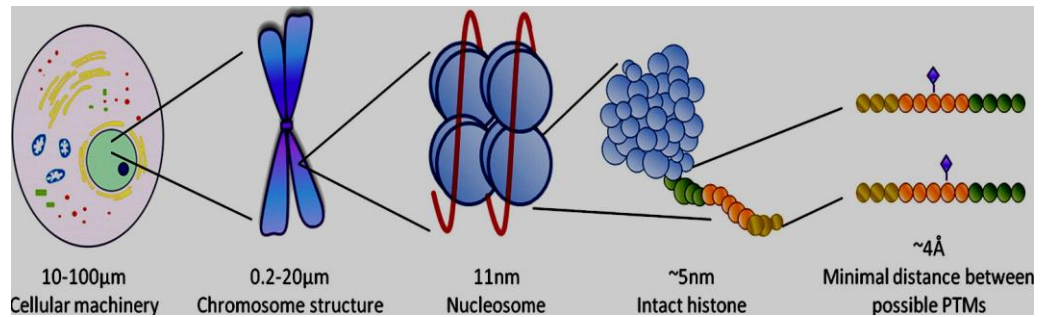


Figure 5.3: A schematic overview of the N-terminal tails of core histones. A minor change in histone modification can lead to a fundamental amendment in the cellular machinery of the green nucleus showed here. Adapted from :Simone et al. [257].

Histone proteolytic processing is associated with the elimination of histone tails resulting in the formation of nucleosomes lacking certain PTMs. This may cause an irreversible change in the chromatin structure as the cleaved tails cannot be repaired or re-ligated, which affects chromatin plasticity. This research study focuses on one histone modification: histone clipping, to further understand the roles played by App and MspA in the clipping of histone tails on the observation of all core histone clipping by App and MspA autotransporters.

Histone clipping is carried out by certain proteases specific to histone tails. Recently, several studies have revealed that microbial proteases can cleave histones and that histone proteolysis has been implicated in the regulation of genes [255, 258]. Indeed, many reports characterized cleavage sites and described the susceptibility or degradation of histones to serine proteases [259-261].

The autotransporter proteins App and MspA belong to the S6 peptidase family, bind to host histones, and can cleave recombinant histone H3. The study focused on further investigating the App and MspA mediated proteolytic cleavage of various histones by utilizing core histones purified from cultured

human cells as cleavage substrates to compare with results obtained using recombinant histones. The recombinant histones lack post-translation modification (PTM), whilst cell-derived histones undergo PTM. Therefore, Hep-2 cell-derived histones will be closer to native histones in cells that meningococci will likely encounter during infection. The comparison will show whether native PTM has any influence on APP- or MspA-mediated histone cleavage.

Histones H2A, H2B, H4 and H1 have antimicrobial properties and thus comprise part of the host innate defence system. Their antimicrobial properties include bacterial cell membrane permeabilization, binding to bacterial DNA and RNA, binding to bacterial lipopolysaccharide (LPS), and entrapment of pathogens as a component of neutrophil extracellular traps (NETs). Histones are released from neutrophils and from dead cells during apoptosis and in response to the presence of endotoxin [262].

5.2. Results

5.2.1. Purification of recombinant His-tagged App and MspA

To examine the proteolytic activity of the meningococcal autotransporters against either cell-derived or recombinant histones, the passenger domains of App, MspA and engineered variants in which the predicted active site serine residues had been mutated, were expressed in *E. coli* BL21-Gold (DE3) cells. Autotransporter proteins were purified as fusions with *E. coli* Trigger Factor (TF) using the cold shock expression vector pColdTF. In each case, optimal expression was obtained at 15°C with IPTG-induction for 24 h (data not shown). To confirm recombinant protein purification, whole-cell lysates from IPTG-induced cultures were separated on SDS-PAGE gels. The analysis showed expected bands of *ca.* 190kDa, which is the predicted size of the App and MspA fusion proteins (consisting of the passenger domain with His-tag and TF-tag) (Figure 5.4).

The identities of the induced bands were confirmed using anti-penta-His antibodies in immunoblot analysis (Figure 5.4 E).

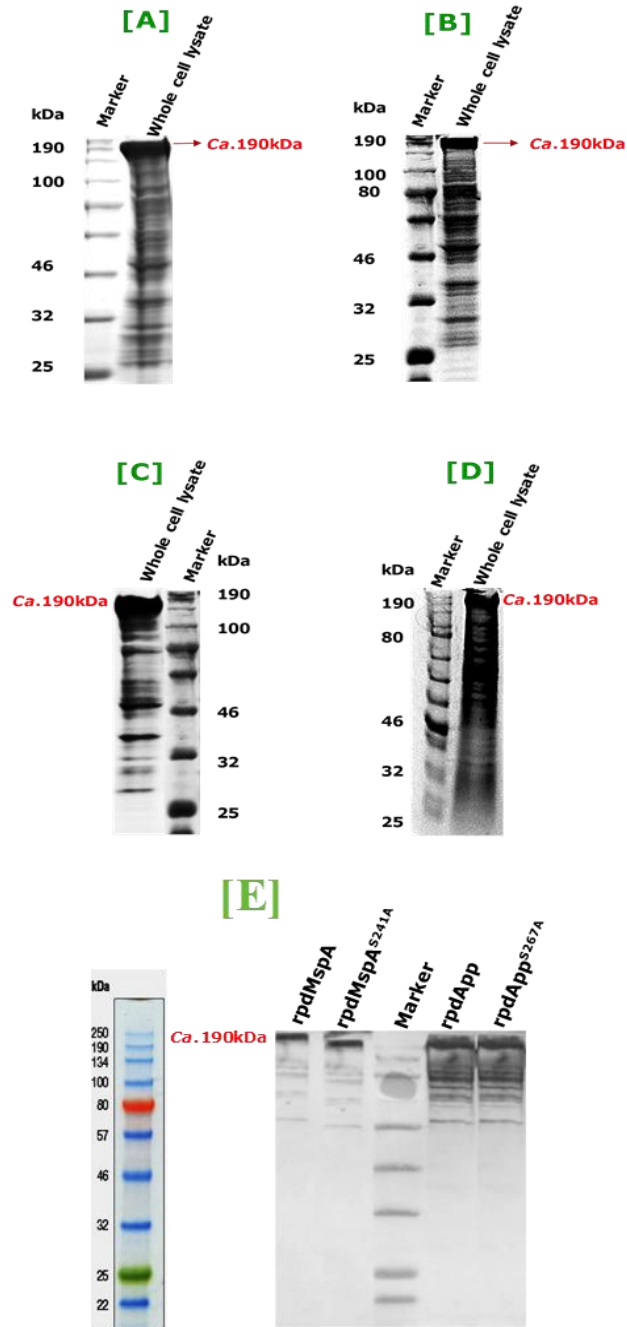


Figure 5.4: Representative images showing the induction of expression of recombinant autotransporter proteins genes in the whole cell lysate. [A]: *rpdApp*, [B]: *rpdApp*^{S267A}, [C]: *rpdMspA* and [D]: *rpdMspA*^{S241A} in IPTG-induced *E. coli* cells, respectively. Immunoblot analysis [E] using anti-penta-His antibodies confirmed recombinant App and MspA expression. *rpdMspA* and *rpdMspA*^{S241A} both are same in size. MspA mutant and all the (feint) bands below

the autotransporter are slightly displaced. It is possible that the gel is 'smiling' (i.e. proteins towards the edge of the gel are slightly retarded compared to those in the middle, presumably reflecting how the current flows through the gel).

5.2.2. Purification of recombinant App and MspA proteins

Recombinant His-tagged rpdApp, rpdApp^{S267A}, rpdMspA and rpdMspA^{S241A} proteins were purified from soluble lysates of IPTG-induced cultures under non-denaturing conditions using an AKTA Prime Plus and Ni-columns. In the purification process, firstly the His-tagged proteins were bound to nickel ions on the purification column. Then non-specifically bound proteins were removed by washing and the recombinant protein eluted using a high-imidazole-containing elution buffer. The corresponding peaks of the elution fractions evident from the purification chromatogram were resolved by SDS-PAGE to confirm the protein purification. The desired bands of *ca.* 190kDa corresponding to rpdApp and rpdMspA were observed (Figure 5.5).

The fractions containing the desired purified proteins were combined and desalted. The identity and purity of the purified rpdApp and rpdMspA proteins were further confirmed with immunoblotting analysis using anti-penta histidine antibodies.

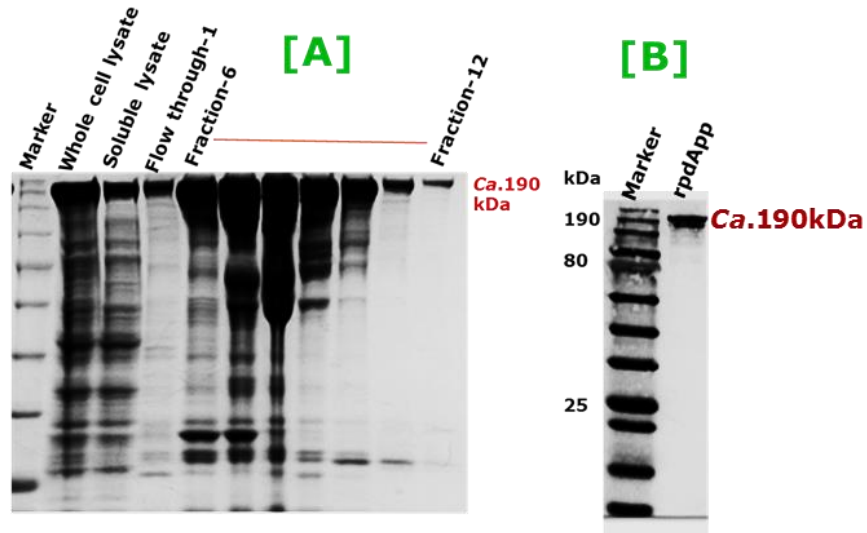


Figure 5.5: Purification of rpdApp protein. SDS-PAGE (left) and immunoblot analysis (right) demonstrating purification of rpdApp. *E. coli* BL21-Gold (DE3) cells harbouring pColdTF-App were grown until the exponential phase and induced with 1 mM IPTG. After 24 h of induction, cells were harvested by centrifugation and the harvested cells used for purification using AKTA prime. The eluate showed the corresponding protein size 190kDa. In panel [A] lane 1: pre-stained protein marker, lane 2: whole cell lysate, lane 3: soluble lysate, lane 4: flow through-1, lane 5 to lane 11: represent the eluted fractions from 6 to 12. [B] Immunoblotting analysis of rpdApp using anti-penta histidine antibody.

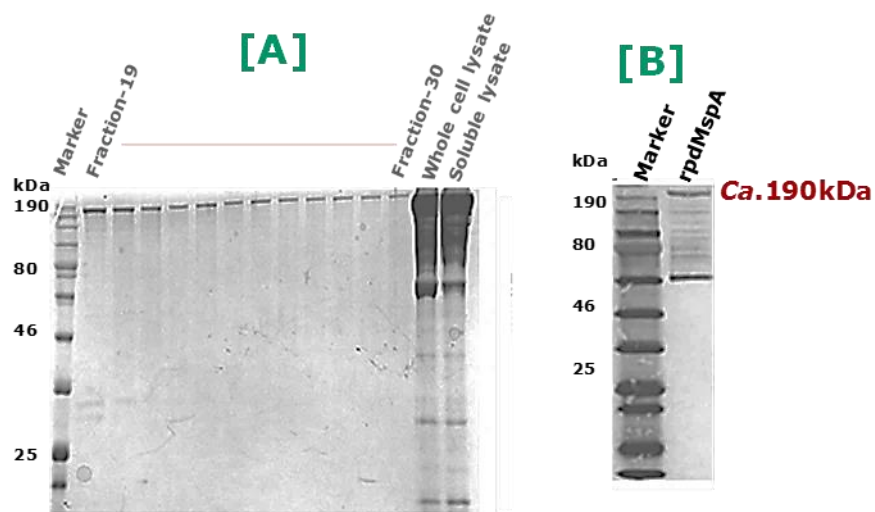


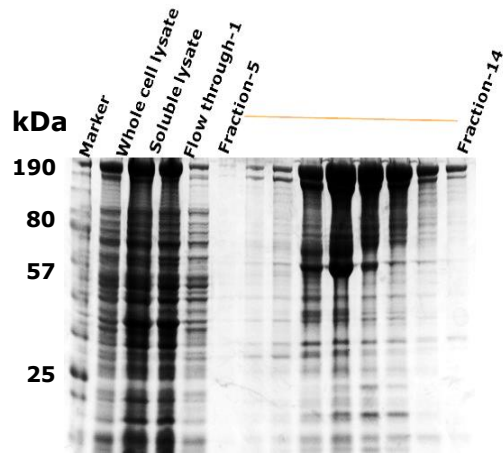
Figure 5.6: Expression and purification of rpdMspA protein. *E.coli* BL21-Gold (DE3) cells harbouring pColdTF-MspA were used. [A] Purified eluted fractions of the proteins were solved on SDS-PAGE. Lane 1: pre-stained protein marker, lane 2 to lane 13: eluted fractions from 19 to 30, lane 14: whole cell lysate, lane 15: soluble lysate. [B] Immunoblotting analysis of rpdMspA using anti-penta histidine antibody.

The extra bands of rpdMspA on blot must have the his-tag on them because they are detected by the anti-penta his Ab. The degradation might be because either the recombinant protein cleaves itself and/or it is degraded by *E. coli* proteases. The prevent of the degradation by including protease inhibitors in the purification buffers couldn't do that because the inhibitors are very difficult to get rid of and needed the purified AT to be functional for the cleavage assays.

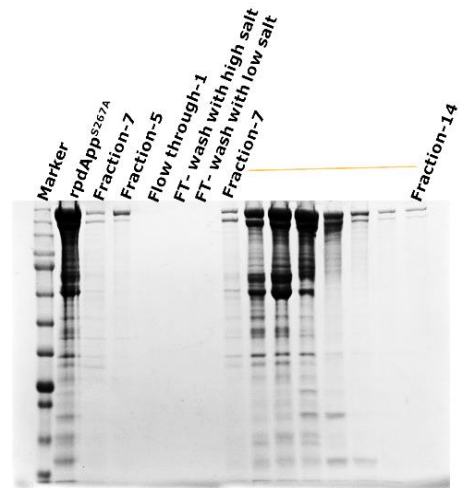
To optimize purity of the mutant proteins, several modifications to the purification process were tested, including using different concentrations of imidazole in the wash buffer, where a high salt buffer was used. The purity of the proteins were monitored using SDS-PAGE and immunoblotting analysis throughout the purification process. In the first optimization experiment (rpdApp^{S267A} prep 1), column-bound rpdApp^{S267A} was washed with 30mM imidazole-containing wash buffer, before being eluted with 500mM imidazole-containing buffer. SDS analysis showed the His-tagged recombinant protein corresponding to the full length rpdApp^{S267A} with more additional indistinct non-specific Proteins (Figure 5.7 A). In an attempt to reduce the impurities in rpdApp^{S267A} prep 1, the purified protein was reloaded onto a fresh, clean Ni-column and washed with high-salt-containing wash buffer and subsequently

rewashed with low salt containing wash buffer and re-purified using AKTA prime plus with IMAC. Unfortunately, this modification was unsuccessful in attempting to improve purity, and no apparent difference observed with the previous pep between the rpdApp^{S267A} prep2, where a high salt wash buffer was used (Figure 5.7 [B]). SDS-PAGE and immunoblotting analysis demonstrated that the same level of purity was obtained where some additional faint bands also come out with rpdApp^{S267A} on the blot ((Figure 5.7 [D]). Consequently, to improve the purity of the rpdApp^{S267A} protein, the next attempt used 50mM imidazole in wash buffer (Figure 5.7 [C]). Afterwards, the purity of all three preps of rpdApp^{S267A} protein was compared by SDS-PAGE and immunoblotting. This confirmed the higher purity of rpdApp^{S267A} protein prep 3, as a result of showing the strong Protein corresponding to rpdApp^{S267A} without so many other additional bands. This prep was therefore used in subsequent cleavage experiments. Similarly, rpdMspA^{S241A} purification was also optimized (Figure 5.8) and 50mM imidazole-containing wash buffer found to be optimum for purification.

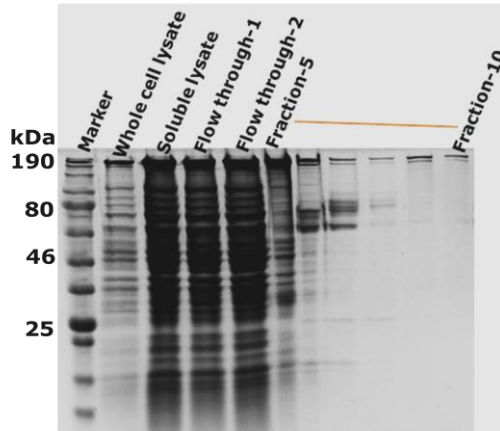
[A]



[B]



[C]



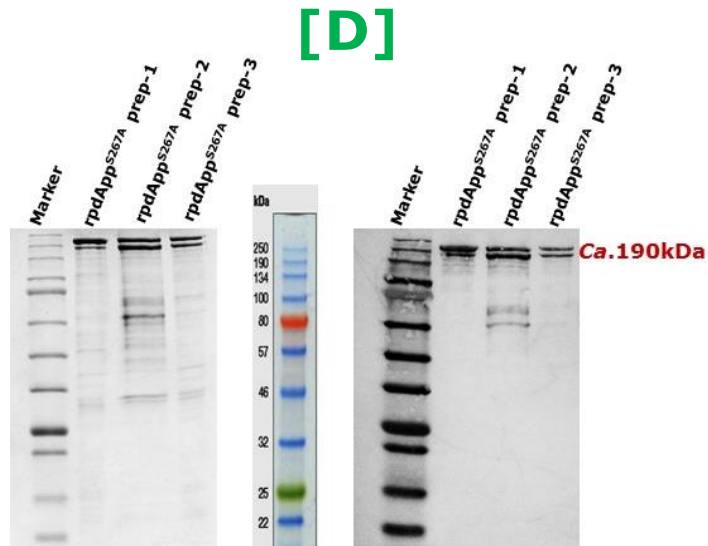


Figure 5.7: Purification of rpdApp^{S267A} protein. [A] rpdApp^{S267A} prep 1 protein purification using 30mM IMD in the wash buffer. [B] Purified rpdApp^{S267A} prep 2 where high salt-containing wash buffer was used in purification. In this purification, rpdApp^{S267A} prep 1 was reloaded on the fresh Ni-column and washed with 1.5M high salt concentration wash buffer and re-purified the protein by AKTA prime plus. [C] rpdApp^{S267A} prep 3 mutant protein purification using 50mM IMD in wash buffer. [D] All the purified preps of rpdApp^{S267A} were analysed by SDS-PAGE (left) and immunoblotting (right) using anti-penta His antibody. Lane 1: pre-stained protein marker, lane 2: rpdApp^{S267A} prep 1, lane 3: rpdApp^{S267A} prep 2, lane 4: rpdApp^{S267A} prep 3. Immunoblotting analysis confirmed the purity of rpdApp^{S267A} protein prep 3 which was eluted with 50mM imidazole-containing wash buffer in purification process. Here, App proteins contains a slightly smaller protein. It is possible that there is partial autocleavage that results in this slightly smaller size protein observed. This MIGHT contain the trigger factor moiety but is unlikely to be a precise cleavage at the fusion site.

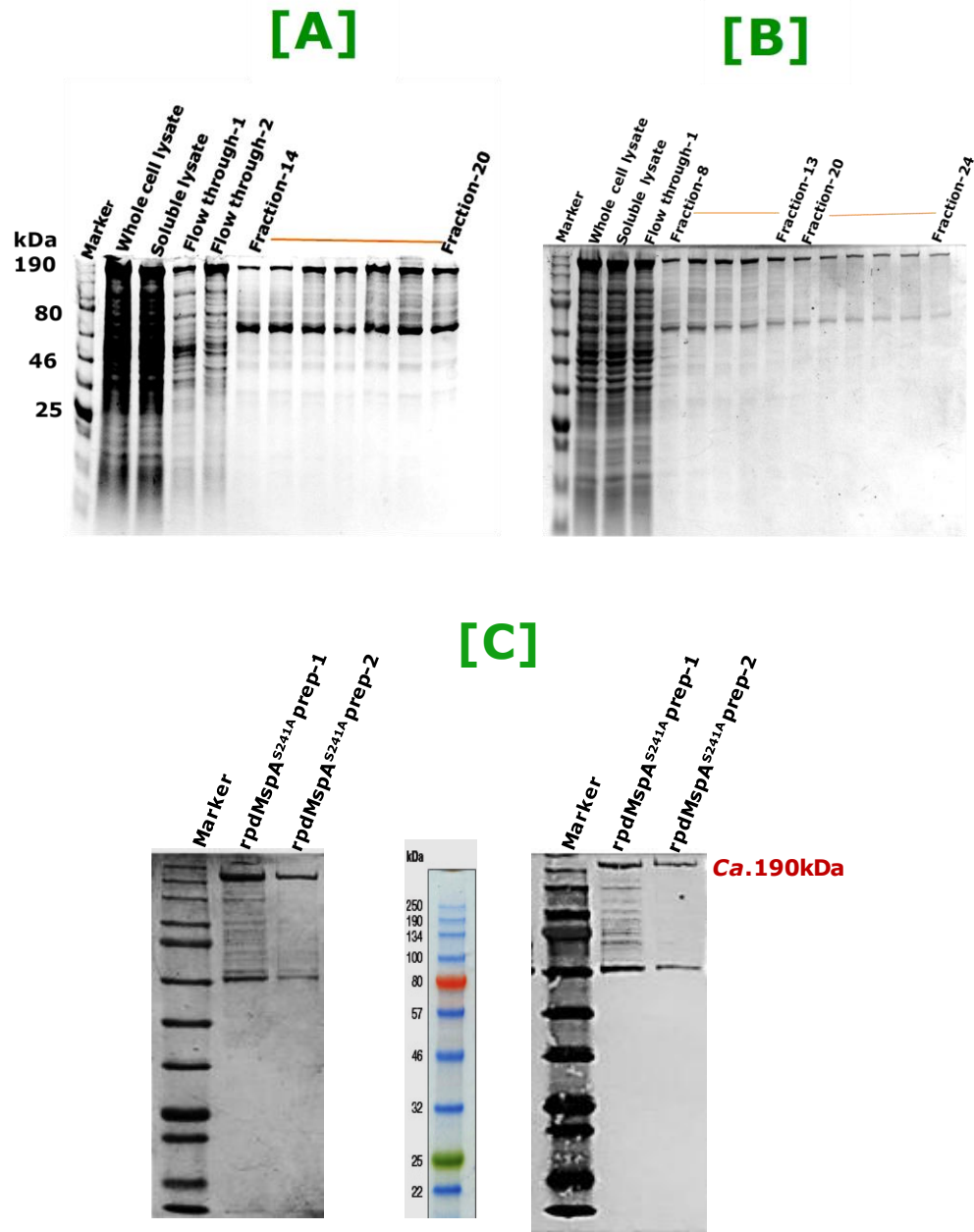


Figure 5.8: rpdMspA^{S241A} expression and purification. *E. coli* BL21-Gold (DE3) cells harbouring pColdTF-MspA^{S241A} were used. [A] Purified rpdMspA^{S241A} prep 1 (used 30mM-containing IMD wash buffer), [B] Purified rpdMspA^{S241A} prep 2 (used 50mM-containing IMD wash buffer). [C] Comparison of the purity of rpdMspA^{S241A} preps. SDS-PAGE (left) and immunoblot analysis (right).. confirmed the presence and purity of His-tagged rpdMspA^{S241A} proteins. rpdMspA^{S241A} prep 2 shows less yield, but higher purity.

5.2.3. Purification of major histones from Hep-2 cells

Our group previously reported the clipping of recombinant histone H3 using rpdApp and rpdMspA. In this present study, we examined the interaction of App and MspA proteins with cell-derived native histones in parallel to recombinant histones because native histones are closer to the *in vivo* scenario than recombinant histones. Cell-derived native histones were purified from Hep-2 cell lysates using the Active motif Histone Purification kit (described in the section 2.20). Aliquots were taken during different stages of the purification process, and the presence of histones visualised by SDS-PAGE analysis (Figure 5.9). The five main classes of histones families: H1, H2A, H2B, H3 and H4 were identified based on the molecular weight of the proteins by staining of the proteins with Coomassie Blue stain. The isolated fractions corresponding to H2A & H2B (elution 1 to 3) showed apparent molecular weights of *ca.* 14-17kDa. H3 histone showed molecular weight of *ca.* 17kDa and co-eluted with the 11kDa H4 histone. H1 histone showed apparent molecular weights of *ca.* 32kDa which are co-eluted with H2A and H2B (elution 1 of H2A and H2B). The concentration of purified histones was determined as 200µg/ml (H2A-H2B) and 80µg/ml (H3-H4) using the BCA protein assay kit.

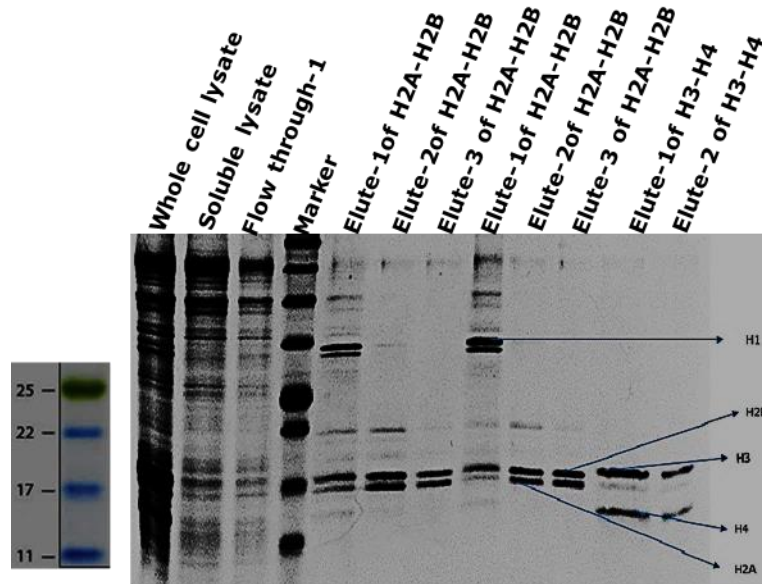


Figure 5.9: Successful histone purification from Hep-2 cells.

16% SDS-PAGE analysis of fractions used in the histone purification process. Lane 1: whole cell lysate, lane 2: soluble lysate, lane 3: flow-through, lane 4: pre-stained molecular marker, lanes 5 to 10: elutions 1, 2 and 3 of the H2A-H2B histones, lanes 11-12: elutions 1 and 2 of the H3-H4 histones. A pre-equilibrated histone purification column was used. Here, the histones aliquots were taken at different stages of two different purification process.

5.2.4. Identification of cell-derived histones

All five classes of histones were extracted and purified from the cell lysate of Hep-2 cells and were initially distinguished by their characteristic molecular weights (H1: 31-33kDa, H2A: 14kDa, H2B: 15-17kDa, H3: 16-17kDa, H4: 10-11kDa). To confirm the identity of the isolated histones, cell-derived H2A, H2B, H3 and H4 were analysed by western blot analysis using specific anti-histones antibodies including anti-Histone-H3 (ab1791), anti-Histone H4 antibody (ab10158), anti-Histone H2A antibody (ab18255) and anti-Histone H2B antibody (ab1790) and compared with the respective human recombinant histone (Figure 5.10).

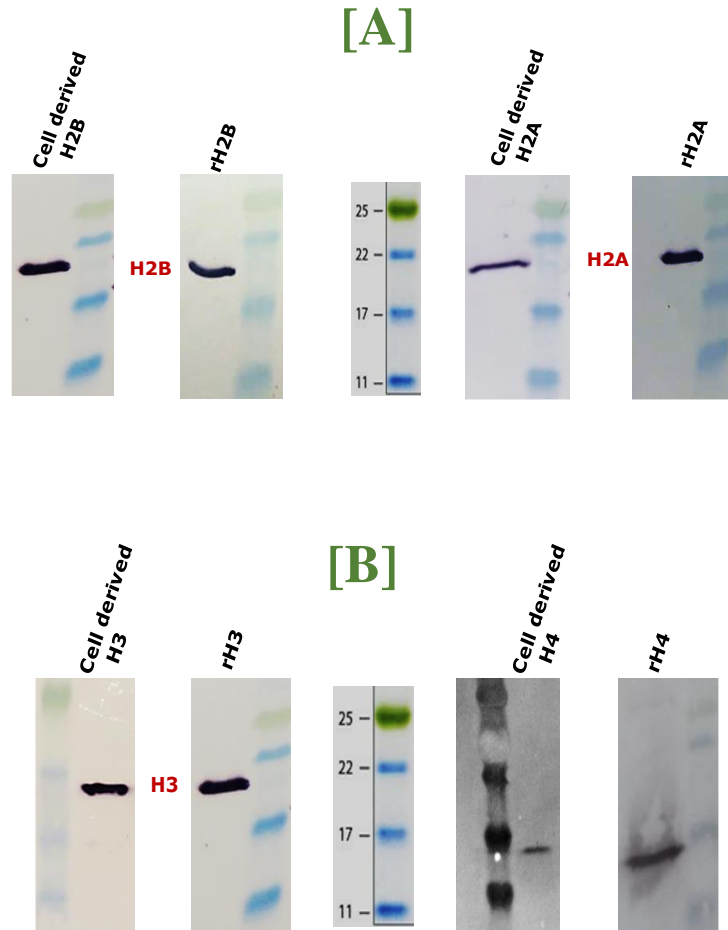


Figure 5.10: Representative immunoblotting images of purified histones. [A] Hep-2-derived H2B and H2A histones compared with recombinant histones. [B] Hep-2-derived H3 and H4 histones compared with recombinant histones. Immunoblotting analysis using 1500ng for r-histone and 3000ng of cell derived histones show histones H2B, H2A, H3 and H4 from Hep-2 cell lysates were similar bands to recombinant H2B, H2A, H3 and H4 histones. These proteins were identified using anti-histone H2B (ab1790; 1:5000 dilution), anti-histone H2A (ab18255; 1:2000 dilution), anti-histone-H3 (ab1791; 1:5000 dilution) and anti-histone H4 (ab10158; 1:4000 dilution), respectively.

5.2.5. Histone clipping assay by App and MspA

Epithelial cell-derived histones were used as cleavage substrates in clipping assays and the results compared to those obtained using recombinant histones.

We examined the ability of rpdApp and rpdMspA to proteolytically cleave human histones (H1, H2A, H2B, H3 and H4) and also used their inactive serine mutants to confirm that cleavage was specifically due to the serine endopeptidase activities of App and MspA. Here, 3µg of Hep-2 cell-derived histones and 1.5ug recombinant histones were used as cleavage substrates in the respective experiments. We used two times more cell derived histones than recombinant histones because we found that the cell-derived histones were not so readily detected as the recombinant histones by the specific antibodies used in immunoblotting experiments.

One possible explanation for this observation would be that the purified forms, unlike the cell-derived histones, were co-eluted with the other histones. Another possibility is that the-cell derived histones processed PTMs that may have reduced the binding of specific antibodies.

In the histone clipping assays, histones were incubated with 40nM autotransporter proteins (rpdApp, rpdApp^{S267A}, rpdMspA and rpdMspA^{S241A}) in a total volume of 40µl of PBS and incubated at 37°C for 16 h. Cleavage reactions were stopped with SDS-PAGE sample buffer and the digestion products resolved by SDS-PAGE and detected by Coomassie blue stain or by immunoblot analysis.

5.2.5.1. H1 clipping assay

Complete degradation of H1 was observed when rpdApp, rpdApp^{S267A}, rpdMspA and rpdMspA^{S241A} were incubated with either rH1 or cell-derived H1 histone at 37°C for 16h. No cleavage was observed in the absence of recombinant TF-tagged autotransporter (PBS alone) or in the presence of TF alone.

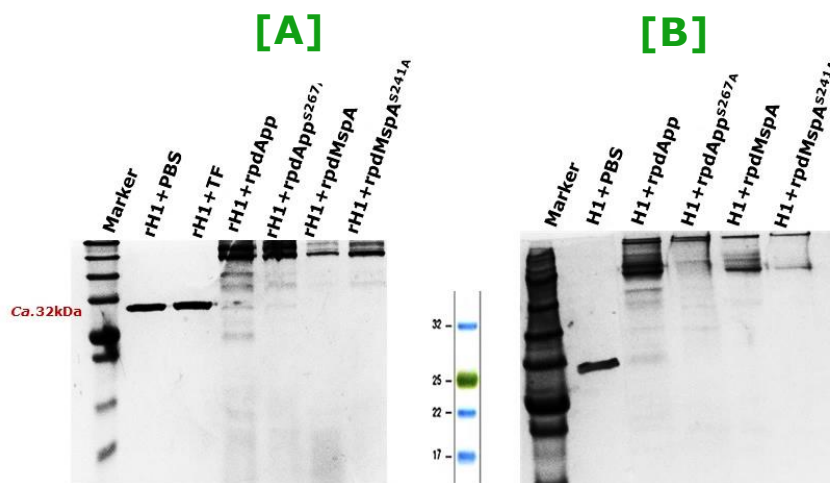


Figure 5.11: Clipping assay utilizing recombinant or cell derived native H1, and recombinant derivatives of App and MspA. **[A]** Cleavage of rH1 by rpdApp, rpdApp^{S267A}, rpdMspA and rpdMspA^{S241A}. **[B]** Cleavage of Hep-2 cell-derived H1 histone by rpdApp, rpdApp^{S267A}, rpdMspA and rpdMspA^{S241A}. Complete degradation of H1 was observed on SDS-PAGE. Here TF and PBS (*i.e.* no autotransporter) were used as negative controls for cleavage. H1 was no longer detected following treatment with either wild-type or inactive mutant derivatives of App and MspA.

5.2.5.2. H2A clipping assay

Using rH2A histones or cell derived H2A, no clipping products were detected using immunoblotting following incubation with App or MspA and their inactive mutant proteins (Figure 5.12). This demonstrated that App and MspA have no proteolytic activity against H2A under the reaction conditions used.

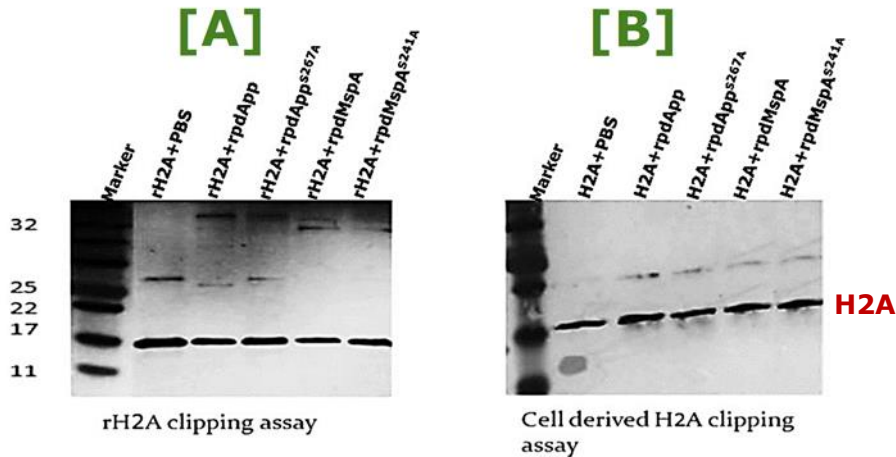


Figure 5.12: Clipping assay utilizing recombinant or cell derived native H2A, and recombinant derivatives of App and MspA. H2A was detected via immunoblot analysis using anti-histone H2A. [A] rH2A clipping assay where recombinant histones were incubated with rpdApp, rpdApp^{S267A}, rpdMspA or rpdMspA^{S241A}. [B] Showing cell derived H2A clipping assay where purified histones were incubated with rpdApp, rpdApp^{S267A}, rpdMspA or rpdMspA^{S241A}. No cleavage activity was apparent.

5.2.5.3. H2B clipping assay

To examine the interaction of histone H2B with App and MspA, histone H2B clipping assays were performed.

Immunoblotting analysis of H2B histone clipping assay, cleavage reactions revealed a faster migrating additional immunoreactive bands of H2B with lower molecular weight ≤ 15 kDa (Figure 5.13 [A] & [B]) in addition to the full size H2B band. A similar band was observed in samples treated with either App and MspA (Figure 5.13 [A]). In the case of cell derived histone, the predicted *ca.* 17-kDa band corresponding to full-length H2B histone almost disappeared in preparations treated with either autotransporter compared to the untreated control (Figure 5.13[B]). Surprisingly, in preparations treated with serine mutant proteins, which were predicted to be non-proteolytically active, similar

results to preparations treated with wild type proteins were observed. This result demonstrated the ability of rpdApp and rpdMspA to proteolytically cleave H2B histones; however, it will be necessary to further investigate and define the particular reason for the observed proteolysis by the serine mutants.

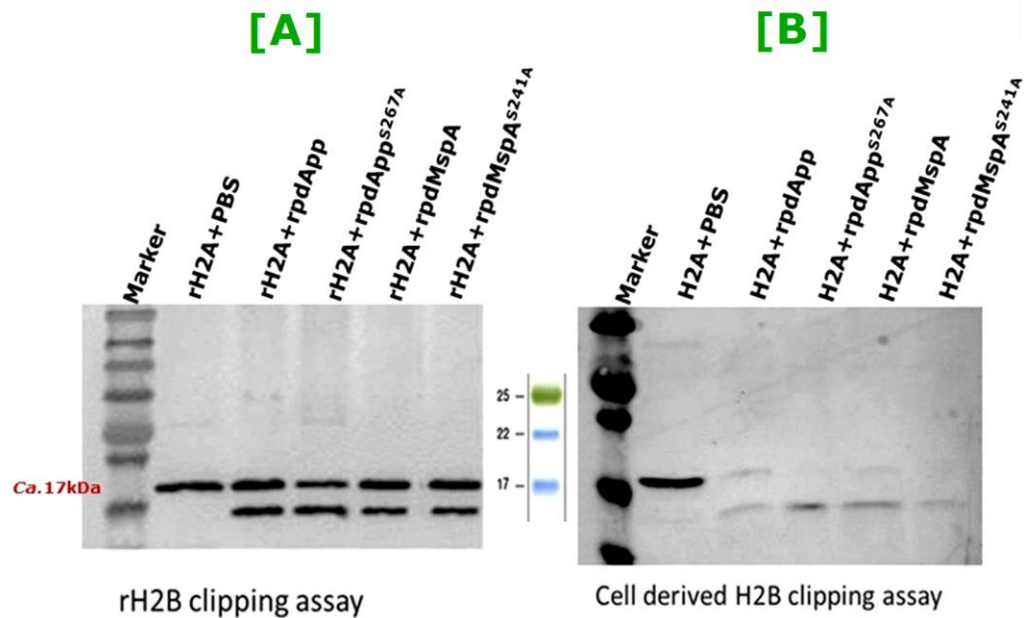


Figure 5.13: Clipping assay utilizing recombinant or cell derived native H2B, and recombinant derivatives of App and MspA. H2B was detected via immunoblot analysis using anti-histone H2B. The recombinant histones and cell derived H2B were used as cleavage substrates and were incubated with rpdApp, rpdApp^{S267A}, rpdMspA and rpdMspA^{S241A} at 37°C for 16h. [A] rH2B clipping assay. [B] Cell-derived H2A clipping assay. The immunoblotting analysis demonstrated the H2B cleavage products with App and MspA treated histones H2B as compared with negative control PBS. Unexpectedly, similar clipping abilities were observed with the serine mutants of rpdApp and rpdMspA.

5.2.5.4. H3 clipping assay

The ability of rpdApp and rpdMspA to cleave native purified histones H3 along with recombinant histones H3 were carried out here. The cleavage reaction was

resolved on 16% SDS-PAGE and followed by immunoblotting with anti-histone-H3 (ab1791).

Immunoblot analysis with C-terminal anti-Histone H3 (ab1791) revealed an additional faster migrating band related to histone H3 while no band was observed in blots probed with the N-terminal-specific anti-Histone-H3 (ab18521). H3-derived cleaved products were observed in cell-derived H3 histone preparations treated with rpdApp or rpdMspA, but not in preparations treated with the serine mutant of App (Figure 5.14).

Surprisingly, the serine mutant of MspA (rpdMspA^{S241A}) cleaved H3 in a manner similar to that of the wild types' proteins. Additional bands observed in preparations of cell derived H3 probed with the polyclonal anti histone H3 (ab1791) presumably corresponded to other co-eluted histones.

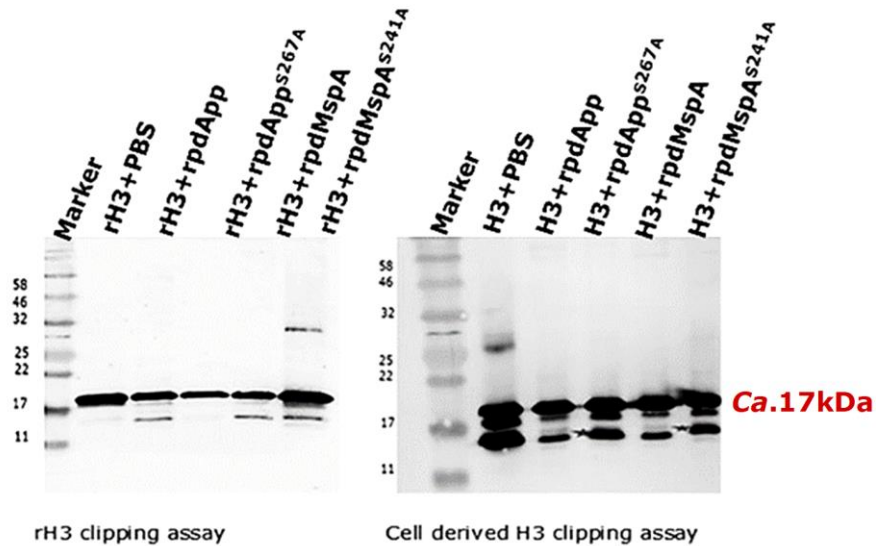


Figure 5.14: Clipping assay utilizing recombinant or cell derived native H3, and recombinant derivatives of App and MspA. H3 was detected via immunoblot analysis anti-Histone-H3 (ab1791). 1.5 μ g recombinant histone or 3 μ g purified cell derived histone H3 were individually incubated with 40nM autotransporter (rpdApp, rpdApp^{S267A}, rpdMspA or rpdMspA^{S241A}). Immunoblot analysis detected clipping products in rH3 and native H3 reactions with rpdApp and rpdMspA, but the absence of specific cleavage product with rpdApp^{S267A}. However, rpdMspA^{S241A} showed similar histone H3 proteolytic activity to rpdMspA.

5.2.5.5. H4 clipping assay

rH4 and Hep-2-derived H4 were both tested in clipping assays with App and MspA autotransporters and their respective catalytic serine residue mutants. Neither App nor MspA had any detectable proteolytic activity against histone H4 under the conditions tested.

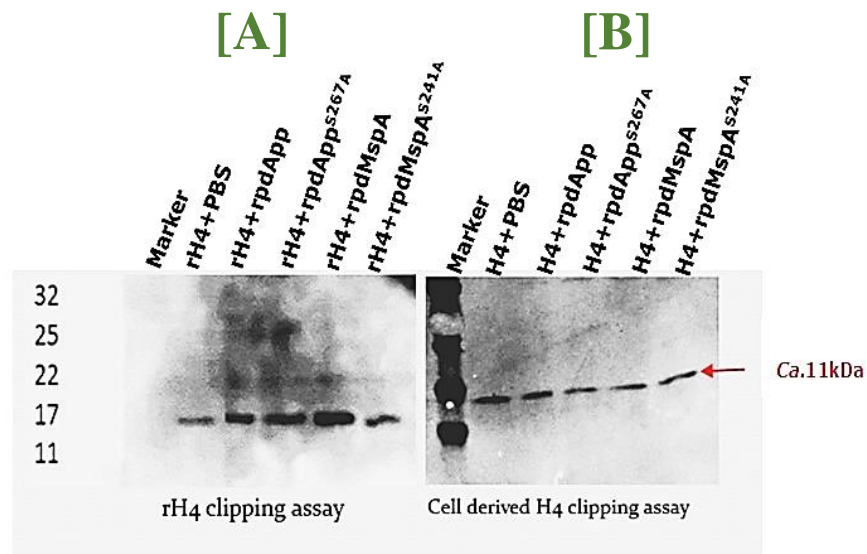


Figure 5.15: Clipping assay utilizing recombinant or cell derived native H4, and recombinant derivatives of App and MspA. H4 was detected via immunoblot analysis using anti-histone H4. [A] Histone rH4 was incubated at 37°C for 16 h with rpdApp, rpdApp^{S267A}, rpdMspA or rpdMspA^{S241A}. [B] Cell-derived H4 clipping assay carried out under the same conditions with the same autotransporters as [A]. The H4 clipping assay showed no evidence for H4 histone clipping by App and MspA.

The result of the histone clipping assays demonstrated histones H1, H2A and H3 were proteolytically processed by App and MspA. Unexpectedly in some cases, the catalytic serine mutants of App and MspA also displayed proteolytic activity towards these histones. The reason for this finding will require further investigation.

5.2.5.6. Effect of serine protease inhibitors on App and MspA mediated clipping of histone H3

In the previous experiment, we found histone-H3 clipping with rpdApp and rpdMspA but not with the serine mutant of App, while the rpdMspA^{S241A} mutant showed cleavage activity against histones that was indistinguishable from that

of its parent. To ensure the histone H3 cleavage was due to serine protease-mediated activity or not, histone clipping assays were undertaken in the presence of the serine protease inhibitor phenylmethylsulfonyl fluoride (PMSF). In the presence of PMSF, either App (wild type/serine mutant) or MspA (wild type/serine mutant) only one band corresponding to the expected size of full-length histone-H3 was detected in samples of treated H3. Interestingly, while the rpdMspA^{S241A} mutant protein demonstrated proteolytic activity, this was entirely abolished in the presence of PMSF (Figure 5.16). PMSF used for reducing proteolysis by sulfonylation of O^γ (hydroxyl oxygen) atom of catalytic site of serine and thereby inactivate the active site and leading to irreversible inhibition of the catalytic site of serine protease and it does not bind to any other serine residues of the protein. However, the possibility that other proteases may be being inhibited cannot be excluded [263]. The finding demonstrates that H3 histones were insensitive to App and MspA in the presence of the serine protease inhibitor, indicating that the observed cleavage was mediated by a serine protease activity, and that this activity was retained by the serine mutant of MspA.

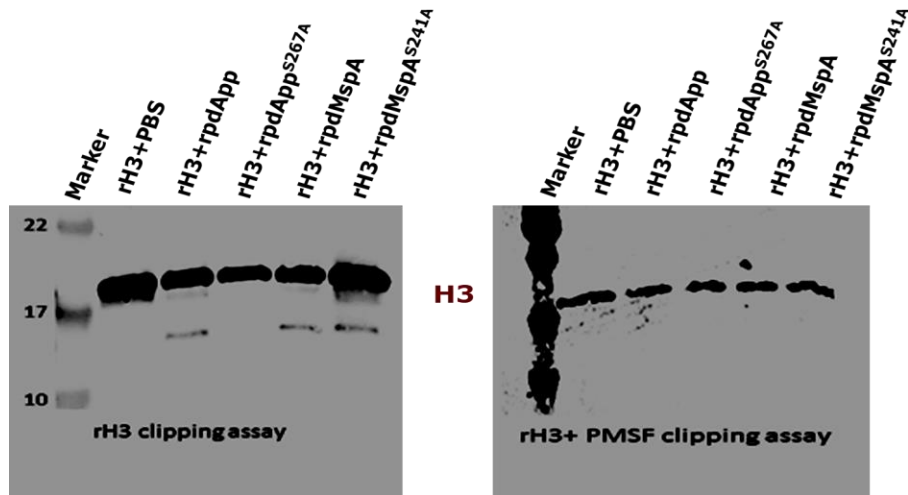


Figure 5.16: The serine protease inhibitor PMSF inhibits App and MspA mediated H3 clipping. The proteolytic activity of rpdApp, rpdApp^{S267A}, rpdMspA and rpdMspA^{S241A} on rH3.1 was examined in the presence or absence of PMSF protease inhibitor. The reactions were incubated with shaking at 37°C for 16 h, subjected to SDS-PAGE, transferred onto nitrocellulose membrane, and probed with anti-histone-H3 (ab1791) to detect histone-H3. In both panels, lane 1: pre-stained protein marker, lane 2: PBS with rH3.1 (negative control), lane 3: rH3 + rpdApp, lane 4: rH3 + rpdApp^{S267A}, lane 5: rH3 + rpdMspA, lane 6: rH3 with rpdMspA^{S241A}. Immuno-reactive bands corresponding to clipped rH3.1 (ca. ≤13 kDa) were only observed in the absence of PMSF and where PMSF was added no cleavage products were observed. However, while similar amounts of protein were loaded onto each gel the bands observed corresponding to the uncleaved protein were less intense than on the corresponding gel of preparations that had not been PMSF-treated, so it is possible that cleavage products below detectable levels were present.

Taken together, these results confirm that App and MspA have serine proteases activities; however, it was found that the MspA mutant retained proteolytic activity even the putative catalytic serine residue. To further address this finding additional mutant derivatives of MspA were generated in which with another member of the catalytic triad was mutated and the resulting protein assayed for its ability to cleave histones.

5.2.6. Defining the reason behind the histone proteolytic processing of serine mutant of MspA

5.2.6.1. Mutation of additional amino acid of the catalytic triad of MspA

To further investigate the residual proteolytic activity of rpdMspA^{S241A}, experiments were designed to mutate an additional amino acid of the catalytic triad of MspA alone or with the serine residue. The catalytic triad of MspA protein is H¹¹¹, D¹³⁵ and S²⁴¹.

Here, we successfully mutated the codon encoding aspartate (D¹³⁵) to encode glutamate (E) in pColdTF-MspA and pColdTFMspA^{S241A} to yield pColdTFMspA^{D135} and pColdTFMspA^{D135ES241A}, respectively.

The recombinant plasmid pColdTF-MspA was used previously in this study to purify the passenger domain of MspA.

To facilitate the mutagenesis of rpdMspA, pColdTF-MspA template plasmids together with Q5 designed primer pairs were used to substitute the desired nucleotides encoding aspartate to glutamate (D¹³⁵ to E) by PCR as using the Q5 site-directed mutagenesis kit (described in the section 2.9.2). PCR-generated products were confirmed by agarose gel electrophoresis (Figure 5.17).

Then the PCR generated products were treated with KLD enzymes (Kinase, Ligase and DpnI enzyme) (described in the section 2.9.3) to ligate PCR-generated blunt ends of the amplified PCR product and the product was used to transform *E. coli* JM109. The desired mutation, the absence of PCR-generated errors and the correct orientation were all confirmed by DNA sequencing.

A mutant of MspA protein was generated in which the aspartate-encoding GAC codon was successfully mutated to the glutamic acid-encoding GAA codon. The

same mutation was introduced in the same way in a construct that already encoded serine mutant rpdMspA^{S241A} and again sequence analysis confirmed the presence of the desired mutations in the final plasmid construct.

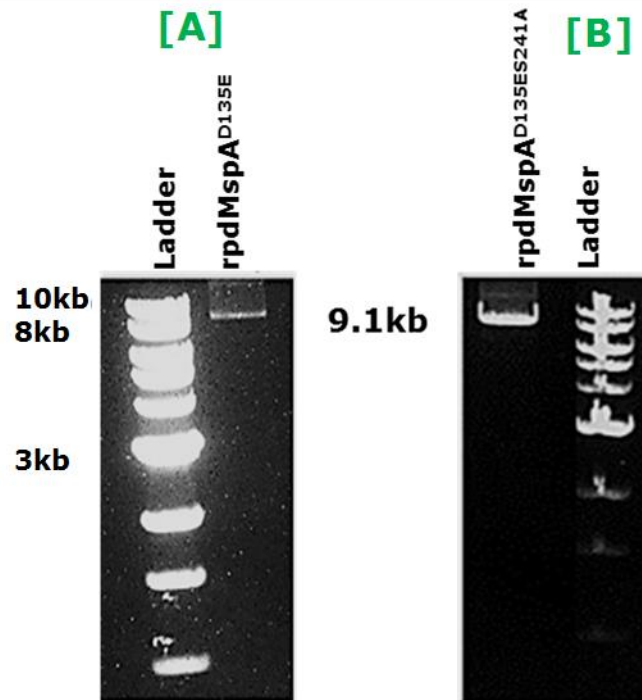


Figure 5.17: PCR amplification of pColdTFMspA^{D135E} and pColdTFMspA^{D135ES241A}. Agarose gel showing the PCR amplification of mutated plasmid derivatives of pColdTF-MspA or pColdTFMspA^{S241A} with mutagenic primers pairs-MspA^{D135E}-F and MspA^{D135E}-R(Table:2.3) to amplify the whole plasmid whilst also generating aspartate to glutamic acid substitutions. [A] Lane 1: 1kb DNA ladder, Lane 2: PCR product corresponding to putative pColdTFMspA^{D135E}, [B] Lane 1: PCR product corresponding to putative pColdTFMspA^{D135ES241A}, lane 2: 1kb DNA ladder.

Confirming by DNA sequencing

MspA mutant (D¹³⁵ to E)

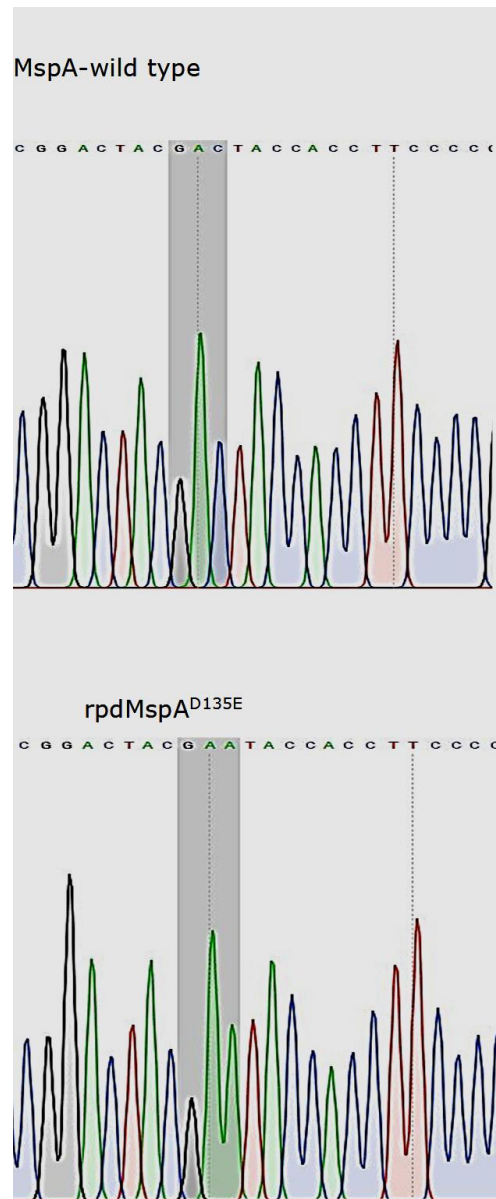
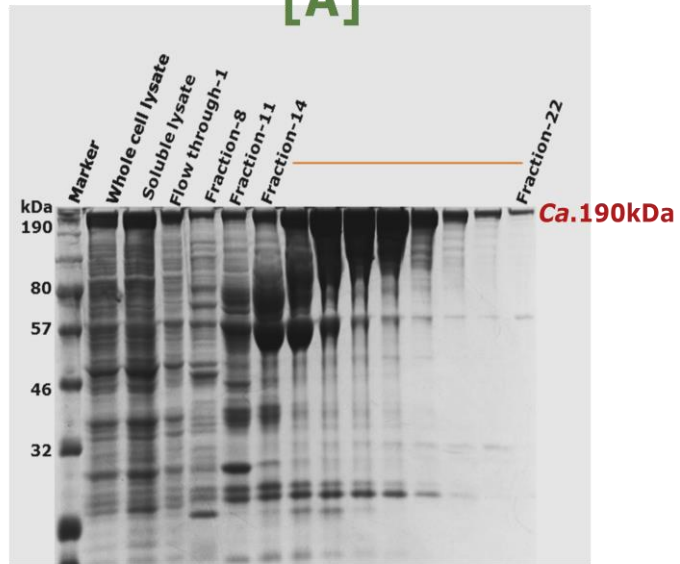


Figure 5.18: DNA sequence chromatograms confirming the desired mutations present in pColdTF-MspA^{D135E}. Here, the highlighted part showing the substitution of triplet codon GAC, encoding aspartate of MspA at position 135 with GAA encoding glutamate (E) to in plasmid pColdTF-MspA^{D135E}.

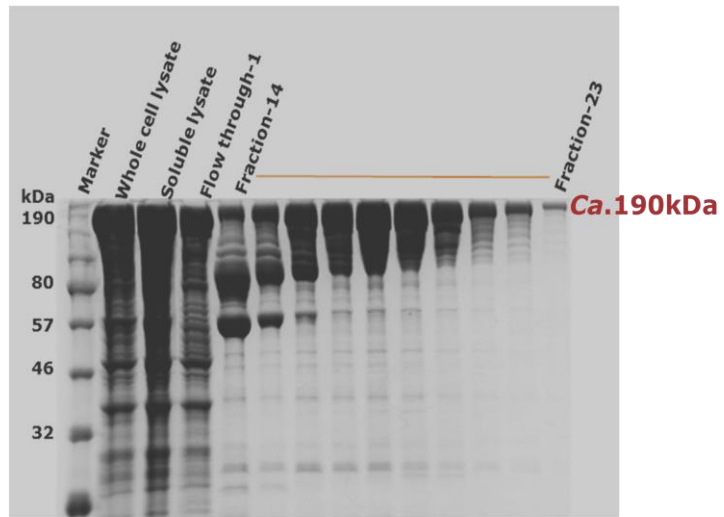
5.2.6.2. rpdMspA^{D135E} and rpdMspA^{D135ES241A} protein purification:

E. coli JM109 cells harbouring plasmids pColdTF-MspA^{D135E} and pColdTFMspA^{D135ES241A} were used to purify the corresponding proteins rpdMspA^{D135E} and rpdMspA^{D135ES241A}, which were purified under native conditions using IMAC as described in section 5.2.1 and 5.2.2. Fractions containing these proteins were identified chromatographically and subsequently resolved on SDS-PAGE (Figure 5.19 [A] & [B]). Both purified proteins were confirmed by immunoblotting using anti-penta-histidine antibodies (Figure 5.19 [C]).

[A]



[B]



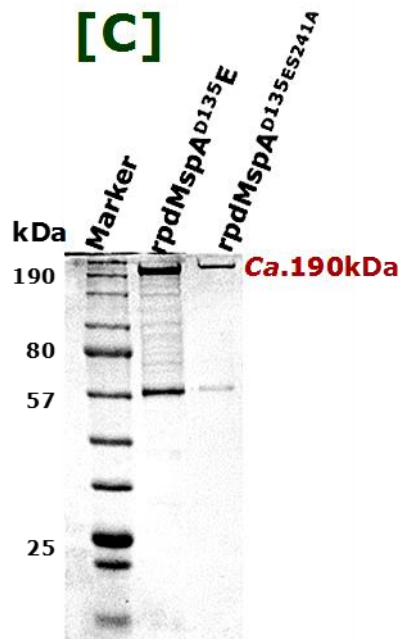


Figure 5.19: SDS-PAGE and immunoblot analysis demonstrating purification of rpdMspA^{D135E} and rpdMspA^{D135ES241A}. [A] rpdMspA^{D135E} protein purification. [B] rpdMspA^{D135ES241A} purification. [C] Immunoblot analysis of purified MspA mutant proteins using anti penta-His antibody. Purification was done with AKTA primer plus using Ni-IMAC using soluble lysate of IPTG-induced *E. coli* JM109 containing rpdMspA^{D135E} or rpdMspA^{D135ES241A}. Sample aliquots were taken throughout the preparation and purification process and were subjected to 10% (v/v) SDS-PAGE. The immunoblot analysis confirms that the purified proteins were his-tagged.

5.2.6.3. Analysis of the proteolytic processing of histones

To investigate whether the putative catalytic triad of MspA is involved in its proteolytic activity against histones, two mutants in addition to the serine mutant of those proteins were generated and tested for their proteolytic activity against histones H1, H2 and H3.

5.2.6.3.1 Investigating the proteolytic processing of histone-H1

In the previous H1 clipping assay (Section 5.2.5.1), non-specific degradation of histone H1 was found with App and MspA wild types and serine mutants. As a consequence, the proteolytic activity of histone H1 was examined using the other mutants in addition to serine or without serine mutants of the catalytic triad of MspA. In parallel, App mutants were tested to compare with the wild types by the same clipping approach (Section 5.2.5.1). The data showed that histone H1 was fully degraded when incubated with either wild type or the mutant variants of App and MspA proteins.

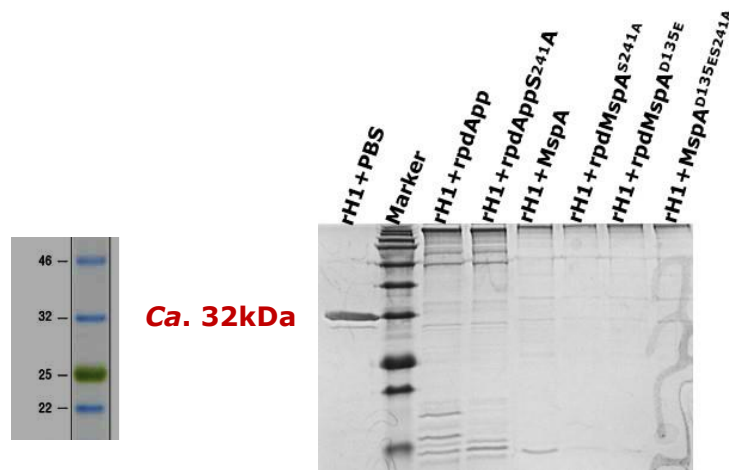


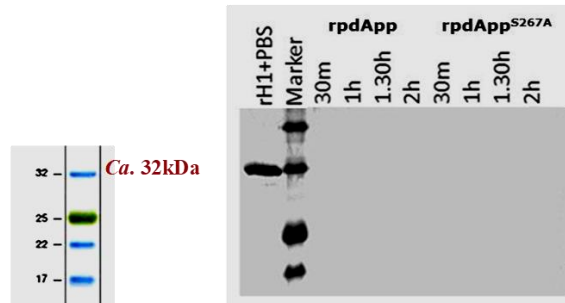
Figure 5.20: rH1 histone cleavage assay with different active and inactive recombinant App and MspA proteins. Recombinant histone H1 was incubated with *rpdApp*, *rpdApp*^{S267A}, *rpdMspA*, *rpdMspA*^{S241A}, *rpdMspA*^{D135E}, *rpdMspA*^{D135ES241A} and PBS (as a negative control) at 37°C for 16 h. After incubation, the cleavage reactions were stopped by the addition of 6 × SDS-PAGE sample buffer and cleavage products subjected to SDS-PAGE. Proteins were stained with coomassie blue stain. The data shows that rH1 was completely degraded by all the App and MspA proteins under the conditions utilized.

To determine the optimal point of histone-H1 clipping by App and MspA proteins, time course and dose response experiments were designed.

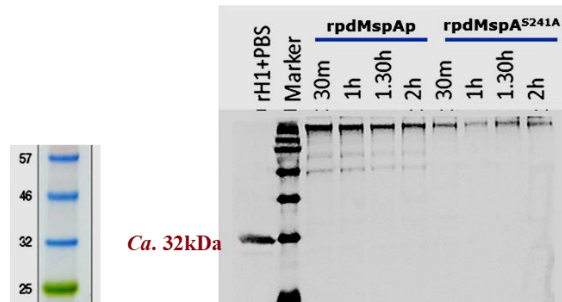
5.2.6.3.2 Time course proteolytic activity experiments of App and MspA

To define the optimal time point for histone-H1 clipping by App and MspA, a time-course experiment of rH1 clipping assay was undertaken. Wild types (rpdApp& rpdMspA) and catalytic triad mutant proteins (rpdApp^{S267A}, rpdMspA^{S241A}, rpdMspA^{D135E}, rpdMspA^{D135ES241A}) of MspA and App were used. Aliquotes of the cleavage reactions were removed at 30 min, 1 h, 1.5 h, 2 h, 4 h, 6 h, 8 h and 12 h time points and resolved on SDS-PAGE. The proteolytic degradation of H1 was complete, however, even at the shortest timepoint with each of the proteases tested.

[A]



[B]



[C]

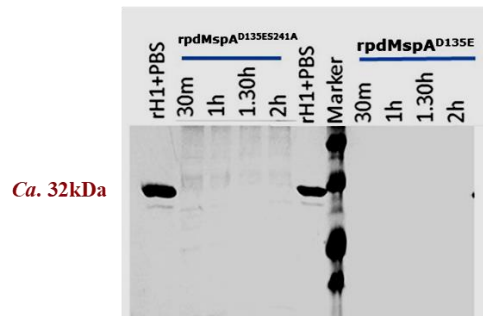


Figure 5.21: Time course experiment for rH1 clipping assay. rH1 was co-incubated with rpdApp, rpdApp^{S267A}, rpdMspA, rpdMspA^{S241A}, rpdMspA^{D135E} or rpdMspA^{D135E}^{S241A} and incubated at 37°C. Aliquots were taken from the cleavage reaction at 30 min, 1h, 1.5h and 2h and subjected to SDS-PAGE. [A] Clipping assay of rH1 by rpdApp and rpdApp^{S267A} (incubated for 30min, 1h, 1.5h, 2h). [B] Proteolytic activity of rpdMspA and rpdMspA^{S241A} proteins on rH1. [C]

Proteolytic activity of rpdMspA^{D135ES241A} and rpdMspA^{D135E}. The data show that all App and MspA fragments completely degraded rH1 within 30 min.

5.2.6.3.3 Titration experiments of App and MspA on histone H1 proteolysis

To further optimise the histone H1 cleavage assays, App and MspA proteins were titrated in these assays. rH1 histones were incubated with 40nM, 10nM, 1nM, 0.1nM or 0.001nM of each protein for 30 min at 37°C and analysed by SDS-PAGE. 1nM to 0.001nM samples are shown in Figure 5.22. Samples incubated with 40nM or 10nM of either protein were fully degraded as previously observed (and are not shown here). 1nM App and MspA proteins treated histone rH1 was cleaved by wild type rpdApp or rpdMspA but not by their respective serine mutants, which were indistinguishable to the negative control containing no protease. These findings confirmed the requirement for the serine component of the catalytic triad in both App and MspA for full activity in this assay. It was also demonstrated the evidence that linker H1 was highly susceptible to proteolytic processing by App and MspA proteins as degradation was observed at very low concentrations of these proteins.

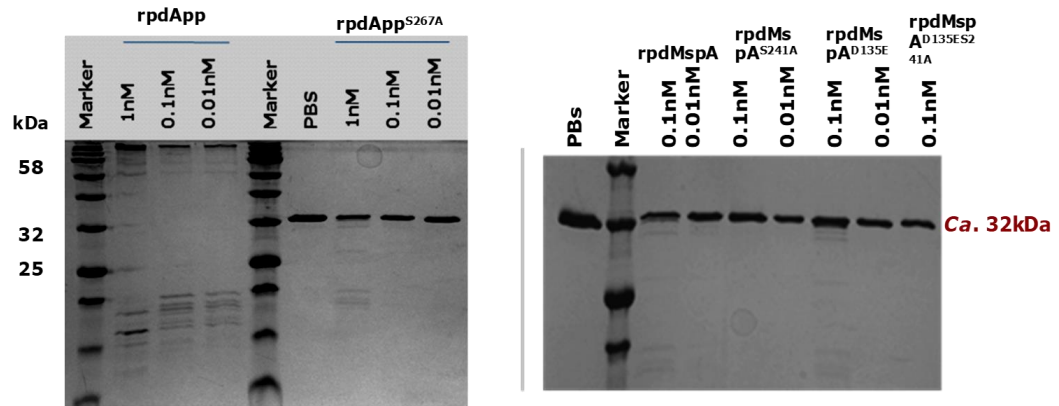


Figure 5.22: Titration experiment to optimise rH1 cleavage assays using recombinant App and MspA proteins. Different concentrations of App and MspA proteins were incubated with 1.5 μ g rH1 at 37°C for 30 min. The reactions were then stopped, and products resolved on SDS-PAGE. rH1 clipping was observed with rpdApp by the degradation of ca. 32kDa band corresponding to rH1. rpdApp and rpdMspA showed cleavage at all the points, but not with the mutant proteins including rpdApp^{S267A}, rpdMspA^{S241A}, rpdMspA^{D135E} and rpdMspA^{D135ES241A}. It showed App and MspA can proteolytic process rH1 with 0.1nM concentration within 2h. rpdApp showed more rapid degradation of rH1 than rpdMspA under the conditions tested where rpdApp showed proteolytic activity at 0.01nM concentration and rpdMspA showed at 0.1nM.

The experiments were further optimised and showed that 0.1nM App or MspA were able to clip the H1 histones within 1hour, whereas no clipping was evidence by serine mutants of these proteins (Figure 5.23).

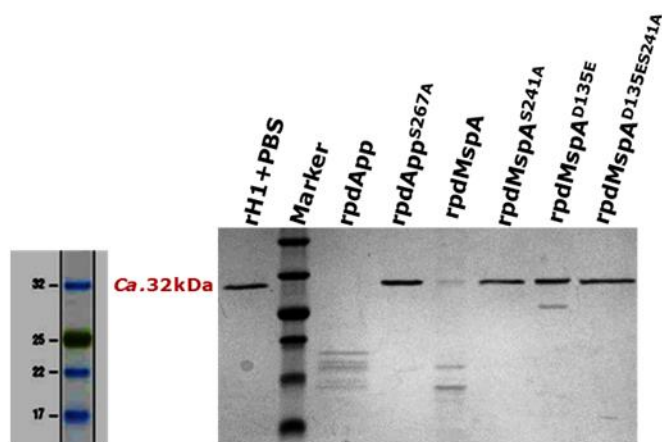


Figure 5.23: Final optimisation of the rH1 clipping assay. 1.5 μ g rH1 was incubated with 0.1nM rpdApp, rpdApp^{S267A}, rpdMspA, rpdMspA^{S241A}, rpdMspA^{D135E}, rpdMspA^{D135ES241A} or PBS (negative control) at 37°C for 1h. Cleavage reactions were stopped by the addition SDS-PAGE sample buffer and the clipping products were analysed on 16% (w/v) SDS-PAGE. rpdApp, rpdMspA and rpdMspA^{D135E} degraded the 32kDa rH1 histone, but intact, full-length rH1 histone bands were observed with the all other mutants of App and MspA and PBS treated negative control.

5.2.6.3.4 Analysis of histone H2B clipping by App and MspA Proteins

To further investigate the histone H2B clipping activity of the serine mutants of App and MspA (results from 5.2.5.3), further experiments were devised using wild types App and MspA and their serine mutant derivatives. The results were consistent with the previous clipping assay where histones H2B cleavage products were observed with all wild types and mutant proteins of App and MspA but this activity was abolished in the presence of PMSF. It was also observed the serine mutant derivative of App retained some activity, but it was much less than that which was observed in preparations treated with the wild type protein

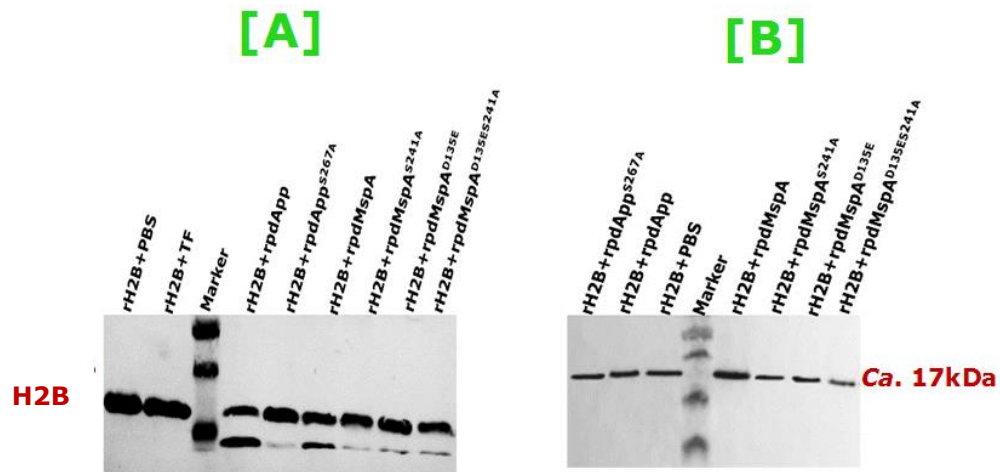


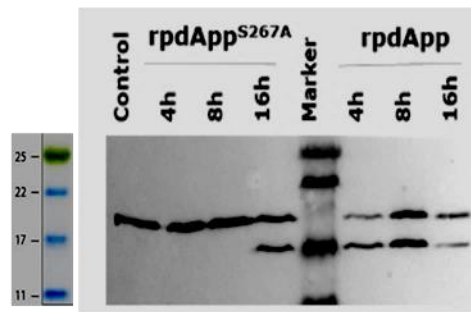
Figure 5.24: Histone H2B clipping assay with recombinant App and MspA wild-type and mutant proteins. [A] rH2B clipping assay. [B] Represents the same rH2B clipping assay, but in the presence of PMSF. Recombinant histone (1.5 μ g) was incubated with 40nM of rpdApp, rpdApp^{S267A}, rpdMspA, rpdMspA^{S241A}, rpdMspA^{D135E}, rpdMspA^{D135ES241A}, TF (negative control) or PBS (negative control) at 37°C for 16 h. Reactions were stopped by addition SDS-PAGE sample buffer and cleavage products were detected using anti-histone H2B (ab1790). This demonstrates cleavage of rH2B by rpdApp and rpdMspA due to the generation of a faster migrating additional H2B-specific band. The yield of this cleavage product is reduced when mutant proteins of App and MspA were utilized. Panel [B] shows that all cleavage could be inhibited by the addition of PMSF indicating serine endopeptidase activity.

5.2.6.3.5 Time-course experiments of histone H2B proteolysis by App and MspA proteins

In the previous experiment of the time dose experiment of H1 histone clipping assay demonstrated the optimal point of App and MspA clipping.

To define the optimal time point for histone-H2B clipping by App and MspA, a time-course experiment of rH2B histone clipping assay was performed. Wild types (rpdApp& rpdMspA) and catalytic triad mutant proteins (rpdApp^{S267A}, rpdMspA^{S241A}, rpdMspA^{D135E}, rpdMspA^{D135ES241A}) of MspA and App were used. Aliquots were taken from the reaction mixture at some time points (4 h, 8 h, 12 h, 16 h) and resolved on SDS-PAGE, transferred onto nitrocellulose membrane and detecting H2B with anti-histone H2B(ab1790). Both rpdApp and rpdMspA showed clipping activity after 4 h of incubation with rH2B. At this time point rpdApp^{S276A}-treated samples displayed no cleavage products, which only became apparent after 16 h (Figure 5.25 [A]). Samples treated with rpdMspA^{D135E} showed evidence of cleavage even at 4 h, although it was less active than the wild type protein. The rpdMspA^{S241A} mutant demonstrated some activity at 12 h, but much less than the wild type, whereas by 16 h cleavage was comparable to that seen in the wild type protein (Figure 5.25 [B]). The double mutant protein rpdMspA behaved similarly to rpdMspA^{S241A} although no activity was apparent at 4 h, 8 h, whereas the histone was fully cleaved at 16 h (Figure 5.25 [B]).

[A]



[B]

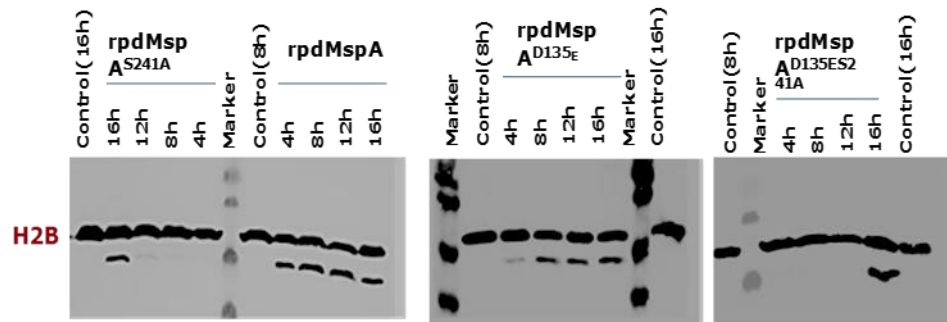


Figure 5.25: Optimizing the incubation time for the rH2B clipping assay. Here 40nM autotransporters (rpdApp, rpdApp^{S267A}, rpdMspA, rpdMspA^{S241A}, rpdMspA^{D135E}, rpdMspA^{D135ES241A}) were incubated with 1.5 μ g rH2B and the cleavage products collected at 4h, 8h, 12h or 16h. [A] rpdApp showed clipping at 4h, whilst clipping products could only be detected in the rpdApp^{S267A} reaction after 16 h. [B] rpdMspA showed clipping at 4h, whilst clipping products appeared later or were less abundant in reactions containing rpdMspA^{S241A} or rpdMspA^{D135ES241A}.

These results indicated that rH2B clipping is mediated by the catalytic triad, but that one or more of the amino acids making up this triad are dispensable if the incubation is prolonged.

The optimisation of the incubation time for H2B clipping assays demonstrated that rH2B clipping by App and MspA is time dependent.

To further optimise the H2B clipping assay, the assay was performed with at different protease concentrations. Firstly, the histone H2B clipping experiment was done using 40nM or 20nM of App or MspA wild type and serine mutant proteins. As expected, reduced proteolytic activity was observed when 20nM of the autotransporter proteins were employed. This result indicated that rpdApp was more active against histone rH2B than rpdMspA.

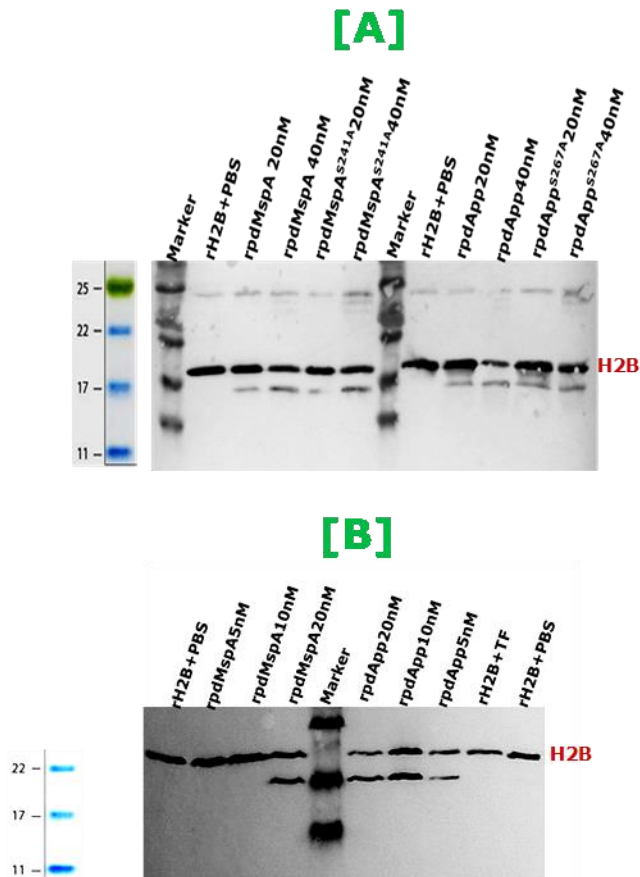


Figure 5.26: Titration experiment to optimise rH2B cleavage assays using recombinant App and MspA proteins. [A] rH2B clipping assay using 20nM or 40nM autotransporter proteins (rpdApp, rpdApp^{S267A}, rpdMspA, rpdMspA^{S241A}). [B] rH2B clipping assay using 5nM, 10nM or 20nM autotransporter proteins

(rpdApp, rpdMspA or TF). Cleavage reactions were incubated for 8h at 37°C, and products detected by immunoblot. rpdApp showed clipping at any concentration being tested here, but rpdMspA showed clipping only at 20nM.

5.2.6.3.6 Role of the catalytic triad in the proteolytic activity of App and MspA in H2B proteolysis

The H2B clipping assay was carried out at the optimal point where serine mutants proteolysis were not showed (Figure 5.27 [A] and [B]). 1.5µg rH2B and 3µg CH2B(cell-derived H2B) clipping assays were repeated with wild type and mutant proteins of App and MspA (in which one or more amino acids making up the catalytic triads of App and MspA were changed) and assays were undertaken for 8 h at 37°C. Cleavage products were observed with rpdApp- and rpdMspA-treated rH2B or cell derived H2B (CH2B), and also in samples treated with rpdMspA^{D135E}. Cleavage products were absent, however, in samples treated with rpdApp^{S267A}, rpdMspA^{S241A}, rpdMspA^{D135ES241A} (Figure 5.27).

These results demonstrated the proteolytic activity of App and MspA towards H2B is mediated by serine protease activity and that the serine residues S276 of App and S241 of MspA are required for this activity but not the aspartic acid residue D135 of MspA. This activity was observed where the histone substrate was generated in bacteria or purified from human cells.

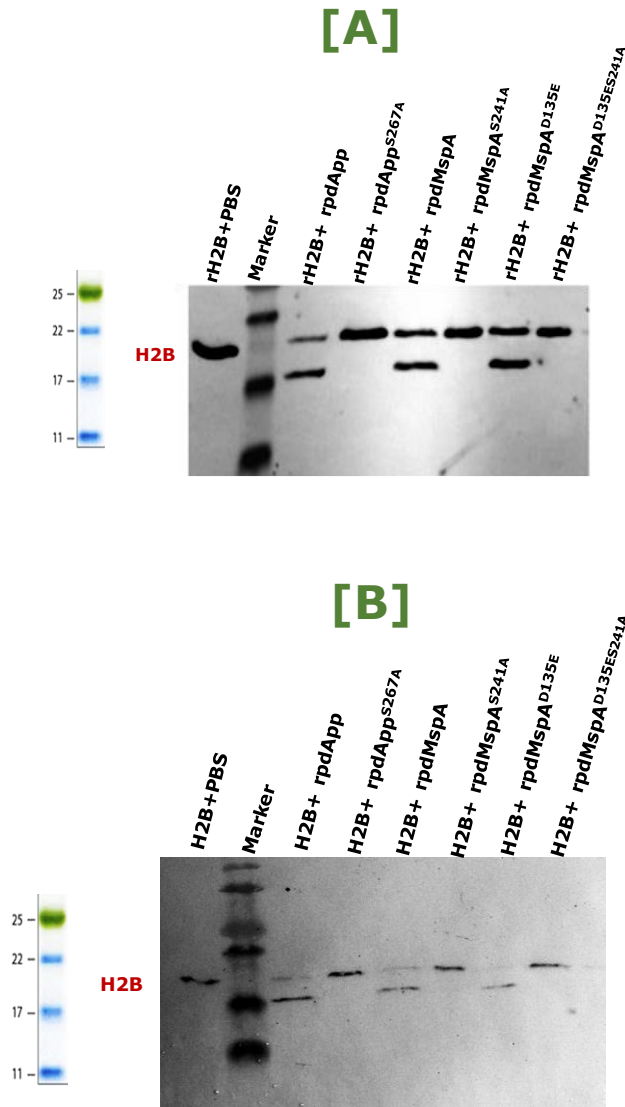


Figure 5.27: Optimized serine protease-mediated histone H2B clipping assay. **[A]** rH2B clipping assay. **[B]** Hep-2 cell-derived H2B clipping assay. 20nM autotransporters (rpdApp, rpdApp^{S267A}, rpdMspA, rpdMspA^{S241A}, rpdMspA^{D135E}, rpdMspA^{D135ES241A}) were incubated with histone H2B for 8 h at 37°C. Reactions were stopped by SDS-PAGE sample buffer and were subjected to immunoblotting analysis using anti C-terminal histone H2B (ab1790) to detect the N-terminal cleavage of histone H2B. No clipping products were observed with serine mutants indicating the importance of the active site serine residue in App and MspA proteolytic processing of N-terminal histone H2B. No differences were apparent between rH2B and Hep-2 derived H2B suggesting that PTMs do not influence cleavage.

5.2.6.3.7 Proteolytic processing of H3 histones by App and MspA

To further characterise the role of the catalytic triad of App and MspA in the proteolytic clipping of H3; the ability of these proteins, as well as the previously tested serine mutants and additional mutations were tested for their ability to cleave this histone. As previously determined the serine residue of App was shown to be important in this activity, although in the later experiments some residual cleavage was observed in the serine mutant. The activity of the serine mutant of MspA was similar to the wild type protein. Mutation of the aspartate residue D135, either alone or in combination with serine S267, also did not have any effect on the ability of this protein to cleave H3 under the conditions tested.

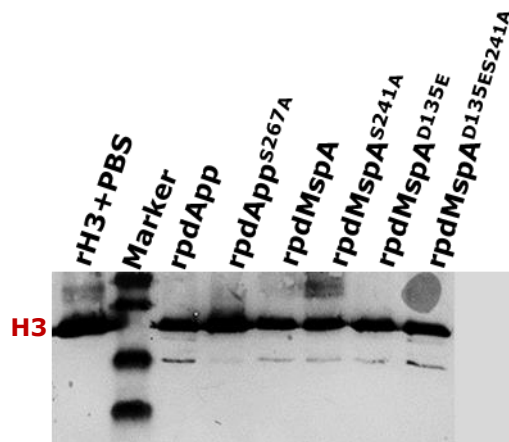


Figure 5.28: rH3 Histone clipping assay with recombinant App and MspA wild types and mutant proteins. Recombinant H3 histones (1.5 μ g) were incubated with 40nM rpdApp, rpdApp^{S267A}, rpdMspA, rpdMspA^{S241A}, rpdMspA^{D135E} and rpdMspA^{D135ES241A} and PBS treated rH3 as a negative control at 37°C for 16 h. The clipping reactions were stopped by adding SDS-PAGE sample buffer and cleavage reaction products were subjected to immunoblotting using polyclonal Ab anti-H3 histone (ab1791). We did not observe any difference between wild type MspA treated histone and MspA mutants treated histones whereas a difference in both rpdApp and rpdApp^{S267A} treated histones.

This data was consistent with the previous findings but also indicate that the aspartate residue of MspA, in addition to the serine residue component of the catalytic triad, was dispensable for the activity of this protease against histone H3. Thus, a time-course analysis of histone-H3 clipping was undertaken in an attempt to determine whether there was any difference in the activity of wild type and catalytic triad mutant versions of this protein against H3.

5.2.6.3.8 Time course proteolytic activity experiments of App and MspA on rH3 histone

To define the optimal point for H3 histone clipping by App and MspA, the time-course proteolysis of histone rH3 experiment were carried out. The assay was also performed with different concentrations of autotransporters where we used 20nM and 40nM wild type and mutant App and MspA proteins. The aliquots of the cleavage reactions were collected at several time points (4 h, 8 h, 12 h, 16 h, 24 h) and the processed fast migrating truncated additional bands of H3 Histones were confirmed with monoclonal anti-H3 histone (ab10799) using immunoblotting analysis.

The clipping of H3 histones were observed with wild type App (rpdApp), MspA (rpdMspA) and rpdMspA^{D135E} mutant but not with any serine mutant (rpdApp^{S267A}, rpdMspA^{S241A}, rpdMspA^{D135ES241A}). This proteolytic activity of App and MspA was also depend on their concentrations (Figure 5.29). In the histone H3 clipping assays, 40nM ATs treated histones showed more intense clipping products than 20nM ATs treated histone H3 (Figure 5.29). Interestingly, 20nM ATs treated histone H3 clipping assays showed the clipping evidence with rpdApp at 4 h incubation whereas the clipping only found with rpdMspA at 16 h incubation and serine mutants' proteolysis were almost concealed. MspA^{D135E}

mutant showed proteolytic ability on rH3 histone after 12h incubation (Figure 5.29 [A]).

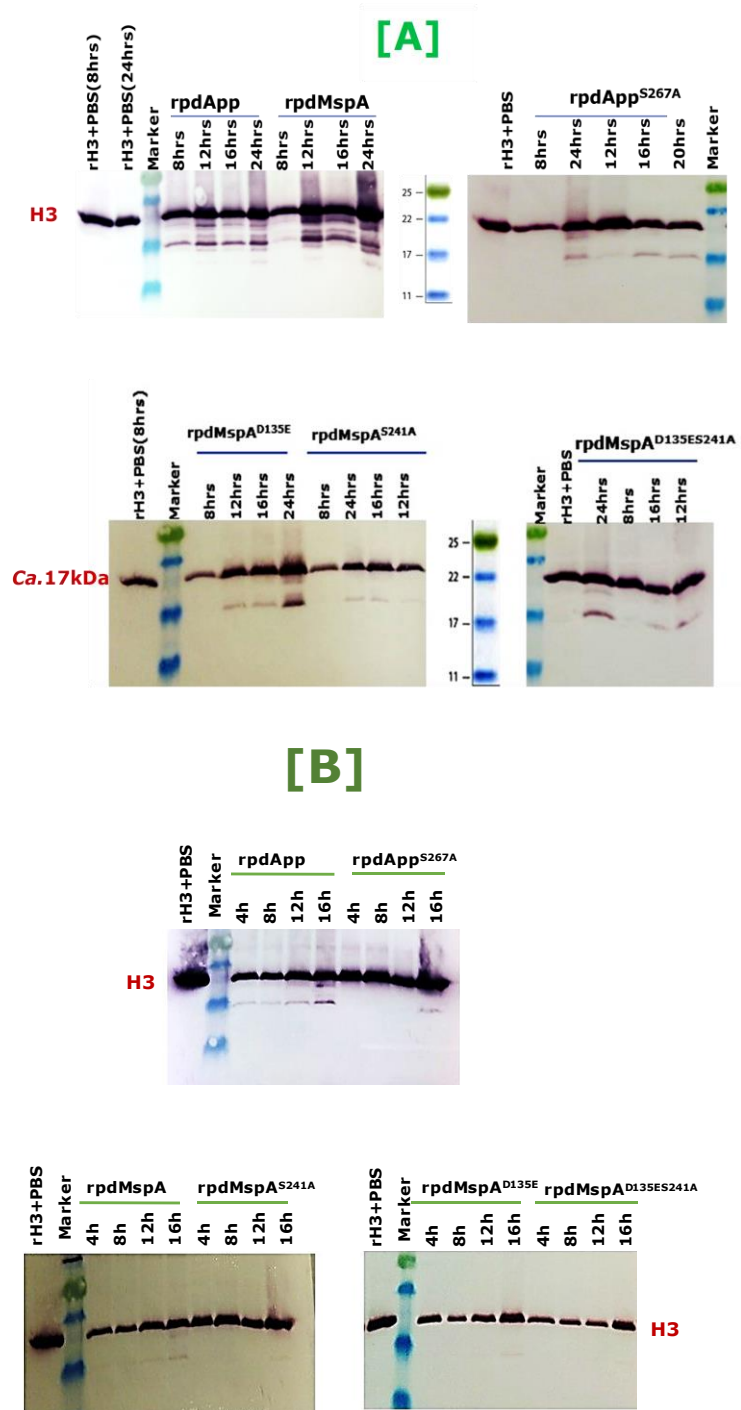


Figure 5.29: Dose-time dependent histones rH3 clipping assays.

Here, [A] 40nM ATs proteins were used for histone rH3 clipping assay [B] 20nM ATs proteins were used for clipping assay. 20nM /40nM autotransporter proteins (rpdApp, rpApp^{S267A}, rpdMspA, rpdMspA^{S241A}, rpdMspA^{D135E} and rpdMspA^{S241AD135E}) were incubated with 1.5ug rH3 and incubated for 24 h. The cleavage products were collected at 4 h, 8 h, 12 h, 16 h and 24 h. 20nM App and MspA showed less truncated clipping products than 40nM ATs. 20nM rpdApp showed cleavage within 4 h where rpdMspA showed clipping after 12 h and faded clipping band was observed with mutants after 16 h incubation. In some clipping assays, the thicker band was observed after 16h incubation, but the same volume of reaction was used in each lane. It may be the reason of the last sample contained precipitated material from the bottom of the tube.

Time-course and dose-response experiments demonstrated the proteolytic processing of histone H3 by App and MspA rapidly increased for long time incubation with high concentrations. The optimal point of clipping assays was where the clipped H3 histones (rH3 and cell derived H3) was found with App and MspA proteins but the full-length size of histones H3 were observed with mutants of App and MspA proteins as with the PBS negative control.

After optimisation, the H3 clipping assay was performed; 40nM autotransporters were co-incubated with either rH3 or CH3 for 8 h. Similar results were obtained when histone rH3 was treated with 20nM autotransporters for 12 h.

The cleavage products were subjected to immunoblotting using C-terminal monoclonal anti-histone H3 (ab10799). The results confirmed rH3 histone clipping by rpdApp and rpdMspA but not with any of the mutants of these proteins, including the aspartate mutation of MspA.

In addition, we observed that MspA wild type (rpdMspA) cleaved CH3 less efficiently than App wild type (rpdApp) (Figure 5.30). The cleavage products of cell derived purified histone-H3 were more prominent with rpdApp treated

histone as compared with rpdMspA treatment, indicating that App was the more active of the two autotransporters against this histone.

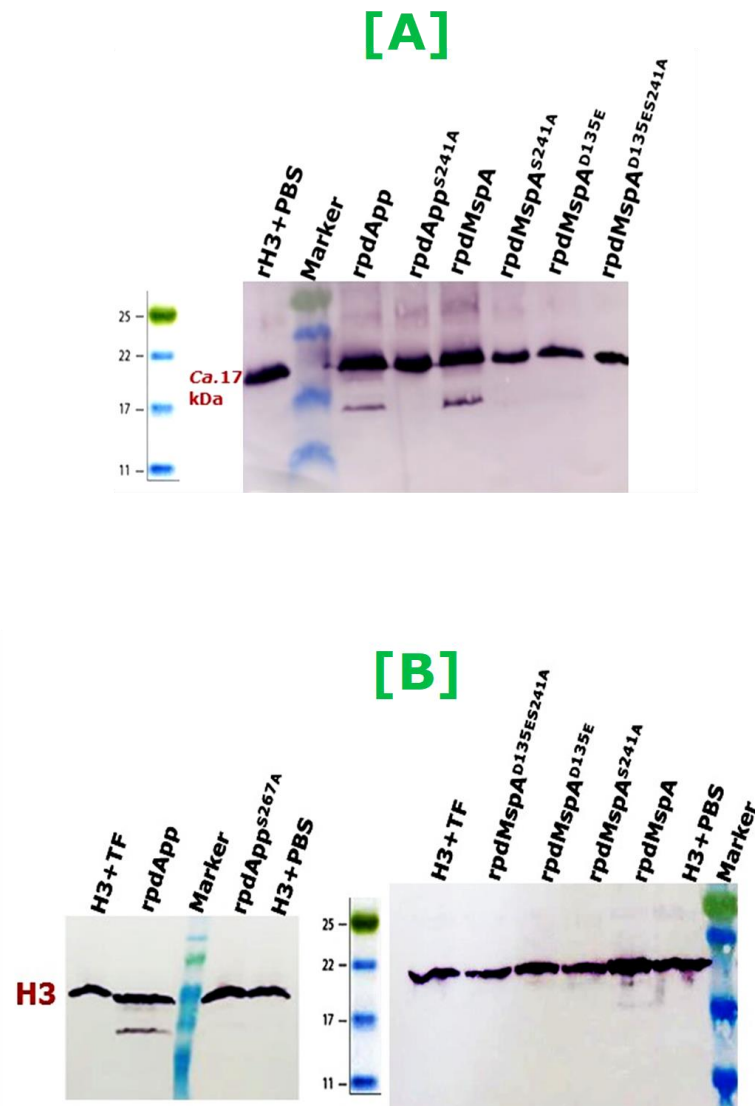


Figure 5.30: Optimised serine protease mediated histone H3 clipping assay. Here, [A] rH3 clipping assay [B] Hep-2 cell-derived H3 clipping assay. In these assays, 40nM autotransporters (rpdApp, rpAppS267A, rpdMspA, rpdMspAS241A, rpdMspAD135E and rpdMspAS241AD135E) were incubated with rH3/CH3 for 8 h at 37°C. After incubation, the cleavage reactions were stopped with SDS-PAGE sample buffer and analysed by immunoblotting with C-terminal monoclonal anti-histone H3 (ab10799) to detect the N-terminal histone H3 tail clipping.

The results described the cleavage products of rH3/CH3 with the rpdApp and rpdMspA according to the faster migrating another additional band <17kDa with the full-length histone. No cleavage with serine mutants demonstrated the N-terminal histone H3 clipping is due to active serine residue. No apparent difference was observed with rH3 and CH3 clipping by rpdApp but MspA showed less efficacy for cell derived histone H3 proteolytic processing.

The overall histone H3 clipping results demonstrated that the time and concentration of autotransporters had dramatic effects on histone H3 proteolysis processing and thus careful optimisation was required to demonstrate the role of the catalytic triad in MspA. The dependence on the catalytic triad was not complete in this case as prolonged incubation with relatively high concentrations of the mutant version of this protease resulted in similar activity to the wild type parent molecule.

5.2.7. Cellular histone clipping assay

The previous experiments were conducted using purified proteins in a very controlled manner and might not reflect the *in vivo* situation very accurately. For example, they do not take into account the fact that the ATs have to bind to host cells and be trafficked to the nucleus before histone clipping can occur. In the experiments described in this section, App and MspA proteins as well as their active site serine mutants into host cells, and after allowing time for binding, trafficking and cleavage, histones were extracted and analysed for evidence of clipping.

5.2.7.1. Cell viability assay

Prior to histone clipping assays in cells, the cellular toxicity of App and MspA proteins were assessed with Hep-2 cells lines using a cell viability assay. The

Hep-2 cells were exposed with 40nM to 400nM rpdApp and rpdMspA and their respective seine mutants and incubated at 37°C for 20 h and monitored post-exposure by phase-contrast microscopy and cell viability was measured using an XTT assay which measured the cell metabolic activity of cells to reduce the tetrazolium salts. A dose-dependent cell death of treated Hep-2 cells was observed when the proteases were added at ≥ 250 nM concentration. However, App and MspA did not reduce cell viability when added at a concentration of 40nM.

No noticeable change of the cell viability was observed between the untreated control and rpdApp- and rpdMspA-treated cells as compared with cells treated with Staurosporine, which was used as a positive control as a known inducer of cellular apoptosis. The lack of toxicity of App and MspA proteins was also confirmed by viable cell counting with trypan blue (not shown) which demonstrated the cell viability actually increased in cells treated with rpdApp or rpdMspA at concentration of 40nM or 200nM. In the XTT assay, metabolic activity of rpdApp- and rpdMspA-treated cells increased compared with untreated negative control cells. Positive control cells treated with Staurosporine showed a significantly reduced metabolic activity (Figure 5.31 and 5.32).

Interestingly, no significant difference was observed between cells treated with the active site serine mutants of the respective proteins compared to untreated control cells. These data revealed that App and MspA proteins could both induce increases in the metabolic activity of host cells. The observation that this effect was not observed in the serine mutants suggests that the effect was dependent on the proteolytic activity of the autotransporter proteins.

[A]



[B]

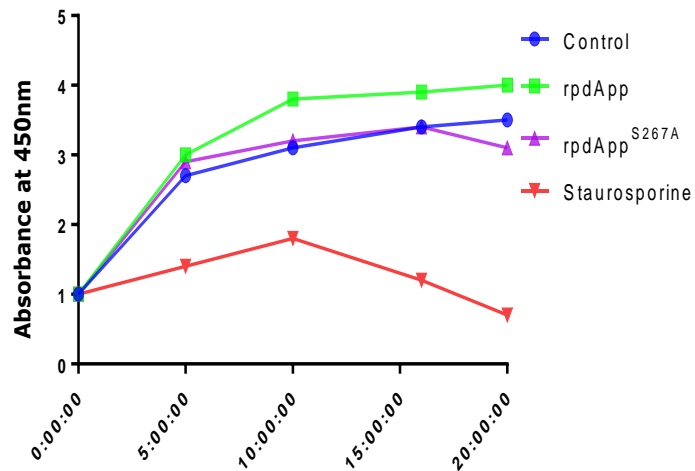
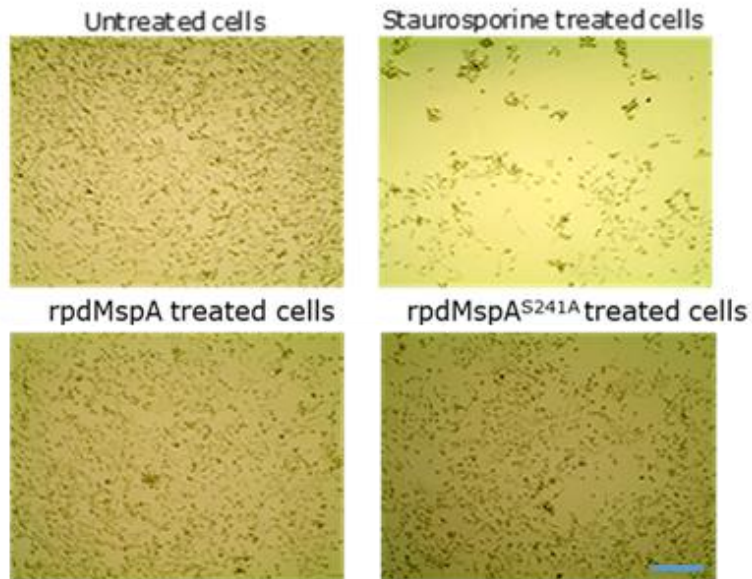


Figure 5.31: Toxicity of recombinant App autotransporter to Hep-2 cells. Here [A] showed the microscopic images of rpdApp, serine mutant of rpdApp, staurosporine toxin treated and untreated Hep-2 cells. [B] cell metabolic activity was monitored with following XTT assay. 1×10^{10} Hep-2 cells were exposed to 40nM rpdApp and rpdApp^{S267A} in triplicate and incubated for 20 h time course

using XTT assay. Untreated Hep-2 cells were used as negative control and Staurosporine (2uM) was used as a positive control. Values presented are the mean \pm SE of three independent separate experiments and were analysed by ANOVA and Tukey's multiple comparison test. The images suggest no deleterious effects of autotransporter exposure. The XTT assay shows significantly increased metabolic activity induced by rpdApp (p value $** < 0.0097$) compared with negative control. The active site serine mutant showed no significant difference compared to control, which indicated the proteolytic processing might be associated with the observed effect on metabolic activities. Staurosporine induced highly significant reduction in absorbance compared to control $p < 0.0001$.

[A]



[B]

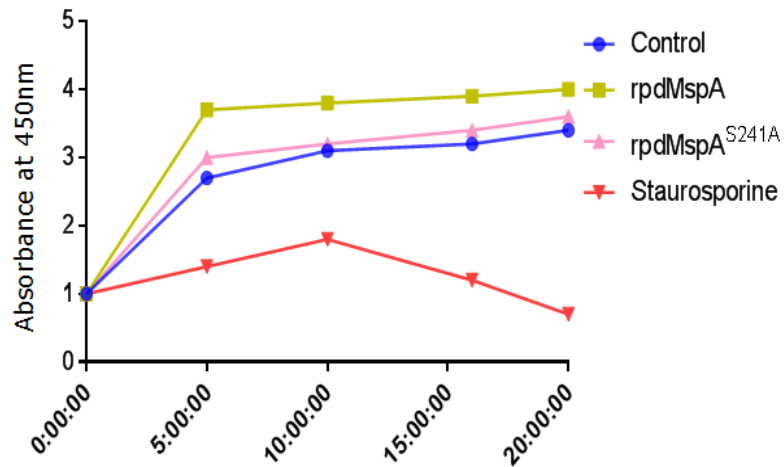


Figure 5.32: Toxicity of recombinant autotransporter MspA to Hep-2 cells. [A] Representative images show the appearance of Hep-2 cells following no treatment, or treatment with rpdMspA, rpdMspA^{S267A} or Staurosporine. [B] Cell metabolic activity has monitored post-exposure using the XTT assay. Values presented are the mean \pm SE of three independent experiments and were

analysed by ANOVA and Tukey's multiple comparison test. The images suggest no deleterious effects of autotransporter exposure. The XTT assay shows significantly increased metabolic activity induced by rpdMspA (p value $* < 0.0218$) as compared with negative control, whereas rpdMspA^{S241A} showed similar absorbance to the untreated cells.

5.2.7.2. Proteolysis of H2B and H3 histones in Hep-2 cells treated with App or MspA

In previous experiments, we demonstrated the proteolysis of purified rH2B/CH2B and rH3/CH3 histones incubated with recombinant App and MspA. It is possible, however, that such proteolysis represents an artefact of the artificial experimental conditions employed. During infection, the autotransporters would need to be transported across the cytosol and into the nucleus of host cells before accessing the histones. To explore the possible proteolytic processing of histones by exogenous App and MspA, Hep-2 cells were exposed to recombinant App or MspA at different concentrations (at 40nM, 80nM, 150nM and 250nM). The most discriminating concentration state was found at 150nM. Hep-2 cells were exposed with 150nM App or MspA for different times prior to lysis and analysis by immunoblotting. The presence of H3 and H2B protein derivatives was confirmed by probing the extracted whole cell lysates of the rpdApp- and rpdMspA-treated Hep-2 cells with C-terminal monoclonal anti-Histone H3 and C-terminal anti-histone H2B. Hep-2 cells were co-incubated with 150nM active rpdApp, rpdMspA and their serine mutant proteins individually, followed by lysis of the treated cells and immunoblotting of the lysed samples. Histones H2B and H3 were both observed to undergo proteolytic processing in cells treated with rpdApp or rpdMspA, which was confirmed by the observation of faster migrating additional bands detected in

lysates of Hep-2 cells probed with their respective anti-histone antibodies that were not observed in lysates of untreated Hep-2 cells (Figure 5.33 [A] & [B]). The analysis showed no proteolysis of histones H2A and H4 (Figure 5.33 [C]), which was consistent with the previous findings when purified proteins (rH2A/CH2A and rH4/CH4) were co-incubated with the proteases. rpdApp-treated cells showed more prominent cleavage products compared with rpdMspA-treated cells. No activity was observed in cells treated with the serine mutants of either rpdApp or rpdMspA.

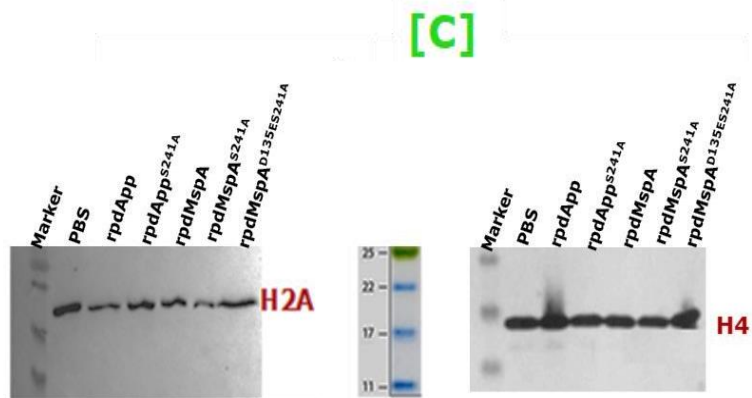
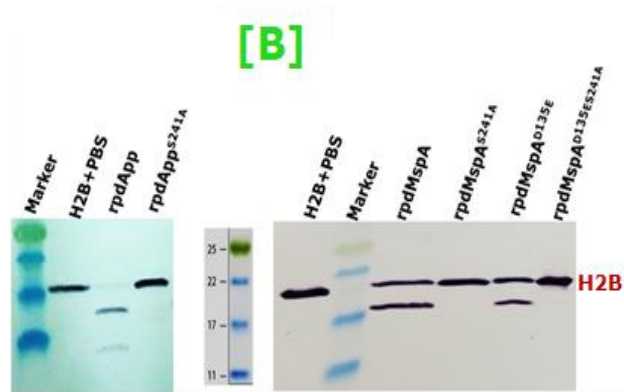
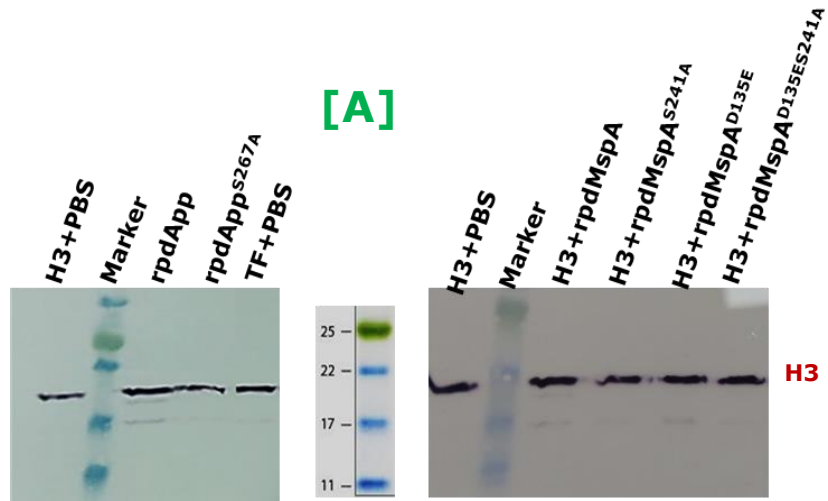


Figure 5.33: Clipped histones formed in Hep-2 cells by App and MspA. **[A]** Immunoblotting of histone H3 from lysates of rpdApp- and rpdMspA-treated

Hep-2 cells, and [B] Immunoblotting analysis of H2B histones from lysates of rpdApp- and rpdMspA-treated Hep-2 cells. [C] Immunoblotting of histone H2A & H4 from lysates of rpdApp- and rpdMspA-treated Hep-2 cells. Hep2 cells were treated with 150nM rpdApp, rpdMspA, rpdApp^{S267A} and rpdMspA^{S241A}, rpdMspA^{D135E} rpdMspA^{D135ES241A} and incubated for 12 h at 37°C. Then the cells were harvested after incubation and the proteins were examined by immunoblotting of cell lysates with their specific anti-histone Abs.

The presence of faster migrating additional bands of histones H3 and H2B by rpdApp and rpdMspA confirmed the histone clipping activity of these both proteins in cells treated with exogenous autotransporters, demonstrating that the proteins can traverse the cell cytosol and enter the nucleus in sufficient quantities to cleave the histones. It also demonstrates that the histones within the nucleus are accessible to the proteolytic activity of rpdApp and rpdMspA.

5.2.8. Cleaved histones H3 and H2B are associated with chromatin

In order to determine whether the cleaved histone products found in whole cells treated with the two autotransporter proteases were associated with chromatin, the rpdApp- and rpdMspA-treated Hep-2 cells or untreated cells were fractionated using the subcellular protein purification kits. Chromatin fractions were resolved on SDS-PAGE (Figure 5.34 [A]) and probed with C-terminal monoclonal anti-histone H3 and C-terminal anti-histone H2B by immunoblotting. Histone H3 and H2B clipped products were observed in the chromatin fractions of protease-treated cells (Figure 5.34 [B]), demonstrating that histones within chromatin are susceptible to the proteolytic activity of the autotransporters, and that the clipped products remain chromatin-associated, suggesting that they remain incorporated into nucleosomes.

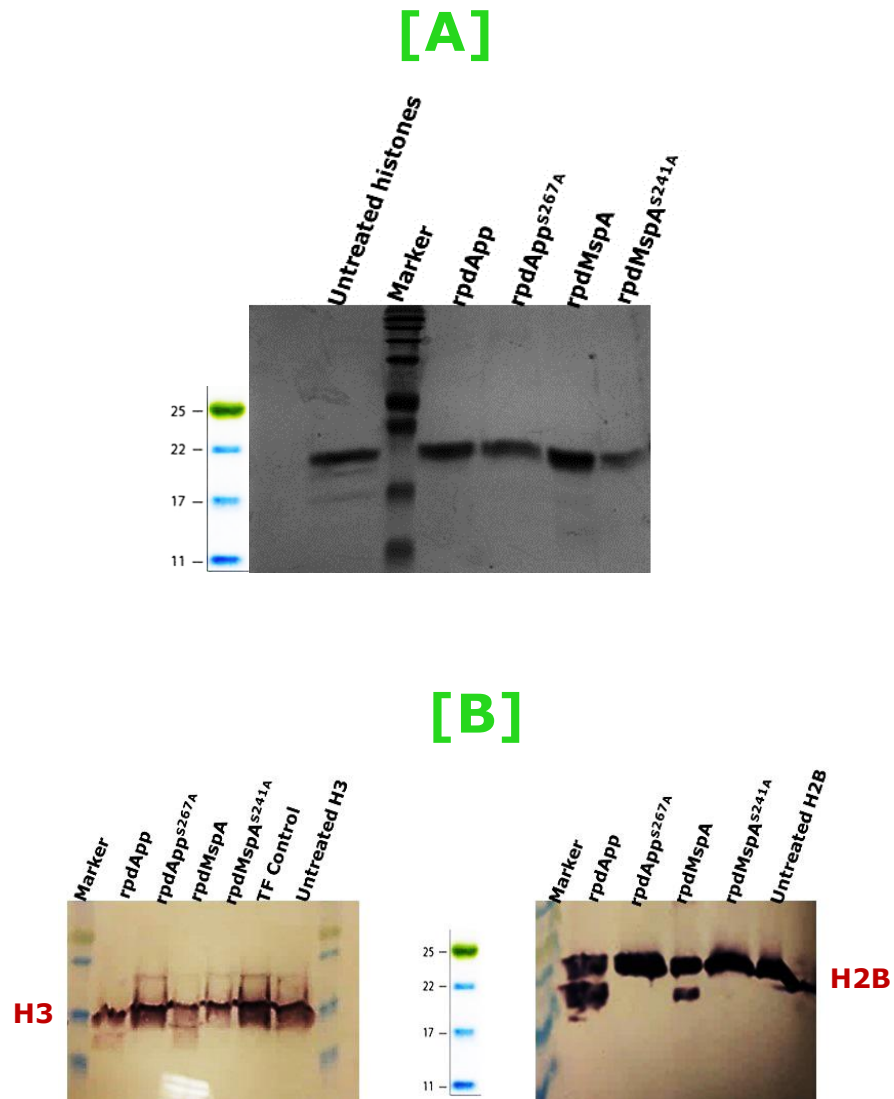


Figure 5.34: Clipped histones accumulated within chromatin. **[A]** The chromatin protein fractions from *rpdApp*- and *rpdMspA*-treated Hep-2 cells were analysed by SDS-PAGE. **[B]** Immunoblotting analysis of H3 and H2B histone clipping from the chromatin fractions. N-terminal cleavage fragments of histone H2B and H3 were associated with chromatin preparations. H1 histone was not found from chromatin fraction.

Collectively our findings demonstrated that App and MspA serine proteases are proteolytically active against H1, H2B and H3 histones, that this activity was dependent at least partially on the presence of an intact catalytic serine protease

triad, and that the activity could be observed in intact cells treated with exogenous proteases. Finally, the histones undergoing proteolysis were contained within chromatin and thus are presumed to be associated with nucleosomes.

5.3. Discussion

In eukaryotic cells, processed histones are an intriguing topic of epigenetics [255]. In eukaryotic cells histones are the central players of chromatin where DNA processes are controlled through a process of imprinting. The histones themselves are regulated by a process of post-translational modification (PTM), which mainly occurs along their N-terminal tails [264]. Genome studies have shown that various modifications in a specific genomic region can lead a 'histone code,' which can define either an 'open' or 'closed' state of chromatin, which in turn can influence gene expression in this region [265]. Histone hydrolysis can cause the irreversible alteration of PTM, which has been reported by several authors [264, 266, 267]. Some outstanding discoveries have demonstrated the proteolysis of histone are processed by proteases including Cathepsin L-cysteine protease [268], Glutamate dehydrogenase [269], Human ESC protease [270], Yeast endopeptidase [271], vacuolar protease B (prb1) in yeast [272], serine type protease in yeast, Foot-and-Mouth disease about a contribution in picorna viral 3C protease -FMDV3C Protease [260], tryptase [273], an cysteine protease of chicken liver [261], a nuclear localised cysteine proteases are associated with histone H3 clipping in colorectal cancer cell lines [274], Jumonji C domain containing proteins -JMJD5 and JMJD7 has been identified as histone proteases [275], protease directed mode of chromatin organisation in *P. falciparum* [276]. The work described here shows that the two meningococcal autotransporter proteins App and MspA are similarly capable of modifying histone proteins within chromatin.

In Eukaryotic cells, the chromosomal DNA is maintained in a compact form along with the histones in the nucleosomes. There are five major histones

families: H1, H2A, H2B, H3 and H4. We successfully purified each of these major histones in fractions including histone H1 alone, histones H2A and H2B and histones H3 and H4. The respective human recombinant histones were shown to be the same size as their cell-derived equivalents by immunoblotting. It was previously reported by our group that the recombinant histone-H3 was susceptible to clipping by App and MspA [215]. However, because recombinant histones produced in *E. coli* may differ from in situ histones within human cells, especially in terms of potential post translational modifications, we wished to extend these findings to human cell derived histones. Thus, we examined all of the human cell derived histone groups for their susceptibility to cleavage by App and MspA autotransporters in parallel with their respective recombinant equivalents.

In this work, pColdTF and *E. coli* expression systems were used to express and to purify the functional passenger domains (rpdApp and rpdMspA) of the meningococcal autotransporters App and MspA and their mutant derivatives. The pColdTF vector used to purify of these proteins contained the *cspA* promoter which enhances the expression of the target proteins at low temperatures (15°C) and also blocks expression of bacterial cell proteins. The trigger factor (TF) fusion improved the solubility of the target protein [277-279], and the N-terminal His-tag facilitated the isolation, purification, and identification of the fusion protein. We successfully purified rpdApp and rpdMspA wild types proteins, as well as mutant derivatives in which specific amino acids belonging to the putative serine protease catalytic triad had been replaced.

The proteolytic activity of both proteins was confirmed and they were both shown to have activity against histones H1, H3 and H2B, but not against histones H2A or H4. In the case of histones H3 and H2B the proteolytic activity

was confirmed to be serine protease activity as it was sensitive to the serine protease inhibitor PMSF. To confirm that the observed activity was serine protease activity, three different mutants of MspA were created by targeting amino acids within the putative catalytic triad: serine and aspartate. These amino acids were mutated individually and in combination and the resulting mutants were analysed for their ability to process histones H1, H2B and H3. When the serine component of the putative catalytic triad within rpdMspA was mutated, the mutant protein retained some activity, which was only distinguished from that of its wild type parent by careful titration and timing of the experiments. Optimization of the experimental design provided evidence to confirm that histone cleavage of App and specifically MspA was dose and time-dependent: findings also supported the study of Xu et al. [280], which reported that activated protein C (APC) can effectively cleave histones in a dose-dependent fashion. In general, rpdApp was more active than rpdMspA, but mutation of its catalytic triad serine residue had a more dramatic effect on the activity of the protein, although in some experiments a small residual activity was retained by the serine mutant of rpdApp.

Linker histone H1 is positioned on top of the nucleosome core particles stabilizing higher-order chromatin structure and is located near the nucleosome of entry and exit site of DNA. H1 promotes the folding of chromatin into its compact form, facilitates the spacing and position of the nucleosome, and regulating gene expression [281]. In our study, we showed that H1 was highly susceptible to proteolysis with App and MspA. We can speculate that H1 proteolysis by App or MspA is likely to alter nucleosome structures and/or position resulting in remodelling of the chromatin complex. Zhang et al. reported Granzymen-A enzyme-mediated complete H1 cleavage and core histone

digestion provides a mechanism for unfolding compacted chromatin and facilitates endogenous DNase access to DNA during T cell and natural killer cell granule-mediated apoptosis [282]. It was also reported, in the *Chlamydia trachomatis* EUO gene encoded protease mediated H1 histone proteolysis resulting in the chromatin de-condensation [283]. A research study reported the evidence that linker histone depletion, including depletion of H1.2, caused cell cycle arrest in the G1-phase, suppresses the expression of cell cycle genes, and decreased nucleosome spacing, H1.4 depletion caused cell death in T47D cells and depletion of individual histone H1 variants have been observed in breast cancer cells [284]. It is thus likely that App and MspA mediated H1 cleavage may cause deregulation of DNA-Histone communication in a way that alters chromatin structure and function.

Some studies reported that the removal of the N terminal tail of H2B modulated nucleosome sliding [285, 286]. In eukaryotes, ATP-dependent chromatin remodelling factors modulate chromatin structure, many of the factors do that via nucleosome sliding. These factors use the energy by ATP hydrolysis to disrupt the histone-DNA interactions which increases the nucleosomal DNA accessibility and also helps to induce the sliding of the histone octamers to adjacent DNA segments ('sliding'), and may even lead to displacement of a histone octamer to a different DNA segment [287]. It was also reported that tryptase enzyme mediated clipping of the N-terminal tail of H2B in mast cells is required to maintain cell identity [273]. In this study, they reported about the absence of tryptase can cause an age-dependent accumulation of the epigenetic mark H2BK5ac which has an extensive effect on the cellular phenotypes accompanying with the change of chromatin of mast cells.

In much the same way, it can be hypothesized that App and MspA- mediated histone H2B clipping may destabilise the H2A-H2B dimer and H3-H4 tetramer interaction, and thus affect nucleosomes solubility.

Histone-H3 is a key factor in the regulation of the gene expression [271]. Thus, it may be an important potential target for pathogen directed proteolysis. Histone H3 can be processed proteolytically at different cleavage sites where the peptide bond is hydrolysed by proteases [255]. As an example, Cathepsin L-cysteine protease is associated with H3 clipping. A previous study from our group showed that App and MspA interact with rH3 histones [215] and here we have shown that in situ-derived histone H3 is cleaved by the bacterial enzymes. The work described here also provides better evidence for cleavage of this histone as the multiple bands detected previously in the case of cell-derived H3 (CH3) by polyclonal anti-Histone H3 (ab1791), which cross-reacts with other human histones, have been resolved to a single band by use of the monoclonal C-terminal anti-histone H3.

In the recombinant histone and native histone clipping assays, the faster-migrating additional histone H3 band was detected with C-terminus-specific monoclonal anti-histone-H3 but not with N-terminus-specific anti-histone antibodies, indicating that H3 was proteolytically processed from N-terminus tail. This is consistent with previous observations of N-terminal clipping of this histone by various with proteases [268, 288].

The N-terminal region -of Histone H3 (1-21a.a) is thought to be a key regulator of gene expression in various systems including *P. falciferum* [276], and cells infected with foot and mouth disease virus (FMDV). In the latter case the virus controls the host cell's transcription by modulating histone H3 N-terminal cleavage [289]. Duncan et al. reported that H3.3 tail cleavage by

Cathepsin L plays a significant role in silencing the transcription of cell cycle-promoting genes [268]. In 2009, Santos-Rosa et al. found a serine protease-H3 endopeptidase and showed that clipped histone H3 was associated with induction of gene expression [271]. Kim et al. has reported the histone H3 N-terminal proteolysis induces gene activation during osteoclast differentiation [290]. Additionally, other studies have supported the theory that histone tail cleavage is associated with cellular processes including stem cell differentiation [270, 288], cellular senescence [291], DNA damaging stress [292] and yeast sporulation [271]. Clipped histones have also been found in chicken liver and *Tetrahymena* micronuclei [267, 269, 293].

Histone N-terminal tail modifications can also alter nucleosomal interactions to disrupt the chromatin structure which can play a crucial role in gene access [294]. Likewise, the clipping of N-terminal histone-H3 by App and MspA may alter the PTM modification of the histone tail and thus may destabilize the surrounding structures. This histone modification may impair transcription of associated genes and may influence additional cellular responses [295].

Chromatin conformation plays a central role in gene expression. In this study, we present the first evidence of histone proteolysis by App and MspA within whole cells. App and MspA mediated histone clipping have been shown here to occur in the chromatin milieu as has been observed in other systems [273]. For example, tryptase was shown to clip H2B within the chromatin and Tvardovskiy et al. demonstrated a relationship between histone clipping and PTM status of histones in human hepatocytes [273, 296]. This histone cleavage within chromatin also provides that in App- and MspA-exposed eukaryotic cells, App and MspA can enter into the nucleus and proteolytically process histones.

The App and MspA mediated histone proteolysis within chromatin suggested to be associated with nucleosome of the host cells. It is known that histone tails contribute in intra –inter nucleosomes interactions and play an essential role in the genomic DNA accessibility. Nucleosomes containing truncated H3/H4 can alter the conformation of nucleosomes which lead to regulate the accessibility DNA binding proteins to nucleosomal DNA [297]. Allis and his colleagues proposed a ‘‘histone code hypothesis’’ in which histone modification can play an important role in chromatin-associated processes [298]. In support of this theory, Nurse et al. reported that the clipping of flexible tails of histones H3 and H4 affects the structure and dynamics of the nucleosome [297], Polach et al. demonstrated that core histone tail domains on the equilibrium constants for dynamic DNA site accessibility in nucleosomes [299], and Lee et al. provided evidence that nucleosome depletion at active regulatory regions genome-wide and may be an important feature of eukaryotic transcriptional regulation [300]. The functional roles of histone cleavage are summarised (Figure 5.35).

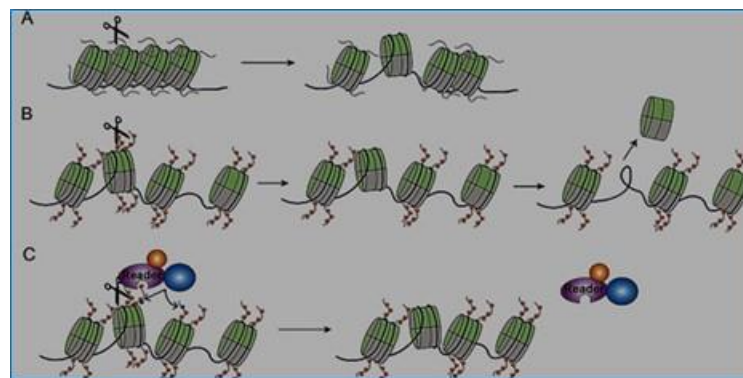


Figure 5.35: Schematic model presentation of the functional roles of histone cleavage in gene expression. (A) Histone clipping can influence chromatin compaction on accessibility. Histone tail clipping by protease enzyme might help to generate open chromatin structures, as a result of that DNA accessibility for transcription factors are increased, in that way contributing to gene activation.

(B) Initiation of histone exclusion. The truncated histone using protease makes unstable in the nucleosome. Histone tail clipping may persuade histone removal, allowing access of transcription factors into DNA in gene activation. (C) Amputation of PTMs and cooperating proteins. Histone tail cleavage may parade to the sweeping of multiple modifications, resulting in obstruction of the recruitment of effector proteins ("Reader" protein) or other PTM flows on histone tails [276, 301]. Adapted from: Sun -Ju Yi et al.[301].

In the same way, App and MspA mediated nucleosome-associated histone tail truncations may increase DNA accessibility, generating an open conformation of the nucleosome and leading to gene activation. Which genes are likely to be affected in this way, however, would need to be further investigated using Next Generation sequencing technologies.

Histone H3 cleavage by the serine proteases App and MspA in whole cells is likely to play an important role in the interaction between meningococcus and host cells during infection and/or meningococcal carriage. Recent findings have collectively made substantial progress towards exploring the possible mechanism of histone cleavage and the downstream consequences of this activity.

Namely, Histones antimicrobial activities play role in host defence system. It is possible that cleavage of histones within these structures may allow the bacteria to escape from these traps.

The current study shows that this area is likely to be important for meningococcal pathogenesis and provides new insights into the role of histone modification on epigenetic regulation during infection.

CHAPTER 6: General discussion

Pathogenic bacteria can employ various strategies to invade and co-opt the host cells to promote their intracellular survival and to modulate the activities of host cells to favour the bacteria. A number of bacterial virulence factors have been described that hijack nuclear processes of the host by translocating to the nucleus and targeting the nuclear proteins. In eukaryotic cells, the nucleus is the site of the vast majority of genes and it is here that gene expression is directed and controlled. Thus, bacterial molecules entering the nucleus, which have been named nucleomodulins, might have permanent genetic or long-term epigenetic effects on the host [302]. Over the last few years it has become evident that some pathogens can reprogram the chromatin to modulate host transcription [276, 303]. Host cell nuclear targeting by secreted proteins of Gram negative bacterial and some viral proteins is a common mechanism employed by microbes to hijack and regulate host transcription [194, 215, 233, 304].

Meningococcal cell surface-associated and secreted virulence factors can enable the bacteria to persist and survive in the host cell; among of these virulence factors autotransporter proteins are an important group. Meningococcal App and MspA autotransporter proteins each contain a serine protease motif (GDSGSP), which is identical to that found in other host targeting SPATEs proteins [180]. Recently it was reported that App, MspA and IgA1 can be internalised into host cells and can subsequently target the host nucleus [194, 215]. Several reports have also demonstrated that nuclear localisation of IgA1protease depends on the presence of the α -peptide [194]. IgA protease has two mutually exclusive secretory events based on the expression/non-expression of the phase-variable surface protease NalP, which is itself an autotransporter [183]. Of the two forms of IgA1 protease, the NalP-dependent secreted form is large molecule of *ca.* 160kDa containing an α -peptide, which in

turn contains the Nuclear localization signal (NLS). Besbes et al. showed that the NLS sequence-containing α -peptide was responsible for nuclear targeting of IgA protease in the host cell [194]. Similarly, App and MspA have two different secreted forms depending on the expression of NalP [183]. It is predicted that a peptide region absent in the smaller forms App and MspA would constitute an α -peptide present in the larger NalP-mediated forms of the two protein. We hypothesized that these larger forms may have roles in the nuclear trafficking of the host cells. How these forms can migrate from bacteria into the host cell nucleus is not clear; specifically, we do not know whether nuclear targeting is NLS dependent. This study was designed to address the hypothesis that nuclear targeting of App and MspA was NLS-dependant, and to define the NLS sequence of the two proteins.

We confirmed the nuclear localization of App and MspA. The DsRed-tagged protein expression approach adopted here to demonstrate nuclear localization was recently employed to study the localisation of IgA1protease [194]. The DsRed-tagged recombinant passenger domains of App and MspA employed corresponded to the larger, α -peptide-containing, forms of the passenger domains of the two proteins. When expressed in two human epithelial cell lines both proteins were localised to the nucleus. Moreover, in cells expressing recombinant App evidence for cellular apoptosis was observed, as we have reported previously [215]. To determine whether the proteolytic activities of the autotransporters were involved in their nuclear trafficking, serine mutants of the passenger domains of each protein were generated and expressed in epithelial cells. Both mutant proteins were translocated to the nucleus in a similar manner to their wild type parents, indicating that the proteolytic activity of the proteins was not required for used for the nuclear

localization approach which demonstrated the proteolytic activity was not required for their nuclear trafficking of these proteins.

Attempts to define functional NLS sequence of App and MspA involved construction of defined mutants lacking predicted NLSs or α -peptide regions. The nuclear localization of two mutant forms of App lacking the predicted NLS and α -peptide region, as well as a defined mutant form lacking the serine residues within the predicted NLS showed significant differences in nuclear trafficking compared to the intact passenger domain. In the absence of this motif, the protein was unable to reach to the nuclear compartment and its translocation was also lower after deletion of the serine residues. This analysis provides experimental evidence to support the hypothesis that the putative NLS sequence is essential for nuclear localization.

App contains a putative autocleavage site at 956F↓NTL959 [214]. This site has not been experimentally proved but is assumed to be the site of processing in the absence of the phase-variable maturation protease NalP [183]. Based on the evidence presented here it is possible that both secreted forms of App would retain nuclear targeting as both would retain the proposed NLS^{933R-940R}. Interestingly, a second putative NLS, ^{1149P-1156R}, which was proposed by van Ulsen et al., which would be predicted to be absent from the autoproteolytically processed form of secreted App but present in the longer NalP-processed form of the protein [183], would appear to be unable to direct the protein to the nucleus as this motif is retained in the deletion mutants $\Delta G^{901-L^{980}}$ and $\Delta G^{901-L^{965}}$, both of which failed to be translocated to the nucleus.

Now that the NLS sequence within MC58 App has been identified, analysis of App sequences from different strains of *N. meningitidis* and *N. gonorrhoeae* would determine the conservation of the APP NLS sequence at the

amino acid level across different lineages. The conservation of the NLS would have important consequences for the relative ability of different App molecules to access the nucleus and exert their functional effects.

By contrast to the findings with App, deletion of a proposed α -peptide of MspA had no significant effect on its nuclear trafficking. No classical NLS-like motif has been proposed for MspA but deletion of the region A¹⁰³⁷-I¹¹³⁹, which approximately corresponds to the α -peptide of App and IgA protease, did not prevent translocation to the nucleus. Interestingly, deletion of the region D⁹⁹⁹-A¹⁰⁷³ resulted in a protein that was not efficiently translocated to the nucleus but rather showed a punctate cytoplasmic localization although a few transfected cells showed nuclear localization of this truncated protein, suggesting that the signal for nuclear localisation had not been removed. The reason for the difference in distribution of this protein compared to the wild type may be due to an instability of the mutant protein, which might be aggregating in the cytoplasm. Unfortunately, we did not find any specific region of MspA for nuclear trafficking. At the beginning of the project we attempted to identify putative NLSs within the MspA passenger domain. The prediction programmes <http://rostlab.org/service/nlsdb>, PredictsNLS-omicX and SeqNLS did not predict any NLSs in MspA, which is why we took a less targeted approach to identifying a region within the predicted α -peptide. Very late in the project, however, an additional prediction programme - cNLS mapper was used. This predicted a possible NLS at position 933N to 961N. Unfortunately, it was too late to generate a deletion mutant specifically targeting this region. Thus, it will be important to generate such a mutant in order to determine whether this motif is required for nuclear localisation of MspA.

There are many challenges towards gaining a full understanding of the contribution of the nuclear targeting of App and MspA during meningococcal disease, and perhaps carriage of *N. meningitidis*. It would be of interest to know whether any alterations in the epigenome occur, for example, that have long-term effects on host cells during meningococcal carriage. The role of nuclear the nuclear targeted autotransporters with respect to gene expression during pathogenesis will also require further study. Transcriptome analysis of cells exposed to nuclear targeting App and/or MspA should shed light on the effects of these proteins on host cell gene expression. Once differentially regulated genes are identified, it will also be possible to determine whether the proteolytic activity of the autotransporters is responsible for these changes by comparing the expression of these genes in cells expressing wild type and proteolytically inactive nuclear targeting variants of the proteins.

It is known that very few bacterial molecules can enter into the eukaryotic cell nuclei and these bacterial virulence factors can potentially reprogram, directly or indirectly, the chromatin-regulatory machinery. Histones are key components of the nuclear machinery that regulates gene transcription and undergoes a broad range of post-translational modifications (PTM) at the N-terminal tail of the protein. PTM of histones is suggested to regulate diverse chromatin-based processes. We have presented the first evidence of histone clipping in the context of whole cells, demonstrating that the chromatin is accessible to the nuclear targeted autotransporters. It was also confirmed that the observed proteolytic processing of histones by App was serine mediated and was time- and dose-dependent. The proteolytic activity of a serine mutant of MspA was unexpected, but not unprecedented [305]. The finding that recombinant histones produced in *E. coli* were processed by the two

autotransporters in the same way as human cell-derived histones and histones *in situ* in human cells indicates that the specificity of the autotransporters for these proteins is not dependent on post-translational modifications that are known to occur within the nucleus.

App and MspA both had maximal activity against the linker histone H1. This histone is likely to be most exposed to the proteases within chromatin compared to the core histones. Nevertheless, both App and MspA were also able to cleave the N-terminal tails of histones H2B and H3, which are thus also shown to be exposed to the proteases after their translocation into the nucleus. It is known that most of the post-translational modification of histones happens on N-terminal tail; cleavage of this tail is thus likely to have important consequences for the activities of these core histones.

Cytotoxic effects of some nuclear targeted bacterial proteins on host cells have been reported. Thus prior to histone clipping assays in whole cells, the toxicity of the protein was examined. At the concentrations used neither App nor MspA were toxic to the cells, which exhibited slightly higher metabolic rates after treatment with the proteins compared to untreated cells or cells treated with staurosporine (as positive control for apoptosis). The reason for the observed increase in cell metabolic activity is not clear, but it is clear that it results from an alteration in the transcription profile of the cells.

Neutrophils are present in very high numbers during meningococcal sepsis and meningitis. One of the mechanisms by which these cells fight bacterial infection is to release large amounts of DNA and associated histones to form extracellular traps. DNA-bound histones can then act to kill bacteria. It is thus possible that the histone clipping activity that has been demonstrated

for the meningococcal autotransporters may play a role in defence against this activity.

However, several questions have been raised: Where is the cleavage site of the histone clipping and what is the fate of the cleaved proteins? What is the influence of histone clipping on gene expression and other cellular processes, for example chromatin-associated DNA replication and repairing? What are the consequences of histone clipping during meningococcal disease and/or carriage?

This study provides insights into the nature of the interaction between the two meningococcal autotransporters and the host cells via nuclear localization and the clipping of nuclear protein histones. These findings are likely to have consequences for our understanding of the complex interactions between this pathogen and its host and may provide important insights more generally in the fields of host-pathogen interactions and in chromatin biology.

References

1. Mace, S.E., *Acute bacterial meningitis*. Emerg Med Clin North Am, 2008. **26**(2): p. 281-317, viii.
2. Tunkel, A.R., et al., *Practice guidelines for the management of bacterial meningitis*. Clin Infect Dis, 2004. **39**(9): p. 1267-1284.
3. Chaudhuri, A., et al., *EFNS guideline on the management of community-acquired bacterial meningitis: report of an EFNS Task Force on acute bacterial meningitis in older children and adults*. Eur J Neurol, 2008. **15**(7): p. 649-659.
4. Stephens, D.S., *Biology and pathogenesis of the evolutionarily successful, obligate human bacterium Neisseria meningitidis*. Vaccine, 2009. **27 Suppl 2**: p. B71-7.
5. Tommassen, J. and J. Arenas, *Biological Functions of the Secretome of Neisseria meningitidis*. Front Cell Infect Microbiol, 2017. **7**: p. 256.
6. Aho, E.L., et al., *Characterization of a class II pilin expression locus from Neisseria meningitidis: evidence for increased diversity among pilin genes in pathogenic Neisseria species*. Infect Immun, 1997. **65**(7): p. 2613-2620.
7. Caugant, D.A., G. Tzanakaki, and P. Kriz, *Lessons from meningococcal carriage studies*. FEMS Microbiol Rev, 2007. **31**(1): p. 52-63.
8. Uiterwijk, A. and P.J. Koehler, *A history of acute bacterial meningitis*. J Hist Neurosci, 2012. **21**(3): p. 293-313.
9. Pizza, M. and R. Rappuoli, *Neisseria meningitidis: pathogenesis and immunity*. Curr Opin Microbiol, 2015. **23**: p. 68-72.
10. Roupael, N.G. and D.S. Stephens, *Neisseria meningitidis: biology, microbiology, and epidemiology*. Methods Mol Biol, 2012. **799**: p. 1-20.
11. Rosenstein, N.E., et al., *Meningococcal disease*. N Engl J Med, 2001. **344**(18): p. 1378-1388.

12. Pace, D. and A.J. Pollard, *Meningococcal disease: clinical presentation and sequelae*. Vaccine, 2012. **30 Suppl 2**: p. B3-9.
13. Koomen, I., et al., *Neuropsychology of academic and behavioural limitations in school-age survivors of bacterial meningitis*. Dev Med & Child Neurol, 2004. **46**(11): p. 724-732.
14. de Souza, A.L. and A.C. Seguro, *Two centuries of meningococcal infection: from Vieusseux to the cellular and molecular basis of disease*. J Med Microbiol, 2008. **57**(Pt 11): p. 1313-1321.
15. Neisser, A., *Ueber cine der Gonorrhoe eigentumliche. Micrococcusform.*, 1879. **7**:: p. 497-500.
16. Greenwood, B., *Manson Lecture. Meningococcal meningitis in Africa*. Trans R Soc Trop Med Hyg, 1999. **93**(4): p. 341-353.
17. Flexner, S., *THE RESULTS OF THE SERUM TREATMENT IN THIRTEEN HUNDRED CASES OF EPIDEMIC MENINGITIS*. J Exp Med, 1913. **17**(5): p. 553-576.
18. Schoenbach, E.B. and J.J. Phair, *The sensitivity of meningococci to sulfadiazine*. Am J Hyg, 1948. **47**(2): p. 177-186.
19. Artenstein, M.S., et al., *Prevention of meningococcal disease by group C polysaccharide vaccine*. N Engl J Med, 1970. **282**(8): p. 417-420.
20. Hung, M.-C. and M. Christodoulides, *The Biology of Neisseria Adhesins*. Biology, 2013. **2**(3): p. 1054-1109.
21. Maiden, M.C., et al., *Multilocus sequence typing: a portable approach to the identification of clones within populations of pathogenic microorganisms*. Proc Natl Acad Sci U S A, 1998. **95**(6): p. 3140-3145.

22. Stephens, D.S., B. Greenwood, and P. Brandtzaeg, *Epidemic meningitis, meningococcaemia, and Neisseria meningitidis*. Lancet, 2007. **369**(9580): p. 2196-2210.
23. Rotman, E. and H.S. Seifert, *The genetics of Neisseria species*. Annu Rev Genet, 2014. **48**: p. 405-431.
24. Liu, T.Y., et al., *Studies on the meningococcal polysaccharides. II. Composition and chemical properties of the group B and group C polysaccharide*. J Biol Chem, 1971. **246**(15): p. 4703-4712.
25. Liu, T.Y., et al., *Studies on the meningococcal polysaccharides. I. Composition and chemical properties of the group A polysaccharide*. J Biol Chem, 1971. **246**(9): p. 2849-2858.
26. Harrison, O.B., et al., *Description and nomenclature of Neisseria meningitidis capsule locus*. Emerg Infect Dis, 2013. **19**(4): p. 566-573.
27. Crum-Cianflone, N. and E. Sullivan, *Meningococcal Vaccinations*. Infect Dis Ther, 2016. **5**(2): p. 89-112.
28. Ala'Aldeen, D.A.A. and D.P.J. Turner, *Neisseria meningitidis*. Principles and Practice of Clinical Bacteriology (Second Edition). Stephen H, Gillespie PMH (ed), 2006: p. 205-220.
29. Frasch, C.E., W.D. Zollinger, and J.T. Poolman, *Serotype antigens of Neisseria meningitidis and a proposed scheme for designation of serotypes*. Rev Infect Dis, 1985. **7**(4): p. 504-510.
30. Manchanda, V., S. Gupta, and P. Bhalla, *Meningococcal disease: history, epidemiology, pathogenesis, clinical manifestations, diagnosis, antimicrobial susceptibility and prevention*. Indian J Med Microbiol, 2006. **24**(1): p. 7-19.

31. Brehony, C., K.A. Jolley, and M.C. Maiden, *Multilocus sequence typing for global surveillance of meningococcal disease*. FEMS Microbiol Rev, 2007. **31**(1): p. 15-26.
32. Jolley, K.A., C. Brehony, and M.C. Maiden, *Molecular typing of meningococci: recommendations for target choice and nomenclature*. FEMS Microbiol Rev, 2007. **31**(1): p. 89-96.
33. Yazdankhah, S.P. and D.A. Caugant, *Neisseria meningitidis: an overview of the carriage state*. J Med Microbiol, 2004. **53**(Pt 9): p. 821-832.
34. Jolley, K.A. and M.C. Maiden, *Automated extraction of typing information for bacterial pathogens from whole genome sequence data: Neisseria meningitidis as an exemplar*. Euro Surveill, 2013. **18**(4): p. 20379.
35. Scheld, W.M., et al., *Pathophysiology of bacterial meningitis: mechanism(s) of neuronal injury*. J Infect Dis, 2002. **186 Suppl 2**: p. S225-233.
36. Hill, D.J., et al., *Cellular and molecular biology of Neisseria meningitidis colonization and invasive disease*. Clin Sci (Lond), 2010. **118**(9): p. 547-564.
37. Guidance for public health management of meningococcal disease in the UK. . **updated August 2019 From 2010/2011.**
38. Ladhani, S.N., et al., *Increase in endemic Neisseria meningitidis capsular group W sequence type 11 complex associated with severe invasive disease in England and Wales*. Clin Infect Dis, 2015. **60**(4): p. 578-585.
39. Oldfield, N.J., et al., *Rise in Group W Meningococcal Carriage in University Students, United Kingdom*. Emerg Infect Dis, 2017. **23**(6): p. 1009-1011.

40. Campbell, H., et al., *Emergency Meningococcal ACWY Vaccination Program for Teenagers to Control Group W Meningococcal Disease, England, 2015-2016*. *Emerg Infect Dis*, 2017. **23**(7): p. 1184-1187.
41. Wilder-Smith, A., *Meningococcal disease: risk for international travellers and vaccine strategies*. *Travel Med Infect Dis*, 2008. **6**(4): p. 182-186.
42. Taha, M.K., et al., *Serogroup W135 meningococcal disease in Hajj pilgrims*. *Lancet*, 2000. **356**(9248): p. 2159.
43. Abad, R., et al., *Molecular characterization of invasive serogroup Y Neisseria meningitidis strains isolated in the Latin America region*. *J Infect*, 2009. **59**(2): p. 104-114.
44. van de Waterbeemd, B., et al., *Improved OMV vaccine against Neisseria meningitidis using genetically engineered strains and a detergent-free purification process*. *Vaccine*, 2010. **28**(30): p. 4810-4816.
45. Theilen, U., et al., *Management of invasive meningococcal disease in children and young people: summary of SIGN guidelines*. *BMJ*, 2008. **336**(7657): p. 1367-1370.
46. Nadel, S. and J.S. Kroll, *Diagnosis and management of meningococcal disease: the need for centralized care*. *FEMS Microbiol Rev*, 2007. **31**(1): p. 71-83.
47. Anderson, J. and I. Lind, *Characterization of Neisseria meningitidis isolates and clinical features of meningococcal conjunctivitis in ten patients*. *Eur J Clin Microbiol Infect Dis*, 1994. **13**(5): p. 388-393.
48. Hart, C.A. and A.P.J. Thomson, *Meningococcal disease and its management in children*. *Bmj*, 2006. **333**(7570): p. 685-690.

49. Hazelzet, J.A., et al., *Complement activation in relation to capillary leakage in children with septic shock and purpura*. *Infect Immun*, 1998. **66**(11): p. 5350-5356.
50. Nielsen, H.E., et al., *Diagnostic assessment of haemorrhagic rash and fever*. *Arch Dis Child*, 2001. **85**(2): p. 160.
51. van der Woude, M.W. and A.J. Baumler, *Phase and antigenic variation in bacteria*. *Clin Microbiol Rev*, 2004. **17**(3): p. 581-611, table of contents.
52. Hammerschmidt, S., et al., *Capsule phase variation in Neisseria meningitidis serogroup B by slipped-strand mispairing in the polysialyltransferase gene (siaD): correlation with bacterial invasion and the outbreak of meningococcal disease*. *Mol Microbiol*, 1996. **20**(6): p. 1211-1220.
53. Hammerschmidt, S., et al., *Modulation of cell surface sialic acid expression in Neisseria meningitidis via a transposable genetic element*. *The EMBO journal*, 1996. **15**(1): p. 192-198.
54. Swain, C.L. and D.R. Martin, *Survival of meningococci outside of the host: implications for acquisition*. *Epidemiol Infect*, 2007. **135**(2): p. 315-320.
55. Schneider, M.C., et al., *Interactions between Neisseria meningitidis and the complement system*. *Trends Microbiol*, 2007. **15**(5): p. 233-240.
56. Spinosa, M.R., et al., *Neisseria meningitidis Capsule Is Important for Intracellular Survival in Human Cells*. *Infect Immun*, 2007. **75**(7): p. 3594.
57. Achtman, M., *Epidemic spread and antigenic variability of Neisseria meningitidis*. *Trends Microbiol*, 1995. **3**(5): p. 186-192.
58. Virji, M., *Pathogenic neisseriae: surface modulation, pathogenesis and infection control*. *Nat Rev Micro*, 2009. **7**(4): p. 274-286.

59. Uria, M.J., et al., *A generic mechanism in Neisseria meningitidis for enhanced resistance against bactericidal antibodies*. J Exp Med, 2008. **205**(6): p. 1423-1434.
60. Tzeng, Y.L., J. Thomas, and D.S. Stephens, *Regulation of capsule in Neisseria meningitidis*. Crit Rev Microbiol, 2016. **42**(5): p. 759-772.
61. Claus, H., et al., *Many carried meningococci lack the genes required for capsule synthesis and transport*. Microbiology, 2002. **148**(Pt 6): p. 1813-1819.
62. Otto, B.R., et al., *Crystal Structure of Hemoglobin Protease, a Heme Binding Autotransporter Protein from Pathogenic Escherichia coli*. J Biol Chem, 2005. **280**.
63. Finne, J., M. Leinonen, and P.H. Makela, *Antigenic similarities between brain components and bacteria causing meningitis. Implications for vaccine development and pathogenesis*. Lancet, 1983. **2**(8346): p. 355-357.
64. Kurzai, O., et al., *Carbohydrate composition of meningococcal lipopolysaccharide modulates the interaction of Neisseria meningitidis with human dendritic cells*. Cell Microbiol, 2005. **7**(9): p. 1319-1334.
65. Becker, S., et al., *A generic system for the Escherichia coli cell-surface display of lipolytic enzymes*. FEBS Lett, 2005. **579**.
66. Jennings, M.P., et al., *The genetic basis of the phase variation repertoire of lipopolysaccharide immunotypes in Neisseria meningitidis*. Microbiology, 1999. **145 (Pt 11)**: p. 3013-3021.
67. Scholten, R.J., et al., *Lipo-oligosaccharide immunotyping of Neisseria meningitidis by a whole-cell ELISA with monoclonal antibodies*. J Med Microbiol, 1994. **41**(4): p. 236-243.

68. Mandrell, R.E. and W.D. Zollinger, *Lipopolysaccharide serotyping of Neisseria meningitidis by hemagglutination inhibition*. Infect Immun, 1977. **16**(2): p. 471-475.
69. Bayliss, C.D., et al., *Neisseria meningitidis Escape from the Bactericidal Activity of a Monoclonal Antibody Is Mediated by Phase Variation of and Enhanced by a Mutator Phenotype*. Infect Immun, 2008. **76**(11): p. 5038.
70. Berrington, A.W., et al., *Phase variation in meningococcal lipooligosaccharide biosynthesis genes*. FEMS Immunol Med Microbiol, 2002. **34**(4): p. 267-275.
71. Zughaier, S.M., et al., *Differential induction of the toll-like receptor 4-MyD88-dependent and -independent signaling pathways by endotoxins*. Infect Immun, 2005. **73**(5): p. 2940-2950.
72. Brandtzaeg, P., et al., *Neisseria meningitidis lipopolysaccharides in human pathology*. J Endotoxin Res, 2001. **7**(6): p. 401-420.
73. Moran, A.P., M.M. Prendergast, and B.J. Appelmelk, *Molecular mimicry of host structures by bacterial lipopolysaccharides and its contribution to disease*. FEMS Immunol Med Microbiol, 1996. **16**(2): p. 105-115.
74. Strom, M.S. and S. Lory, *Structure-function and biogenesis of the type IV pili*. Annu Rev Microbiol, 1993. **47**: p. 565-596.
75. Craig, L. and J. Li, *Type IV pili: paradoxes in form and function*. Curr Opin Struct Biol, 2008. **18**(2): p. 267-277.
76. Virji, M., et al., *Identification of Epitopes Recognized by Monoclonal Antibodies SM1 and SM2 Which React with All Pili of Neisseria gonorrhoeae but Which Differentiate between Two Structural Classes of Pili Expressed by Neisseria meningitidis and the Distribution of Their Encoding Sequences in the Genomes of Neisseria spp*. Microbiology, 1989. **135**(12): p. 3239-3251.

77. Tzeng, Y.L. and D.S. Stephens, *Epidemiology and pathogenesis of Neisseria meningitidis*. *Microbes Infect*, 2000. **2**(6): p. 687-700.
78. Brown, D.R., et al., *Systematic Functional Analysis Reveals That a Set of Seven Genes Is Involved in Fine-Tuning of the Multiple Functions Mediated by Type IV Pili in Neisseria meningitidis*. *Infect Immun*, 2010. **78**(7): p. 3053.
79. Carbonnelle, E., et al., *A systematic genetic analysis in Neisseria meningitidis defines the Pil proteins required for assembly, functionality, stabilization and export of type IV pili*. *Mol Microbiol*, 2006. **61**(6): p. 1510-1522.
80. Nassif, X., *Interaction mechanisms of encapsulated meningococci with eucaryotic cells: what does this tell us about the crossing of the blood-brain barrier by Neisseria meningitidis?* *Curr Opin Microbiol*, 1999. **2**(1): p. 71-77.
81. Bille, E., et al., *A chromosomally integrated bacteriophage in invasive meningococci*. *J Exp Med*, 2005. **201**(12): p. 1905-1913.
82. Doulet, N., et al., *Neisseria meningitidis infection of human endothelial cells interferes with leukocyte transmigration by preventing the formation of endothelial docking structures*. *J Cell Biol*, 2006. **173**(4): p. 627-637.
83. Johansson, L., et al., *CD46 in meningococcal disease*. *Science*, 2003. **301**(5631): p. 373-375.
84. Kirchner, M., D. Heuer, and T.F. Meyer, *CD46-independent binding of neisserial type IV pili and the major pilus adhesin, PilC, to human epithelial cells*. *Infect Immun*, 2005. **73**(5): p. 3072-3082.
85. Bernard, S.C., et al., *Pathogenic Neisseria meningitidis utilizes CD147 for vascular colonization*. *Nat Med*, 2014. **20**(7): p. 725-731.

86. Helaine, S., et al., *PilX, a pilus-associated protein essential for bacterial aggregation, is a key to pilus-facilitated attachment of Neisseria meningitidis to human cells*. Mol Microbiol, 2005. **55**(1): p. 65-77.
87. Imhaus, A.F. and G. Dumenil, *The number of Neisseria meningitidis type IV pili determines host cell interaction*. Embo j, 2014. **33**(16): p. 1767-1783.
88. Fussenegger, M., et al., *Transformation competence and type-4 pilus biogenesis in Neisseria gonorrhoeae--a review*. Gene, 1997. **192**(1): p. 125-134.
89. Merz, A.J., M. So, and M.P. Sheetz, *Pilus retraction powers bacterial twitching motility*. Nature, 2000. **407**(6800): p. 98-102.
90. Orihuela, C.J., et al., *Laminin receptor initiates bacterial contact with the blood brain barrier in experimental meningitis models*. J Clin Invest, 2009. **119**(6): p. 1638-1646.
91. Alqahtani, F., et al., *Deciphering the complex three-way interaction between the non-integrin laminin receptor, galectin-3 and Neisseria meningitidis*. Open biol, 2014. **4**(10): p. 140053.
92. Coureuil, M., et al., *Meningococcus Hijacks a beta2-adrenoceptor/beta-Arrestin pathway to cross brain microvasculature endothelium*. Cell, 2010. **143**(7): p. 1149-1160.
93. Virji, M., *The structural basis of CEACAM-receptor targeting by neisserial Opa proteins: Response*. Trends in Microbiology, 2000. **8**(6): p. 260-261.
94. Zhu, P., G. Morelli, and M. Achtman, *The opcA and (psi)opcB regions in Neisseria: genes, pseudogenes, deletions, insertion elements and DNA islands*. Mol Microbiol, 1999. **33**(3): p. 635-650.

95. Toleman, M., E. Aho, and M. Virji, *Expression of pathogen-like Opa adhesins in commensal Neisseria: genetic and functional analysis*. Cell Microbiol, 2001. **3**(1): p. 33-44.
96. Unkmeir, A., et al., *Fibronectin mediates Opc-dependent internalization of Neisseria meningitidis in human brain microvascular endothelial cells*. Mol Microbiol, 2002. **46**(4): p. 933-946.
97. Muenzner, P., et al., *Carcinoembryonic antigen family receptor specificity of Neisseria meningitidis Opa variants influences adherence to and invasion of proinflammatory cytokine-activated endothelial cells*. Infect Immun, 2000. **68**(6): p. 3601-3607.
98. Chen, T., et al., *Several carcinoembryonic antigens (CD66) serve as receptors for gonococcal opacity proteins*. J Exp Med, 1997. **185**(9): p. 1557-1564.
99. de Jonge, M.I., et al., *Functional activity of antibodies against the recombinant OpaJ protein from Neisseria meningitidis*. Infect Immun, 2003. **71**(5): p. 2331-2340.
100. Wang, X., et al., *Immune Homeostatic Macrophages Programmed by the Bacterial Surface Protein NhhA Potentiate Nasopharyngeal Carriage of Neisseria meningitidis*. MBio, 2016. **7**(1): p. e01670-15.
101. Massari, P., et al., *Cutting edge: Immune stimulation by neisserial porins is toll-like receptor 2 and MyD88 dependent*. J Immunol, 2002. **168**(4): p. 1533-1537.
102. van der Ende, A., C.T. Hopman, and J. Dankert, *Multiple mechanisms of phase variation of PorA in Neisseria meningitidis*. Infect Immun, 2000. **68**(12): p. 6685-6690.

103. Tommassen, J., et al., *Isolation of Neisseria meningitidis mutants deficient in class 1 (porA) and class 3 (porB) outer membrane proteins*. Infect Immun, 1990. **58**(5): p. 1355-1359.
104. Van Der Ley, P., et al., *Topology of outer membrane porins in pathogenic Neisseria spp.* Infect Immun, 1991. **59**(9): p. 2963-2971.
105. Derrick, J.P., et al., *Structural and Evolutionary Inference from Molecular Variation in Neisseria Porins*. Infect Immun, 1999. **67**(5): p. 2406.
106. Massari, P., Y. Ho, and L.M. Wetzler, *Neisseria meningitidis porin PorB interacts with mitochondria and protects cells from apoptosis*. Proc Natl Acad Sci U S A, 2000. **97**(16): p. 9070-9075.
107. Massari, P., et al., *Improved purification of native meningococcal porin PorB and studies on its structure/function*. Protein Expr Purif, 2005. **44**(2): p. 136-146.
108. Kozjak-Pavlovic, V., et al., *Bacterial Porin Disrupts Mitochondrial Membrane Potential and Sensitizes Host Cells to Apoptosis*. PLOS Pathog, 2009. **5**(10): p. e1000629.
109. Schmitt, C., et al., *A Functional Two-Partner Secretion System Contributes to Adhesion of Neisseria meningitidis to Epithelial Cells*. J Bacteriol, 2007. **189**(22): p. 7968-7976.
110. Tala, A., et al., *The HrpB-HrpA two-partner secretion system is essential for intracellular survival of Neisseria meningitidis*. Cell Microbiol, 2008. **10**(12): p. 2461-2482.
111. Girard, V. and M. Mourez, *Adhesion mediated by autotransporters of Gram-negative bacteria: structural and functional features*. Res Microbiol, 2006. **157**(5): p. 407-416.

112. Henderson, I.R., F. Navarro-Garcia, and J.P. Nataro, *The great escape: structure and function of the autotransporter proteins*. Trends Microbiol, 1998. **6**.
113. Grifantini, R., et al., *Identification of iron-activated and -repressed Fur-dependent genes by transcriptome analysis of Neisseria meningitidis group B*. Proc Natl Acad Sci U S A, 2003. **100**(16): p. 9542-9547.
114. Noinaj, N., et al., *Structural basis for iron piracy by pathogenic Neisseria*. Nature, 2012. **483**(7387): p. 53-58.
115. Fletcher, L.D., et al., *Vaccine potential of the Neisseria meningitidis 2086 lipoprotein*. Infect Immun, 2004. **72**(4): p. 2088-2100.
116. Masignani, V., et al., *Vaccination against Neisseria meningitidis using three variants of the lipoprotein GNA1870*. J Exp Med, 2003. **197**(6): p. 789-799.
117. Madico, G., et al., *The meningococcal vaccine candidate GNA1870 binds the complement regulatory protein factor H and enhances serum resistance*. J Immunol, 2006. **177**(1): p. 501-510.
118. Schneider, M.C., et al., *Functional significance of factor H binding to Neisseria meningitidis*. J Immunol, 2006. **176**(12): p. 7566-7575.
119. Seib, K.L., et al., *Factor H-Binding Protein Is Important for Meningococcal Survival in Human Whole Blood and Serum and in the Presence of the Antimicrobial Peptide LL-37*. Infect Immun, 2009. **77**(1): p. 292.
120. McNeil, L.K., et al., *Role of factor H binding protein in Neisseria meningitidis virulence and its potential as a vaccine candidate to broadly protect against meningococcal disease*. Microbiol Mol Biol Rev, 2013. **77**(2): p. 234-252.

121. Martin, N.G. and M.D. Snape, *A multicomponent serogroup B meningococcal vaccine is licensed for use in Europe: what do we know, and what are we yet to learn?* *Exp Rev Vaccines*, 2013. **12**(8): p. 837-858.
122. Sim, R.J., et al., *Underestimation of meningococci in tonsillar tissue by nasopharyngeal swabbing.* *Lancet*, 2000. **356**(9242): p. 1653-1654.
123. Van Deuren, M., P. Brandtzaeg, and J.W. van der Meer, *Update on meningococcal disease with emphasis on pathogenesis and clinical management.* *Clin Microbiol Rev*, 2000. **13**(1): p. 144-166.
124. Diaz Romero, J. and I.M. Otschoorn, *Current status of meningococcal group B vaccine candidates: capsular or noncapsular?* *Clin Microbiol Rev*, 1994. **7**(4): p. 559-575.
125. Schembri, M.A., D. Dalsgaard, and P. Klemm, *Capsule shields the function of short bacterial adhesins.* *J Bacteriol*, 2004. **186**(5): p. 1249-1257.
126. Stephens, D.S., P.A. Spellman, and J.S. Swartley, *Effect of the (α 2 \rightarrow 8)-Linked Polysialic Acid Capsule on Adherence of *Neisseria meningitidis* to Human Mucosal Cells.* *J Infect Dis*, 1993. **167**(2): p. 475-478.
127. Klein, N.J., et al., *The influence of capsulation and lipooligosaccharide structure on neutrophil adhesion molecule expression and endothelial injury by *Neisseria meningitidis*.* *J Infect Dis*, 1996. **173**(1): p. 172-179.
128. Stephens, D.S., et al., *Pili and outer membrane appendages on *Neisseria meningitidis* in the cerebrospinal fluid of an infant.* *J Infect Dis*, 1982. **146**(4): p. 568.
129. Hopper, S., et al., *Effects of the immunoglobulin A1 protease on *Neisseria gonorrhoeae* trafficking across polarized T84 epithelial monolayers.* *Infect Immun*, 2000. **68**(2): p. 906-911.

130. Plant, L., et al., *Lipooligosaccharide structure contributes to multiple steps in the virulence of Neisseria meningitidis*. Infect Immun, 2006. **74**(2): p. 1360-1367.
131. Lécuyer, H., X. Nassif, and M. Coureuil, *Two strikingly different signaling pathways are induced by meningococcal type IV pili on endothelial and epithelial cells*. Infect Immun, 2012. **80**(1): p. 175-186.
132. Waage, A., et al., *The complex pattern of cytokines in serum from patients with meningococcal septic shock. Association between interleukin 6, interleukin 1, and fatal outcome*. J Exp Med, 1989. **169**(1): p. 333-338.
133. Hoffman, O. and R.J. Weber, *Pathophysiology and treatment of bacterial meningitis*. Ther Adv Neurol Disord, 2009. **2**(6): p. 1-7.
134. M.D, D.A., *INFECTIONS OF THE NERVOUS SYSTEM*. <http://neuropathology-web.org/chapter5/chapter5aSuppurative.html>, 2016.

Chapter 5

135. Nau, R. and W. Bruck, *Neuronal injury in bacterial meningitis: mechanisms and implications for therapy*. Trends Neurosci, 2002. **25**(1): p. 38-45.
136. Gotschlich, E.C., I. Goldschneider, and M.S. Artenstein, *Human immunity to the meningococcus. IV. Immunogenicity of group A and group C meningococcal polysaccharides in human volunteers*. J Exp Med, 1969. **129**(6): p. 1367-1384.
137. Bilukha, O.O. and N. Rosenstein, *Prevention and control of meningococcal disease. Recommendations of the Advisory Committee on Immunization Practices (ACIP)*. MMWR Recomm Rep, 2005. **54**(Rr-7): p. 1-21.

138. Reingold, A.L., et al., *Age-specific differences in duration of clinical protection after vaccination with meningococcal polysaccharide A vaccine*. Lancet, 1985. **2**(8447): p. 114-118.
139. Gold, R., et al., *Kinetics of antibody production to group A and group C meningococcal polysaccharide vaccines administered during the first six years of life: prospects for routine immunization of infants and children*. J Infect Dis, 1979. **140**(5): p. 690-697.
140. Jodar, L., et al., *Development of vaccines against meningococcal disease*. Lancet, 2002. **359**(9316): p. 1499-1508.
141. Finne, J., et al., *An IgG monoclonal antibody to group B meningococci cross-reacts with developmentally regulated polysialic acid units of glycoproteins in neural and extraneural tissues*. J Immunol, 1987. **138**(12): p. 4402-4407.
142. Nedelec, J., et al., *Evidence for autoimmune antibodies directed against embryonic neural cell adhesion molecules (N-CAM) in patients with group B meningitis*. J Neuroimmunol, 1990. **29**(1-3): p. 49-56.
143. Stein, D.M., et al., *Are antibodies to the capsular polysaccharide of Neisseria meningitidis group B and Escherichia coli K1 associated with immunopathology?* Vaccine, 2006. **24**(3): p. 221-228.
144. Nadel, S., *Prospects for eradication of meningococcal disease*. Archives of disease in childhood, 2012. **97**(11): p. 993-998.
145. Holst, J., et al., *Properties and clinical performance of vaccines containing outer membrane vesicles from Neisseria meningitidis*. Vaccine, 2009. **27**: p. B3-B12.
146. Giuliani, M.M., et al., *A universal vaccine for serogroup B meningococcus*. Proc Nat Acad Sci, 2006. **103**(29): p. 10834.

147. Harris, S.L., et al., *The bivalent factor H binding protein meningococcal serogroup B vaccine elicits bactericidal antibodies against representative non-serogroup B meningococci*. *Vaccine*, 2018. **36**(45): p. 6867-6874.
148. Brehony, C., D.J. Wilson, and M.C.J. Maiden, *Variation of the factor H-binding protein of Neisseria meningitidis*. *Microbiology (Reading, England)*, 2009. **155**(Pt 12): p. 4155-4169.
149. Costa, T.R., et al., *Secretion systems in Gram-negative bacteria: structural and mechanistic insights*. *Nat Rev Microbiol*, 2015. **13**(6): p. 343-359.
150. Economou, A., et al., *Secretion by numbers: protein traffic in prokaryotes*. *Mol Microbiol*, 2006. **62**(2).
151. Stathopoulos, C., et al., *Secretion of virulence determinants by the general secretory pathway in gram-negative pathogens: an evolving story*. *Microbes Infect*, 2000. **2**(9): p. 1061-1072.
152. Berks, B.C., T. Palmer, and F. Sargent, *The Tat protein translocation pathway and its role in microbial physiology*. *Adv Microb Physiol*, 2003. **47**: p. 187-254.
153. van Ulsen, P. and J. Tommassen, *Protein secretion and secreted proteins in pathogenic Neisseriaceae*. *FEMS Microbiol Rev*, 2006. **30**(2): p. 292-319.
154. Wooldridge, K., *Bacterial Secreted Proteins: Secretory Mechanisms and Role in Pathogenesis*. 2009: Caister Academic Press.
155. Hooda, Y., et al., *Slam is an outer membrane protein that is required for the surface display of lipidated virulence factors in Neisseria*. *Nature Microbiology*, 2016. **1**(4): p. 16009.

156. Henderson, I.R., R. Cappello, and J.P. Nataro, *Autotransporter proteins, evolution and redefining protein secretion*. Trends Microbiol, 2000. **8**(12): p. 529-532.
157. Grijpstra, J., et al., *Autotransporter secretion: varying on a theme*. Res Microbiol, 2013. **164**(6): p. 562-582.
158. Dautin, N. and H.D. Bernstein, *Protein secretion in gram-negative bacteria via the autotransporter pathway*. Annu Rev Microbiol, 2007. **61**: p. 89-112.
159. Henderson, I.R., et al., *Type V protein secretion pathway: the autotransporter story*. Microbiol Mol Biol Rev, 2004. **68**(4): p. 692-744.
160. van Ulsen, P., *Protein folding in bacterial adhesion: secretion and folding of classical monomeric autotransporters*. Adv Exp Med Biol, 2011. **715**: p. 125-142.
161. Wells, T.J., et al., *Autotransporter proteins: novel targets at the bacterial cell surface*. FEMS Microbiol Lett, 2007. **274**(2): p. 163-172.
162. Henderson, I.R. and J.P. Nataro, *Virulence functions of autotransporter proteins*. Infect Immun, 2001. **69**(3): p. 1231-1243.
163. Rutherford, N. and M. Mourez, *Surface display of proteins by Gram-negative bacterial autotransporters*. Microbial Cell Factories, 2006. **5**(1): p. 1-15.
164. Ieva, R., K.M. Skillman, and H.D. Bernstein, *Incorporation of a polypeptide segment into the beta-domain pore during the assembly of a bacterial autotransporter*. Mol Microbiol, 2008. **67**(1): p. 188-201.
165. Ruiz-Perez, F., et al., *Roles of periplasmic chaperone proteins in the biogenesis of serine protease autotransporters of Enterobacteriaceae*. J Bacteriol, 2009. **191**(21): p. 6571-6583.

166. Purdy, G.E., C.R. Fisher, and S.M. Payne, *IcsA Surface Presentation in Shigella flexneri Requires the Periplasmic Chaperones DegP, Skp, and SurA*. J Bacteriol, 2007. **189**(15): p. 5566.
167. Volokhina, E.B., et al., *Role of the periplasmic chaperones Skp, SurA, and DegQ in outer membrane protein biogenesis in Neisseria meningitidis*. J Bacteriol, 2011. **193**(7): p. 1612-1621.
168. Sauri, A., et al., *Autotransporter beta-domains have a specific function in protein secretion beyond outer-membrane targeting*. J Mol Biol, 2011. **412**(4): p. 553-567.
169. Desvaux, M., et al., *The general secretory pathway: a general misnomer?* Trends Microbiol, 2004. **12**(7): p. 306-309.
170. Albrecht, R. and K. Zeth, *Crystallization and preliminary X-ray data collection of the Escherichia coli lipoproteins BamC, BamD and BamE*. Acta Crystallogr Sect F Struct Biol Cryst Commun, 2010. **66**(Pt 12): p. 1586-1590.
171. Ieva, R., et al., *Sequential and spatially restricted interactions of assembly factors with an autotransporter beta domain*. Proc Natl Acad Sci U S A, 2011. **108**(31): p. E383-391.
172. Drobnak, I., E. Braselmann, and P.L. Clark, *Multiple driving forces required for efficient secretion of autotransporter virulence proteins*. J Biol Chem, 2015. **290**(16): p. 10104-10116.
173. Hendrixson, D.R., et al., *Structural determinants of processing and secretion of the Haemophilus influenzae hap protein*. Mol Microbiol, 1997. **26**.
174. Pohlner, J., et al., *Gene structure and extracellular secretion of Neisseria gonorrhoeae IgA protease*. Nature, 1987. **325**.
175. Sallusto, F., et al., *Dendritic cells use macropinocytosis and the mannose receptor to concentrate macromolecules in the major histocompatibility complex*

- class II compartment: downregulation by cytokines and bacterial products.* J Exp Med, 1995. **182**(2): p. 389-400.
176. Łyskowski, A., J. Leo, and A. Goldman, *Structure and Biology of Trimeric Autotransporter Adhesins.* Adv Exp Med Biol, 2011. **715**: p. 143-158.
177. Linke, D., et al., *Trimeric autotransporter adhesins: variable structure, common function.* Trends Microbiol, 2006. **14**(6): p. 264-270.
178. Ait-Tahar, K., et al., *Auto-transporter A protein of Neisseria meningitidis: a potent CD4+ T-cell and B-cell stimulating antigen detected by expression cloning.* Mol Microbiol, 2000. **37**(5): p. 1094-1105.
179. Henderson, I.R., et al., *Type V Protein Secretion Pathway: the Autotransporter Story.* Microbiol Mol Biol Rev, 2004. **68**(4): p. 692-744.
180. Hadi, H.A., et al., *Identification and characterization of App: an immunogenic autotransporter protein of Neisseria meningitidis.* Mol Microbiol, 2001. **41**(3): p. 611-623.
181. Turner, D.P., K.G. Wooldridge, and D.A. Ala'Aldeen, *Autotransported serine protease A of Neisseria meningitidis: an immunogenic, surface-exposed outer membrane, and secreted protein.* Infect Immun, 2002. **70**(8): p. 4447-4461.
182. Turner, D.P., et al., *Characterization of MspA, an immunogenic autotransporter protein that mediates adhesion to epithelial and endothelial cells in Neisseria meningitidis.* Infect Immun, 2006. **74**(5): p. 2957-2964.
183. van Ulsen, P., et al., *A Neisserial autotransporter NalP modulating the processing of other autotransporters.* Mol Microbiol, 2003. **50**(3): p. 1017-1030.
184. Dufailu, O.A., et al., *Uptake of Neisserial autotransporter lipoprotein (NalP) promotes an increase in human brain microvascular endothelial cell metabolic activity.* Microb Pathog, 2018. **124**: p. 70-75.

185. Chiou, C.S., et al., *Molecular epidemiology and emergence of worldwide epidemic clones of Neisseria meningitidis in Taiwan*. BMC Infect Dis, 2006. **6**: p. 25.
186. Ruiz-Perez, F. and J.P. Nataro, *Bacterial serine proteases secreted by the autotransporter pathway: classification, specificity, and role in virulence*. Cell Mol Life Sci, 2014. **71**(5): p. 745-770.
187. Pohlner, J., et al., *Uptake and nuclear transport of Neisseria IgA1 protease-associated alpha-proteins in human cells*. Mol Microbiol, 1995. **17**(6): p. 1073-1083.
188. Roussel-Jazede, V., et al., *Variable processing of the IgA protease autotransporter at the cell surface of Neisseria meningitidis*. Microbiology, 2014. **160**(Pt 11): p. 2421-2431.
189. Roussel-Jazede, V., et al., *Lipidation of the autotransporter NalP of Neisseria meningitidis is required for its function in the release of cell-surface-exposed proteins*. Microbiology, 2013. **159**(Pt 2): p. 286-295.
190. Plaut, A.G., et al., *Neisseria gonorrhoeae and Neisseria meningitidis: extracellular enzyme cleaves human immunoglobulin A*. Science, 1975. **190**(4219): p. 1103-1105.
191. Almogren, A., et al., *Structural and functional consequences of cleavage of human secretory and human serum immunoglobulin A1 by proteinases from Proteus mirabilis and Neisseria meningitidis*. Infect Immun, 2003. **71**(6): p. 3349-3356.
192. Mulks, M.H., et al., *IgA proteases of two distinct specificities are released by Neisseria meningitidis*. J Exp Med, 1980. **152**(5): p. 1442-1447.

193. Lin, L., et al., *The Neisseria type 2 IgA1 protease cleaves LAMP1 and promotes survival of bacteria within epithelial cells*. Mol Microbiol, 1997. **24**(5): p. 1083-1094.
194. Besbes, A., et al., *Hyperinvasive Meningococci Induce Intra-nuclear Cleavage of the NF- κ B Protein p65/RelA by Meningococcal IgA Protease*. PLoS Pathog, 2015. **11**(8): p. e1005078.
195. Jose, J., et al., *Human T-Cell Response to Meningococcal Immunoglobulin A1 Protease Associated-Proteins*. Scand. J. Immunol, 2000. **51**: p. 176-185.
196. Arenas, J., et al., *Involvement of three meningococcal surface-exposed proteins, the heparin-binding protein NhbA, the alpha-peptide of IgA protease and the autotransporter protease NalP, in initiation of biofilm formation*. Mol Microbiol, 2013. **87**(2): p. 254-268.
197. Oldfield, N.J., et al., *Prevalence and phase variable expression status of two autotransporters, NalP and MspA, in carriage and disease isolates of Neisseria meningitidis*. PloS one, 2013. **8**(7): p. e69746.
198. Serruto, D., et al., *Neisseria meningitidis GNA2132, a heparin-binding protein that induces protective immunity in humans*. Proc Natl Acad Sci U S A, 2010. **107**(8): p. 3770-3775.
199. Del Tordello, E., et al., *Neisseria meningitidis NalP cleaves human complement C3, facilitating degradation of C3b and survival in human serum*. Proc Natl Acad Sci U S A, 2014. **111**(1): p. 427-432.
200. Arenas, J., et al., *The meningococcal autotransporter AutA is implicated in autoaggregation and biofilm formation*. Environ Microbiol, 2015. **17**(4): p. 1321-1337.

201. Arenas, J., et al., *Expression of the Gene for Autotransporter AutB of Neisseria meningitidis Affects Biofilm Formation and Epithelial Transmigration*. Front Cell Infect Microbiol, 2016. **6**: p. 162.
202. Ochiai, K., et al., *Effect of co-aggregation on the pathogenicity of oral bacteria*. J Med Microbiol, 1993. **39**(3): p. 183-190.
203. Peak, I.R., et al., *Identification and characterisation of a novel conserved outer membrane protein from Neisseria meningitidis*. FEMS Immunol Med Microbiol, 2000. **28**(4): p. 329-334.
204. Scarselli, M., et al., *Neisseria meningitidis NhhA is a multifunctional trimeric autotransporter adhesin*. Mol Microbiol, 2006. **61**(3): p. 631-644.
205. Griffiths, N.J., et al., *Meningococcal surface fibril (Msf) binds to activated vitronectin and inhibits the terminal complement pathway to increase serum resistance*. Mol Microbiol, 2011. **82**(5): p. 1129-1149.
206. Sjölander, H., et al., *Meningococcal Outer Membrane Protein NhhA Is Essential for Colonization and Disease by Preventing Phagocytosis and Complement Attack*. Infect Immun, 2008. **76**(11): p. 5412.
207. Frosch, M. and U. Vogel, *Structure and Genetics of the Meningococcal Capsule*. Handbook of Meningococcal Disease, 2006: p. 145-162.
208. Martin, P., et al., *Experimentally revised repertoire of putative contingency loci in Neisseria meningitidis strain MC58: evidence for a novel mechanism of phase variation*. Mol Microbiol, 2003. **50**(1): p. 245-257.
209. Metruccio, M.M., et al., *A novel phase variation mechanism in the meningococcus driven by a ligand-responsive repressor and differential spacing of distal promoter elements*. PLoS Pathog, 2009. **5**(12): p. e1000710.

210. Capecchi, B., et al., *Neisseria meningitidis NadA is a new invasin which promotes bacterial adhesion to and penetration into human epithelial cells*. Mol Microbiol, 2005. **55**(3): p. 687-698.
211. Franzoso, S., et al., *Human monocytes/macrophages are a target of Neisseria meningitidis Adhesin A (NadA)*. J Leuko Biol, 2008. **83**(5): p. 1100-1110.
212. Comanducci, M., et al., *NadA, a novel vaccine candidate of Neisseria meningitidis*. J Exp Med, 2002. **195**(11): p. 1445-1454.
213. van Ulsen, P., et al., *In vivo expression of Neisseria meningitidis proteins homologous to the Haemophilus influenzae Hap and Hia autotransporters*. Pathog Dis, 2001. **32**(1): p. 53-64.
214. Serruto, D., et al., *Neisseria meningitidis App, a new adhesin with autocatalytic serine protease activity*. Mol Microbiol, 2003. **48**(2): p. 323-334.
215. Khairalla, A.S., et al., *Nuclear trafficking, histone cleavage and induction of apoptosis by the meningococcal App and MspA autotransporters*. Cell Microbiol, 2015. **17**(7): p. 1008-1020.
216. Arenas, J. and J. Tommassen, *Meningococcal Biofilm Formation: Let's Stick Together*. Trends Microbiol, 2017. **25**(2): p. 113-124.
217. Linehan, S.A., et al., *Mannose receptor and its putative ligands in normal murine lymphoid and nonlymphoid organs: In situ expression of mannose receptor by selected macrophages, endothelial cells, perivascular microglia, and mesangial cells, but not dendritic cells*. J Exp Med, 1999. **189**(12): p. 1961-1972.
218. Aisen, P., *Transferrin receptor 1*. Int J Biochem Cell Biol, 2004. **36**(11): p. 2137-2143.

219. Bhavsar, A.P., J.A. Guttman, and B.B. Finlay, *Manipulation of host-cell pathways by bacterial pathogens*. *Nature*, 2007. **449**(7164): p. 827-834.
220. Lara-Tejero, M. and J.E. Galán, *A Bacterial Toxin That Controls Cell Cycle Progression as a Deoxyribonuclease I-Like Protein*. *Science*, 2000. **290**(5490): p. 354.
221. Stephens, D.S. and M.M. Farley, *Pathogenic Events During Infection of the Human Nasopharynx with Neisseria meningitidis and Haemophilus influenzae*. *Clin Infect Dis*, 1990. **13**(1): p. 22-33.
222. Birkness, K.A., et al., *A tissue culture bilayer model to study the passage of Neisseria meningitidis*. *Infect Immun*, 1995. **63**(2): p. 402-409.
223. Warren, H.S., R.G. Gonzalez, and D. Tian, *Case 38-2003*. *N Engl J Med*, 2003. **349**(24): p. 2341-2349.
224. Deghmane, A.-E., et al., *Differential modulation of TNF- α -induced apoptosis by Neisseria meningitidis*. *PLoS pathog*, 2009. **5**(5): p. e1000405.
225. Zarantonelli, M.L., et al., *Hyperinvasive genotypes of Neisseria meningitidis in France*. *Clin Microbiol Infect*, 2008. **14**(5): p. 467-472.
226. Poulsen, K., et al., *Cloning and sequencing of the immunoglobulin A1 protease gene (iga) of Haemophilus influenzae serotype b*. *Infect Immun*, 1989. **57**(10): p. 3097-3105.
227. St. Geme III, J.W. and S. Falkow, *A Haemophilus influenzae IgA protease-like protein promotes intimate interaction with human epithelial cells*. *Mol Microbiol*, 1994. **14**(2): p. 217-233.
228. Benz, I. and M.A. Schmidt, *Structures and functions of autotransporter proteins in microbial pathogens*. *Int J Med Microbiol*, 2011. **301**(6): p. 461-468.
229. Izaurralde, E. and S. Adam, *Transport of macromolecules between the nucleus and the cytoplasm*. *Rna*, 1998. **4**(4): p. 351-364.

230. Pemberton, L.F., G. Blobel, and J.S. Rosenblum, *Transport routes through the nuclear pore complex*. *Curr Opin Cell Biol*, 1998. **10**(3): p. 392-399.
231. Lee, J.H., et al., *Prediction and screening of nuclear targeting proteins with nuclear localization signals in Helicobacter pylori*. *J Microbiol Methods*, 2012. **91**(3): p. 490-496.
232. Benabdillah, R., et al., *Identification of a nuclear targeting signal in YopM from Yersinia spp.* *Microb Pathog*, 2004. **36**(5): p. 247-261.
233. Okuda, J., et al., *Shigella effector IpaH9.8 binds to a splicing factor U2AF35 to modulate host immune responses*. *Biochem Biophys Res Commun*, 2005. **333**(2): p. 531-539.
234. Agterberg, M., H. Adriaanse, and J. Tommassen, *Use of outer membrane protein PhoE as a carrier for the transport of a foreign antigenic determinant to the cell surface of Escherichia coli K-12*. *Gene*, 1987. **59**.
235. Xiao, C.Y., S. Hubner, and D.A. Jans, *SV40 large tumor antigen nuclear import is regulated by the double-stranded DNA-dependent protein kinase site (serine 120) flanking the nuclear localization sequence*. *J Biol Chem*, 1997. **272**(35): p. 22191-22198.
236. Ozawa, M., et al., *Contributions of Two Nuclear Localization Signals of Influenza A Virus Nucleoprotein to Viral Replication*. *J Virol*, 2007. **81**(1): p. 30.
237. Lee, J.C., et al., *Prediction of bacterial proteins carrying a nuclear localization signal and nuclear targeting of HsdM from Klebsiella pneumoniae*. *J Microbiol*, 2009. **47**(5): p. 641.
238. Howard, E.A., et al., *The VirD2 protein of A. tumefaciens contains a C-terminal bipartite nuclear localization signal: implications for nuclear uptake of DNA in plant cells*. *Cell*, 1992. **68**(1): p. 109-118.

239. Xiao, C.Y., P. Jans, and D.A. Jans, *Negative charge at the protein kinase CK2 site enhances recognition of the SV40 large T-antigen NLS by importin: effect of conformation*. FEBS Lett, 1998. **440**(3): p. 297-301.
240. Kuwahara, H., M. Nishizaki, and H. Kanazawa, *Nuclear Localization Signal and Phosphorylation of Serine350 Specify Intracellular Localization of DRAK2*. J Biochem, 2007. **143**(3): p. 349-358.
241. Jans, D.A., C.Y. Xiao, and M.H. Lam, *Nuclear targeting signal recognition: a key control point in nuclear transport?* Bioessays, 2000. **22**(6): p. 532-344.
242. McSweeney, L.A. and L.A. Dreyfus, *Nuclear localization of the Escherichia coli cytolethal distending toxin CdtB subunit*. Cell Microbiol, 2004. **6**(5): p. 447-458.
243. Haraga, A. and S.I. Miller, *A Salmonella enterica Serovar Typhimurium Translocated Leucine-Rich Repeat Effector Protein Inhibits NF- κ B-Dependent Gene Expression*. Infect Immun, 2003. **71**(7): p. 4052-4058.
244. Briggs, L.J., et al., *The cAMP-dependent protein kinase site (Ser312) enhances dorsal nuclear import through facilitating nuclear localization sequence/importin interaction*. J Biol Chem, 1998. **273**(35): p. 22745-22752.
245. Mancini, A., et al., *The M-CSF receptor substrate and interacting protein FMIP is governed in its subcellular localization by protein kinase C-mediated phosphorylation, and thereby potentiates M-CSF-mediated differentiation*. Oncogene, 2004. **23**(39): p. 6581-6589.
246. Matangkasombut, O., et al., *Cytolethal Distending Toxin from Aggregatibacter actinomycetemcomitans Induces DNA Damage, Cell Cycle Arrest, and Caspase- Independent Death in a Saccharomyces cerevisiae; Model*. Infect Immun, 2010. **78**(2): p. 783.

247. McSweeney, L.A. and L.A. Dreyfus, *Nuclear localization of the Escherichia coli cytolethal distending toxin CdtB subunit*. Cell Microbiol, 2004. **6**(5): p. 447-458.
248. Pennini, M.E., et al., *Histone Methylation by NUE, a Novel Nuclear Effector of the Intracellular Pathogen Chlamydia trachomatis*. PLOS Pathog, 2010. **6**(7): p. e1000995.
249. Choi, C.H., et al., *Acinetobacter baumannii outer membrane protein A targets the nucleus and induces cytotoxicity*. Cell Microbiol, 2008. **10**(2): p. 309-319.
250. Pulliam, K.F., et al., *The Classical Nuclear Localization Signal Receptor, Importin- α , Is Required for Efficient Transition Through the G/S Stage of the Cell Cycle in Saccharomyces cerevisiae*. Genetics, 2009. **181**(1): p. 105-118.
251. Lange, A., et al., *Classical nuclear localization signals: definition, function, and interaction with importin α* . J Biol Chem, 2007. **282**(8): p. 5101-5105.
252. Sa E Cunha, C., et al., *Neisseria meningitidis Opc invasin binds to the cytoskeletal protein alpha-actinin*. Cell Microbiol, 2009. **11**(3): p. 389-405.
253. Kornberg, R.D., *Chromatin structure: a repeating unit of histones and DNA*. Science, 1974. **184**(4139): p. 868-871.
254. Draizen, E.J., et al., *HistoneDB 2.0: a histone database with variants--an integrated resource to explore histones and their variants*. Database (Oxford), 2016. **2016**.
255. Zhou, P., et al., *Histone cleavage as a mechanism for epigenetic regulation: current insights and perspectives*. Curr Mol Med, 2014. **14**(9): p. 1164-1172.

256. Azad, G.K., et al., *Modifying Chromatin by Histone Tail Clipping*. J Mol Biol, 2018. **430**(18, Part B): p. 3051-3067.
257. Sidoli, S., L. Cheng, and O.N. Jensen, *Proteomics in chromatin biology and epigenetics: Elucidation of post-translational modifications of histone proteins by mass spectrometry*. J Proteomics, 2012. **75**(12): p. 3419-3433.
258. Anderson, D., et al., *Extensive and varied modifications in histone H2B of wild-type and histone deacetylase 1 mutant Neurospora crassa*. Biochemistry, 2010. **49**(25): p. 5244-5257.
259. Dhaenens, M., et al., *Histone proteolysis: A proposal for categorization into 'clipping' and 'degradation'*. Bioessays, 2015. **37**(1): p. 70-79.
260. Falk, M.M., et al., *Foot-and-mouth disease virus protease 3C induces specific proteolytic cleavage of host cell histone H3*. J Virol, 1990. **64**(2): p. 748-756.
261. Panda, P., et al., *Purification and characterization of a novel histone H2A specific protease (H2Asp) from chicken liver nuclear extract*. Gene, 2013. **512**(1): p. 47-54.
262. Kawasaki, H. and S. Iwamuro, *Potential roles of histones in host defense as antimicrobial agents*. Infect Disord Drug Targets, 2008. **8**(3): p. 195-205.
263. Sharma, A. and K.V. Radha Kishan, *Serine protease inhibitor mediated peptide bond re-synthesis in diverse protein molecules*. FEBS Letters, 2011. **585**(21): p. 3465-3470.
264. Bhaumik, S.R., E. Smith, and A. Shilatifard, *Covalent modifications of histones during development and disease pathogenesis*. Nat Struct Mol Biol, 2007. **14**(11): p. 1008-1016.
265. Rodriguez-Paredes, M. and M. Esteller, *Cancer epigenetics reaches mainstream oncology*. Nat Med, 2011: p. 330-339.

266. Zhang, K., et al., *Distinctive core histone post-translational modification patterns in Arabidopsis thaliana*. PLoS One, 2007. **2**(11): p. e1210.
267. David Allis, C., et al., *Proteolytic processing of histone H3 in chromatin: a physiologically regulated event in tetrahymena micronuclei*. Cell, 1980. **20**(1): p. 55-64.
268. Duncan, E.M., et al., *Cathepsin L proteolytically processes histone H3 during mouse embryonic stem cell differentiation*. Cell, 2008. **135**(2): p. 284-294.
269. Mandal, P., et al., *Unexpected histone H3 tail-clipping activity of glutamate dehydrogenase*. J Biol Chem, 2013. **288**(26): p. 18743-187457.
270. Vossaert, L., et al., *Identification of histone H3 clipping activity in human embryonic stem cells*. Stem Cell Res, 2014. **13**(1): p. 123-134.
271. Santos-Rosa, H., et al., *Histone H3 tail clipping regulates gene expression*. Nat Struct Mol Biol, 2009. **16**(1): p. 17-22.
272. Xue, Y., et al., *PRB1 is required for clipping of the histone H3 N terminal tail in Saccharomyces cerevisiae*. PLoS One, 2014. **9**(2): p. e90496.
273. Melo, F.R., et al., *Tryptase-catalyzed core histone truncation novel epigenetic regulatory mechanism in mast cells*. J Allergy and Clin Immunol, 2017. **140**(2): p. 474-485.
274. Haugen, M.H., et al., *Nuclear legumain activity in colorectal cancer*. PLoS one, 2013. **8**(1): p. e52980.
275. Liu, H., et al., *Clipping of arginine-methylated histone tails by JMJD5 and JMJD7*. Proc Natl Acad Sci USA, 2017. **114**(37): p. E7717-E7726.
276. Herrera-Solorio, A.M., et al., *Clipped histone H3 is integrated into nucleosomes of DNA replication genes in the human malaria parasite Plasmodium falciparum*. EMBO reports, 2019: p. e46331.

277. Lakshmipathy, S.K., et al., *Identification of nascent chain interaction sites on trigger factor*. J Biol Chem, 2007. **282**(16): p. 12186-12193.
278. Hoffmann, A., et al., *Trigger factor forms a protective shield for nascent polypeptides at the ribosome*. J Biol Chem, 2006. **281**(10): p. 6539-6545.
279. Martinez-Hackert, E. and W.A. Hendrickson, *Promiscuous substrate recognition in folding and assembly activities of the trigger factor chaperone*. Cell, 2009. **138**(5): p. 923-934.
280. Xu, J., et al., *Extracellular histones are major mediators of death in sepsis*. Nat Med, 2009. **15**(11): p. 1318-1321.
281. Cutter, A.R. and J.J. Hayes, *Linker histones: novel insights into structure-specific recognition of the nucleosome*. Biochem Cell Biol, 2016. **95**(2): p. 171-178.
282. Zhang, D., et al., *Induction of rapid histone degradation by the cytotoxic T lymphocyte protease Granzyme A*. J Biol Chem, 2001. **276**(5): p. 3683-3690.
283. Kaul, R., et al., *The chlamydial EUO gene encodes a histone H1-specific protease*. J Bacteriol, 1997. **179**(18): p. 5928-5934.
284. Sancho, M., et al., *Depletion of human histone H1 variants uncovers specific roles in gene expression and cell growth*. PLoS Genet, 2008. **4**(10): p. e1000227.
285. Iwasaki, W., et al., *Contribution of histone N-terminal tails to the structure and stability of nucleosomes*. FEBS open bio, 2013. **3**: p. 363-369.
286. Hamiche, A., et al., *Histone tails modulate nucleosome mobility and regulate ATP-dependent nucleosome sliding by NURF*. Proc Nat Acad Sci, 2001. **98**(25): p. 14316-14321.
287. Becker, P.B. and W. Horz, *ATP-dependent nucleosome remodeling*. Annu Rev Biochem, 2002. **71**: p. 247-273.

288. Mandal, P., G.K. Azad, and R.S. Tomar, *Identification of a novel histone H3 specific protease activity in nuclei of chicken liver*. *Biochem Biophys Res Commun*, 2012. **421**(2): p. 261-267.
289. Tesar, M. and O. Marquardt, *Foot-and-mouth disease virus protease 3C inhibits cellular transcription and mediates cleavage of histone H3*. *Virology*, 1990. **174**(2): p. 364-374.
290. Kim, K., et al., *MMP-9 facilitates selective proteolysis of the histone H3 tail at genes necessary for proficient osteoclastogenesis*. *Genes Dev*, 2016. **30**(2): p. 208-219.
291. Duarte, L.F., et al., *Histone H3.3 and its proteolytically processed form drive a cellular senescence programme*. *Nat Commun*, 2014. **5**: p. 5210.
292. Shen, J., et al., *JMJD5 cleaves monomethylated histone H3 N-tail under DNA damaging stress*. *EMBO reports*, 2017. **18**(12): p. 2131-2143.
293. Allis, C.D. and J.C. Wiggins, *Proteolytic processing of micronuclear H3 and histone phosphorylation during conjugation in Tetrahymena thermophila*. *Exp Cell Res*, 1984. **153**(2): p. 287-298.
294. Biswas, M., et al., *Role of histone tails in structural stability of the nucleosome*. *PLoS Comput Biol*, 2011. **7**(12): p. e1002279.
295. Fullgrabe, J., N. Hajji, and B. Joseph, *Cracking the death code: apoptosis-related histone modifications*. *Cell Death Differ*, 2010. **17**(8): p. 1238-1243.
296. Tvardovskiy, A., et al., *Top-down and Middle-down Protein Analysis Reveals that Intact and Clipped Human Histones Differ in Post-translational Modification Patterns*. *Mol Cell Proteomics*, 2015. **14**(12): p. 3142-3153.

297. Nurse, N.P., et al., *Clipping of flexible tails of histones H3 and H4 affects the structure and dynamics of the nucleosome*. Biophys J, 2013. **104**(5): p. 1081-1088.
298. Jenuwein, T. and C.D. Allis, *Translating the histone code*. Science, 2001. **293**(5532): p. 1074-1080.
299. Polach, K.J., P.T. Lowary, and J. Widom, *Effects of core histone tail domains on the equilibrium constants for dynamic dna site accessibility in nucleosomes*¹¹Edited by P. E. Wright. J Mol Biol, 2000. **298**(2): p. 211-223.
300. Lee, C.-K., et al., *Evidence for nucleosome depletion at active regulatory regions genome-wide*. Nat Genet, 2004. **36**(8): p. 900-905.
301. Yi, S.J. and K. Kim, *Histone tail cleavage as a novel epigenetic regulatory mechanism for gene expression*. BMB Rep, 2018. **51**(5): p. 211-218.
302. Bierne, H. and P. Cossart, *When bacteria target the nucleus: the emerging family of nucleomodulins*. Cell Microbiol, 2012. **14**(5): p. 622-633.
303. Lebreton, A., et al., *A Bacterial Protein Targets the BAHD1 Chromatin Complex to Stimulate Type III Interferon Response*. Science, 2011. **331**(6022): p. 1319.
304. Capozzo, A.V., et al., *Expression of foot and mouth disease virus non-structural polypeptide 3ABC induces histone H3 cleavage in BHK21 cells*. Virus Res, 2002. **90**(1-2): p. 91-99.
305. Brewer, J.M., et al., *Significance of the enzymatic properties of yeast S39A enolase to the catalytic mechanism*. Biochim Biophys Acta, 1998. **1383**(2): p. 351-355.

Appendix

10% Acrylamide mini gels Separating (resolving) gel master mix: 2.5 ml Buffer A, 3.3 ml Acrylamide/Bis-acrylamide (30%, w/v), 4.1 ml dH₂O, 30 µl 10% (w/v) Ammonium persulfate (APS), 30 µl Tetramethylethylenediamine (TEMED).

16% Acrylamide mini gels Separating (resolving) gel master mix: 2.5 ml Buffer A, 5.3 ml Acrylamide/Bis-acrylamide (30%, w/v), 2.2 ml dH₂O, 30 µl 10% (w/v) Ammonium persulfate (APS), 30 µl Tetramethylethylenediamine (TEMED).

Stacking gel master mix: 1.3 ml Buffer B, 1 ml Acrylamide/ Bis-acrylamide (30%, w/v), 2.7 ml dH₂O, 10 µl 10% (w/v) APS, 10 µl TEMED.

Agarose gel; preparation of 0.7-1.0% agarose gel was done by dissolving 0.7-1 g of agarose powder (sigma) in 100 ml 1× TAE buffer and syber safe stain was added.

Alkaline phosphatase buffer; 15.7 g Tris-HCl, 5.8 g NaCl, 0.2 g MgCl₂·6H₂O, 1000 ml dH₂O, adjust the pH to 9.5.

Antibiotics: All antibiotics were purchased from Sigma-Aldrich, UK, prepared according to the recommended concentration, sterilised by filtration, and stored at 4°C.

Kanamycin (50 mg ml⁻¹ stock solution prepared in dH₂O)

Ampicillin: (100 mg ml⁻¹ stock solution prepared in dH₂O)

Spectinomycin (50 mg ml⁻¹ stock solution prepared in dH₂O)

Blocking buffer (Milk): 5% (w/v) skimmed milk powder in 0.1% (v/v) PBST.

Blocking buffer: 1-5% (w/v) Bovine serum albumin (Sigma-Aldrich A3912) in PBS-T and sterilize by filtration (0.22 µm filter).

BSA: Bovine serum Albumin, (Sigma A3912) as lyophilized powder (MW ca. 66 kDa) was prepared in sterile PBS according to the concentration needed.

Buffers for protein purification under native condition:

Elution buffer; 50mM NaH₂PO₄, 300mM NaCl, 500mM imidazole, and pH adjusted to 7.5 using NaOH.

Lysis Buffer; 50mM NaH₂PO₄, 300 mM NaCl, 10mM imidazole, and pH adjusted to 7.5 using NaOH.

Wash buffer; 50 mM NaH₂PO₄, 300 mM NaCl, 20 mM imidazole, and pH adjusted to 7.5 using NaOH.

Complete medium for cell culture: DMEM medium supplemented with 10% (v/v) Fetal Bovine Serum (FBS), 1% (v/v) Penicillin/Streptomycin, and 1% (v/v) Epithelial Cell Growth Supplement (ScienCell Research Labs.).

DMEM medium: DMEM (Dulbecco's Modified Eagle's Medium) Contains 1000 mg/L glucose, L-glutamine, and sodium bicarbonate.

DNA loading dye (6×); 10 mM Tris-HCl (pH 7.6), 0.03% Bromophenol blue, 0.03% Xylene cyanol FF, 60% glycerol, 60 mM Ethylenediaminetetraacetic acid (EDTA).

Fixing solution (4% paraformaldehyde): 40 g of paraformaldehyde powder was added to the pre-heated 800 mL of PBS at 60°C. pH was slowly adjusted at 6.9 by 1 N NaOH, final volume made up to 1L with PBS.

IPTG (Isopropyl-β-D-1-thiogalactopyranoside [FW 238.8]); to prepare 1 M stock solution, 0.23 g of IPTG was dissolved in 1 ml dH₂O, sterilized by filtration and stored at -20°C.

LB (Lysogeny broth); Tryptone 10 g, Yeast extract 5 g and Sodium chloride 10 g for 1000 ml dH₂O.

LB agar; Tryptone 10 g, Yeast extract 5 g, Sodium chloride 10g, Microbial tested agar 15 g for 1000 ml of dH₂O, pH 7.0 ± 0.2 at 25°C.

Permeabilization solution: 0.5 g of BSA in 50 ml of mixture of 0.1% of Triton X-100 (v/v) in PBS.

Phosphate buffered saline solution (PBS); prepared by dissolving 1 tablet of Phosphate buffered saline (Dulbecco, Oxoid) in 100 ml dH₂O and autoclave, this gives sodium chloride 0.16 mol, Potassium chloride 0.003 mol, Disodium hydrogen phosphate 0.008 mol and Potassium dihydrogen phosphate 0.001 mol with a pH value of 7.4.

Radio-immunoprecipitation assay (RIPA) buffer: 5 ml of RIPA buffer (Sigma-Aldrich) supplemented with ½ tablet of PhosSTOP complete ultra-protease inhibitor tablet (Roche) and ½ tablet of complete mini EDTA-free protease inhibitor cocktail tablet.

SDS running buffer (10×); (30.3 g (0.25 M) Tris base, 187.7 g (2.5 M) Glycine, 950 ml dH₂O, 10 g SDS (1%), made up to 1000 ml with dH₂O, mix well.

SDS-PAGE Coomassie Staining Solution: 50% (v/v) methanol 10%(v/v) acetic acid, Coomassie Blue 12g/L(Sigma-Aldrich) in 1L.

SDS-PAGE Destaining Solution: 30%(v/v) Methanol, 10%(v/v) Acetic Acid and 60% (v/v) water in 1L).

SDS-sample buffer (6×); 375mM M Tris-HCl (pH 6.8), 9% SDS, 50% Glycerol, 9% β-mercaptoethanol, 0.03% Bromophenol blue.

Sodium dodecyl sulphate (SDS)-separating (resolving) buffer (Buffer A): 181.7 g Tris base, 40 ml 10% (w/v) SDS, made up to 1L with dH₂O, pH adjusted at 8.8.

SDS-stacking buffer (Buffer B): 60.6 g Tris base, 40 ml 10% (w/v) SDS, made up to 1L with dH₂O, pH adjusted at 6.8.

Semi-dry transfer buffer: 5.82 g Tris, 2.93 g Glycine, 3.75 ml 10% SDS, 200 ml methanol, made up to 1L with dH₂O, pH adjusted at 9.

Sodium carbonate buffer (coating buffer): 9.3 g of Sodium Carbonate (Na_2CO_3) and 1 g Sodium Bicarbonate (NaH_2CO_3), made up to 1L with dH_2O , pH adjusted at 9.4.

Stripping Buffer (Glycine-HCl, pH 2.5); 1.5 g Glycine, 200 ml dH_2O , adjust the pH to 2.5 with 5 M HCl.

Washing buffer (PBS-T): 0.05-0.1% (v/v) Tween20 in PBS.

Working concentration was 1000x dilution from the prepared stock.

Amino Acid Abbreviations

Amino acid	Three-letter abbreviation	One-letter abbreviation
Alanine	Ala	A
Arginine	Arg	R
Asparagine	Asn	N
Aspartate	Asp	D
Cysteine	Cys	C
Glutamate	Glu	E
Glutamine	Gln	Q
Glycine	Gly	G
Histidine	His	H
Isoleucine	Ile	I
Leucine	Leu	L
Lysine	Lys	K
Methionine	Met	M
Phenylalanine	Phe	F
Proline	Pro	P
Serine	Ser	S
Threonine	Thr	T
Tryptophan	Trp	W
Tyrosine	Tyr	Y
Valine	Val	V

The annealing temperatures of the primers used in this study.

Primer	Annealing Temperature(°C)
AppdelRed-AmpF1	62
AppdelRed-AmpR1	
AppReddel ^{901 to 980} mt1-F5	65
AppReddel ^{901 to 980} mt1-R5	
AppReddel ^{908 to 965} mt2-F2	67
AppReddel ^{908 to 965} mt2-R2	
MspAReddel ^{1037 to 1139} mt1-F4	72
MspAReddel ^{1037 to 1139} mt1-R4	
MspAReddel ^{999 to 1073} mt2-F3	71
MspAReddel ^{999 to 1073} mt2-R3	
MspAdelRed-AmpF1	62
AppRed ^{S267A} -F	60
AppRed ^{S267A} -R	
MspARed ^{S241A} -F	61
MspARed ^{S241A} -R	
MspA ^{D135E} -F	72
MspA ^{D135E} -R	
AppRedNLS ^{SS936&939AA} -F	71
AppRedNLS ^{SS936&939AA} -R	